

**Refined isotopic compositions of K, Ca
and a complementary comparison
of the ^{40}K - ^{40}Ca , ^{40}K - ^{40}Ar and ^{87}Rb - ^{87}Sr chronometers.**

Inauguraldissertation
der Philosophisch-naturwissenschaftlichen Fakultät
der Universität Bern

vorgelegt von
Mariia Dèzes
aus der Ukraine

Leiter der Arbeit:
Prof. Dr. Igor M. Villa
Prof. Dr. Thomas F. Nägler
Institut für Geologie, Universität Bern

Von der Philosophisch-naturwissenschaftlichen Fakultät angenommen.

Bern, Februar 4, 2016

Der. Dekan:
Prof. Dr. G. Colangelo

Original document saved on the web server of the University Library of Bern



This work is licensed under a
Creative Commons Attribution-Non-Commercial-No derivative works 2.5 Switzerland licence. To see the
licence go to <http://creativecommons.org/licenses/by-nc-nd/2.5/ch/> or write to Creative Commons, 171
Second Street, Suite 300, San Francisco, California 94105, USA.

Copyright Notice

This document is licensed under the Creative Commons Attribution-Non-Commercial-No derivative works 2.5 Switzerland.

<http://creativecommons.org/licenses/by-nc-nd/2.5/ch/>

You are free:



to copy, distribute, display, and perform the work

Under the following conditions:



Attribution. You must give the original author credit.



Non-Commercial. You may not use this work for commercial purposes.



No derivative works. You may not alter, transform, or build upon this work..

For any reuse or distribution, you must take clear to others the license terms of this work.

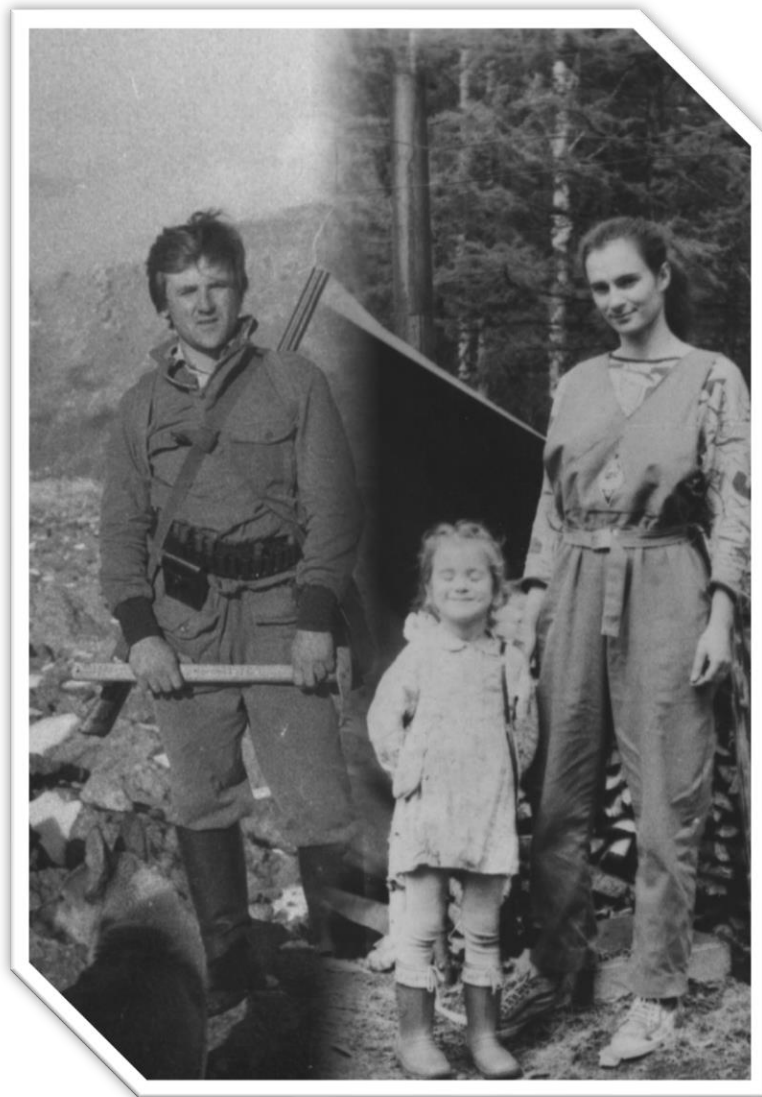
Any of these conditions can be waived if you get permission from the copyright holder.

Nothing in this license impairs or restricts the author's moral rights according to Swiss law.

The detailed license agreement can be found at:

<http://creativecommons.org/licenses/by-nc-nd/2.5/ch/legalcode.de>

To my parents



Acknowledgements

I am infinitely grateful to my parents for my geological upbringing, that they took me with them on their geological field expeditions, for living with them in tents, growing up with packs of wolf-dogs, seeing bear's footprints, eating larch needles and flying above Siberian forest ocean in an incredibly loud military helicopter. For their patience, when I asked the names of each rock I saw on the way, their tolerance for my endless stone collections and their encouraging my interest in the fascinating geochemical life of our planet.

I am in debt to Igor, who guided me through these years of my PhD, who was patient to my falls, helpful in my complications, tolerable to my mistakes, supportive, when nothing was working, who was as happy as me, when I succeeded, and thanks to whom I discovered the intriguing world of geochronology.

I appreciate Thomas's cheerfulness, his constant support and valuable advices, his positive attitude, even when neither I nor Igor were sure it is going to work, and thanks to whom I discovered an exciting world of chemistry.

I am grateful to Klaus for puzzling discussions, for always having time for a PhD student in his incredibly busy schedule, and thanks to whom I got captivated with cosmochemistry.

I am grateful to our Isotope geology group: Ben, Emelie, Nikolas, Chloe, Jonas, Om, Alessandro, Dipankar, Edel; Dea, Dănu, Hauke, Kirsten, Gabi, Kurt – for being the best.

My special thanks are doing to my dear friends at the Geological institute, who made my life in Bern happy and fun: Laura, Sara, Glenn, Daniele, Dima; and to the new generation of party animals: Anne C., Laura, Andrea, Frank, Camille, Anne K., Nasim, Veit, Lena, Francesco and many others!

Special thanks from all my heart are going to Regina without whom life would not be as fun as it is!

Special appreciations to Ulli who helped me with math and was always cheerful!

Thanks to all institute people for making this place friendly and enjoyable to work!

I appreciate the help of Illia, who came all the way from Ukraine to clean filaments, when I was piled under a lab work. Thanks are going to all my family for support, borsch, vareniki, salo and their generous love.

And this work would not be completed without the help of dear Pierre, who was so kind to feed me the last months and to proof read all these dozens of pages.

Summary

The K-Ar geochronometer and its more sophisticated Ar-Ar version are among the most used methods in geochronology. Recently the EarthTime initiative started the attempt to calibrate the Geochronological Time Scale with a precision of 0.1% by intercalibrating orbital tuning, absolute dating and relative dating. This requires the absolute dating to be of a precision of 0.1%. Such a precision is achievable on modern mass-spectrometers for the measurements of isotope ratios; however the accuracy of the Ar-Ar dating system strongly depends on the accuracy of the constants incorporated into the age equation.

Three constants are used for Ar-Ar age calculations: 1) the age of the irradiation flux monitor; 2) the ^{40}K isotopic abundance and 3) the ^{40}K decay constant and its branching ratio. The first one has been an object of calibrations during the last two decades; and an age of some irradiation standards is claimed to be known with a precision of 0.1%. We did not focus on this problem and just briefly discuss the issue of the age of the Fish Canyon Tuff sanidine irradiation standard in Chapter 3. Two other constants are the subject of this study.

The natural K isotopic composition has been measured in 1975 with the gravimetric method, which yielded a high precision for the $^{41}\text{K}/^{39}\text{K}$ value, but an insufficient precision for the $^{40}\text{K}/^{39}\text{K}$ ratio, which is one of the key values for K-Ar and Ar-Ar dating. The isotopic compositions of two standards NIST SRM 918a and SRM 918b have been measured in the frame of this study and compared with the bulk Earth isotopic composition. I measured K isotopic composition on a thermal ionization mass spectrometer (TIMS Triton *Plus*) with the application of three different amplifiers, which allowed to acquire a wide dynamic range with high precision. Three measurement techniques have been applied: total evaporation, block total evaporation and conventional block measurements. Due to a high instrumental fractionation, total evaporation measurements did not give consistent results, thus the $^{40}\text{K}/^{39}\text{K}$ ratios have been normalized to the fixed and precise $^{41}\text{K}/^{39}\text{K}$ ratio of Garner et al. (1975) [Garner E.L. et al. 1975. J. Res. Natl. Bur. Stand. 79A, 713-725]. The resulting best estimate for the $^{40}\text{K}/^{39}\text{K}$ ratio is $0.000\,125\,116 \pm 57$ (2σ), corresponding to an isotopic abundance $^{40}\text{K}/\text{K} = (1.1668 \pm 8) \times 10^4$. This value is identical with previous estimations, but the uncertainty is five times better, which brings the uncertainty of ^{40}K isotopic abundance from 0.35% to the desired level below 0.1%.

^{40}K decay constants are more complicated to measure. Radioactive ^{40}K decays to ^{40}Ca and to ^{40}Ar ; the decay to Ar presumably has three paths, two of which can be measured and one that is calculated theoretically. Therefore the uncertainty on the ^{40}K decay constants is relatively high, which limits the accuracy of the Ar-Ar dating tool. In this work the estimation of the ^{40}K decay constants is approached by intercalibration of K-Ca and Ar-Ar with U-Pb and Rb-Sr ages of well-characterized magmatic samples with simple geological histories. This task itself relied on two subtasks: 1) developing a high precision K-Ca dating method and 2) dating samples with a well-known geological history, using the K-Ca, Ar-Ar and Rb-Sr methods, and comparing the obtained ages with published U-Pb reference ages.

High precision K-Ca dating relies upon high precision Ca measurements. A unique high precision method for the simultaneous measurements of the full range of Ca isotopes was

developed, which makes use of a TIMS Triton *Plus* especially designed for Ca measurements. This allowed to measure $^{40}\text{Ca}/^{44}\text{Ca}$ ratios with an outstanding reproducibility of 0.06‰. The method was first used to compare the internal consistency of published Ca isotopic compositions. The isotopic compositions of two Ca standards, NIST SRM 915a and SRM 915b, were found to be identical within uncertainty and in line with published values. Small samples measured in the frame of this study (<1µg) suffered from an intense instrumental fractionation, which cannot anymore be sufficiently corrected with a simple exponential law. Therefore the use of an additional term for the exponential fractionation correction, which eliminates the offset due to an insufficient instrumental fractionation correction, is suggested and applied here.

Finally K-Ca combined with Rb-Sr and Ar-Ar dating was performed on four samples. Potential samples for intercalibration should be of considerable age with a “point-like” geological history which limits the choice to well described and already dated samples. Quantitative element profiles and semi-quantitative mapping by electron microprobe were essential to ensure that our samples did not suffer from recrystallization or any other post-emplacement processes. For the Archean Siilinjärvi carbonatite Rb-Sr and low precision Ar-Ar and K-Ca dating indicate the occurrence of a post-emplacement metamorphic event at 1869 Ma. The other three samples appear to have a “point-like” geological history. A sample from the Triassic Bolgokhtokh intrusion, Kotuy, Russia, was dated with the Ar-Ar system and yielded an 225 Ma age, however microscopic investigations showed a very prominent zonation, which prevented the use of this sample for the decay constant intercalibration. The Rubikon lepidolite, Namibia, yielded an 505 Ma Rb-Sr age consistent with a previously published U-Pb age. The low precision K-Ca age we obtained did not allow us, so far, to use this sample for the ^{40}K decay intercalibration. The fourth sample from the Phalaborwa carbonatite complex not only shows a “point-like” geological history, but also yielded high precision Rb-Sr and K-Ca ages. The Rb-Sr age for this sample is coincident with previously reported U-Pb ages for this complex and K-Ca as well as Ar-Ar ages are ca. 1% younger. Results from this last sample allowed us to assess the ^{40}K total decay constant. Within a reported range of the ^{40}K branching ratios the most suitable decay constant is the one published by Min et al. (2000) [Min, K., Mundil, R., Renne, P.R., Ludwig, K.R., 2000. *Geochim. Cosmochim. Acta* 64, 73-98]. This constant is lower than the currently recommended value and has been previously reported to be the best-fit constant also for Ar-Ar and U-Pb ages intercalibrations.

Thus this work presents a newly determined $^{40}\text{K}/\text{K}$ ratio with a precision of 0.07%, as well as a narrowed down range of plausible ^{40}K decay constants, and confirms the best fit total decay constant for ^{40}K geochronometers. It also describes high precision static Ca measurements, recommends the most consistent Ca isotopic composition, determines isotopic compositions of two widely used Ca standards and finally proposes an improved fractionation correction for small Ca samples.

Table of contents:

Introduction.....	1
1. Short historical outline.....	3
2. K dating systems.....	5
3. K decay constants	6
3.1. Physical methods of ^{40}K decay constant determination	6
3.2. Geological methods	8
4. ^{40}K abundance.....	9
5. Outline of the thesis	11
References.....	12
Chapter 1.	
High precision determination of the terrestrial ^{40}K abundance	15
1. Introduction.....	18
2. Methodology	19
2.1. Standards	19
2.2. Filaments	20
2.3. Mass spectrometry	21
2.3.1. TIMS amplifier configurations.....	21
2.3.2. TIMS measurement protocols	21
3. Results and discussion	23
3.1. In run normalized measurements.....	23
3.2. Conventional total evaporation measurements.....	25
3.3. Block total evaporation measurements.....	30
4. Conclusions.....	32
Acknowledgements.....	33
Appendix.....	33
References.....	34
Chapter 2.	
TIMS measurements of full range of natural Ca isotopes with internally consistent fractionation correction.....	37
1. Introduction.....	40
1.1. Reference materials	41
1.2. Reference isotopic compositions	41
1.3. Fractionation corrections	42
2. Analytical methods	44
3. Results and discussion	46
3.1. Internal consistency check of Ca isotopic compositions	46
3.2. Improved exponential correction law for Ca.....	48
3.3. Ca isotopic composition of SRM915a and SRM915b.....	53
4. Conclusions.....	55

Appendix	56
References	56
Chapter 3.	
Assessing the ^{40}K decay constant with ^{87}Rb - ^{87}Sr , ^{40}K - ^{40}Ca and ^{40}Ar - ^{39}Ar chronometers intercalibration	59
1. Introduction.....	61
1.1. ^{40}K decay constant determination.....	62
1.2. ^{40}K decay constant in geochronology	63
1.3. Our approach	63
2. Samples ..	64
3. Method ...	68
3.1. Sample preparation	68
3.2. Measurements	68
3.3. K-Ca mixed spike calibration	69
4. Results.....	70
5. Discussion	84
5.1. Ar-Ar flux monitor	84
5.2. “Point-like” event	85
5.3. ^{40}K decay constant	87
6. Conclusions.....	90
Acknowledgements.....	90
References	91
General conclusions	95
Appendix 1. Clean laboratory protocols	A-1-1
Appendix 2. Sample description	A-2-1
Appendix 3. Measurement protocols	A-3-1
Appendix 2. K-Ca mixed spike calibration.....	A-4-1



Introduction

1. Short historical outline

The age of the Earth and the time of the creation have occupied human imagination for thousands of years. Ancient Greeks, Romans, Egyptians, Hebrews, Sumerian, Chinese and many other civilizations have tried to estimate the time of the creation with results varying from 2'000 to 300'000 years before their time. Most estimates derived from the Old Testament converged at around 4'000 BC (or exactly on October 26, 4004 BC at 9:00am if the Archbishop James Ussher is to be believed). By the 19th century it had become clear to most scientists that the Earth had to be much older than calculated from the Bible, it's age, however, was scarcely settled; some scientists even postulated that the Earth was of unlimited age (Hutton, Lyell). By mid-1800 several attempts were made to calculate the age of the Earth on a scientific basis: Using the time it would take for the Sun to condense down to its current diameter and brightness from the nebula of gas and dust from which it was born, Hermann von Helmholtz calculated in 1858 the Earth's age at about 20 Ma. This age estimate was shortly followed by Lord Kelvin's (at the time still William Thomson) attempt to calculate the age of the Earth based on the time it would take for the totally molten Earth to cool to its present temperature. In his first attempt in 1862 he calculated an age of 98 Ma, conceding however for a maximum age of 400 Ma. Lord Kevin would then continuously revise his age downwards to finally settle in 1897 for 24 Ma. This was clearly not sufficiently old to account for many geological process or for the theory of evolution. Actually Charles Darwin himself estimated (with a somewhat "Ussherian" precision) that the geological processes that formed a specific region in England had to have taken 306'662'400 years to complete. This age which was published in the first edition of *On the origin of species* in 1859, was however removed by Darwin from the third edition of his book because it proved to be too contentious. By the end of the 19th century, and somewhat closer to reality, John Perry produced in 1895 an age-of-Earth estimate of 2 to 3 billion years (*England et al.*, 2007) using a model of a convective mantle and thin crust.

Great discoveries of the twenty centuries were about to come and change the entire understanding of the history of the Earth. Radioactivity was first discovered by Henri Becquerel in 1896 and further findings by Ernest Rutherford, Paul Villard, Marie Skłodowska and Pierre Curie, Frederick Soddy and others made it possible to come to the idea of the radioactive clock counting the absolute age of the universe, the Earth and even of individual processes.

Absolute dating was first suggested by Ernest Rutherford in 1904. He proposed that a radioactive element decaying with α particle emission creates helium atoms, which will be captured in the structure of the element. The amount of daughter elements is proportional to the age of the system. Bertram B. Boltwood and Ernest Rutherford investigated another decay path of radium to uranium and ultimately to lead. This work

made it possible to perform the first geochronological dating of rock samples with ages ranging from 410 million to 2.2 billion years (Ga) (Boltwood, 1907). Arthur Holmes picked up the baton of radiometric dating. In 1927, he published *The Age of the Earth, an Introduction to Geological Ideas* in which he presented a range of samples with ages between 1.6 and 3.0 Ga.

So far only the U-Pb system was used as a geochronological tool. But in 1913 the idea of isotopes was introduced and in 1921 Aston discovered the ^{39}K and ^{41}K isotopes. Nine years later, Holmes (1932) suggested that the decay of potassium into calcium could be used as a geochemical tracer for granite petrogenesis and as a geological clock to directly estimate the age of the Earth. He stipulated that ^{41}K was radioactive, which fortunately was not the case. Later in 1935 Nier presented evidence of the ^{40}K isotope existence. Von Weizsäcker (1937) discussed the decay modes of ^{40}K . He concluded that ^{40}K undergoes decay to ^{40}Ca and ^{40}Ar . The decay to ^{40}Ar was predicted on the basis of the amount of Ar in Earth's atmosphere, which is 1000 more than expected compared to other noble gases. He also pointed out that ^{40}Ar should be present in old K-bearing minerals. Aldrich and Nier (1948) confirmed Von Weizsäcker's latter prediction and demonstrated that old orthoclase, microcline, sylvite and langbeinite contain radiogenic ^{40}Ar . This laid the foundations for the K-Ar dating system. The K-Ca system, first suggested as a dating tool, was used seldomly starting from 1950, due to ^{40}Ca to be the most abundant Ca isotope, which swamp the presents of ^{40}Ca radiogenic.



1937 was also a vital year for another dating system, which became one of the most used geochronological and geochemical tools after the 1950s. It was the year ^{87}Rb was discovered to be radioactive: Hahn and Walling (1938) discussed the possibility of dating Rb-bearing minerals and five years later Hahn et al. (1943) performed the first age determination with this geochronometer.

The flourishing of geochronology started after the creation of the first mass-spectrometer by Alfred O. C. Nier (Fig.1). He used it to isolate ^{235}U and to demonstrate that this isotope undergoes fission. Alfred Nier also developed the sector mass spectrometer configuration now known as Nier-Johnson geometry, which proved to be instrumental for the exact dating of geological events. Thanks to his invention the isotopes started to be widely used for geochemical and geochronological purposes. Numerous isotopic systems have been discovered and widely used for a range of geological studies and age

estimations. This study focusses on the ^{40}K decay system which plays an important role in the reconstruction of Earth's history.

2. K dating systems.

^{40}K undergoes decays to ^{40}Ar and ^{40}Ca (Fig.2) and thus has a potential for two dating systems: ^{40}K - ^{40}Ar and ^{40}K - ^{40}Ca . The ^{40}K - ^{40}Ar method since being invented by Aldrich and Nier (1948) was improved and described by multiple researchers (e.g. Merrihue, 1965, Schaeffer and Zähringer, 1966; Dalrymple, 1991). The ^{40}K - ^{40}Ar method requires separate measurements of K and Ar concentrations on different mass-spectrometers. To avoid this inconvenience, a more sophisticated version of ^{40}Ar - ^{39}Ar dating was developed by Merrihue and Turner (1966) and the optimization of this method with J parameter was described by Turner (1971). Since its invention ^{40}Ar - ^{39}Ar dating became one of the most used methods in geochronology and is therefore also well described in the literature. This contrasts with the ^{40}K - ^{40}Ca dating method, which, due to its extreme complexity, is much less documented. Thus we describe the ^{40}K - ^{40}Ca system in more details.

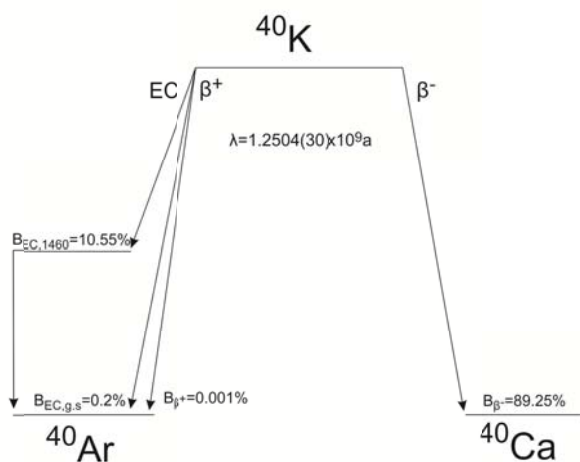


Fig.2. ^{40}K decay scheme (Bé et al., 2014)

The ^{40}K - ^{40}Ca system was first discussed by Holmes (1932) and Ahrens (1951). One of the main obstacles in the development of this method is the high abundance of common ^{40}Ca which swamps the radiogenic excess of ^{40}Ca . The attempts to use ^{40}K - ^{40}Ca dating were made for samples with high K/Ca ratio starting from 1950s, but the method remained exotic due to its complexity.

Attempts to use K-Ca for sedimentary rocks were so far limited and did not give precise ages although the scatter of isochron data may be interpreted as a range of crystallization ages (Plevaya et al., 1958; Wilhelm and Ackermann, 1972; Heumann et al., 1979; Baadsgaard 1987; Gopalan 2008; Robinson Cacil and Ducea, 2011, Nelson and McCulloch, 1989). Dating of magmatic minerals was more successful, K-Ca ages in many cases agreed with Rb-Sr or even sometimes with U-Pb ages (Coleman, 1971; Ovchinnikova et al., 1980; Marshall and DePaolo, 1982; Gopalan and Kumar, 2008; Harrison et al., 2010). Nögler and Villa (2000) obtained coincident ^{40}Ar - ^{39}Ar and ^{40}K - ^{40}Ca ages for a sanidine sample and calculated the branching ratio for the ^{40}K total decay constant from radiogenic Ca/Ar ratios. In those cases

where K-Ca ages were younger than Rb-Sr ages (Fletcher et al., 1997), the discrepancies were attributed to the sequential closure of these two systems. In some cases K-Ca dating did not give a reasonable ages at all (Nelson and McCulloch, 1989). With the improvement of mass-spectrometers from the 1990s on, ^{40}K - ^{40}Ca dating started to be used also for extraterrestrial studies (Shih et al., 1993, 1994; Bogard et al., 1994). The latest attempts to use the K-Ca isotopic system and to date extraterrestrial materials resulted in a precision of 2-8% (Simon et al., 2011; Yokoyama et al., 2013; Yokoyama et al., 2015).

3. ^{40}K decay constants

Therefore use of the ^{40}K - ^{40}Ca dating tool was limited to the attempts described above. On the contrary ^{40}Ar - ^{39}Ar system became widely used for determination of the ages for the majority of the Geologic Time Scale units (Gradstein et al., 2012; Smith et al., 1998). Its accuracy and reproducibility play an important role in the reconstruction of the Earth's history. When other systems like U-Pb or ^{87}Rb - ^{87}Sr started to be widely used, the age discrepancies between different dating approaches raised the questions whether they have geological meaning or can be explained solely by inaccurate constants.

The ages of isotopic systems relies on the constants used for the calculations. The general formula for age determination is:

$$R = R_0 + R_{P/D}(e^{\lambda t} - 1),$$

Eq.1.

where R is the isotopic ratio, R_0 is the initial ratio and $R_{P/D}$ is the parent/daughter ratio, λ is the decay constant and t is the time since a system was closed. Hence the decay constant is one of the crucial parameter of the age equation. It is mostly determined with physical methods. Physicists uses the half-life ($T_{1/2}$) as a measure of the decay speed, which has a relationship to λ as $T_{1/2} = \ln 2 / \lambda$.

3.1. Physical methods of ^{40}K decay constant determination

The lifetimes of various radioactive isotopes have a wide range from *ca.* 10^{-22} sec to 10^{21} years and thus require different methods for lifetime measurements. Radioactive isotopes used for absolute geological methods mostly have long lifetimes ($>10^8$ years) and are still present on Earth. The decay of such nuclei can be counted with the scintillation counting method. The isotope of interest is chemically separated in macroscopic quantities and mounted as a source in the scintillation spectrometer. After a radioactive isotope decays, the daughter isotope stays in the source but decay particles or gamma-rays are emitted. The ionization trails of such emission can be recorded as e-trajectories. Emitted particles and gamma-rays are caught in scintillators which generate light in proportion to the energy of particle. The amount of events within a certain time-frame is then counted and the half-life can be determined.

Introduction

The first attempts to determine the half-life of ^{40}K have been made in 1948 when Orban measured the partial electron capture decay constant to be $0.5 \times 10^9 \text{a}$, which is approximately 20 times lower than the actual value. In the subsequent years both electron capture and β^- decay were measured by numerous workers; over 40 published papers did however not achieve much consistency. The latest attempts to measure the ^{40}K decay constant were made with liquid scintillation counting.

The half-life of ^{40}K has been determined by Grau Malonda and Grau Carles (2002) of both β^- rays and electron capture contributions. The source was prepared as a KNO_3 solution mixed with Insta-gel. The average activity for 7 samples was $A = 12.24 \pm 0.014 \text{ Bq/g}$ calculated to ^{40}K isotopic concentration of 0.01167%, which gave a half-life of $T_{1/2} = 1.248 \pm 0.004 \text{ Ga}$. Later Kossert and Gunter (2004) have used the same method with aqueous solutions of both KNO_3 and KCl on four samples measured on three scintillators. The resulting activity was $A = 12.2318 \pm 0.0063 \text{ Bq/g}$ calculated to ^{40}K isotopic concentration of 0.01167% for KNO_3 samples. The resulting half-life was $T_{1/2} = 1.248 \pm 0.003 (\pm 0.23\%) \text{ Ga}$. The branching ratio used for calculations was from Bé et al., (1999): β^- decay branch $B_{\beta^-} = 89.14 \pm 0.13\%$, electron capture with measured gamma-emission of 1460 keV $B_{\text{EC},1460} = 10.66 \pm 0.13\%$, electron capture to the ground state $B_{\text{ECgs}} = 0.2 \pm 0.1\%$.

Almost all physics literature describing measurements of ^{40}K half-lives, with the exception of the publication of Grau Malonda and Grau Carles (2002), has been summarized on the web-site <http://www.nucleide.org/NucData.htm> with last updates up to February 2014 (Bé et al, 2004, Bé et al, 2014). Based on these data, the total half-life of $T_{1/2} = 1.2504 \pm 0.0030 \text{ Ga}$ is recommended. The branching ratios were calculated from the values published in the 1940-60s $T_{1/2\beta^-}$ and $T_{1/2\text{EC},1460}$. Another part of branching ratio belonging to β^+ transition was chosen from three available very imprecise measurements (Engelkemeir et al., 1962; Leutz et al., 1965; Tilley and Madansky, 1959), though its contribution is negligible. The branch of electron capture to Ar ground state cannot be measured and was calculated theoretically. The suggested branching ratios were $B_{\beta^-} = 89.25 \pm 0.19\%$, $B_{\text{EC},1460} = 10.55 \pm 0.11\%$, $B_{\text{ECgs}} = 0.20 \pm 0.10\%$, $B_{\beta^+} = 0.00100 \pm 0.00012\%$, which sums up $B_{\text{Ca}} = 89.25 \pm 0.17 (\pm 0.19\%)$, $B_{\text{Ar}} = 10.75 \pm 0.15 (\pm 1.40\%)$, all uncertainties 1σ . One has to specify that the publication of Bé et al (2014) and its later updates are evaluated with a statistical approach assuming Gaussian distribution of the data (Fig.2). They did not evaluate uncertainties of published decay constants for systematic errors and thus the dataset uncertainties were treated as repeatability of results (Type A evaluation (JCGM, 2012)).

The constants of Bé et al (2014) are the most recent, which are proposed by the physics community. Although the proposed uncertainty of total half-life is only 0.24%, the uncertainty on the branching ratio is quite significant. Depending on the adopted branching

ratio the total half-life calculated out of partial half-lives can vary. Especially crucial for the Ar-Ar dating is the uncertainty of the B_{Ar} branch which is now 1.4%.

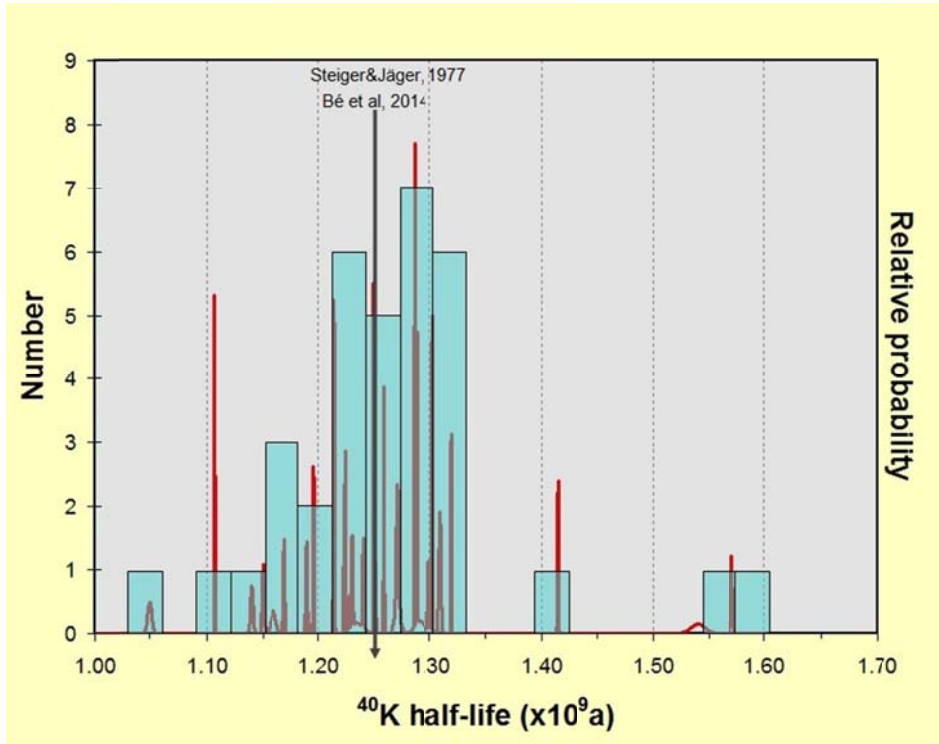


Fig.2. The distribution of ^{40}K half-lives measured with physical methods. With an arrow marking the values recommended in the geochronological and physics communities.

3.2. Geological methods

Due to imprecise physical measurements of the K decay constants, and because until 2009 the uncertainty on the total $T_{1/2}$ was higher than 1%, the geochronological community strived to evaluate ^{40}K decay constants with intercomparison of the Ar-Ar, K-Ar and U-Pb ages. A first attempt was made in 1956 by Wetherill et al. (1956), they compared Ar-Ar ages of 12 samples with ages spreading from 4500 to 265 Ma. Despite the fact that some samples had an Ar-Ar age 7% lower than the U-Pb age, their decay constant was incorporated into the compilation of ^{40}K decay constants and was used for some time by the western geochronological community. Russian geochronologists used the same λ_{β} but much lower λ_{40Ar} (Dalrymple, 1979). Later Steiger and Jäger (1977) published ^{40}K decay constants based on the activity measurement evaluation of Beckinsale and Gale (1969) recalculated to precise $^{40}\text{K}/\text{K}$ value of (Garner et al., 1975). Till this day the constants of Steiger and Jäger (1977) for the K-Ca-Ar system remain the recommended ones (Begemann et al., 2001) with values $\lambda_{\beta}=4.962 \cdot 10^{-10} \text{a}^{-1}$ and $\lambda_{40Ar}=0.581 \cdot 10^{-10} \text{a}^{-1}$, $\lambda_{\text{tot}}=5.543 \cdot 10^{-10} \text{a}^{-1}$ and they agree with the values of Bé et al (2014). Based on the comparison of U-Pb and ^{40}Ar - ^{39}Ar ages Min et al. (2000) argued that the ^{40}K total decay constant is too high. They mentioned $5.37 \cdot 10^{-10} \text{a}^{-1}$ to better fit to the observed ages. One

age comparison was however not enough to recommend the adoption of a new decay constant and therefore Min et al. (2000) recommended the use of the values by Endt and van der Leun (1973) of $\lambda_{\beta^-} = 4.884 \pm 0.099 \times 10^{-10} \text{ a}^{-1}$ and $\lambda_{40\text{Ar}} = 0.580 \pm 0.014 \times 10^{-10} \text{ a}^{-1}$, $\lambda_{\text{tot}} = 5.464 \times 10^{-10} \text{ a}^{-1}$. Similar work of Kwon et al. (2002) on five reference samples with ages spanning from 1.9 ka to 4.5 Ga resulted in an estimated total decay constant of $\lambda_{\text{tot}} = 5.4755 \pm 0.0170 \times 10^{-10} \text{ a}^{-1}$ (1σ). Krumrei et al. (2006) obtained a spread of Ar-Ar ages for the Ilimaussaq complex, which were 1-2% younger than the U-Pb ages; based on this offset they confirmed that the decay constant of Kwon et al. (2002) give coinciding Ar-Ar and U-Pb ages. Renne et al. (2010) performed the comparison of U-Pb and Ar-Ar ages for 17 samples to determine simultaneously an age for the Fish Canyon sanidine standard used as a flux monitor for Ar-Ar dating and a decay constants for the ^{40}K system and obtained $\lambda_{40\text{Ar}} = 0.5755 \pm 0.0016 \times 10^{-10} \text{ a}^{-1}$ and $\lambda_{\beta^-} = 4.9737 \pm 0.0093 \times 10^{-10} \text{ a}^{-1}$, $\lambda_{\text{tot}} = 5.5492 \times 10^{-10} \text{ a}^{-1}$; later elimination of liquid scintillation data from the calculation resulted in $\lambda_{40\text{Ar}} = 0.5757 \pm 0.0016 \times 10^{-10} \text{ a}^{-1}$ and $\lambda_{\beta^-} = 4.9548 \pm 0.0134 \times 10^{-10} \text{ a}^{-1}$, $\lambda_{\text{tot}} = 5.5305 \times 10^{-10} \text{ a}^{-1}$ (Renne et al., 2011).

An important part of the ^{40}Ar - ^{39}Ar age calculation is the branching ratio of ^{40}K decay $B_{\text{Ca}}/B_{\text{Ar}}$. The uncertainty of the decay constant is claimed to be known to 0.2-0.5%, but the uncertainty on the branching ratio is still approximately 1.5%. The only independent approach to estimate the branching ratio from molar amount of radiogenic Ar and Ca was performed by Nagler and Villa (2000) on one sample and resulted in $B_{40\text{Ar}} = 0.1067$ and $B_{\beta^-} = 0.8933$ (with 1% uncertainty).

This short overview reveals the disagreement in a fundamental key constituent part of the age equation. The available compilation of the ^{40}K decay constant and the branching ratio (Be et al., 2004) is coincident with those of Steiger and Jager (1977) currently used in the geochronological community. However these values are proven to be not optimal for ^{40}Ar - ^{39}Ar dating and need to be assessed with diverse approaches. Moreover, decay constants are not the only constants used for age determination.

4. ^{40}K abundance.

Nowadays the precision and accuracy of the ^{40}Ar - ^{39}Ar dating system are the objects of improvement. The international scientific initiative *EarthTime* (www.earthtime.org), whose main goal is the sequencing of Earth's history through the integration of high-precision geochronology and quantitative chronostratigraphy, is aiming for a precision of 0.1% uncertainty in the absolute age determination. Modern mass-spectrometric techniques can reach a permille level of precision, but the precision and accuracy of the ages cannot be fully achieved without high accuracy of various constants included into the age equation. Though the decay constant is one of the most important constants in such calculations, it is not the only one which can affect the accuracy of the age determination.

Another two constants of the ^{40}Ar - ^{39}Ar system are the ^{40}K isotopic abundance and the age of the flux monitor. Usually, natural samples of a known age are used as flux monitors during the irradiation of samples for Ar-Ar dating. Natural samples are used as standards because no metrological traceable standard is available. The age of such samples has been an object of thorough recalibration for the last decade; for example the Fish Canyon sanidine standard, also used in this study as a flux monitor, has been intercalibrated with orbital tuning ages and reached a precision of 0.1% (e.g. Kuiper et al, 2008; Rivera et al, 2011). Recalibrating the standards used as flux monitors is not part of this study.

^{40}K isotopic abundance also is included into ^{40}Ar - ^{39}Ar age determination. It was measured by Burnett et al. (1966) and Garner et al. (1975) and the latter one was adopted by the International Union of Pure and Applied Chemistry and to this day is the basis of the IUPAC recommendation for the terrestrial K isotope composition (de Laeter et al., 2003). This value has an uncertainty of 0.35% which is significant in comparison to the precision of the modern mass-spectrometers and published Ar-Ar ages.

5. Outline of this thesis

The main object of this study is to improve the widely used Ar-Ar dating system by assessing the constants included in the equation. We focused on two constants: the ^{40}K isotopic abundance and the ^{40}K decay constants with its branching ratio.

K isotopic composition of the terrestrial samples was obtained for two standards whose composition is close to the mean Earth. The results of this study are present in **Chapter 1**. Potassium was measured on a thermal ionization mass spectrometer with three techniques: total evaporation, block total evaporation and conventional block measurements. Due to the light mass of this element, it suffered extensive fractionation during measurements and the total evaporation procedure did not give consistent results. Thus the $^{40}\text{K}/^{39}\text{K}$ ratio had to be fractionation corrected to the fixed $^{41}\text{K}/^{39}\text{K}$ ratio of Garner et al. (1975) obtained with a high precision gravimetric method. The $^{41}\text{K}/^{39}\text{K}$ value of Garner et al (1975) is sufficiently precise and consistent with the mean Earth. Our $^{40}\text{K}/^{39}\text{K}$ is the most precise estimation obtained so far and reduces the uncertainty of $^{40}\text{K}/^{44}\text{K}$ from 0.35% to 0.07%.

The ^{40}K decay constants are more difficult to reevaluate. Our approach is to assess it with the geological age intercalibration method. We dated samples of a well-known age and geologically “point-like” history with ^{40}Ar - ^{39}Ar , ^{40}K - ^{40}Ca and ^{87}Rb - ^{87}Sr geochronometers. The discrepancy between the reference age and the obtained ^{40}Ar - ^{39}Ar and ^{40}K - ^{40}Ca ages is due to a ^{40}K decay constant offset. This method relies on high precision K-Ca dating which is impossible without accurate and precise measurements of Ca isotopic composition. Measurements were performed on a unique TIMS Triton *Plus* specially designed for Ca measurements. These measurements allowed to obtain the isotopic composition of two Ca standards, evaluate the internal consistency of different published Ca isotopic compositions and to test the fractionation correction methods. This work is shown in **Chapter 2**. **Chapter 3** brings up the issues of geological decay constants intercalibration. ^{87}Rb - ^{87}Sr , ^{40}Ar - ^{39}Ar and ^{40}K - ^{40}Ca dating were performed on four samples. These ages are compared with each other and with a reference U-Pb age and the best estimate for the ^{40}K decay constant is presented.

References:

- Ahrens, L.H., 1951. The feasibility of a calcium method for the determination of geological age. *Geochimica et Cosmochimica Acta* 1, 312-316.
- Aldrich, L.T., Nier, A.O., 1948. Argon 40 in Potassium Minerals. *Physical Review* 74, 876-877.
- Baadsgaard, H., 1987. Rb-Sr and K-Ca isotope systematics in minerals from potassium horizons in the prairie evaporite formation, Saskatchewan, Canada. *Chemical Geology (Isotope Geoscience Section)* 66, 1-15.
- Bé, M.-M., Christè, V., Dulieu, C., Browne, E., Chechev, V., Kuzmenko, N., Helmer, R., Nichols, A., Schönfeld, E., Dersch, R., 2004. Table of Radionuclides, A=1 to 150 ed. Bureau International Des Poids et Mesures, Pavillon de Breteuil, F-92310 Sèvres, p. 285.
- Bé, M.-M., Duchemin, B., Browne, E., Wu, S.-C., Chechev, V., Helmer, R., Schönfeld, E., 1999. Report CE A, ISBN 2-7272-0211-3.
- Bé, M.-M., Dulieu, C., Mougeot, X., Kellett, M., 2014. HALF-LIVES. Table of recommended values, 2014 ed. Bureau International Des Poids et Mesures, Pavillon de Breteuil, F-92310 Sèvres, p. 13.
- Beckinsale, R.D., Gale, N.H., 1969. A reappraisal of the decay constants and branching ratio of ^{40}K . *Earth and Planetary Science Letters* 6, 289-294.
- Begemann, F., Ludwig, K.R., Lugmair, G.W., Min, K., Nyquist, L.E., Patchett, P.J., Renne, P.R., Shih, C.Y., Villa, I.M., Walker, R.J., 2001. Call for an improved set of decay constants for geochronological use. *Geochimica et Cosmochimica Acta* 65, 111-121.
- Bogard, D.D., Garrison, D.H., Shih, C.Y., Nyquist, L.E., 1994. ^{39}Ar - ^{40}Ar dating of two lunar granites: The age of Copernicus. *Geochimica et Cosmochimica Acta* 58, 3093-3100.
- Boltwood, B.B., 1907. Ultimate disintegration products of the radioactive elements; Part II, Disintegration products of uranium. *American Journal of Science Series 4 Vol. 23*, 78-88.
- Coleman, M.L., 1971. Potassium-calcium dates from pegmatitic micas. *Earth and Planetary Science Letters* 12, 399-405.
- Dalrymple, G.B., 1979. Critical tables for conversion of K-Ar ages from old to new constants. *Geology* 7, 558-560.
- Dalrymple, G.B., 1991. *The Age of the Earth*, 474 pp. Stanford University Press, Stanford.
- de Laeter, J.R., Böhlke, J.K., De Bièvre, P., Hidaka, H., Peiser, H.S., Rosman, K.J.R., Taylor, P.D.P., 2003. Atomic weights of the elements. Review 2000 (IUPAC Technical Report), *Pure and Applied Chemistry*, p. 683.
- Endt, P.M., van der Leun, C., 1973. Energy levels of A=21-44 nuclei (V). *Nuclear Physics* 214, 1-625.
- Engelkemeir, D.W., Flynn, K.F., Glendenin, L.E., 1962. Positron Emission in the Decay of K^{40} . *Physical Review* 126, 1818-1822.
- England, P.C., Molnar, P., Richter, F.M., 2007. Kelvin, Perry and the Age of the Earth. *American scientist* 95, 342.
- Fletcher, I.R., McNaughton, N.J., Pidgeon, R.T., Rosman, K.J.R., 1997. Sequential closure of K-Ca and Rb-Sr isotopic systems in Archaean micas. *Chemical Geology* 138, 289-301.
- Garner, E., Murphy, T., Gramlich, J., Paulsen, P., Barnes, I., 1975. Absolute Isotopic Abundance Ratios and the Atomic Weight of a Reference Sample of K. *J. Res. Natl. Bur. Stand., A* 79, 713-725.
- Gopalan, K., 2008. Conjunctive K-Ca and Rb-Sr dating of glauconites. *Chemical Geology* 247, 119-123.
- Gopalan, K., Kumar, A., 2008. Phlogopite K-Ca dating of Narayanpet kimberlites, south India: Implications to the discordance between their Rb-Sr and Ar/Ar ages. *Precambrian Research* 167, 377-382.
- Gradstein, F.M., Ogg, J.G., Schmitz, M., Ogg, G., 2012. The Geologic Time Scale. *Newsletters on stratigraphy* 45, 171-188.
- Grau Malonda, A., Grau Carles, A., 2002. Half-life determination of ^{40}K by LSC. *Applied Radiation and Isotopes* 56, 153-156.
- Hahn, O., Straßmann, F., Matthauch, J., Ewald, H., 1943. Geologische Altersbestimmungen nach der Strontiummethode. *Chem.-Ztg* 67, 55-56.
- Hahn, O., Walling, E., 1938. Über die Möglichkeit geologischer Altersbestimmungen rubidiumhaltiger Mineralien und Gesteine. *Zeitschrift für anorganische und allgemeine Chemie* 236, 78-82.
- Harrison, T.M., Heizler, M.T., McKeegan, K.D., Schmitt, A.K., 2010. In situ ^{40}K - ^{40}Ca 'double-plus' SIMS dating resolves Klokken feldspar ^{40}K - ^{40}Ar paradox. *Earth and Planetary Science Letters* 299, 426-433.
- Heumann, K., Kubassek, E., Schwabenbauer, W., Stadler, I., 1979. Analytisches Verfahren zur K/Ca-Altersbestimmung geologischer Proben. *Z. Anal. Chem.* 297, 35-43.

- Holmes, A., 1932. The Origin of Igneous Rocks. *Geological Magazine* 69, 543-558.
- Hunziker, J.C., 1979. Potassium Argon Dating, in: Jäger, E., Hunziker, J. (Eds.), *Lectures in Isotope Geology*. Springer Berlin Heidelberg, pp. 52-76.
- JCGM, 2012. Joint Committee for Guides in Metrology - The International Vocabulary of Metrology - Basic and General Concepts and Associated Terms, 3rd ed., JCGM 200:2012. JCGM.
- Kossert, K., Gunther, E., 2004. LSC measurements of the half-life of ^{40}K . *Applied radiation and isotopes* : including data, instrumentation and methods for use in agriculture, industry and medicine 60, 459-464.
- Krumrei, T.V., Villa, I.M., Marks, M.A.W., Markl, G., 2006. A $^{40}\text{Ar}/^{39}\text{Ar}$ and U/Pb isotopic study of the Ilimaussaq complex, South Greenland: Implications for the ^{40}K decay constant and for the duration of magmatic activity in a peralkaline complex. *Chemical Geology* 227, 258-273.
- Kuiper, K.F., Deino, A., Hilgen, F.J., Krijgsman, W., Renne, P.R., Wijbrans, J.R., 2008. Synchronizing Rock Clocks of Earth History. *Science* 320, 500-504.
- Kwon, J., Min, K., Bickel, P.J., Renne, P.R., 2002. Statistical Methods for Jointly Estimating the Decay Constant of ^{40}K and the Age of a Dating Standard. *Mathematical Geology* 34, 457-474.
- Leutz, H., Schulz, G., Wenninger, H., 1965. The decay of potassium-40. *Z. Physik* 187, 151-164.
- Marshall, B.D., DePaolo, D.J., 1982. Precise age determination and petrogenetic studies using the K-Ca method. *Geochimica et Cosmochimica Acta* 46, 2537-2545.
- Merrihue, C., 1965. Trace-element determinations and potassium-argon dating by mass spectroscopy of neutron-irradiated samples. *Trans. Amer. Geophys. Union* 46, 125.
- Merrihue, C., Turner, G., 1966. Potassium-argon dating by activation with fast neutrons. *Journal of Geophysical Research* 71, 2852-2857.
- Min, K., Mundil, R., Renne, P.R., Ludwig, K.R., 2000. A test for systematic errors in Ar-Ar geochronology through comparison with U-Pb analysis of a 1.1-Ga rhyolite. *Geochimica et Cosmochimica Acta* 64, 73-98.
- Nägler, T.F., Villa, I.M., 2000. In pursuit of the 40K branching ratios: K-Ca and ^{39}Ar - ^{40}Ar dating of gem silicates. *Chemical Geology (Isotope Geoscience Section)* 169, 5-16.
- Nelson, D.R., McCulloch, M.T., 1989. Petrogenetic application of the ^{40}K - ^{40}Ca radiogenic decay scheme - A reconnaissance study. *Chemical Geology (Isotope Geoscience Section)* 79, 275-293.
- Renne, P.R., Balco, G., Ludwig, K.R., Mundil, R., Min, K., 2011. Response to the comment by W.H. Schwarz et al. on "Joint determination of ^{40}K decay constants and $^{40}\text{Ar}^*/^{40}\text{K}$ for the Fish Canyon sanidine standard, and improved accuracy for $^{40}\text{Ar}/^{39}\text{Ar}$ geochronology" by P.R. Renne et al. (2010). *Geochimica et Cosmochimica Acta* 75, 5097-5100.
- Renne, P.R., Mundil, R., Balco, G., Min, K., Ludwig, K.R., 2010. Joint determination of ^{40}K decay constants and $^{40}\text{Ar}^*/^{40}\text{K}$ for the Fish Canyon sanidine standard, and improved accuracy for $^{40}\text{Ar}/^{39}\text{Ar}$ geochronology. *Geochimica et Cosmochimica Acta* 74, 5349-5367.
- Rivera, T.A., Storey, M., Zeeden, C., Hilgen, F.J., Kuiper, K., 2011. A refined astronomically calibrated $^{40}\text{Ar}/^{39}\text{Ar}$ age for Fish Canyon sanidine. *Earth and Planetary Science Letters* 311, 420-426.
- Robinson Cecil, M., Ducea, M., 2011. K-Ca ages of authigenic sediments: examples from Paleozoic glauconite and applications to low-temperature thermochronometry. *Int J Earth Sci (Geol Rundsch)* 100, 1783-1790.
- Schaeffer, O.A., Zähringer, J., 1966. Potassium argon dating. Springer Science & Business Media.
- Shih, C.Y., Nyquist, L.E., Bogard, D.D., Wiesmann, H., 1994. K-Ca and Rb-Sr dating of two lunar granites: Relative chronometer resetting. *Geochimica et Cosmochimica Acta* 58, 3101-3116.
- Shih, C.Y., Nyquist, L.E., Wiesmann, H., 1993. K-Ca chronology of lunar granites. *Geochimica et Cosmochimica Acta* 57, 4827-4841.
- Simon, J.I., Shih, C.Y., Nyquist, L.E., 2011. K-Ca and Rb-Sr dating of lunar granite 14321 revisited, 42 Lunar and Planetary Science Conference, The Woodlands, Texas. , p. 2754.
- Smith, P.E., Evensen, N.M., York, D., Odin, G.S., 1998. Single-Grain ^{40}Ar - ^{39}Ar Ages of Glauconies: Implications for the Geologic Time Scale and Global Sea Level Variations. *Science* 279, 1517-1519.
- Steiger, R.H., Jäger, E., 1977. Subcommittee on geochronology: convention on the use of decay constants in geo- and cosmochronology. *Earth and Planetary Science Letters* 36, 359-362.
- Tilley, D.R., Madansky, L., 1959. Search for Positron Emission in K40. *Physical Review* 116, 413-415.
- Turner, G., 1971. Argon 40-argon 39 dating: the optimization of irradiation parameters. *Earth and Planetary Science Letters* 10, 227-234.
- Von Weizsäcker, C.F., 1937. Über die Möglichkeit eines dualen β -Zerfalls von Kalium. *Physikalische Zeitschrift* 38, 623-624.

Wetherill, G.W., Wasserburg, G.J., Aldrich, L.T., Tilton, G.R., Hayden, R.J., 1956. Decay Constants of K^{40} as Determined by the Radiogenic Argon Content of Potassium Minerals. *Physical Review* 103, 987-989.

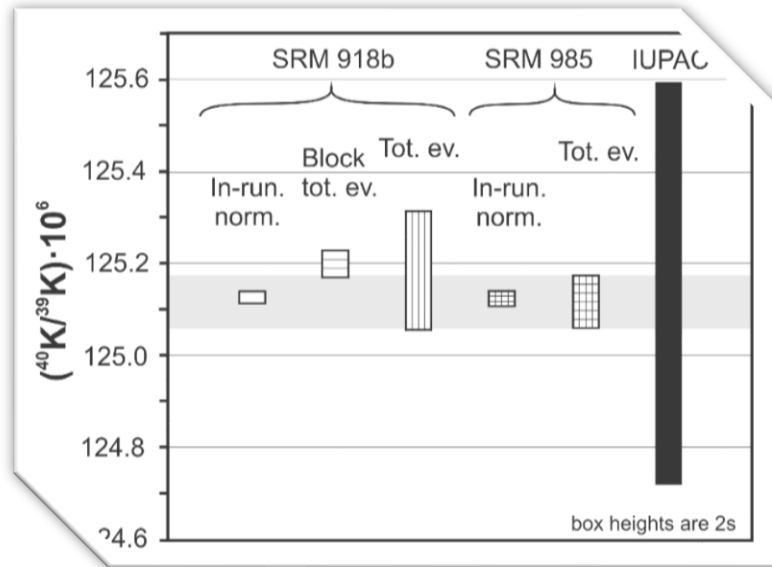
Wilhelm, H.G., Ackermann, W., 1972. Altersbestimmung nach der K-Ca-Methode an Sylvinit des Oberen Zechsteines des Werragebietes. *Zeitschrift für Naturforschung A* 27, 1256-1259.

Yokoyama, T., Misawa, K., Okano, O., Shih, C.Y., Nyquist, L.E., Simon, J.I., Tappa, M.J., Yoneda, S., 2013. K-Ca dating of alkali-rich fragments in the Y-74442 and bhola LL-chondritic. 44th Lunar and Planetary Science Conference (2013), 1972.

Yokoyama, T., Misawa, K., Okano, O., Shih, C.Y., Nyquist, L.E., Simon, J.I., Tappa, M.J., Yoneda, S., 2015. Early solar system alkali fractionation events recorded by K-Ca isotopes in the Yamato-74442 LL-chondritic breccia, 46th Lunar and Planetary Science Conference, p. 1695.

Овчинникова, Г.В., Левчинков, О.А., Варшавская, Е.С., Кутявин, Е.П., Яковлева, С.З., 1980. Сравнительное изучение K-Ca, Rb-Sr и K-Ar систем в лепидолитах. *Геохимия* 8, 1166-1173.

Полевая, Н.И., Титов, Н.Е., Беляев, В.С., Спрингсон, В.Д., 1958. Опыт применения кальциевого метода для определения абсолютного возраста сильвинитов. *Геохимия* 8, 718-726.



Chapter 1

High precision determination of the terrestrial ^{40}K abundance

High precision determination of the terrestrial ^{40}K abundance

Maria O. Naumenko¹, Klaus Mezger¹, Thomas F. Nägler¹, Igor M. Villa^{1,2}

1-Institut für Geologie, Universität Bern, Baltzerstrasse 1+3, 3012 Bern, Switzerland

2-Università di Milano Bicocca, Piazza della Scienza 4, 20126 Milano, Italy

Corresponding author: Maria Naumenko, naumenko@geo.unibe.ch

Published in Geochimica et Cosmochimica Acta 122 (2013) 353-362

Abstract

Recent improvements in the precision of mass spectrometric measurements have reduced the uncertainty of K-Ar and ^{39}Ar - ^{40}Ar ages measured on geological materials. Now the major sources of uncertainty are the uncertainties on the ^{40}K decay constant and the absolute abundance of ^{40}K . In order to improve on this situation we determined the abundance of the ^{40}K isotope in terrestrial standards.

A ThermoFischer Triton+ thermal ionization mass spectrometer was used for K isotope ratio measurements of the NIST K standard reference materials SRM 918b and SRM 985. Ion beams were measured in Faraday cups with amplifiers equipped with 10^{10} , 10^{11} and $10^{12} \Omega$ resistors. Three measurement protocols were used: (A) dynamic measurement with in-run fractionation correction by normalization to the IUPAC recommended isotope ratio $^{41}\text{K}/^{39}\text{K} = 0.0721677$; (B) total evaporation; (C) a modified total evaporation with interblock baseline measurements. Different measurement protocols were combined with different loading procedures. The best results were obtained by loading samples on single oxidized tantalum filaments with 0.1M H_3PO_4 . The total ion yields (ionization + transmission) were tested for the evaporation procedures (B) and (C) and ranged up to 48 %.

The resulting best estimate for the $^{40}\text{K}/^{39}\text{K}$ ratio is $0.000\,125\,116 \pm 57$ (2σ), corresponding to an isotopic abundance $^{40}\text{K}/\text{K} = (1.1668 \pm 8; 2\sigma) \times 10^{-4}$.

1. Introduction

Potassium is the eighth most abundant chemical element in the Earth's crust and a major element in several rock-forming minerals. The isotope ^{40}K is radioactive and undergoes β^- decay to ^{40}Ca and electron capture (and possibly β^+ decay) to ^{40}Ar . The decay of ^{40}K to ^{40}Ar is one of the most widely applied geochronological tools (e.g., Begemann et al., 2001), because it has the potential to yield highly precise and accurate ages. In the case of ^{40}K the physical quantities that control the achievable age uncertainty are the decay constants for electron capture, λ_{EC} , and for β^- decay, λ_{β} , and the ^{40}K abundance. Ideally uncertainties of these constants should be lower or at least of similar magnitude as uncertainties obtained during mass spectrometric measurements. Due to recent large improvements in performance of mass-spectrometers the uncertainty of the $^{40}\text{K}/\text{K}$ isotope abundance has become larger than the sample measurement uncertainty. We report here an improved precision for the $^{40}\text{K}/\text{K}$ ratio.

The decay constants adopted by the IUGS Subcommittee on Geochronology ($\lambda_{\beta} = 4.962 \times 10^{-10} \text{ a}^{-1}$, $\lambda_{\text{EC}} = 0.581 \times 10^{-10} \text{ a}^{-1}$; Steiger and Jäger, 1977) result in an accuracy and precision no better than 2% for K-Ar ages (Min et al, 2000). Another important source of uncertainty in age equations [1] and [2] is the isotopic abundance $^{40}\text{K}/\text{K}$.

$$^{40}\text{Ar} = ^{40}\text{Ar}_I + ^{40}\text{K} \frac{\lambda_{\text{EC}}}{\lambda_{\beta} + \lambda_{\text{EC}}} \times (e^{(\lambda_{\beta} + \lambda_{\text{EC}}) \times t} - 1) \quad [\text{Eq.1}]$$

$$^{40}\text{Ca} = ^{40}\text{Ca}_I + ^{40}\text{K} \frac{\lambda_{\beta}}{\lambda_{\beta} + \lambda_{\text{EC}}} \times (e^{(\lambda_{\beta} + \lambda_{\text{EC}}) \times t} - 1) \quad [\text{Eq.2}]$$

where I corresponds to the initial content of isotopes, λ_{β} and λ_{EC} are decay constants due β^- decay and electron capture, respectively, t is the time elapsed since initiation of the system.

The $^{40}\text{K}/\text{K}$ isotope abundance was measured on terrestrial materials by Burnett et al. (1966) and Garner et al. (1975). Burnett et al. (1966) determined the instrumental mass fractionation by comparing the measured $^{39}\text{K}/^{41}\text{K}$ ratio of selected geological samples to the $^{39}\text{K}/^{41}\text{K}$ ratio of 0.074239 determined by Nier (1950). The appropriate fractionation correction was then applied to the measured $^{40}\text{K}/^{41}\text{K}$ ratio. Garner et al. (1975) reported analyses of the newly produced NIST Standard Reference Material SRM 985 by comparing it to six different gravimetrically calibrated synthetic reference solutions, prepared from chemically purified K highly enriched in ^{39}K and ^{41}K . A special purification procedure (crystallization of potassium perchlorate) was performed to reduce impurities to low ppm levels. If the instrumental fractionation of the raw data of Burnett et al. (1966) is corrected with the $^{39}\text{K}/^{41}\text{K}$ ratio of Garner et al. (1975), the $^{40}\text{K}/^{41}\text{K}$ ratio becomes 0.0001287 ± 6 , a value fairly close to that reported by Garner et al. (1975).

The isotope abundances measured by Garner et al (1975), viz. $^{39}\text{K}/\text{K} = 0.9325811(\pm 292)$, $^{40}\text{K}/\text{K} = 0.00011672(\pm 41)$, $^{41}\text{K}/\text{K} = 0.0673022(\pm 292)$, were adopted by the International Union of Pure and Applied Chemistry and to this day are the basis of the

IUPAC recommendation for the terrestrial K isotope composition (De Laeter et al., 2003). For geochronologic applications, these values result in a $^{40}\text{K}/\text{K}$ isotope abundance that has an uncertainty of 0.35% and is thus a significant contributor to the total K-Ar age uncertainty.

In the last two decades there has been an intense collective endeavor to reduce measurement uncertainties of the K-Ar dating system. A major effort has been made to reduce the analytical and systematic uncertainties on the ^{40}K decay constants (Min et al., 2000; Nagler & Villa, 2000; Kwon et al., 2002; Grau & Grau, 2002; Kossert & Gunter, 2004; Krumrei et al., 2006; Renne et al., 2010; Schwarz et al., 2011). The most recently published uncertainty on the λ_{EC} and λ_{β} decay constants is $\pm 0.27\%$ (Renne et al., 2010). This implies that the least precisely known term in the K-Ar age equation is the isotopic abundance of ^{40}K with its uncertainty of 0.35%.

A reduction of the uncertainties in geochronology to the level of 0.1% is also one of the goals of the international scientific initiative *EarthTime* (www.earthtime.org), whose main goal is sequencing Earth history through the integration of high-precision geochronology and quantitative chronostratigraphy. It is especially remarkable that biostratigraphy is credited with achieving a relative age resolution of 0.2 Ma for Paleozoic strata, i.e. an uncertainty of 0.05 % (Gradstein et al., 2004). The present uncertainty on the $^{40}\text{K}/\text{K}$ isotope abundance is almost an order of magnitude larger, effectively limiting the accuracy of the K-Ar isotopic geochronometer and thus impairing its usefulness. Reducing the uncertainty for the K-Ar dating system helps to obtain a higher accuracy for absolute ages for rocks and minerals that allows to better constrain the absolute timing of geologic events and the rates of processes. It also allows for a more reliable correlation of ages obtained with different chronometers. Highly accurate ages allow to correlate geological processes on a regional to a global scale in order to provide a highly-resolved, calibrated time scale.

2. Methodology

2.1 Standards

For most of the high precision K measurements reported here, a solution of the NIST SRM 918b K standard reference material was used. This material consists of KCl purified to 999.27 ± 0.14 mg/g and according to the certificate contains only the following detectable trace impurities: Br 45 $\mu\text{g/g}$, Na 35 $\mu\text{g/g}$, Rb 2.6 $\mu\text{g/g}$, and Si 1.8 $\mu\text{g/g}$. The SRM 918b powder was dissolved in milli-QTM water to create K solutions having concentrations of 13 ng/ μl , 26 ng/ μl , 52 ng/ μl and 100 ng/ μl , suitable for filament loading. For the first precise determination of K isotope abundances Garner et al. (1975) used NIST SRM 985 which is now out of stock. A small amount of SRM 985 available to us was used for a few in-run fractionation corrected measurements using $^{41}\text{K}/^{39}\text{K} = 0.0721677$ for normalization (Garner et al., 1975) and total evaporation runs.

A Ca-doped K element concentration standard solution (with a nominal Ca/K element ratio of 0.002) was used to determine the sensitivity of the K isotope ratio measurement on the TIMS to Ca interference. These measurements helped to identify the optimum filament currents for K ionization of different setups (single and double filament), filament materials (tantalum or rhenium), and loading additives. At the same time discrimination of Ca relative to K under these various conditions was empirically determined.

All total evaporation and block total evaporation measurements were performed with 26 ng/ μ L loads; a solution with 52 ng/ μ L was used for in-run fractionation corrected measurements.

2.2 Filaments

Rhenium and tantalum single filaments were degassed prior to loading (zone-refined Re for 40 min at 1.5 A and 90 min at 4 A; zone-refined Ta 30 min at 2 A and 70 min at 4 A) and then oxidized in air for one week and one month, respectively. A suitable amount (1-2 μ L) of the K standard solution was loaded on the filament and almost dried down with a current of 0.5 A for Re and 1 A for Ta; then it was covered with 1 μ L of an activator (a Ta₂O₅ loading solution (Birck, 1986) for the rhenium filaments or 0.1M H₃PO₄ (cleaned with exchange resin added to the beaker) for the tantalum filaments) and then evaporated to complete dryness by slowly heating up the filament until the activator fumed around 2 A for Re and 3 A for Ta. The K blank for the Ta₂O₅ loading solution was 30 pg, and for the 0.1 M H₃PO₄ loading solution 5 pg which is less than 0.02% of the total K load.

For K isotope analyses different filament arrangements were tested. Double filaments (Re and Ta) would be expected to cause a much lower mass fractionation due to the predominance of ionization over evaporation. However, we found two drawbacks to double filaments during this study. The first and foremost is that during the initial tests with a Ca-doped K element concentration standard solution the Ca interferences were higher and occurred earlier in the run. Three tests out of 5 with pure SRM918b gave a significantly elevated ⁴⁰K/³⁹K ratio (0.000 129 - 0.000 130). This may be due to an additional Ca contribution coming from the hot ionization filament and/or filament holder, or may be due to the different ionization properties of K and Ca when loaded as chloride without the emission enhancers, compared to the loading protocol used with single filaments. The second is that the practical realization of the total evaporation runs was much less straightforward than with single filaments, as it requires increasing the current simultaneously for both, the ionization and the evaporation filament with different heating rates. However, this is not possible due to the limitations provided by the software and lack of manual control of the mass spectrometer. Because of the better uncertainties on the resulting isotope ratio measurements, further analyses were performed using single filaments.

Both rhenium and tantalum filaments were tested for the total evaporation measurement protocol. Loading a pure KCl solution resulted in short-lived, unstable ion beams. Loading with the Ta-activator on Re and with phosphoric acid on Ta filaments was more effective: 25 ng of K normally yielded an optimum intensity of 3 nA for 1-2 h without becoming exhausted. Tantalum filaments were chosen as the best option for total evaporation measurements due to the better total ion yield and lower blank.

2.3 Mass spectrometry

Potassium isotope compositions were measured on a ThermoFischer Triton+ thermal ionization mass spectrometer (TIMS) at the Institut für Geologie, Universität Bern. Measuring the abundance of ^{40}K is challenging due to two main constraints: the very large dynamic range of K isotopes and the large isotope fractionation during sample analysis. The first problem can be tackled using different amplifier configurations; the second one by in-run normalization to the certified $^{41}\text{K}/^{39}\text{K}$ ratio (for unspiked samples) or by applying a total evaporation analysis protocol.

2.3.1 TIMS amplifier configurations

The K ion beams were measured simultaneously in Faraday cups with 10^{10} , 10^{11} , $10^{12}\ \Omega$ resistors (table 1). Since ^{40}K is a very minor isotope precise measurement of its abundance requires high ion beam intensities of the more abundant K isotopes. This problem can be addressed by using amplifiers with different resistors that provide linear amplification in different signal intensity ranges.

Amplifier gains were intercalibrated by supplying a fixed voltage (corresponding to about 33 pA) off-line. Because of the two orders of magnitude range in collector currents resulting from the fixed voltage calibration, additional intercalibration tests were performed in-run in dynamic mode by switching the 40 pA signal of ^{39}K from $10^{10}\ \Omega$ (faraday cup L2) to $10^{11}\ \Omega$ (central faraday cup) and the 3 pA signal of ^{41}K from $10^{12}\ \Omega$ (faraday cup H2) to $10^{11}\ \Omega$ (central faraday cup) and back each cycle. The standard deviation for in-run gain intercalibrations was about 0.01%.

Baseline measurements were performed mainly in defocused mode when the beam is deflected before entering the magnet. Additionally, baselines on masses 39.85 and 40.15 were measured for a total of ten filaments in different turrets while the ion beam was focused. Baselines measured with the beam in focus were always statistically indistinguishable from the electronic background. Additionally an evaluation of the tails from peaks ^{31}K and ^{41}K was performed applying the secondary electron multiplier SEM (see appendix). Contributions of the tails on mass 40 are 0.003%. While this is about a third of the uncertainty of our most precise measurements (in-run normalized measurements, see below) it is an order of magnitude less important than the overall accuracy assigned to the abundance of the ^{40}K proposed here.

2.3.2. TIMS measurement protocols

Both amplifier configurations described in Table 1 were used for three measurement protocols: (1) in-run fractionation corrected measurements, (2) classic total evaporation and (3) block total evaporation.

Table 1. Amplifier configurations.

	Configuration 1			Configuration 2		
Cup	L2	C	H2	L2	C	H2
Resistor ($10^n \Omega$)	11	12	11	10	12	11
Isotope	^{39}K	^{40}K	^{41}K	^{39}K	^{40}K	^{41}K
Average measured current intensity (pA)	300	0.04	22	3000	0.4	220
Relative gain $\pm 1\sigma$	1.01665 \pm 2	0.100801 \pm 2	1.01444 \pm 2	10.02 \pm 1	0.100801 \pm 2	1.01444 \pm 2
Baseline average (fA)	-2	-3	-2	10	-3	-2

The tantalum filament was heated up to 1.2 A at a rate of 50 mA/min, so as to reach a ^{39}K signal sufficient for focusing and peak centering. When the ^{41}K signal reached 3 pA, the beam was centered. This starting procedure takes up to 15 minutes. Keeping track of the time and beam current during the centering and focusing procedure is necessary, as this may form a significant contribution of the total evaporation. When using configuration 1 (Table 1), the filament current was reduced to keep the beam at the lowest intensity needed for focusing and peak centering. In-run fractionation corrected measurements and block total evaporation measurements were done with automatic centering of the ^{40}K signal during acquisition. All measurements were performed in static mode.

In-run fractionation corrected measurements consisted of 15 blocks with 15 cycles with 8s integration time per cycle and 6s idle time between integrations. The filament was heated between blocks. One hundred baseline cycles of 1.05s each were measured between blocks in defocused mode with a pre-baseline waiting time of 15s to allow for the relatively slow decay on the $10^{12} \Omega$ resistor. $^{40}\text{K}/^{39}\text{K}$ ratios were calculated in-run with internal fractionation correction to the recommended IUPAC $^{41}\text{K}/^{39}\text{K} = 0.0721677$ (De Laeter et al, 2003).

Total evaporation (Fiedler, 1995) is a measurement protocol that uses a steadily increasing filament current without any interruption until the sample is totally consumed. The main aim of this method is to overcome progressive sample fractionation (at least the part due to sample depletion) by collecting “all” ions from the beginning to the end of the evaporation. Classic total evaporation has the disadvantage that focusing is only performed at the beginning of the run when the intensity of the signal is still small. This can result in possible loss of intensity if the focusing conditions change over time. During preliminary, semi-manual tests we observed that attempts to optimize the intensity by refocusing in mid-run did not increase the K signal, which showed a very stable behavior throughout the run. On the basis of these tests it was decided to follow the classical total evaporation procedure without interrupting the run for focusing. Ionization efficiency can approach 100 % for K as it is easily ionized (DePaolo, 1988), however, the total ion yield is lower since it also

involves the transmission efficiency of the mass spectrometer and (at least theoretically) the possibility to lose some part of signal due to a focus change. In our K measurements between 1 % and 48 % of all ions were collected. Measurements with a total ion yield <6 % were discarded. Measurement parameters for both amplifier configurations 1 and 2 (Table 1) were: integration time 4 s, idle time 1s. The time required for totally evaporating the samples was 1-4 h depending on the amplifier configuration and ionization efficiency. Data reduction was performed off-line.

Block total evaporation or “NBL-modified total evaporation” (Richter and Goldberg, 2003) is similar to the in-run fractionation corrected measurement protocol, the main difference being that the data acquisition is prolonged until the sample is totally evaporated. The measurement is divided into blocks, each block consisting of 15 cycles with 4s integration time each and 6s idle time. Baselines are measured for every block and the ^{40}K peak is centered every 5 blocks; the filament current is adjusted between blocks if required.

3. Results and discussion

3.1. In-run normalized measurements

The normalization value chosen for in-run normalized measurements was $^{41}\text{K}/^{39}\text{K} = 0.0721677$ as determined by Garner et al. (1975). These authors very probably used a linear law for a fractionation correction, but it is not explicitly stated in their study. As we do not have access to their raw data, we estimated the influence of the different fractionation corrections on our own raw data. It was noted that the linear law is in good accordance with Rayleigh and exponential fractionation laws over a large range of sample evaporated (Habfast, 1998). Application of a linear law correction instead of an exponential correction resulted in a maximum deviation of 0.005% towards lower values; this bias is well within the uncertainty given by Garner et al. (1975) for their corrected results. Twenty in-run normalized measurements for SRM 918b in three different filament turrets with in-run fractionation correction according to the exponential law built into the Triton+ instrument software were performed in late 2012 and are shown in Table 2a and in Fig. 1. Two different amplifier configurations were applied for this procedure (Table 1). Six filaments with SRM 985 were measured in two different filament turrets with the amplifier configuration 2 in early 2013. Results are presented in Table 2b and Fig. 1.

The long-term reproducibility is consistent with the individual in-run measurement uncertainty. The weighted mean of twenty $^{40}\text{K}/^{39}\text{K}$ measurements for SRM 918b is $0.000\ 125\ 127 \pm 12$ and for SRM 985 (6 runs) is $0.000\ 125\ 123 \pm 16$. Assuming the two standard reference materials are derived from the same K source, their fractionation-corrected $^{40}\text{K}/^{39}\text{K}$ ratios can be averaged, which results in a weighted average of $0.000\ 125\ 126 \pm 10$. Corrected for the contribution from the tailing of neighboring masses on ^{40}K (0.003%), the value is $0.000\ 125\ 122 \pm 10$. These results are indistinguishable from

$^{40}\text{K}/^{39}\text{K}$ ratio of $0.000\,125\,158 \pm 436$ measured by Garner et al. (1975), but much more precise; they are also indistinguishable from the $^{40}\text{K}/^{39}\text{K} = 0.000\,125\,112 \pm 37$ for terrestrial material published by Wielandt and Bizzarro (2010).

Table 2. Results of in-run fractionation correction measurements for a) SRM 918b and b) SRM 985. Weighted mean (bold values) calculated by Isoplot 3.75 (Ludwig, 2012).

Date	Run	$(^{40}\text{K}/^{39}\text{K}) \cdot 10^6$	$\pm 2\sigma \cdot 10^6$
<i>(a)</i>			
19.11.12	1	125.122	0.038
19.11.12	2	125.144	0.036
19.11.12	3	125.136	0.078
19.11.12	4	125.135	0.103
26.11.12	5	125.125	0.052
26.11.12	6	125.148	0.062
26.11.12	7	125.111	0.039
26.11.12	8	125.126	0.058
26.11.12	9	125.119	0.041
26.11.12	10	125.106	0.041
26.11.12	11	125.127	0.062
26.11.12	12	125.123	0.047
26.11.12	13	125.131	0.230
26.11.12	14	125.145	0.232
26.11.12	15	125.189	0.062
26.11.12	16	125.110	0.047
26.11.12	17	125.107	0.241
26.11.12	18	125.131	0.052
26.11.12	19	125.130	0.040
26.11.12	20	125.171	0.278
Wtd. Mean		125.127	0.012
MSWD = 0.42, probability = 0.99			
<i>(b)</i>			
15.02.13	1	125.121	0.043
15.02.13	2	125.136	0.044
15.02.13	3	125.119	0.034
15.02.13	4	125.127	0.038
15.02.13	5	125.120	0.044
15.02.13	6	125.118	0.035
Wtd. Mean		125.123	0.016
MSWD = 0.117, probability = 0.99			

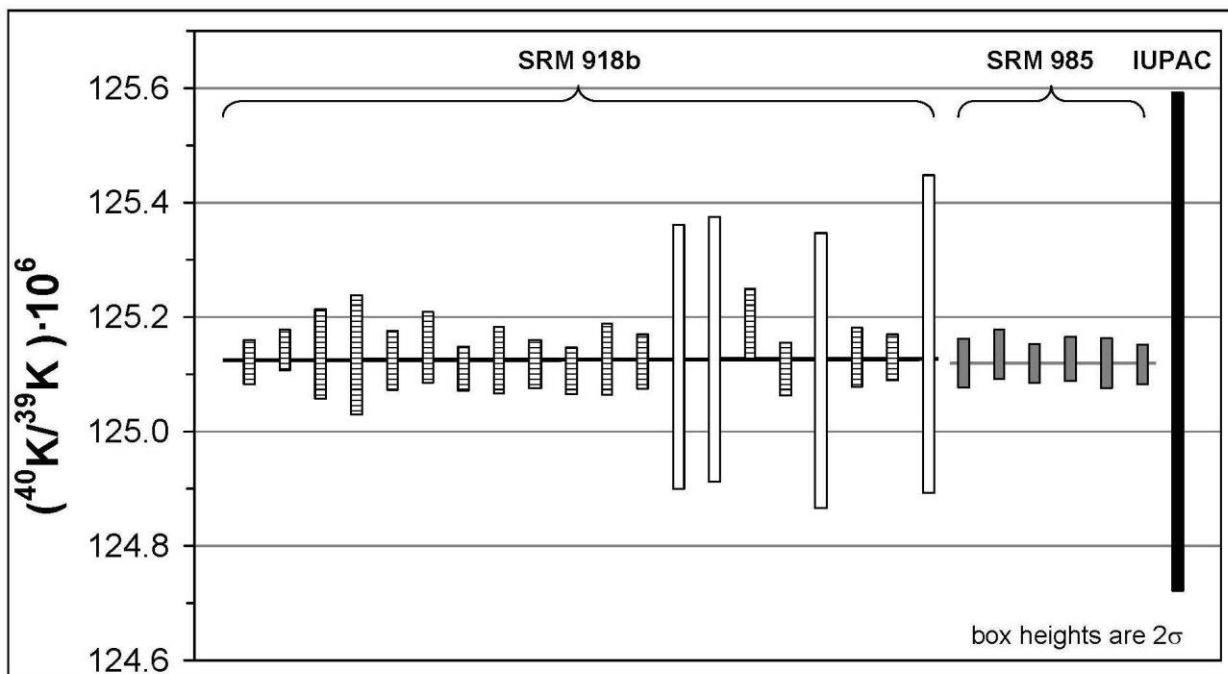


Fig. 1. Results of in-run normalized $^{40}\text{K}/^{39}\text{K}$ measurements. SRM 918b: white bars, amplifier configuration 1; grey bars, amplifier configuration 2; SRM 985: dark grey bars, amplifier configuration 2; IUPAC value (De Laeter et al., 2003): black bar.

3.2. Conventional total evaporation measurements

Total evaporation analyses are less precise than in-run normalized measurements, but they have the advantage that the determination of both $^{40}\text{K}/^{39}\text{K}$ and $^{41}\text{K}/^{39}\text{K}$ ratios is independent of the choice of a normalization value, and that they allow to estimate any excess of isotope 40 (due to isobaric interference of Ca or any other possible contamination, see below). As such, the two analytical approaches should be viewed as complementary. One difficulty with the total evaporation protocol is optimizing the amount of K that is loaded on the filament. As the ionization efficiency of K approaches 100 %, a sample size of 100 ng requires 8-10 h for a single measurement. Such long measurements are unlikely to provide reliable results due to unavoidable electronic instabilities that affect baselines and amplifiers. In a total evaporation measurement following the published procedure of Fiedler (1995), peak centering and focusing are reduced to a minimum to reduce the loss of counted ions under changing fractionation conditions as the run progresses. Typically, focusing of the beam and peak-centering for ^{39}K and ^{41}K are done only at the beginning of the run, as well as the baseline measurement. No baseline is measured subsequently. Decreasing the amount of K used for an analysis would reduce the measurement time, but would at the same time increase the importance of the (fixed) Ca interference introduced during loading relative to the minor ^{40}K isotope. Since K and Ca are ionized at different times during the measurement, it could be anticipated that Ca interference should be negligible. Possible interference can be diagnosed by comparison of

experimental and theoretical fractionation slopes. An excessively shallow slope shows an increase of isotope 40 and is a good tracer of any contamination affecting this minor isotope.

Table 3. Different fractionation laws, theoretical and experimental slopes of the $^{40}\text{K}/^{39}\text{K}$ vs. $^{41}\text{K}/^{39}\text{K}$ diagram. Atomic masses used for calculations are from (De Laeter et al, 2003).

Exponential law	1.973
Rayleigh law	1.961
Equilibrium law	1.949
Wielandt and Bizzaro (2010) experimental	1.958
This work (N = 24)	1.932-1.972

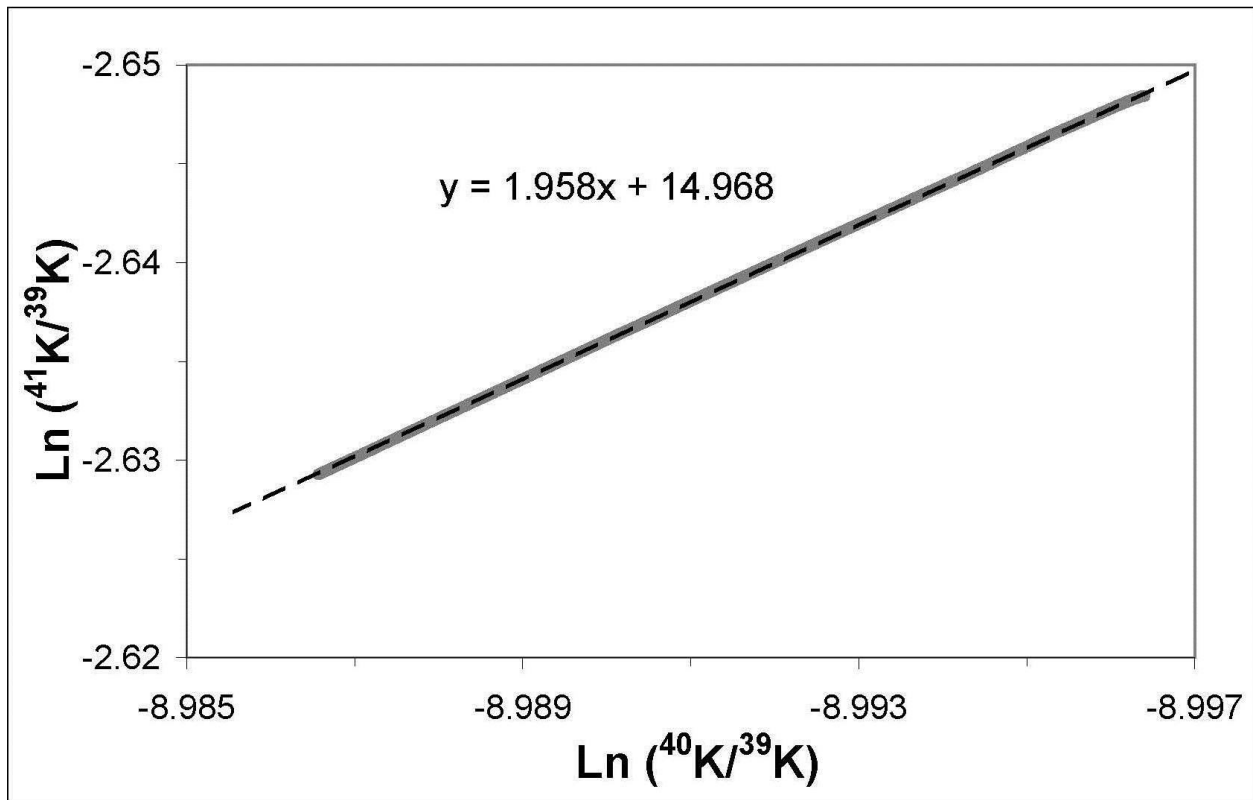


Fig. 2. Example of the fractionation evolution of K isotopes. The slope $f = 1.958$ is a fit to the total evaporation data for a single run, and represents the experimental exponent according to the exponential fractionation law.

Experimental fractionation slopes were calculated from the uncorrected $^{40}\text{K}/^{39}\text{K}$ and $^{41}\text{K}/^{39}\text{K}$ raw data, which change owing to mass fractionation during the run. Combining equation (A4) from Russell et al (1978) for $^{40}\text{K}/^{39}\text{K}$ and $^{41}\text{K}/^{39}\text{K}$

$$\begin{cases} \left(\frac{^{40}\text{K}}{^{39}\text{K}} \right)_M = \left(\frac{^{40}\text{K}}{^{39}\text{K}} \right)_C \left(\frac{m_{40}}{m_{39}} \right)^p \\ \left(\frac{^{41}\text{K}}{^{39}\text{K}} \right)_M = \left(\frac{^{41}\text{K}}{^{39}\text{K}} \right)_C \left(\frac{m_{41}}{m_{39}} \right)^p \end{cases} \quad [\text{Eq. 3}]$$

and expressing $\left(\frac{m_{41}}{m_{39}}\right)^p$ as $\left(\frac{m_{40}}{m_{39}}\right)^{fp}$ we can derive

$$\left[\frac{\left(\frac{^{40}\text{K}}{^{39}\text{K}}\right)_M}{\left(\frac{^{40}\text{K}}{^{39}\text{K}}\right)_C} \right] = \left[\frac{\left(\frac{^{41}\text{K}}{^{39}\text{K}}\right)_M}{\left(\frac{^{41}\text{K}}{^{39}\text{K}}\right)_C} \right]^f \quad [\text{Eq. 4}]$$

where M and C mean measured and normalized ratios respectively, m is the mass of the isotope, p is the fractionation factor (function of time, but independent of mass) and f is a time-independent, mass-dependent coefficient.

The exponential fractionation law yields:

$$f = \frac{\ln\left(\frac{m_{41}}{m_{39}}\right)}{\ln\left(\frac{m_{40}}{m_{39}}\right)} = 1.973 \quad [\text{Eq. 5}]$$

Theoretical coefficients for other fractionation laws can be calculated following Ranen and Jacobsen (2008) and are presented in Table 3 together with those obtained experimentally by Wielandt and Bizzarro (2010) and in the present study. For the estimates the atomic masses from De Laeter et al. (2003) were used. An example is shown in Fig 2 where raw total evaporation data are plotted in log-log coordinates. The slope f , obtained by fitting the total evaporation raw data points, ranges from 1.932 to 1.972 in our data set. Small deviations from the theoretical slope can be caused by a fractionation behavior deviating from the exponential law at the beginning of the run.

The data obtained by total evaporation measurements were reduced off-line. The sum of all intensities for each isotope (typically 1000-2000 cycles) was used to obtain ratios and represents a single total evaporation run in Table 4a and 4b. We follow Bürger et al. (2010, p.68) in considering the repeatability (“external reproducibility”) as the correct measure of the uncertainty, and in considering the “internal standard error” as an underestimate of the actual measurement uncertainty. Each individual cycle records mass-dependent instrumental fractionation due to two distinct mechanisms. The first one is related to a Rayleigh-type reservoir fractionation during sample evaporation, and always results in light isotopes being preferentially ionized at the beginning of the measurement, with heavy isotopes dominating the residual and the last part of the measurement. The second one is caused by the incomplete transmission of ions from the filament past the source slits, which depends on the source focusing conditions; since total transmission yields in the runs judged reliable ranged from 6 to 48 %, the summation is able to remove the reservoir effect, but not the ion transmission effect, which affects each measurement to an unknown degree. Thus, the summed data lie along the fractionation line, albeit at unknown location relative to the true unfractionated value. An additional complication is that these two mechanisms operate to different extents and in different proportions during a measurement. As the filament is heated, a part of the sample is evaporated from hotspots

and undergoes progressive fractionation due to both Rayleigh fractionation and focusing-dependent incomplete transmission. Later during the measurements, as this hotspot shifts, its fractionation behavior changes and other hotspots at different locations on the filament undergo a similar Rayleigh fractionation but a different focusing-dependent transmission fractionation. The combined effect of these fractionation processes is empirically described by an exponential law (Russell et al, 1978).

Table 4. Total evaporation results for: (a) SRM 918b (b) SRM 985. All analyses used amplifier configuration 2. Unc.avg. means uncorrected average. Corr.avg. (in bold) is the average of the fractionation-corrected ratios, regressed to $^{41}\text{K}/^{39}\text{K}=0.721677$.

Date	Run	$(^{40}\text{K}/^{39}\text{K}) \cdot 10^6$	$^{41}\text{K}/^{39}\text{K}$	Slope	Total ion yield %
<i>(a)</i>					
29.10.12	1	125.258	0.07225	1.848	48
29.10.12	2	125.167	0.07219	1.899	30
29.10.12	3	125.271	0.07228	1.898	16
29.10.12	4	125.179	0.07218	1.929	21
29.10.12	5	125.186	0.07212	1.751	6
29.10.12	6	125.518	0.07229	1.661	8
29.10.12	7	125.262	0.07218	1.748	11
29.10.12	8	125.112	0.07205	1.729	8
05.11.12	9	125.348	0.07240	1.932	15
05.11.12	10	125.206	0.07224	1.971	20
05.11.12	11	125.092	0.07211	1.940	14
05.11.12	12	125.190	0.07227	1.937	15
05.11.12	13	125.561	0.07263	1.880	9
05.11.12	14	125.300	0.07230	1.891	8
05.11.12	15	125.550	0.07263	1.969	15
05.11.12	16	125.488	0.07252	1.904	7
Unc.avg.		125.293	0.07229		
2 std.dev		0.311	0.00035		
Corr. avg.		125.185			
2 std dev.		0.130			
MSWD = 0.112, Probability = 1.0					
<i>(b)</i>					
13.02.13	1	125.054	0.07210		
13.02.13	2	125.179	0.07210	1.963	9
15.02.13	3	125.221	0.07221	1.929	7
20.02.13	4	125.122	0.07226	1.940	16
20.02.13	5	125.145	0.07216	1.972	19
20.02.13	6	125.078	0.07220	1.956	40
20.02.13	7	125.099	0.07213	1.955	36
20.02.13	8	125.066	0.07215	1.930	26
Unc.avg.		125.120	0.07218	1.950	20
2 std.dev		0.117	0.07217		
Corr. avg.		125.116			
2 std dev.		0.057			
MSWD = 0.107, Probability = 0.996					

The total evaporation data that scatter along the fractionation line can be corrected after the runs are completed (Fig.3). Strictly speaking, this makes the results of the total evaporation runs not a conventional total evaporation, as an additional fractionation correction was performed to bring the measured $^{41}\text{K}/^{39}\text{K}$ ratio in agreement with the IUPAC recommendation. The rationale for applying this correction in the case of K has to do with the relative importance of the two competing fractionation processes: Rayleigh-type reservoir and focusing-dependent transmission. An alkali metal such as K undergoes a practically complete ionization. Therefore, the effect of the Rayleigh fractionation is factored away by using the sum of the beam intensities. However, the fractionation due to focusing is not removed by the summation. An unfractionated value can be found by using an independently determined normalization value on the fractionated total evaporation results, as was done for Nd isotope ratios by Wakaki et al. (2007). In the present study the IUPAC $^{41}\text{K}/^{39}\text{K}$ ratio that lies in the “Mean Earth” field (Fig. 4) is used as a normalization value. The unfractionated $^{40}\text{K}/^{39}\text{K}$ can be found from simple interpolation along the fractionation line (Fig.3). The fractionation corrected $^{40}\text{K}/^{39}\text{K}$ average ratios for sixteen SRM 918b and eight SRM 985 analyses are $0.000\,125\,185 \pm 113$ and $0.000\,125\,116 \pm 57$ (2σ), respectively.

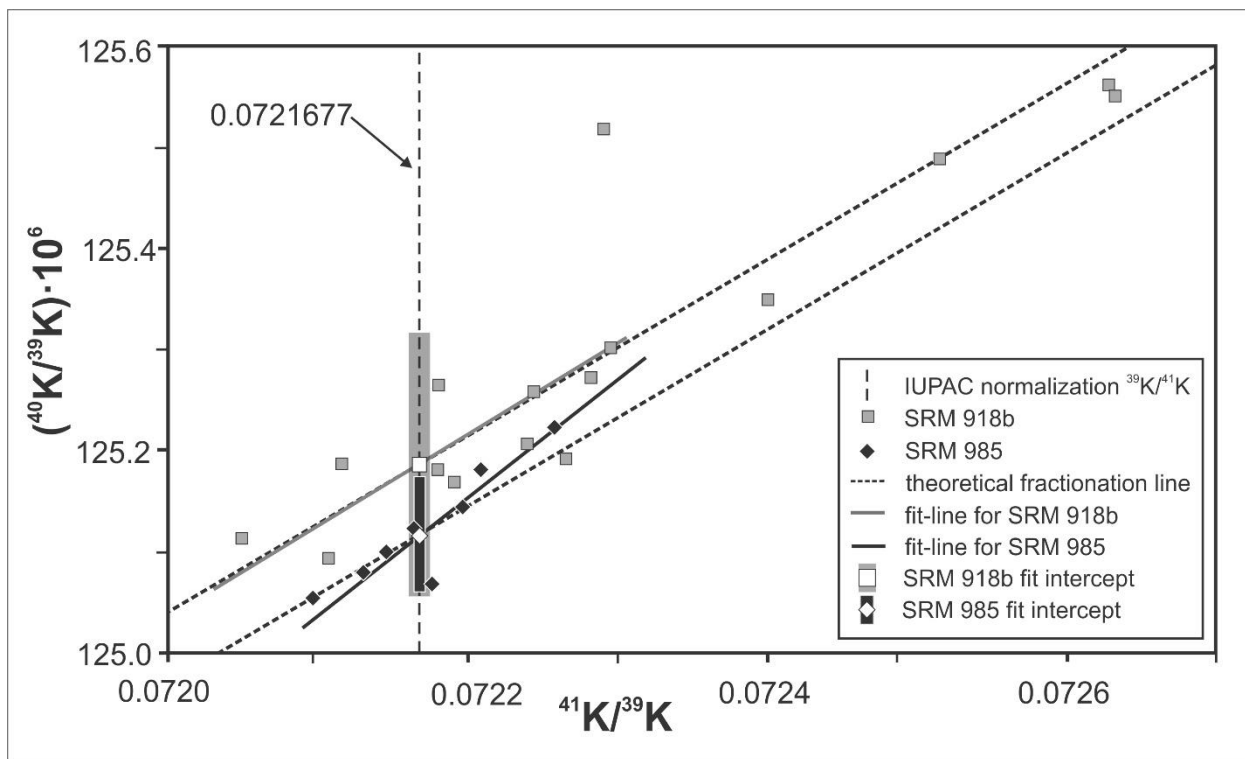


Fig. 3. Total evaporation results. Filled squares: SRM 918b; black diamonds: SRM 985. The dispersion of the points is due to isotope fractionation, as shown by the fact that regression lines are close to the theoretical slope of the mass-dependent fractionation (dashed line). The two overlapping vertical bars are the intercepts of the regressions for $^{41}\text{K}/^{39}\text{K} = 0.0721677$ with a 2σ uncertainty. The grey bar is drawn broader for reasons of graphic clarity.

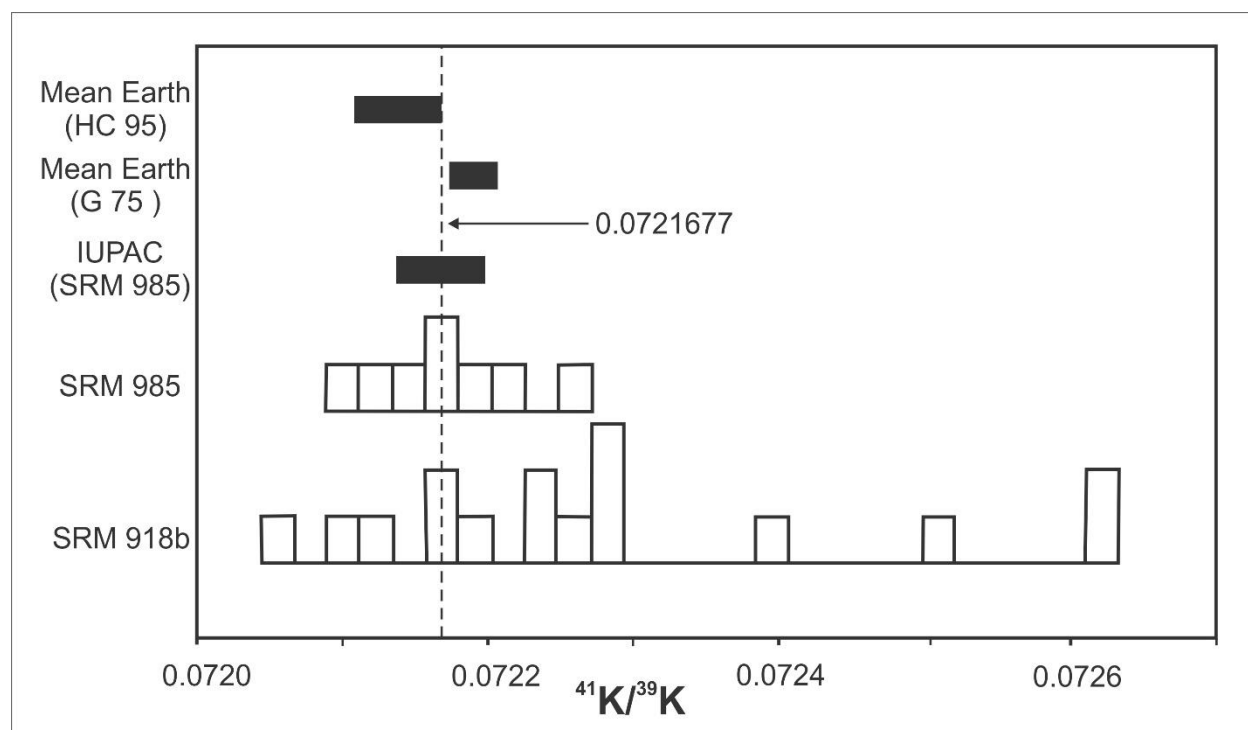


Fig. 4. $^{41}\text{K}/^{39}\text{K}$ ratios for different materials. Mean Earth (HC 95) is the value proposed by Humayun and Clayton (1995). Mean Earth (G 75) is the recalculated value of the Garner et al. (1975) data presented by Humayun and Clayton (1995). The IUPAC value is from De Laeter et al. (2003) who based their recommendation on the SRM 985 measurement by Garner et al. (1975). The two histograms for SRM 918b and SRM 985 represent total evaporation runs without mass fractionation correction from the present study.

3.3. Block total evaporation measurements

The block total evaporation is expected to be a very precise method for the determination of the absolute abundances of K isotopes, as it combines advantages of the in-run normalized measurements and conventional total evaporation methods: high in-run precision, baseline measurements and peak centering between blocks together with the possibility to collect “all” ions and to avoid Rayleigh artifacts. However, it has the disadvantage that not all ions are counted, especially at the beginning and the end of the run. Loss of ions at the beginning of the run is unavoidable due to the focusing and centering procedures, and can be reduced to a minimum as was described in the previous section. Loss of ions also occurs at the end of the run, when the signal is still present but not high enough for a precise measurement; this results in fast automatic filament heating and accelerated evaporation of the rest of the sample. The part of the measurement that is not integrated by this protocol is towards the end of the run, which corresponds to the segment of total evaporation runs with the highest depletion of light isotopes.

The total ion yield of the block total evaporation measurements ranged from 2 to 7 % (Table 5), which is much lower than the total ion yield of conventional total evaporation measurements (Table 4). It can be explained at least in part by the time required for inter-block procedures (baseline, peak-centering and heating), which use up approximately half

Chapter 1. High precision determination of the terrestrial ^{40}K abundance.

of the run time, during which no intensity is recorded. The loss of these ions does not greatly affect the final result, as the losses are evenly distributed during the analysis, and the summed ratios still represent the whole sample. A larger effect on the final result is caused by the uncontrolled loss of 2-3 % of the material at the end of the run that is enriched in heavy isotopes.

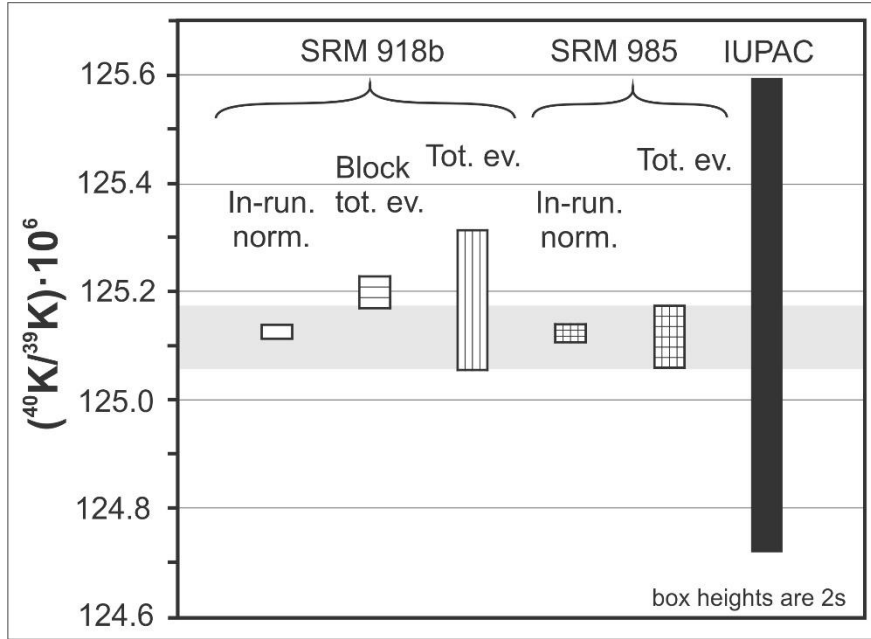
The weighted mean of normalized $^{40}\text{K}/^{39}\text{K}$ ratios obtained with the block total evaporation protocol agrees with the IUPAC value (Table 5) and is statistically the same as that of the in-run normalized measurements protocol (Table 2). The difference in measurement uncertainties of the two analytical sessions reflects the two different amplifier configurations.

Each of three analysis protocols has the potential to produce systematic artifacts, but the artifacts are different for each protocol and uncorrelated with each other. The very close similarity of the three data-sets for SRM 918b and two data-sets for SRM 985 (Fig. 5), is strong evidence that the true $^{40}\text{K}/^{39}\text{K}$ isotope ratio lies between 0.000 1250 and 0.000 1253. The in-run normalized value gives a weighted average $^{40}\text{K}/^{39}\text{K}$ of $0.000\ 125\ 122 \pm 10$ ($2\ \sigma$). The fractionation-corrected high transmission total evaporation $^{40}\text{K}/^{39}\text{K}$ ratios for SRM 918b ($=0.000\ 125\ 185 \pm 130$) and SRM 985 ($=0.000\ 125\ 116 \pm 57$) are analytically indistinguishable from the in-run normalized values. Because of the larger number of analyses, we consider the fractionation-corrected total evaporation values as conservative, most robust determination of the terrestrial $^{40}\text{K}/^{39}\text{K}$ isotopic ratio.

Table 5. Block total evaporation results for SRM 918b. The first 7 analyses used amplifier configuration 1, the last 3 used configuration 2.

Date	$(^{40}\text{K}/^{39}\text{K}) \cdot 10^6$	2σ	$^{41}\text{K}/^{39}\text{K}$	2σ	Total ion yield %
30.07.12	125.124	1.570	0.072118	0.000409	2
30.07.12	125.061	0.710	0.072061	0.000206	5
30.07.12	125.269	0.634	0.072131	0.000192	5
28.08.12	125.166	0.709	0.071940	0.000199	5
28.08.12	125.288	0.850	0.072170	0.000294	5
28.08.12	125.078	1.263	0.072092	0.000361	5
28.08.12	125.287	1.175	0.072150	0.000315	5
19.11.12	125.177	0.137	0.072217	0.000049	5
19.11.12	125.156	0.172	0.072238	0.000043	7
19.11.12	125.203	0.031	0.072198	0.000030	6
Wtd. Mean	125.200	0.029	0.072205	0.000029	
	MSWD=0.081, probability=1		MSWD = 1.5, probability = 0.15		

Fig. 5. Comparison of the results of SRM 918b and 985 obtained by different techniques and recommended IUPAC value for $^{40}\text{K}/^{39}\text{K}$ previously measured by Garner et al (1975) on SRM 985. The “best estimate” for $^{40}\text{K}/^{39}\text{K}$ in natural samples is: $0.000\ 125\ 116 \pm 57\ (2\sigma)$ and marked with a grey horizontal bar.



4. Conclusions

The $^{40}\text{K}/^{39}\text{K}$ ratio was measured by thermal ionization mass spectrometry. High precision data were obtained by three different measurement protocols for two standard reference materials. The most accurate results were obtained with an amplifier configuration that uses 10^{10} , 10^{11} and $10^{12}\ \Omega$ resistors on Faraday cups. The data for in-run normalization and total evaporation protocols were corrected for the instrumental fractionation by the normalization to IUPAC $^{41}\text{K}/^{39}\text{K}$. The results all agree with the terrestrial $^{40}\text{K}/^{39}\text{K}$ value suggested by IUPAC, but have much higher precision. The $^{40}\text{K}/^{39}\text{K}$ for the SRM985, which has been a standard for terrestrial K abundance since 1975, is $0.000\ 125\ 122 \pm 16$ (in-run normalization), $0.000\ 125\ 116 \pm 57$ (fractionation-corrected total evaporation). These values within their uncertainties are coincident with the previously accepted IUPAC value of $0.000\ 125\ 158 \pm 436$.

The proposed $^{40}\text{K}/^{39}\text{K} = 0.000\ 125\ 116 \pm 57\ (2\sigma)$ for SRM 985 agrees with the previously accepted IUPAC value of $0.000\ 125\ 158 \pm 436$ but has a significantly improved measurement uncertainty. This ratio corresponds to an isotopic abundance $^{40}\text{K}/\text{K} = (1.1668 \pm 8) \cdot 10^{-4}$, taking into account the 0.046% uncertainty on the IUPAC $^{41}\text{K}/^{39}\text{K}$ (De Laeter J.R. et al, 2003)

The bias of K-Ar and K-Ca dating systems contributed by the uncertainty in the abundance of ^{40}K is now reduced from 0.35% to 0.05%. However, in order to reach the goal of the Earthtime initiative to determine ages with an absolute uncertainty of 0.1% of the total age requires further calibration of reference materials used for ^{40}Ar - ^{39}Ar dating,

and further improvements in the determination of the ^{40}K branching ratio and the value for the total decay constant of ^{40}K .

Acknowledgements:

We are thankful to M. Humayun who kindly granted us some amount of SRM 985. We also grateful to Associate Editor D.A. Papanastassiou and three anonymous reviewers for their profound comments promoted improvements of this paper.

Appendix

A scan (800 steps) from mass 39.2 to 40.8 (Fig. A1) was performed with the secondary electron multiplier (SEM), to estimate the relevant abundance sensitivity. The ^{40}K intensity was 960 000 cps corresponding roughly to 0.16 pA, which is less than half of the signal used for data accumulation. The intensity of K beams was lowered to reduce possibility of damaging of the SEM.

The tail from the wide and strong ^{39}K peak can be observed close to the mass 40. At the region of 39.9 this tail is 40 cps, which corresponds to $7 \cdot 10^{-6}$ pA. The ^{41}K tail superimposed with a tail from ^{39}K on mass 40.1 is 25 cps ($4 \cdot 10^{-6}$ pA). Below the ^{40}K peak the tail intensity is 32 cps ($5 \cdot 10^{-6}$ pA), which is 0.003 % of the ^{40}K peak intensity. Thus the abundance sensitivity in the region of mass 40 is 2 ppb.

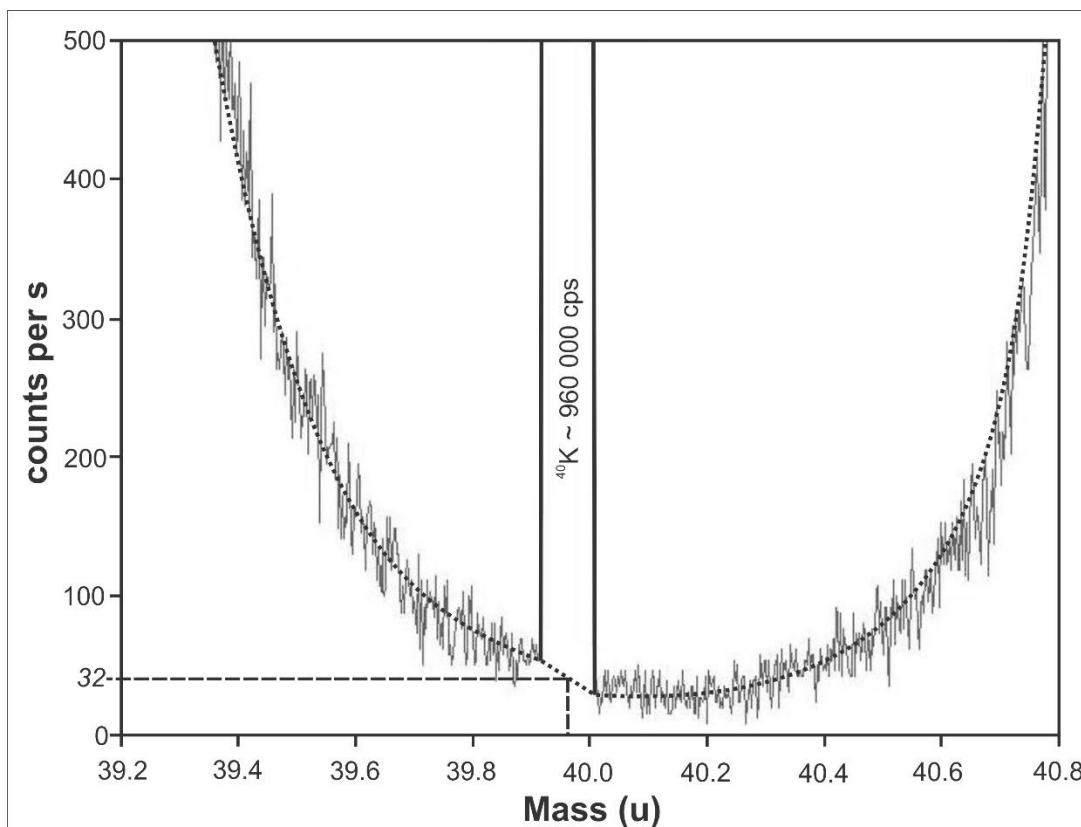


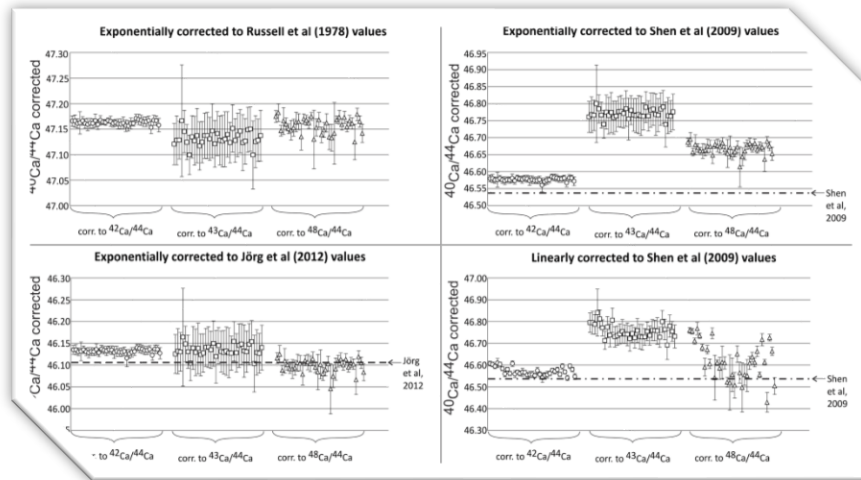
Fig. A1. Mass scan performed with SEM at the area of ^{40}K , with a ^{40}K intensity was 960 000 cps that corresponds to 0.16 pA.

References

- Begemann F., Ludwig K.R., Lugmair G.W., Min K., Nyquist L.E., Patchett P.J., Renne P.R., Shih C.-Y., Villa I.M. and Walker R.J., 2001 Call for an improved set of decay constants for geochronological use. *Geochimica et Cosmochimica Acta* 65, 111–121.
- Birck J.R., 1986 Precision K-Rb-Sr isotopic analysis: application to Rb-Sr chronology. *Chemical Geology* 56, 73-83.
- Bürger S., Essex R.M., Mathew K.J., Richter S. and Thomas R.B., 2010. Implementation of Guide to the expression of Uncertainty in Measurement (GUM) to multi-collector TIMS uranium isotope ratio metrology. *International Journal of Mass Spectrometry* 294, 65-76.
- Burnett D.S., Lippolt H.J. and Wasserburg G.J., 1966. The relative isotopic abundance of ^{40}K in terrestrial and meteoritic samples. *Journal of Geophysical Research* 71, 1249-1269.
- De Laeter J.R., Böhlke J.K., De Bivre P., Hidaka H., Peiser H.S. Rosman K.J. and Taylor P.D.P., 2003. Atomic weights of the elements: review 2000 (IUPAC Technical report). *Pure and Applied Chemistry* 75, 683-800.
- DePaolo D.J., 1988. Neodymium Isotope Geochemistry. An Introduction. Springer, New York, 187 p.
- Fiedler R., 1995. Total evaporation measurements: experience with multi-collector instruments and a thermal ionization quadrupole mass spectrometer. *International Journal of Mass Spectrometry. Ion Proc.* 146, 91-97.
- Garner E.L., Murphy T.J., Gramlich J.W., Paulsen P.J. and Barnes I.L., 1975. Absolute isotopic abundance ratios and atomic weight of a reference sample of potassium. *J. Res. Natl. Bur. Stand.* 79A, 713-725.
- Gradstein F.M., Ogg J.G., and Smith A.G., 2004. A geologic time scale-2004. Cambridge University Press, Cambridge, 589 p.
- Grau Malonda A. and Grau Carles A., 2002. Half-life determination of ^{40}K by LSC. *Applied. Radiation and Isotopes* 56, 153-156.
- Habfast K. (1998) Fractionation correction and multiple collectors in thermal ionization isotope ratio mass spectrometry. *International Journal of Mass Spectrometry.* 176, 133-148.
- Humayun M. and Clayton R.N., 1995. Precise determination of the isotopic composition of potassium: Application to terrestrial rocks and lunar soils. *Geochimica et Cosmochimica Acta* 59, 2115-2130.
- Kossert K. and Günter E., 2004. LSC measurements of the half-life of ^{40}K . *Applied. Radiation and Isotopes* 60, 459-464.
- Krumrei T.V., Villa I.M., Marks M. A.W., and Markl G., 2006. A $^{40}\text{Ar}/^{39}\text{Ar}$ and U/Pb isotopic study of the Ilímaussaq complex, South Greenland: Implications for the ^{40}K decay constant and for the duration of magmatic activity in a peralkaline complex. *Chemical Geology* 227, 258-273.
- Kwon J.Y., Min K.W., Bickel P.J. and Renne P.R., 2002. Statistical methods for jointly estimating the decay constant of K-40 and the age of a dating standard. *Mathematical Geology* 34, 457-475.
- Ludwig K.R., 2012. Isoplot 3.75. A Geochronological Toolkit for Microsoft Excel. Berkeley Geochronology Center Spec. Publ. 5.
- Min K., Mundil R., Renne P.R. and Ludwig K.R., 2000. A test for systematic errors in $^{40}\text{Ar}/^{39}\text{Ar}$ geochronology through comparison with U/Pb analysis of a 1.1-Ga rhyolite. *Geochimica et Cosmochimica Acta* 64, 73-98.
- Nägler T.F. and Villa I.M., 2000. In pursuit of the ^{40}K branching ratios: K-Ca and ^{39}Ar - ^{40}Ar dating of gem silicates. *Chemical Geology* 169, 5-16.
- Nier A.O., 1950. A redetermination of the relative abundances of the isotopes of carbon, nitrogen, oxygen, argon, and potassium. *Phys. Rev.* 77, 789.
- Ranen M.C. and Jacobsen S.B., 2008. Fractionation corrections for high-precision multi-collector thermal ionization mass spectrometry. 29th Lunar and Planetary Science Conference, Abstr. 1966.
- Renne P.R., Mundil R., Balco G., Min K. and Ludwig K.R., 2010. Joint determination of ^{40}K decay constants and $^{40}\text{Ar}^*/^{40}\text{K}$ for the Fish Canyon sanidine standard, and improved accuracy for $^{40}\text{Ar}/^{39}\text{Ar}$ geochronology. *Geochimica et Cosmochimica Acta* 74, 5349-5367.

Chapter 1. High precision determination of the terrestrial ^{40}K abundance.

- Richter S. and Goldberg S.A., 2003. Improved techniques for high accuracy isotope ratio measurements of nuclear materials using thermal ionization mass spectrometry. *International Journal of Mass Spectrometry* 229, 181-197.
- Russell W.A, Papanastassiou D.A and Tombrello T.A., 1978. Ca isotope fractionation on the Earth and other solar system materials. *Geochimica et Cosmochimica Acta* 42, 1075-1090.
- Steiger R.H. and Jäger E., 1977. Subcommittee on geochronology: Convention on the use of decay constants in geo- and cosmochronology. *Earth and Planetary Science Letters* 36, 359-362.
- Schwarz W.H., Kossert K, Tieloff M. and Hopp J., 2011. Comment on the “Joint determination of ^{40}K decay constants and $^{40}\text{Ar}^*/^{40}\text{K}$ for the Fish Canyon sanidine standard, and improved accuracy for $^{40}\text{Ar}/^{39}\text{Ar}$ geochronology” by Paul R. Renne et al. *Geochimica et Cosmochimica Acta* 75, 5094-5096.
- Wakaki S., Shibata S.-N. and Tanaka T., 2007. Isotope ratio measurements of trace Nd by the total evaporation normalization (TEN) method in thermal ionization mass spectrometry. *International Journal of Mass Spectrometry* 264, 137-163.
- Wielandt D. and Bizzarro M., 2011. A TIMS-based method for the high precision measurements of the three-isotope potassium composition of small samples. *Journal of Analytical. Atomic Spectrometry* 26, 366-377.



Chapter 2

TIMS measurements of full range of natural Ca isotopes with internally consistent fractionation correction

TIMS measurements of full range of natural Ca isotopes with internally consistent fractionation correction

Maria O. Naumenko-Dèzes^{1,*}, Claudia Bouman², Thomas F. Nägler¹, Klaus Mezger¹, Igor M. Villa^{1,3}

1-Institute für Geologie, Universität Bern, Baltzerstrasse 1+3, 3012 Bern, Switzerland

2-Thermo Fisher Scientific, Hanna-Kunath-Strasse. 11, 28199 Bremen, Germany

3-Università di Milano Bicocca, Piazza della Scienza 4, 20126 Milano, Italy

Corresponding author: Maria O. Naumenko-Dèzes, marie@geosphere.ch

Published in International Journal of Mass Spectrometry 387 (2015) 60-68

Abstract

This study presents static measurements of the Ca isotopic composition of standard reference materials SRM 915 a/b on a Triton *Plus*TM thermal ionization mass spectrometer with a specially developed Faraday cup array allowing simultaneous measurement of ⁴⁰Ca and ⁴⁸Ca. The total amount of Ca in all analyses was kept < 1 µg. With this setup the measurement uncertainties were 0.06 ‰ for ⁴⁰Ca/⁴⁴Ca and 0.12 ‰ for ⁴⁸Ca/⁴⁰Ca. Measuring all isotopes simultaneously better allows to test the internal consistency of different Ca isotope abundances reported in the literature. The exponential law was observed to correct incompletely instrumental mass fractionation. An improved fractionation correction based on the exponential law is proposed. It changes the ⁴⁰Ca/⁴⁴Ca ratio of SRM 915a (corrected relative to ⁴²Ca/⁴⁴Ca = 0.31221; ⁴⁸Ca/⁴⁴Ca = 0.08871) from 47.1635 ± 0.0028 to 47.1649 ± 0.0047. The measurements of SRM 915b were performed with different analytical conditions (runs were prolonged till complete filament load depletion). Even if the ⁴⁰Ca/⁴⁴Ca ratio of SRM 915b, when corrected with the simple exponential law, appears different (47.1532 ± 0.0038) from that of SRM 915a, it becomes coincident (47.1613 ± 0.0028) when corrected with a second-order refinement. This supports the use of the improved exponential law to obtain internally consistent Ca isotope ratio for natural samples.

1. Introduction

Calcium is the fifth most abundant element in the terrestrial planets. It has five stable isotopes ^{40}Ca , ^{42}Ca , ^{43}Ca , ^{44}Ca , ^{46}Ca and the long lived ^{48}Ca with a half-life of 4×10^{19} a. The Ca isotope abundances are of great importance for multiple disciplines like astrophysics, biology and geology, as they provide information on nucleosynthetic processes in stars, and act as a proxy for paleoclimate, changes in biological cycles, fractionation in plants and animals, condensation and evaporation processes in the Early Solar System and present-day surface processes on Earth, as well as K-Ca geochronology (e.g. Skulan et al., 1997; Gopalan and Kumar, 2008; Caro et al., 2010; Fantle, 2010).

Such a wide spread of possible applications requires a uniform base to make different studies comparable. In geological applications a substantial obstacle to data intercomparison is the usage of (a) different reference materials (National Institute for Standards and Technology, NIST, Standard Reference Materials SRM 915a and SRM 915b; sea water; in-house reference solutions; *etc.*); (b) different Ca isotope ratios published by different authors (e.g.; Russell et al., 1978; Schmitt et al., 2001; de Laeter et al., 2003; Simon et al., 2009); and (c) different mass-dependent fractionation correction laws (linear, power, Rayleigh, exponential, improved exponential; see § 3.2.).

The most commonly used methods for Ca isotope measurements are thermal ionization mass spectrometry (TIMS, both single- and multicollector) and multicollector inductively coupled plasma mass spectrometry (MC-ICP-MS). Common issues with both measurements are isobaric interferences (^{40}K and, in the case of ICP-MS, ^{40}Ar), high abundance range ($^{40}\text{Ca} = 96.9\%$, $^{43}\text{Ca} = 0.135\%$; ^{46}Ca (0.004%) is generally not reported due to its very high measurement uncertainty) and wide mass range (8 amu difference between ^{40}Ca and ^{48}Ca). Single collector set ups were used e.g. by Russell et al. (1978), Skulan et al. (1997) and Nagler and Villa (2000). The use of single collectors even in the late 90ties and early this millennium is partly due to the problem of the large relative mass range of Ca, and concomitant issues with the focal plane and collector setups in multicollector instruments. Multicollector measurements were found to give very good internal precision, but poor external reproducibility, at least in part related to focussing issues (e.g. Skulan et al., 1997). However, single collector measurement requires stable beams over long measuring times. More recently, two approaches were used to cope with the wide mass range in multicollector setups: either the number of measured isotopes was limited (e.g. Holmden, 2005; Gopalan et al., 2006; Schiller et al., 2012) or the isotopes were measured in two separate groups, the first pass including masses 40, 42, 43, 44 and a second pass including masses 44, 46, 48 (e.g. Heuser et al., 2002; Amini et al., 2009; Lehn et al., 2013). The former is unfavorable if the subject of interest is mass-dependent isotope fractionation; the latter if the signal is short-lived, notably in case when small amounts of radiogenic ^{40}Ca are to be analyzed. For the present study the Ca isotope compositions of SRM 915a and SRM 915b were determined by measuring the whole range of Ca isotopes from mass 40 to 48 simultaneously in static mode using a multicollector configuration

(Bouman et al., 2011) adapted specifically for this purpose on a Thermo Scientific Triton *Plus*TM TIMS at the Universität Bern. Static measurements have advantages over multidynamic measurements: for example, any non-uniform signal decrease causes no drift in isotope ratios; moreover, as stable and long-lived signals are not an absolute requirement, sample loading is less critical.

1.1 Reference materials.

Diverse materials have been used as reference materials for Ca isotope measurements: museum- grade fluorite (Nägler and Villa, 2000), seawater (Zhu and MacDougall, 1998; Schmitt et al., 2001), calcium carbonate NIST SRM 915a /915b (e.g. Heuser et al., 2002; Farkaš et al., 2007; Simon et al., 2009 ; Caro et al., 2010; Jörg et al., 2012) and other materials (A.N.U. *Tridacna* standard, in house ultrapure CaCO₃) (Fletcher et al., 1997a; Fletcher et al., 1997b; Skulan et al., 1997). The community endeavored to agree on a uniform basis for Ca studies. Hippler et al. (2003) compared three intra-laboratory reference materials with SRM 915a, which at that time was commonly available. Eisenhauer et al. (2004) suggested to use SRM 915a as an international Ca standard. At present SRM 915a is no longer available and has been replaced with SRM 915b. Two studies compared their two isotope compositions after internal mass fractionation correction and report no detectable difference (Hindshaw et al., 2011; Schiller et al., 2012).

1.2 Reference isotopic compositions

The isotopic composition of standards is an essential parameter that becomes crucial when studying natural isotopic fractionation. A comparison of the data obtained by different laboratories strongly depends on the choice of isotope ratio used as a reference. Currently all isotopic compositions recommended by IUPAC have been determined by mass spectrometry taking into account instrumental fractionation effects in the best possible way (de Laeter et al., 2003), as none can be determined with uncertainties < 1% by absolute gravimetric methods. However studies of fractionation processes require one or two orders of magnitude lower uncertainties. Therefore the geochemical community has agreed on using certain reference materials, defining one of their isotope ratios by convention (with a zero uncertainty by definition). This requires that the outcome of a mass fractionation correction be independent of the isotope ratio chosen as normalization. The case of Ca will be discussed in detail in § 3.1.

Russell et al. (1978) determined the Ca isotope composition of various terrestrial and extraterrestrial materials using the double spike technique. Their double spike was prepared gravimetrically, and isotopic compositions were measured on a single collector TIMS. Data were corrected for instrumental mass-dependent isotope fractionation with different mathematical approaches; Russell et al. (1978) concluded that the exponential law was most accurate. Recently several studies have attempted to re-determine the isotopic composition of Ca. Three approaches have been used so far: (1) mass spectrometer measurements with normalization to one fixed value; (2) total evaporation measurements,

where a sample is measured on TIMS while continuously heating the filament until the sample is completely exhausted; as nominally all ions are collected, their summation should cancel out artefacts due to Rayleigh fractionation on the filament (Fiedler, 1995; Schmitt et al., 2001; Jörg et al., 2012); (3) a vector presentation of TIMS data developed by Shen et al. (2009). An overview of these methods is given by Boulyga (2010) and Jörg et al. (2012).

The present study reviews the isotopic compositions obtained with each of the three approaches (Russell et al., 1978; Jörg et al., 2012; Shen et al., 2002) and provides an internal consistency check for each. The fractionation corrected Ca isotopic compositions are different in these three studies. Russell et al. (1978) proposed $^{42}\text{Ca}/^{44}\text{Ca} = 0.31221$ and $^{40}\text{Ca}/^{44}\text{Ca} = 47.153$ using the gravimetrically defined $^{42}\text{Ca}/^{48}\text{Ca}$ ratio as fixed values. Jörg et al. (2012) proposed $^{42}\text{Ca}/^{44}\text{Ca} = 0.30886$ and $^{40}\text{Ca}/^{44}\text{Ca} = 46.106$ on the basis of the best total evaporation value, whereby they assumed that the measured Ca isotope ratios are only controlled by Langmuir fractionation from the filament, which should be cancelled out in total evaporation measurements. Using $^{42}\text{Ca}/^{44}\text{Ca}$ ratio as correction ratio they derived an isotopic composition of Ca, which differs from that proposed by Russell et al. (1978). The vector analytical method of Shen et al. (2002) is based on a 3D model, with coordinates $x = ^{40}\text{Ca}/^{48}\text{Ca}$, $y = ^{44}\text{Ca}/^{48}\text{Ca}$, $z = ^{42}\text{Ca}/^{48}\text{Ca}$, whereby the true spike or true natural composition can be determined without the need of a reference ratio. Their model assumes a linear mass-dependent fractionation during the measurement. Shen et al. (2002) tested the validity of this assumption by comparing the fractionation-corrected $^{40}\text{Ca}/^{44}\text{Ca}$ normalized to $^{42}\text{Ca}/^{44}\text{Ca} = 0.31031$ with exponential and linear laws. They calculated that the difference between linear and exponential law corrections is < 50 ppm in all cases in their study.

1.3. Fractionation corrections

The new static setup allows using various approaches to correct for instrumental mass fractionation. For unspiked samples traditionally the $^{42}\text{Ca}/^{44}\text{Ca}$ ratio is chosen to correct all other ratios (e.g. Skulan et al., 1997; Hindshaw et al., 2011; Schiller et al., 2012), but also other ratios can be used (Jungck et al., 1984). The application of $^{48}\text{Ca}/^{44}\text{Ca}$ to correct for instrumental fractionation during analysis could appear advantageous over the commonly used $^{42}\text{Ca}/^{44}\text{Ca}$ ratio, as the pair ^{48}Ca - ^{44}Ca has almost the same mass difference as the pair ^{40}Ca - ^{44}Ca . The wider mass range of the correction ratio can be expected to decrease the uncertainty on the normalized $^{40}\text{Ca}/^{44}\text{Ca}$ ratio provided that the fractionation during mass spectrometric analysis follows a simple, well-understood mathematical equation. In the present study the variation of $^{40}\text{Ca}/^{44}\text{Ca}$ is examined as a function of the normalization ratio chosen to correct for mass dependent fractionation.

As already noted by Russell et al. (1978), and reproduced in the present study, the exponential law is the closest empirical representation for the behavior of the isotope fractionation during a mass spectrometer run. The exponential correction for Ca is

$$\frac{\left(\frac{{}^{40}\text{Ca}}{{}^{44}\text{Ca}}\right)_M}{\left(\frac{{}^{40}\text{Ca}}{{}^{44}\text{Ca}}\right)_C} = \left(\frac{\left(\frac{{}^i\text{Ca}}{{}^{44}\text{Ca}}\right)_M}{\left(\frac{{}^i\text{Ca}}{{}^{44}\text{Ca}}\right)_T}\right)^p \quad [\text{Eq. 1}]$$

where M stands for measured, C for corrected, T for the chosen "true value".

$$p = \frac{\ln\left(\frac{m_i}{m_{44}}\right)}{\ln\left(\frac{m_{40}}{m_{44}}\right)}$$

where m_i is the mass of isotope ${}^i\text{Ca}$, with $i = 42$ or 43 or 48 .

While it is generally accepted that the exponential law gives the best empirical fit for the fractionation correction (Russell et al., 1978; Hart and Zindler, 1989; Schiller et al., 2012), it is intuitive that there may be processes during measurements that do not follow the exponential law. This was first mentioned by Russell et al. (1978). Later Jungck et al. (1984) used ${}^{40}\text{Ca}/{}^{44}\text{Ca}$ for correction of the ${}^{48}\text{Ca}/{}^{44}\text{Ca}$ ratio and proposed a modification to the exponential law to eliminate a small residual effect. According to Hart and Zindler (1989), the exponential law might be the best fit only for a limited range of the measurement; they explained such behavior due to reservoir mixing (see below). As pointed out by Naumenko et al. (2013), there are at least two heterogeneous sources of isotope fractionation: the evaporation of ions from the filament, which follows Rayleigh-type fractionation (if the hotspot on the filament is smaller than the area covered by the sample, there may be the additional complication of reservoir mixing as discussed by Hart and Zindler (1989)); and the incomplete transmission of ions emitted from the filament into the collectors, due to the impossibility to focus the whole ion emission that spans a half-space with 2π geometry. This latter point is borne out by the fact that even for elements such as K, whose ionization efficiency approaches 100 %, the total ion yield is rarely higher than 20 %; the missing ions entail a mass-dependent fractionation.

Caro et al. (2010) noticed that at the end of the run there is an evident fractionation trend that is not corrected by the exponential law. Similar residual trends after exponential fractionation correction were observed by Lehn and Jacobson (2015). They further noted that this effect followed the "average mass rule" (Wasserburg et al., 1981), i.e. the residual trend per atomic mass unit was largest for isotope pairs (e.g. ${}^{44}\text{Ca}/{}^{48}\text{Ca}$ vs. ${}^{40}\text{Ca}/{}^{42}\text{Ca}$). Gopalan et al. (2006) and Lehn et al. (2013) proposed a workaround that circumvents the "average mass rule", namely using a double spike having an average mass sufficiently close to the Ca isotope ratios of interest.

An observation of incomplete fractionation correction with the exponential law was also made for Nd isotopes. Upadhyay et al (2008) studied the reservoir mixing and fractionation for Nd isotopes and found up to +70 ppm shift on ${}^{146}\text{Nd}/{}^{144}\text{Nd}$ ratio due to incomplete fractionation correction with the exponential law. Caro et al. (2006) compared the Nd isotope fractionation with and without a magnet inserted in the source during TIMS measurements in positive ion mode. Normally without the magnet the reproducibility of Nd

measurements was 2 ppm for the $^{142}\text{Nd}/^{144}\text{Nd}$ ratio. With inserted magnet the reproducibility was 10 ppm for the same ratio. Caro et al. (2003) suggested an additional correction term to the commonly used exponential correction law. The present study also focuses on the incomplete fractionation correction of Ca with conventional exponential law and test the possibility of applying the additional correction term proposed by Caro et al. (2003) to Ca isotopes.

2. Analytical Methods

The Thermo Scientific Triton *Plus*TM multicollector TIMS used for the present measurements was equipped with a specially developed extra large Faraday cup (L5) for the analysis of ^{40}Ca and a special Faraday cup (H4) with extended mass range for ^{48}Ca , allowing simultaneous measurement of masses 40 to 48 amu (Fig. 1, supplementary materials Fig.S1). Additional zoom lenses and beam dispersion were used to optimally center each beam in the fixed Faraday cups.

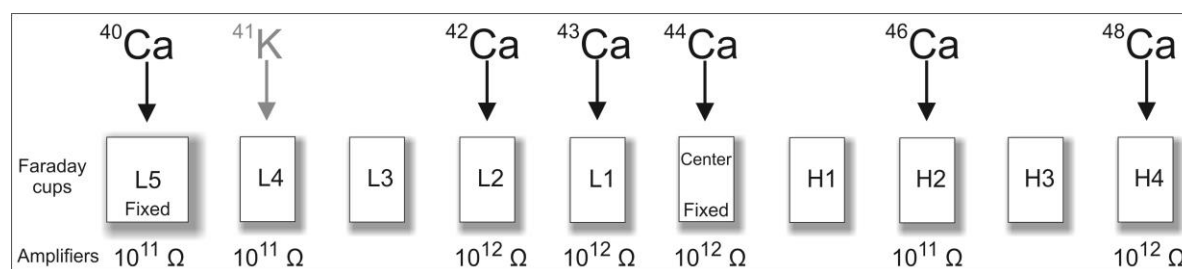


Fig. 1. Scheme of the Faraday cup configuration and amplifiers employed.

The intensity of ^{41}K was monitored on the low-mass cup L4; no K interference was observed in either SRM 915 solution. Since Ca isotopes have high abundance ranges the application of different amplifiers (10^{11} and $10^{12} \Omega$) gave the opportunity to measure high (^{40}Ca) and low (^{43}Ca) intensity beams simultaneously with reduced uncertainties. During the measurements ^{40}Ca was detected with the $10^{11} \Omega$ resistor, signals for ^{42}Ca , ^{43}Ca , ^{44}Ca and ^{48}Ca were amplified with $10^{12} \Omega$ resistors. An additional improvement of the analytical setup would be using a $10^{10} \Omega$ amplifier for the ^{40}Ca beam, allowing measurements with ten times higher Ca amounts, which should further reduce the relative uncertainty by a factor of 3.17. As the present study focused on the analysis of small samples of terrestrial and extraterrestrial samples, it was not anticipated that ^{40}Ca signal intensities would exceed 100-200 pA, and it was decided to sacrifice precision deriving from large ^{40}Ca signals in exchange for accuracy deriving from excluding any potential instrumental artefact caused by non-linear response when comparing small sample signals with large SRM signals. Typical intensities for standards with a high Ca concentration (ca. 0.5 - 1 μg) were ca. 350 pA for ^{40}Ca and ca. 0.5 pA for ^{43}Ca . Gain calibrations were performed every 24 h with a fixed voltage of 3 V applied to each cup and amplifier.

The present study reports Ca isotope compositions measured on NIST standard reference materials SRM 915a and SRM 915b. In view of the geochronological

applications it was desirable to limit sample sizes to $< 1\mu\text{g}$ Ca. In the following "high concentration measurements" refers to Ca loads on the filament of 0.5 - 1 μg and "low concentration measurements" to Ca loads ≈ 100 ng. The simultaneous acquisition ensures high precision measurements of low Ca samples even with unstable signal intensities.

Single zone-refined rhenium filaments were used. After welding, filaments and filament holders were prewashed for 20 s with 1 M HCl and purified Milli-QTM water to dissolve any possible Ca contamination; afterwards filaments were degassed for 45 min at 1500 mA, 30 min at 2000 mA and 70 min at 4000 mA with subsequent oxidizing at room temperature for at least two weeks. SRM solution concentrations were adjusted so that only 1 μl was loaded on filament, so as to keep the ionization hotspot as small as possible. A loading solution containing Ta₂O₅ (Birck, 1986; Nagler and Villa, 2000) was loaded on top of the standard. Filaments were kept at 100 mA during loading, after drying they were brought to glowing at ca. 2500 mA for approximately 5 s. The Ca loading blank was < 30 pg.

During measurements filaments were slowly heated (50 mA/min) until the filament current reached 2800 mA, at which point the signal was focused. Heating resumed with a ramp rate of 25 mA/min up to 3200-3400 mA (ca. 1450⁰C) when the ⁴⁰Ca beam reached 50 pA or 300 pA for low and high concentration measurements respectively. Ramp rates were further decreased to 15 mA/min until the ⁴⁰Ca signal reached the target intensity of 100 pA and 350 pA respectively. The signal was kept on target with an automatic filament current adjustment between blocks. Typical runs consisted of 100 or 150 cycles, except for the total evaporation, each ten cycles being grouped in one block. Each cycle was acquired for 8 s, with 6 s idle time. Peaks were centered before the measurement. Baselines were acquired at the beginning of a run and every three blocks. The signal was focused several times during heating and every 5 blocks during the measurement.

Raw data were corrected online for baseline and amplifier gain. Two off-line instrumental mass-dependent fractionation corrections were tested and compared: (i) exponential law (Eq.1) using six different normalizations: ⁴⁸Ca/⁴⁴Ca, ⁴³Ca/⁴⁴Ca and ⁴²Ca/⁴⁴Ca ratios as proposed by Russell et al. (1978) and by Jorg et al. (2012); (ii) exponential and linear laws using the same three ratios as proposed by Shen et al. (2009). The exponential law using ⁴³Ca/⁴⁴Ca as correction ratio will not be discussed here on account of the low intensity of ⁴³Ca and the ensuing high measurement uncertainty, which is then propagated to the corrected ratios. Uncertainties for weighted means are reported at the 95 % confidence level (1.96 σ), for single measurements with 1 σ standard deviation.

Six total evaporation runs for SRM915a and two for SRM915b (ca. 500 ng and ca. 1000 ng each, respectively) were performed. Total evaporation data were processed in two modes for comparison. The cumulative mode presents data as a summation of isotope intensities, which supposedly minimize the Rayleigh fractionation effects. The cycle mode

allows to eliminate outliers and to calculate the uncertainty of each run based on the scatter of cycles.

It has been reported that Faraday cups in TIMS can suffer degradation from the high intensity ^{40}Ca beam (e.g. Simon et al, 2009; Caro et al, 2010; Hindshaw et al, 2011). The extra large ^{40}Ca Faraday Cup collector was exposed to a total Ca load of *ca.* 64 μg during the preparation of this paper. No drift in $^{40}\text{Ca}/^{44}\text{Ca}$ ratios was observed over the period of June 2014 till February 2015 within the uncertainty of individual measurements. The reproducibility of $^{40}\text{Ca}/^{44}\text{Ca}$ for SRM 915a and SRM 915b is presented in the electronic supplement (Fig.S2 and S3).

3. Results and discussion

3.1 Internal consistency check of Ca isotopic compositions

The internal consistency check for published Ca isotopic compositions was performed using the $^{40}\text{Ca}/^{44}\text{Ca}$ ratio for SRM 915a/b corrected with the exponential law (Eq.1). It is expected that an internally consistent set of Ca isotope ratios will result in a fractionation corrected $^{40}\text{Ca}/^{44}\text{Ca}$ that does not change depending on the correction ratio. In the following, the term “correction ratio” specifies which ratio ($^{42}\text{Ca}/^{44}\text{Ca}$, $^{43}\text{Ca}/^{44}\text{Ca}$ or $^{48}\text{Ca}/^{44}\text{Ca}$) was used to correct the instrumental isotope fractionation of $^{40}\text{Ca}/^{44}\text{Ca}$. The term “correction value” specifies the Ca isotopic composition of the correction ratio as published in three different studies (Russell et al., 1978; Shen et al., 2009; Jörg et al., 2012). The three correction ratios being different in the three cited studies, one obtains nine values for the corrected $^{40}\text{Ca}/^{44}\text{Ca}$ ratio (Table 1, Fig. 2).

correction ratio correction values	$^{42}\text{Ca}/^{44}\text{Ca}$	$^{43}\text{Ca}/^{44}\text{Ca}$	$^{48}\text{Ca}/^{44}\text{Ca}$
Russell et al., 1978. $(^{40}\text{Ca}/^{44}\text{Ca})^{\text{R}}$ 47.153 \pm 3	$(^{40}\text{Ca}/^{44}\text{Ca})^{\text{R}}_{42}$ 47.163 \pm 3	$(^{40}\text{Ca}/^{44}\text{Ca})^{\text{R}}_{43}$ 47.129 \pm 17	$(^{40}\text{Ca}/^{44}\text{Ca})^{\text{R}}_{48}$ 47.163 \pm 5
Jörg et al., 2012. $(^{40}\text{Ca}/^{44}\text{Ca})^{\text{J}}$ 46.106 \pm 19	$(^{40}\text{Ca}/^{44}\text{Ca})^{\text{J}}_{42}$ 46.132 \pm 4	$(^{40}\text{Ca}/^{44}\text{Ca})^{\text{J}}_{43}$ 46.132 \pm 18	$(^{40}\text{Ca}/^{44}\text{Ca})^{\text{J}}_{48}$ 46.100 \pm 6
Shen et al., 2009. $(^{40}\text{Ca}/^{44}\text{Ca})^{\text{Sh}}$ 46.537 \pm 2	$(^{40}\text{Ca}/^{44}\text{Ca})^{\text{Sh}}_{42}$ 46.576 \pm 4	$(^{40}\text{Ca}/^{44}\text{Ca})^{\text{Sh}}_{43}$ 46.768 \pm 19	$(^{40}\text{Ca}/^{44}\text{Ca})^{\text{Sh}}_{48}$ 46.669 \pm 6

Table 1. $^{40}\text{Ca}/^{44}\text{Ca}$ ratio corrected to three correction ratios assuming three different Ca isotopic compositions published in three different papers. Superscripts R, J and Sh refer to Russell et al. (1978), Jörg et al. (2010), and Shen et al. (2009), respectively. Subscripts 42, 43, 48 denote the "correction ratio" ($^{42}\text{Ca}/^{44}\text{Ca}$, $^{43}\text{Ca}/^{44}\text{Ca}$, $^{48}\text{Ca}/^{44}\text{Ca}$) used in the calculation.

The first triplet of corrected $^{40}\text{Ca}/^{44}\text{Ca}$ ratios shown in Table 1 was calculated by assuming as "correction ratios" the $^{42}\text{Ca}/^{44}\text{Ca}$, $^{43}\text{Ca}/^{44}\text{Ca}$ and $^{48}\text{Ca}/^{44}\text{Ca}$ ratios as measured

by Russell et al. (1978). They are denoted by the superscript "R" and the subscript referring to the respective correction ratio: $(^{40}\text{Ca}/^{44}\text{Ca})^{\text{R}}_{42}$, $(^{40}\text{Ca}/^{44}\text{Ca})^{\text{R}}_{43}$, $(^{40}\text{Ca}/^{44}\text{Ca})^{\text{R}}_{48}$ (see Table 1). If the exponential law is accurate and the Ca isotope compositions reported by Russell et al. (1978) are internally consistent, then the three calculated ratios must coincide: $(^{40}\text{Ca}/^{44}\text{Ca})^{\text{R}}_{42} = (^{40}\text{Ca}/^{44}\text{Ca})^{\text{R}}_{43} = (^{40}\text{Ca}/^{44}\text{Ca})^{\text{R}}_{48}$. Fig. 2 shows that indeed the calculated $^{40}\text{Ca}/^{44}\text{Ca}$ ratios are identical amongst each other. The same procedure was performed with the isotopic composition published by Jörg et al. (2012). The results of our recalculation of our raw data, using the ratios proposed by Jörg et al. (2012) as "correction ratios", are shown in Table 1 with the superscript "J". The recalculated $^{40}\text{Ca}/^{44}\text{Ca}$ values are not consistent at the 2σ level, but they are consistent at the 3σ level.

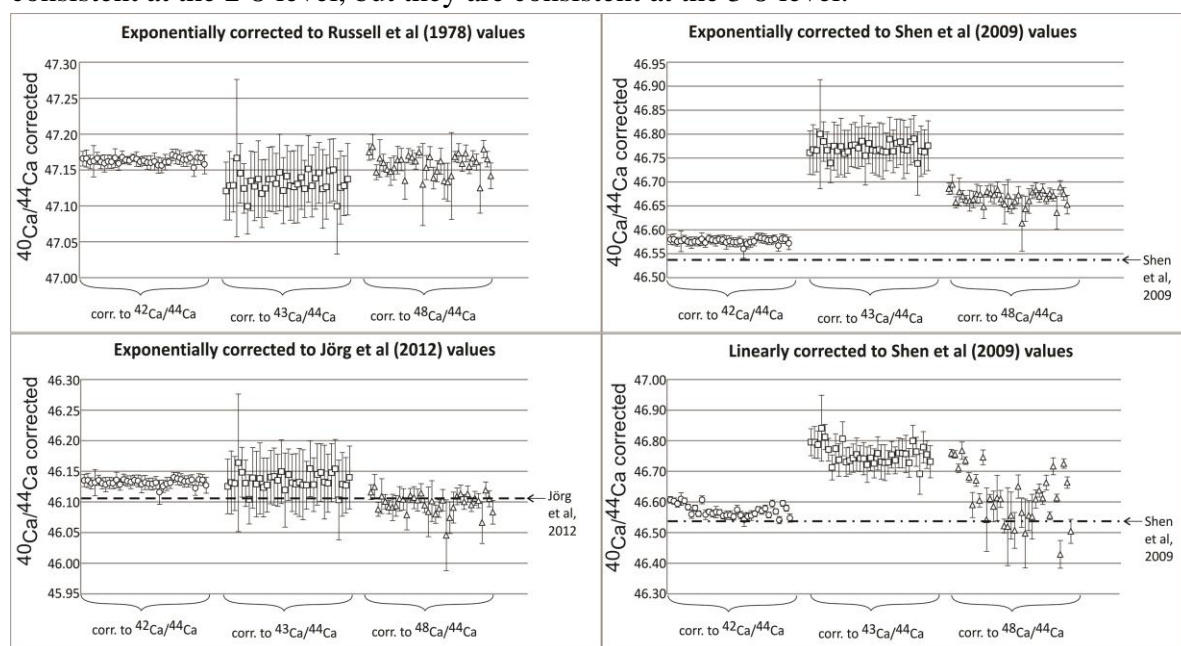


Figure 2. Comparison of the normalization protocols for 25 high intensity measurements of SRM 915a. The $^{40}\text{Ca}/^{44}\text{Ca}$ ratio was corrected with the exponential law applying three "correction ratios" $^{42}\text{Ca}/^{44}\text{Ca}$ (circles), $^{43}\text{Ca}/^{44}\text{Ca}$ (squares) and $^{48}\text{Ca}/^{44}\text{Ca}$ (triangles) provided by three distinct studies (Russell et al., 1978; Shen et al., 2009 and Jörg et al., 2012). The dashed lines refer to the $^{40}\text{Ca}/^{44}\text{Ca}$ ratios for SRM 915a by Shen et al (2009) and 915b by Jörg et al (2012); note that Russell et al (1978) did not have SRM 915a available. Our results show that when the $^{42}\text{Ca}/^{44}\text{Ca}$ ratio of Jörg et al (2012) is used to correct the measured $^{40}\text{Ca}/^{44}\text{Ca}$ ratio, the resulting $^{40}\text{Ca}/^{44}\text{Ca}$ ratio is inconsistent with that proposed by Jörg et al (2012) at the 0.5 ‰ level. The inconsistency with the Shen et al (2009) normalization is 5 ‰. Linear fractionation corrections were applied to $^{40}\text{Ca}/^{44}\text{Ca}$ using the values of Shen et al. (2009). The Ca isotope composition from Shen et al. (2009) yields distinct values for $^{40}\text{Ca}/^{44}\text{Ca}$ depending which "correction ratio" is used during the instrumental mass-dependent fractionation correction.

The third internal consistency check using the isotopic compositions presented by Shen et al. (2009) shows that the calculated $(^{40}\text{Ca}/^{44}\text{Ca})^{\text{Sh}}$ ratios are inconsistent amongst each other and with the $^{40}\text{Ca}/^{44}\text{Ca}$ ratio proposed by Shen et al. (2009) as the "true" value (Fig. 2). One probable cause for this lack of internal consistency is that Shen et al. (2009) applied a linear fractionation correction. The linearity check was performed for mass

differences $\Delta m=2$ and $\Delta m=4$. Shen et al. (2009) extrapolated the linear correction to isotope ratios with higher mass range: $^{40}\text{Ca}/^{48}\text{Ca}$, $^{44}\text{Ca}/^{48}\text{Ca}$ and $^{42}\text{Ca}/^{48}\text{Ca}$. These ratios have large mass differences and their fractionation does not strictly follow the linear law. The inaccuracy of the linear law to correct the $^{48}\text{Ca}/^{44}\text{Ca}$ ratio was first demonstrated by Russell et al. (1978), who found a systematic bias of $> 5 \text{ ‰}$. Using $^{40}\text{Ca}/^{48}\text{Ca}$ for the correction gives an even greater shift. This implies that the assumption of linear fractionation vectors for $^{40}\text{Ca}/^{48}\text{Ca}$, $^{44}\text{Ca}/^{48}\text{Ca}$ and $^{42}\text{Ca}/^{48}\text{Ca}$ in the vector analytical method is not applicable.

3.2 Improved exponential correction law for Ca

Similarly to Jungck et al. (1984), Hart and Zindler (1989), Upadhyay et al (2008) and Caro et al. (2010), in the present work it was observed that the $^{40}\text{Ca}/^{44}\text{Ca}$ ratio in very long runs showed a residual trend after the exponential fractionation correction. This residual trend can reach 0.5 ‰ when the "correction ratio" was $^{42}\text{Ca}/^{44}\text{Ca}$ and 1.5 ‰ when the "correction ratio" was $^{48}\text{Ca}/^{44}\text{Ca}$. Fig. 3 shows the behavior of $^{40}\text{Ca}/^{44}\text{Ca}$ corrected with $^{42}\text{Ca}/^{44}\text{Ca}$ (open circles) and $^{48}\text{Ca}/^{44}\text{Ca}$ (triangles) as a function of the number of measured cycles.

In the plot chosen to assess the functional form of the fractionation correction, namely $X = (^{40}\text{Ca}/^{44}\text{Ca})_{\text{measured}} / (^{40}\text{Ca}/^{44}\text{Ca})_{\text{corrected}}$, $Y = (^{48}\text{Ca}/^{44}\text{Ca})_{\text{measured}} / (^{48}\text{Ca}/^{44}\text{Ca})_{\text{corrected}}$ (Russell et al., 1978), both abscissa and ordinate are a measure of the progressively increasing mass fractionation. When the filament is approaching exhaustion, the abscissa and ordinate of the present measurements drop to much lower values than those of the corresponding figure of Russell et al. (1978), that is, the fractionation is more extreme. The corrected isotope ratios still all lie on the line labelled "exponential", indicating that at least to first order the dominant process that causes isotope fractionation can be best described with the exponential fractionation law.

Fig. 4b additionally displays a time-series of the progressively increasing mass fractionation. The trajectory trends downward, meaning that the correction of the $^{40}\text{Ca}/^{44}\text{Ca}$ ratio with the exponential law based exclusively on the $^{42}\text{Ca}/^{44}\text{Ca}$ ratio becomes increasingly inaccurate as the run approaches complete sample exhaustion.

A similar observation of incomplete fractionation correction of the Nd isotope ratios with the exponential law was made by Caro et al. (2006). They also pointed out a correlation factor $r^2 = 0.6-0.8$ between corrected ratios. A similar correlation factor $r^2 = 0.7$ is seen between $(^{40}\text{Ca}/^{44}\text{Ca})_{\text{R}_{42}}$ and $(^{48}\text{Ca}/^{44}\text{Ca})_{\text{R}_{42}}$ (Fig. 5). Caro et al (2006) proposed an additional, second-order-correction term to the commonly used exponential correction law. The adaptation to Ca, shown here, of the equation proposed for Nd by Caro et al. (2006, eq. 4) eliminates the residual trend for the corrected Ca isotope ratios (closed circles in Fig. 3). This equation requires two fixed correction ratios: one to estimate the fractionation factor and second one to estimate the mass dependence of the residual trend:

Chapter 2. TIMS measurements of full range of Ca isotopes

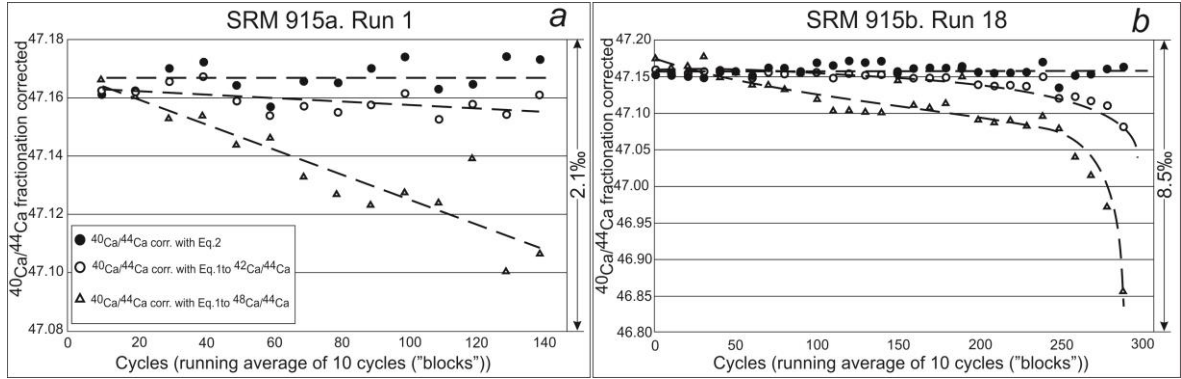


Fig. 3. Example of fractionation correction of SRM 915a runs with the exponential law (eq.1) (open circles and triangles) and with eq.2 (filled circles); note that the scale is expanded relative to Fig.2. The conventional procedure of taking the average of all blocks gives divergent values: triangles give 47.142 ± 12 and 47.043 ± 77 for SRM 915a run 1 and SRM 915b run 18.3, respectively; open circles give correspondingly 47.159 ± 4 and 47.127 ± 22 . The correction following eq. 2 (filled circles) gives 47.167 ± 6 and 47.157 ± 19 ; the extent of the bias in the example of SRM 915a is 0.4‰ for the $(^{40}\text{Ca}/^{44}\text{Ca})_{R_{48}}$ ratio and 0.05‰ for the $(^{40}\text{Ca}/^{44}\text{Ca})_{R_{42}}$ ratio. Especially the latter is a second-order effect which could be overlooked, were it not for the monotonic trend most clearly visible at high depletion (Fig.3b)

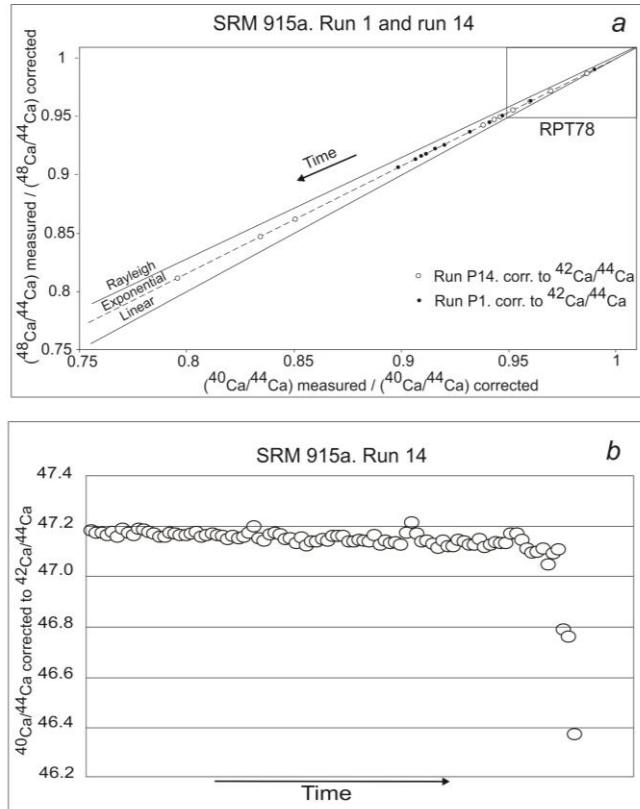


Fig. 4. Exponential behaviour of two SRM 915a runs. The range marked "RPT78" refers to the similar figure published by Russell et al (1978).

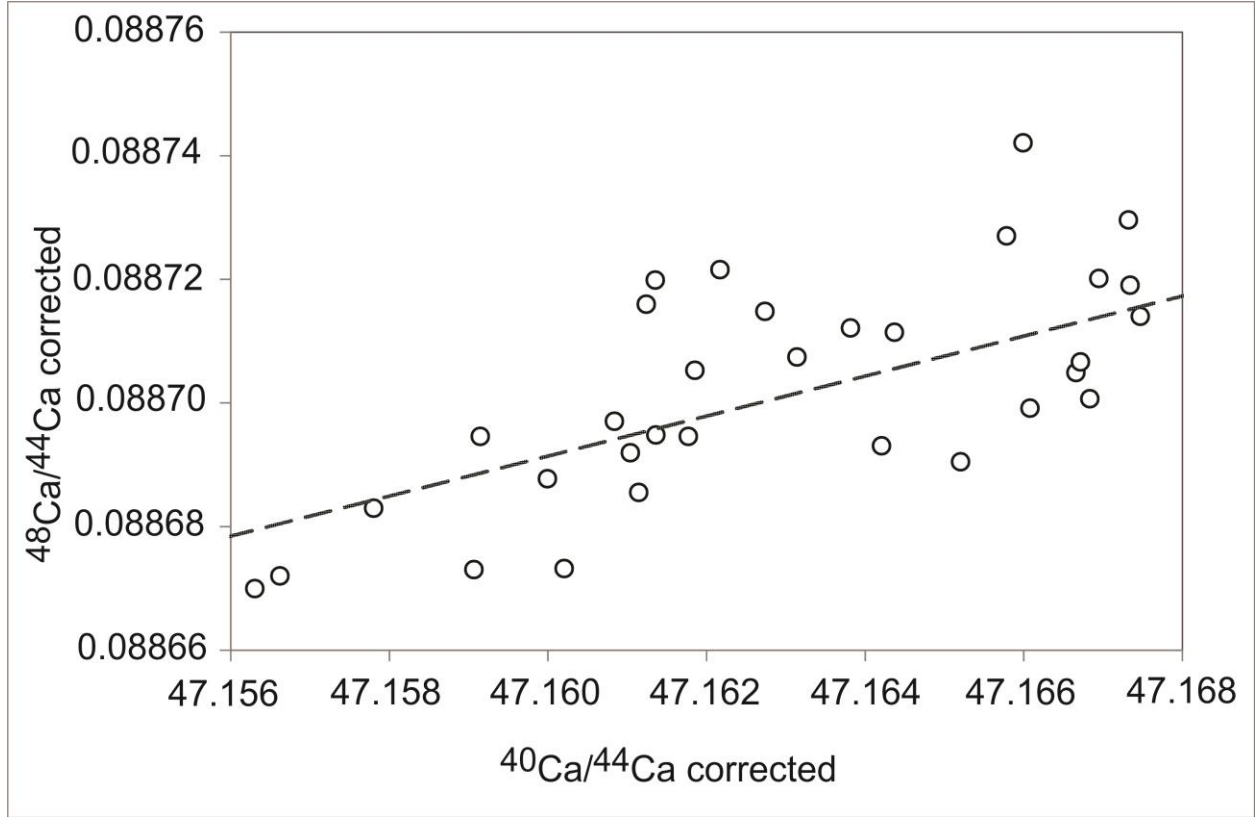


Fig. 5. The correlation coefficient of $R^2=0.7$ between $^{40}\text{Ca}/^{44}\text{Ca}$ and $^{48}\text{Ca}/^{44}\text{Ca}$ corrected to $^{42}\text{Ca}/^{44}\text{Ca}$ with the simple exponential law. Results for SRM 915a, 34 measurements.

$$\frac{\left(\frac{^{40}\text{Ca}}{^{44}\text{Ca}}\right)_M}{\left(\frac{^{40}\text{Ca}}{^{44}\text{Ca}}\right)_C} = \left(\frac{\left(\frac{^{48}\text{Ca}}{^{44}\text{Ca}}\right)_M}{\left(\frac{^{48}\text{Ca}}{^{44}\text{Ca}}\right)_T}\right)^{f(^{40}\text{Ca})} \cdot \left(\frac{\left(\frac{^{42}\text{Ca}}{^{44}\text{Ca}}\right)_C}{\left(\frac{^{42}\text{Ca}}{^{44}\text{Ca}}\right)_T}\right)^A \quad [\text{Eq. 2}]$$

where M stands for measured, C for corrected, T for “true”; f and A will be defined below. In this example the values from Russell et al. (1978) are used: $\left(\frac{^{48}\text{Ca}}{^{44}\text{Ca}}\right)_T = 0.08871$, $\left(\frac{^{42}\text{Ca}}{^{44}\text{Ca}}\right)_T = 0.31221$. The first term is the exponential correction law following Russell et al. (1978) and the second term is the correction coefficient which accounts for mass discrepancies between corrected and correction ratios derived by Caro et al. (2003). In this example $^{40}\text{Ca}/^{44}\text{Ca}$ is corrected with $^{48}\text{Ca}/^{44}\text{Ca}$ (the exponential term) and $^{42}\text{Ca}/^{44}\text{Ca}$ is used to estimate the mass-dependent drift of the corrected value. The fractionation factor, $f(^{40}\text{Ca})$, is given by:

$$f(^{40}\text{Ca}) = \frac{\ln\left(\frac{m_{40}}{m_{44}}\right)}{\ln\left(\frac{m_{48}}{m_{44}}\right)} \quad [\text{Eq. 3}]$$

In the second term of equation 2, $\left(\frac{^{42}\text{Ca}}{^{44}\text{Ca}}\right)_c$ is calculated from the conventional exponential correction law (modified Eq. 1):

$$\frac{\left(\frac{^{42}\text{Ca}}{^{44}\text{Ca}}\right)_M}{\left(\frac{^{42}\text{Ca}}{^{44}\text{Ca}}\right)_c} = \left(\frac{\left(\frac{^{48}\text{Ca}}{^{44}\text{Ca}}\right)_M}{\left(\frac{^{48}\text{Ca}}{^{44}\text{Ca}}\right)_T}\right)^{f(^{42}\text{Ca})} \quad [\text{Eq. 4}]$$

where $f(^{42}\text{Ca})$ is calculated from an equation similar to Eq. 3:

$$f(^{42}\text{Ca}) = \frac{\ln\left(\frac{m_{42}}{m_{44}}\right)}{\ln\left(\frac{m_{48}}{m_{44}}\right)} \quad [\text{Eq. 5}]$$

The coefficient A in Eq. 2 is given by:

$$A = \frac{\ln\left(\frac{m_{40}}{m_{44}}\right) \cdot \ln\left(\frac{m_{40}}{m_{48}}\right)}{\ln\left(\frac{m_{42}}{m_{44}}\right) \cdot \ln\left(\frac{m_{42}}{m_{48}}\right)} \quad [\text{Eq. 6}]$$

This additional term corrects Ca fractionation over most of the range. Fig. 3 illustrates the difference between three fractionation corrections. Simply correcting $^{40}\text{Ca}/^{44}\text{Ca}$ with $^{48}\text{Ca}/^{44}\text{Ca}$ (open triangles) produces a steep trend (ca. 1-3 ‰ over the duration of the run); correcting $^{40}\text{Ca}/^{44}\text{Ca}$ with $^{42}\text{Ca}/^{44}\text{Ca}$ (open circles) results in a smaller, but still evident trend. Only the additional term in eq. 2 (closed circles) completely removes the trend. There can be extreme cases, when the sample on the filament is exhausted, when the last few cycles yield extremely highly fractionated ratios. In these instances, not even eq. 2 corrects the fractionation completely (even if the bias is reduced below 1 ‰). Such data have to be eliminated manually.

For large samples ($> 1 \mu\text{g Ca}$), if a sample does not approach exhaustion during a run, the simple exponential law correction of $^{40}\text{Ca}/^{44}\text{Ca}$ to $^{42}\text{Ca}/^{44}\text{Ca}$ is sufficient and an application of Eq. 2 makes no detectable difference relative to Eq. 1. Sample sizes $< 1 \mu\text{g Ca}$ can show a decreasing trend in $^{40}\text{Ca}/^{44}\text{Ca}$ (see Fig. 3), a sign of incomplete correction that requires eq. 2. In the present study 19 out of 35 high intensity measurements for SRM 915a show no obvious trend with the simple exponential correction to $^{42}\text{Ca}/^{44}\text{Ca}$; 11 measurements show a visible trend over the range of a run; another five measurements might have signs of incomplete correction at the end of a run. We consider a trend to be present when weighted error fitting of the data returns an uncertainty envelope that does not include the horizontal line (i.e. the slope differs from zero by more than 2σ of the calculated slope uncertainty). The data for SRM 915a, shown in the supplementary materials, hint at an offset between $^{40}\text{Ca}/^{44}\text{Ca}$ corrected with $^{43}\text{Ca}/^{44}\text{Ca}$ and with $^{42}\text{Ca}/^{44}\text{Ca}$. Currently it is not possible to judge if this shift is significant, and if so, if it is due to incomplete exponential correction or some other factors.

The correction with $^{48}\text{Ca}/^{44}\text{Ca}$ yields isotope ratios for $^{40}\text{Ca}/^{44}\text{Ca}$ that show a downward fractionation trend in most of the measurements. The use of $^{48}\text{Ca}/^{44}\text{Ca}$ as the "correction ratio", or of any other ratio with a large mass range (e.g. $^{48}\text{Ca}/^{42}\text{Ca}$, $^{48}\text{Ca}/^{43}\text{Ca}$),

is possible only with utilization of Eq. 2. This can be critical when using double spikes (e.g. ^{48}Ca - ^{43}Ca , ^{48}Ca - ^{42}Ca , ^{46}Ca - ^{42}Ca , ^{46}Ca - ^{43}Ca). The incomplete fractionation correction produces an artifact on the corrected value by shifting $^{40}\text{Ca}/^{44}\text{Ca}$ towards lower values (see Fig. 3).

Similar behavior is also seen in total evaporation runs where the fractionation is pushed to the limit (the data for the eight total evaporation runs can be found in supplementary materials Table S3, fig.S4, S5). The fractionation corrected total evaporation runs, displayed in cycle mode, show similar signs of incomplete fractionation correction at the end of each run. Sometimes incomplete fractionation correction can be seen during the whole run and even in cumulative mode (supplementary materials Fig.S6 and S7). Smaller Ca loads were observed to have lower total ion yields; these runs suffer most strongly from incomplete fractionation correction (see fig.S4 and S5 for P17). The uncorrected total evaporation $^{40}\text{Ca}/^{44}\text{Ca}$ ratios vary between 42.8 and 44.2 for SRM915a. These values are ca. 7-9 % lower relative to those by Russell et al. (1978). The breadth of their variation, ± 1.5 %, might be due to the loss of ions either at the beginning of a run, when the signal is focused, or at the end when the signal is decreasing rapidly. The total evaporation approach also neglects the importance of fractionation during source focusing of the ions. As the total Ca ion yield in ideal cases is given by DePaolo (1988) as 0.1 %, the present total evaporation runs with lower yields (0.02 - 0.09 %) (see Table S3) are likely to have undergone additional mass fractionation.

A unified approach to mass fractionation correction may be possible according to the following argumentation. The very cause of mass fractionation in thermal ionization mass spectrometry is incompletely understood. A number of effects undoubtedly play a role: Rayleigh distillation of the evaporating filament load, optical aberrations that occur when ions emitted in non-axial directions are deflected back into axis, superposed ion emission from filament domains at different temperatures, etc. The relative importance of these effects is variable, and the equations governing them are different. No quantitative mathematical-physical formulation from first principles has been successfully attempted to date. What is available are empirical equations that can be interpolated between, but not extrapolated beyond, controlled laboratory constraints. The hypothesis by Russell et al. (1978) that mass fractionation follows an exponential law amounts to stating that, to first order, the sum of the effects listed above is described by Eq. 1. It provides no physical model why the functional form of mass fractionation should be exactly exponential.

The second-order term in Eq. 2 is an empirical correction of the empirical law in Eq. 1. As such, it is not based on first principles. It is required because the exponential law breaks down for very large depletions of the sample load. It is likely that a source of residual trends is the use of one single equation to describe a superposition of heterogeneous physical process.

Filament reservoir mixing as a predominant source of non-exponential mass fractionation is not a satisfactory explanation for the observations of the present study. When the filament load is almost entirely depleted at the end of a long run it is expected that the remaining Ca reservoirs on the filament be closest to thermal equilibrium relative to the beginning of the measurement. The present observations suggest that sample with the lowest incidence of reservoir mixing have the most extreme residual trends.

The static measurement of the whole range of Ca isotopes allows to study fractionation processes with improved precision. The application of eq. 2 to correct the instrumental mass-dependent fractionation strongly reduces artifacts due to an incomplete fractionation correction.

3.3 Ca isotopic composition of SRM 915a and SRM 915b

Thirty one low intensity and 28 high intensity measurements of SRM 915b are compared with 8 low intensity and 35 high intensity measurements of SRM 915a. The raw $^{40}\text{Ca}/^{44}\text{Ca}$ data were corrected with a simple exponential fractionation law (Eq. 1) using different "correction ratios" (as described in § 3.1.), as well as with the improved exponential law according to Eq. 2. The raw and corrected data are shown in the supplementary materials. As the Russell et al. (1978) correction values are the most internally consistent ones (see § 3.1.), they will be used in the following to compare the present results with other studies. The isotopic composition of SRM 915a and SRM 915b obtained here with the conventional exponential law (Eq. 1) is presented in Table 2. The $^{40}\text{Ca}/^{44}\text{Ca}$ ratio obtained following Eq. 2 is presented in Table 3 together with a comparison with data from the literature. The uncertainty of our results is limited by the sample size chosen for this study, $< 1 \mu\text{g}$.

For SRM 915a the corrected $^{40}\text{Ca}/^{44}\text{Ca}$ ratio (Table 3, Fig. 6) is identical with that obtained by Caro et al. (2010). There is no resolvable difference between $(^{40}\text{Ca}/^{44}\text{Ca})_{42}^{\text{R}} = 47.1635 \pm 28$, $(^{40}\text{Ca}/^{44}\text{Ca})_{48}^{\text{R}} = 47.1627 \pm 43$, and $^{40}\text{Ca}/^{44}\text{Ca} = 47.1649 \pm 47$ when Eq. 2 is used for fractionation correction, even though incomplete fractionation correction at the permil level can be seen in Fig. 3. Furthermore, the measured $^{48}\text{Ca}/^{40}\text{Ca}$ ratio of SRM 915a was corrected using $^{42}\text{Ca}/^{44}\text{Ca} = 0.31221$ (Russell et al., 1978) as the normalization ratio and yielded $^{48}\text{Ca}/^{40}\text{Ca} = 0.00188081 \pm 23$ [0.12 ‰] with Eq. 1 for 43 high intensity measurements (see supplementary materials).

	$^{40}\text{Ca}/^{44}\text{Ca}$	$^{42}\text{Ca}/^{44}\text{Ca}$	$^{43}\text{Ca}/^{44}\text{Ca}$	$^{48}\text{Ca}/^{44}\text{Ca}$
Russell et al., 1978	47.153 \pm 3	0.31221 \pm 2	0.06486 \pm 1	0.08871 \pm 2
Caro et al., 2010	47.1622 \pm 16	fixed to 0.31221		N.D.
This study SRM 915a	47.1635 \pm 28	fixed to 0.31221	0.0648716 \pm 68	0.0887045 \pm 88
This study SRM 915b	47.1532 \pm 38	fixed to 0.31221	0.0648707 \pm 63	0.088683 \pm 12

Table 2. Isotope compositions of SRM 915a and SRM 915b obtained in this study with the exponential law (eq.1) and normalization to $^{42}\text{Ca}/^{44}\text{Ca} = 0.31221$ (Russell et al., 1978). Values for this study are calculated in Isoplot 3.75 (Ludwig, 2012) as weighted mean. Absolute uncertainties, expressed at the 95 % confidence level (1.96 σ), are referred to the last digits. The Ca isotopic composition reported by Caro et al. (2010) does not include the $^{48}\text{Ca}/^{44}\text{Ca}$ ratio. Additional data can be found in the electronic supplement.

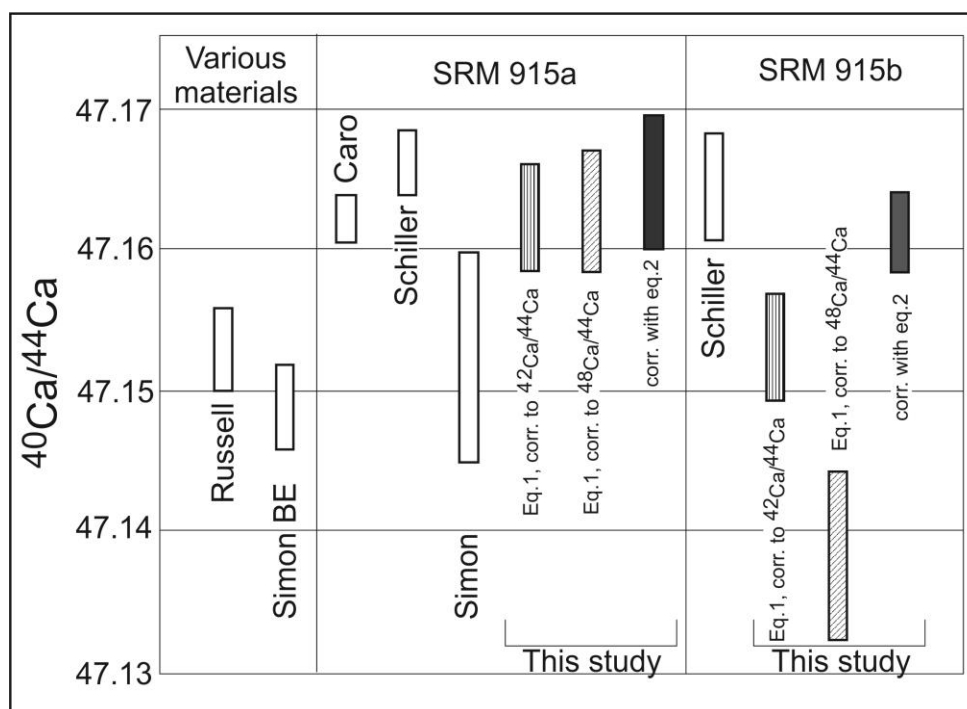


Fig. 6. Comparison of published $^{40}\text{Ca}/^{44}\text{Ca}$ values for NIST SRM 915 a/b and other materials. All literature data were normalized to $^{42}\text{Ca}/^{44}\text{Ca}=0.31221$ of Russell et al (1978), the assumed fractionation laws are noted in table 3. "BE" means Bulk Earth (Simon et al., 2009). "Corr." refers to the diverse corrections assessed in the present study.

Publication	Sample	$^{40}\text{Ca}/^{44}\text{Ca}$	\pm	Method		
				Mass spectrometer / method / measured masses	Approach	Correction law for the instrumental mass dependent fractionation
Russell et al 1978	various materials	47.153	0.003	single collector TIMS	double spike	Exponential
Simon et al 2009	Bulk Earth	47.1487	0.003	m.c. TIMS, static, 40-44	norm. to $^{42}\text{Ca}/^{44}\text{Ca}=0.31222$	Exponential
Shen et al 2008	SRM 915a	46.537	0.002	m.c. TIMS, dynamic, 40-48	vector analytical	"Linear"
Simon et al 2009	SRM 915a	47.1525	0.0074	m.c. TIMS, static, 40-44	norm. to $^{42}\text{Ca}/^{44}\text{Ca}=0.31222$	Exponential
Caro et al 2010	SRM 915a	47.1622	0.0016	m.c. TIMS, dynamic, 40-44	norm. to $^{42}\text{Ca}/^{44}\text{Ca}=0.31222$	Exponential
Schiller et al 2012	SRM 915a	47.1662	0.0023	m.c. TIMS, static, 40-44	norm. to $^{42}\text{Ca}/^{44}\text{Ca}=0.31222$	Power
This work	SRM 915a	47.1635	0.0028	m.c. TIMS, static, 40-48	norm. to $^{42}\text{Ca}/^{44}\text{Ca}=0.31222$	Exponential (Eq.1)
	SRM 915a	47.1627	0.0043	m.c. TIMS, static, 40-48	norm. to $^{48}\text{Ca}/^{44}\text{Ca}=0.08871$	Exponential (Eq.1)
	SRM 915a	47.1649	0.0047	m.c. TIMS, static, 40-48	norm. to $^{48}\text{Ca}/^{44}\text{Ca}=0.08871$ and $^{42}\text{Ca}/^{44}\text{Ca}=0.31222$	Improved exponential (Eq. 2)
Schiller et al 2012	SRM 915b	47.1645	0.0038	m.c. TIMS, static, 40-44	norm to $^{42}\text{Ca}/^{44}\text{Ca}=0.31221$	Power
Jörg et al 2012	SRM 915b	46.106	0.019	m,c TIMS, dynamic, 40-48	average of total evaporation and Langmuir recalculation of incipient emission	No correction
This work	SRM 915b	47.1532	0.0038	m.c. TIMS, static, 40-48	norm. to $^{42}\text{Ca}/^{44}\text{Ca}=0.31222$	Exponential (Eq.1)
	SRM 915b	47.1384	0.0060	m.c. TIMS, static, 40-48	norm. to $^{48}\text{Ca}/^{44}\text{Ca}=0.08871$	Exponential (Eq.1)
	SRM 915b	47.1613	0.0028	m.c. TIMS, static, 40-48	norm. to $^{48}\text{Ca}/^{44}\text{Ca}=0.08871$ and $^{42}\text{Ca}/^{44}\text{Ca}=0.31222$	Improved exponential (Eq. 2)

Table 3. Comparison of published $^{40}\text{Ca}/^{44}\text{Ca}$ values. The values in this work are calculated in Isoplot 3.75 (Ludwig, 2012) as weighted mean for 8 low intensity and 35 high intensity measurements of SRM 915a; 31 low intensity and 28 high intensity measurements for SRM 915b. Uncertainties in this work are calculated as 95% conf. (1.96 σ) error. M.c. TIMS states for multicollector thermal ionization mass spectrometer, norm. for normalization.

The $^{40}\text{Ca}/^{44}\text{Ca}$ ratios of SRM 915b, corrected for fractionation using Eq. 1, $(^{40}\text{Ca}/^{44}\text{Ca})_{42}^{\text{R}} = 47.1532 \pm 38$ and $(^{40}\text{Ca}/^{44}\text{Ca})_{48}^{\text{R}} = 47.1384 \pm 60$, are analytically different from the corresponding corrected ratios of SRM 915a. This cannot be due to discrepant "correction values" of the "correction ratio", as the weighted mean of $^{48}\text{Ca}/^{44}\text{Ca}$ (corrected with $^{42}\text{Ca}/^{44}\text{Ca}$) is 0.088683 ± 12 , and thus identical to the Russell et al. (1978) value of 0.08871 ± 2 . This points instead to an incomplete fractionation correction of $^{40}\text{Ca}/^{44}\text{Ca}$ with the exponential law (Eq. 1) when $^{48}\text{Ca}/^{44}\text{Ca}$ is utilized as "correction ratio". This effect was more prominent for SRM 915b than for SRM 915a because of a different measurement protocol. Each filament with SRM 915b was measured several times until the sample was strongly depleted. As a consequence the $^{40}\text{Ca}/^{44}\text{Ca}$ ratio was incompletely corrected with Eq. 1. The application of Eq. 2 removes the offset and brings the $^{40}\text{Ca}/^{44}\text{Ca} = 47.1613 \pm 28$ in agreement with SRM 915a.

The reproducibility of results for low Ca concentration samples (100-200 ng) was studied in detail on SRM 915b as such concentrations are likely to be encountered for some specific cases like K-Ca dating of minerals. Low Ca concentrations in natural samples and Al residues after column separation lead to short, unstable signals during data acquisition. The uncertainty of such measurements can be decreased with measurements of the full range of Ca isotopes, as the static method is less demanding for signal stability. Even short-lived signals can be measured with sufficient precision. A 0.5 ‰ uncertainty on the $^{40}\text{Ca}/^{44}\text{Ca}$ ratio was obtained for 100 ng samples exponentially corrected to $^{42}\text{Ca}/^{44}\text{Ca}$.

4. Conclusions

1. No Faraday cup degradation was observed over the period of eight months.
2. The simultaneous acquisition of all Ca isotopes by use of a specially developed collector geometry allows sub-permil precision of Ca isotope measurements of sub- μg samples.
3. Precise measurement of ^{40}Ca - ^{48}Ca makes it possible both to assess the internal consistency of different fractionation corrections from the literature and to propose an improved mathematical formulation.
4. The $^{40}\text{Ca}/^{44}\text{Ca}$ ratios of SRM 915a (47.1649 ± 0.0047) and SRM 915b (47.1613 ± 0.0028) obtained in the present study are indistinguishable from that measured by Caro et al. (2010) on SRM 915a.
5. The Ca isotopic composition proposed by Shen et al. (2009) is internally inconsistent and cannot be used for correction of TIMS measurements with an exponential fractionation law.
6. An incomplete mass fractionation correction using Eq. 1 is observed when measurements were pushed to large depletions of the filament load. Eq. 2 is required to remove this inaccuracy.

Appendix A. Supplementary data

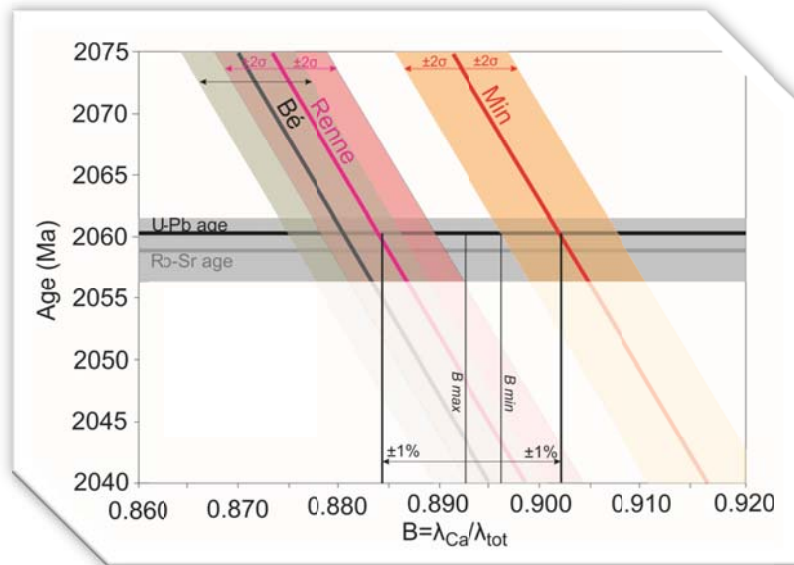
Supplementary data associated with this article can be found in the online version, at <http://dx.doi.org/10.1016/l.ijms.2015.07.012>

References

- Amini, M., Eisenhauer, A., Böhm, F., Holmden, C., Kreissig, K., Hauff, F., Jochum, K.P., 2009. Calcium Isotopes ($\delta^{44}/^{40}\text{Ca}$) in MPI-DING Reference Glasses, USGS Rock Powders and Various Rocks: Evidence for Ca Isotope Fractionation in Terrestrial Silicates. *Geostandards and Geoanalytical Research* 33, 231-247.
- Birck, J.L., 1986. Precision K-Rb-Sr isotopic analysis: Application to Rb-Sr chronology. *Chemical Geology* 56, 73-83.
- Boulyga, S.F., 2010. Calcium isotope analysis by mass spectrometry. *Mass Spectrometry Reviews* 29, 685-716.
- Bouman, C., Tuttas, D., Deerberg, M., Schwieters, J.B., 2011. Advances in high precision Ca isotope ratio measurements using TIMS. *Mineralogical Magazine* 75, 561.
- Caro, G., Bourdon, B., Birck, J.-L., Moorbath, S., 2003. ^{146}Sm - ^{142}Nd evidence from Isua metamorphosed sediments for early differentiation of the Earth's mantle. *Nature* 423, 428-432.
- Caro, G., Bourdon, B., Birck, J.-L., Moorbath, S., 2006. High-precision $^{142}\text{Nd}/^{144}\text{Nd}$ measurements in terrestrial rocks: Constraints on the early differentiation of the Earth's mantle. *Geochimica et Cosmochimica Acta* 70, 164-191.
- Caro, G., Papanastassiou, D.A., Wasserburg, G.J., 2010. ^{40}K - ^{40}Ca isotopic constraints on the oceanic calcium cycle. *Earth and Planetary Science Letters* 296, 124-132.
- de Laeter, J.R., Böhlke, J.K., De Bièvre, P., Hidaka, H., Peiser, H.S., Rosman, K.J.R., Taylor, P.D.P., 2003. Atomic weights of the elements. Review 2000 (IUPAC Technical Report), *Pure and Applied Chemistry*, p. 683.
- DePaolo, D.J., 1988. Neodymium Isotope Geochemistry. An introduction. Springer-Verlag, Berlin/Heidelberg/ New York/ London/ Paris/ Tokyo.
- Eisenhauer, A., Nögler, T.F., Stille, P., Kramers, J.D., Gussone, N., Bock, B., Fietzke, J., Hippler, D., Schmitt, A.-D., 2004. Proposal for international agreement on Ca notation resulting from discussions at workshops on stable isotope measurements held in Davos (Goldschmidt 2002) and Nice (EGS-AGU-EUG 2003). *Geostandards and Geoanalytical Research* 28, 149-151.
- Fantle, M.S., 2010. Evaluating the Ca isotope proxy. *American Journal of Science* 310, 194-230.
- Farkaš, J., Böhm, F., Wallmann, K., Blenkinsop, J., Eisenhauer, A., van Geldern, R., Munnecke, A., Voigt, S., Veizer, J., 2007. Calcium isotope record of Phanerozoic oceans: Implications for chemical evolution of seawater and its causative mechanisms. *Geochimica et Cosmochimica Acta* 71, 5117-5134.
- Fiedler, R., 1995. Total evaporation measurements: experience with multi-collector instruments and a thermal ionization quadrupole mass spectrometer. *International Journal of Mass Spectrometry and Ion Processes* 146, 91-97.
- Fletcher, I.R., Maggi, A.L., Rosman, K.J.R., McNaughton, N.J., 1997a. Isotopic abundance measurements of K and Ca using a wide-dispersion multi-collector mass spectrometer and low-fractionation ionisation techniques. *International Journal of Mass Spectrometry and Ion Processes* 163, 1-17.
- Fletcher, I.R., McNaughton, N.J., Pidgeon, R.T., Rosman, K.J.R., 1997b. Sequential closure of K-Ca and Rb-Sr isotopic systems in Archaean micas. *Chemical Geology* 138, 289-301.
- Gopalan, K., Kumar, A., 2008. Phlogopite K-Ca dating of Narayanpet kimberlites, south India: Implications to the discordance between their Rb-Sr and Ar/Ar ages. *Precambrian Research* 167, 377-382.
- Gopalan, K., Macdougall, D., Macisaac, C., 2006. Evaluation of a ^{42}Ca - ^{43}Ca double-spike for high precision Ca isotope analysis. *International Journal of Mass Spectrometry* 248, 9-16.
- Hart, S.R., Zindler, A., 1989. Isotope fractionation laws: a test using calcium. *International Journal of Mass Spectrometry and Ion Processes* 89, 287-301.
- Heuser, A., Eisenhauer, A., Gussone, N., Bock, B., Hansen, B.T., Nögler, T.F., 2002. Measurement of calcium isotopes ($\delta^{44}\text{Ca}$) using a multicollector TIMS technique. *International Journal of Mass Spectrometry* 220, 385-397.
- Hindshaw, R.S., Reynolds, B.C., Wiederhold, J.G., Kretzschmar, R., Bourdon, B., 2011. Calcium isotopes in a proglacial weathering environment: Damma glacier, Switzerland. *Geochimica et Cosmochimica Acta* 75, 106-118.

Chapter 2. TIMS measurements of full range of Ca isotopes

- Hippler, D., Schmitt, A.-D., Gussone, N., Heuser, A., Stille, P., Eisenhauer, A., Nögler, T.F., 2003. Calcium isotopic composition of various reference materials and seawater. *Geostandards and Geoanalysis* 27, 13-19.
- Holmden, C., 2005. Measurement of $\delta^{44}\text{Ca}$ using a ^{43}Ca - ^{42}Ca double-spike TIMS technique, Summary of Investigations 2005, CD-ROM ed. Saskatchewan Geological Survey, Sask. Industry Resources, p. 7.
- Jörg, G., Amelin, Y., Kossert, K., Lierse v. Gostomski, C., 2012. Precise and direct determination of the half-life of ^{41}Ca . *Geochimica et Cosmochimica Acta* 88, 51-65.
- Jungck, M.H.A., Shimamura, T., Lugmair, G.W., 1984. Ca isotope variations in Allende. *Geochimica et Cosmochimica Acta* 48, 2651-2658.
- Lehn, G.O., Jacobson, A.D., 2015. Optimization of a ^{48}Ca - ^{43}Ca double-spike MC-TIMS method for measuring Ca isotope ratios ($\delta^{44}/^{40}\text{Ca}$ and $\delta^{44}/^{42}\text{Ca}$): limitations from filament reservoir mixing. *Journal of Analytical Atomic Spectrometry*.
- Lehn, G.O., Jacobson, A.D., Holmden, C., 2013. Precise analysis of Ca isotope ratios ($\delta^{44}/^{40}\text{Ca}$) using an optimized ^{43}Ca - ^{42}Ca double-spike MC-TIMS method. *International Journal of Mass Spectrometry* 351, 69-75.
- Ludwig, K.R., 2012. Isoplot3_75, A Geochronological Toolkit for Microsoft Excel, 3.75 ed, Berkley Geochronology Center
- Nögler, T.F., Villa, I.M., 2000. In pursuit of the ^{40}K branching ratios: K-Ca and ^{39}Ar - ^{40}Ar dating of gem silicates. *Chemical Geology (Isotope Geoscience Section)* 169, 5-16.
- Naumenko, M.O., Mezger, K., Nögler, T.F., Villa, I.M., 2013. High precision determination of the terrestrial ^{40}K abundance. *Geochimica et Cosmochimica Acta* 122, 353-362.
- Ramakumar, K.L., Fiedler, R., 1999. Calibration procedures for a multicollector mass spectrometer for cup efficiency, detector amplifier linearity, and isotope fractionation to evaluate the accuracy in the total evaporation method. *International Journal of Mass Spectrometry* 184, 109-118.
- Russell, W.A., Papanastassiou, D.A., Tombrello, T.A., 1978. Ca isotope fractionation on the Earth and other solar system materials. *Geochimica et Cosmochimica Acta* 42, 1075-1090.
- Schiller, M., Paton, C., Bizzarro, M., 2012. Calcium isotope measurement by combined HR-MC-ICPMS and TIMS. *Journal of Analytical Atomic Spectrometry* 27, 38-49.
- Schmitt, A.-D., Bracke, G., Stille, P., Kiefel, B., 2001. The calcium isotope composition of modern seawater determined by thermal ionisation mass spectrometry. *Geostandards Newsletter* 25, 267-275.
- Shen, J.J.-S., Lee, D.-C., Liang, W.-T., 2009. Absolute Ca isotopic measurements using an improved double spike technique. *Terr. Atmos. Ocean. Sci.* 20, 455-464.
- Simon, J.I., DePaolo, D.J., Moynier, F., 2009. Calcium Isotope Composition of Meteorites, Earth, and Mars. *The Astrophysical Journal* 702, 707-715.
- Skulan, J., DePaolo, D.J., Owens, T., 1997. Biological control of calcium isotopic abundances in the global calcium cycle. *Geochimica et Cosmochimica Acta* 61, 2505-2510.
- Upadhyay, D., Scherer, E.E., Mezger, K., 2008. Fractionation and mixing of Nd isotopes during thermal ionization mass spectrometry: implications for high precision $^{142}\text{Nd}/^{144}\text{Nd}$ analyses. *Journal of Analytical Atomic Spectrometry* 23, 561.
- Wasserburg, G.J., Jacobsen, S.B., DePaolo, D.J., McCulloch, M.T., Wen, T., 1981. Precise determination of Sm-Nd ratios, Sm and Nd isotopic abundances in standard solutions. *Geochimica et Cosmochimica Acta* 45, 2311-2323.
- Zhu, P., MacDougall, J.D., 1998. Calcium isotopes in the marine environment and the oceanic calcium cycle. *Geochimica et Cosmochimica Acta* 62, 1691-1698.



Chapter 3

Assessing the ^{40}K decay constant with
 ^{87}Rb - ^{87}Sr , ^{40}K - ^{40}Ca and ^{40}Ar - ^{39}Ar
 chronometer intercalibration.

Assessing the ^{40}K decay constant with ^{87}Rb - ^{87}Sr , ^{40}K - ^{40}Ca and ^{40}Ar - ^{39}Ar chronometers intercalibration.

Mariia O. Naumenko-Dèzes^{1*}, Thomas F. Nägler¹, Igor M. Villa^{1,2}

¹ *Institute für Geologie, Universität Bern, Baltzerstrasse 1+3, 3012, Bern*

² *Università di Milano Bicocca, Piazza della Scienza 4, 20126 Milano, Italy*

* corresponding author marie@geosphere.ch

In preparation to Geochimica et Cosmochimica Acta

Abstract:

Ar-Ar is one of the most used dating systems. This method has been reported to give ages *ca.* 1% younger than U-Pb ages. This offset may be attributed to an inaccurate ^{40}K decay constant. We attempted to intercalibrate four dating systems taking as a reference U-Pb, as a monitor Rb-Sr and assessing the offset of K-Ca and Ar-Ar ages. Four samples with a known U-Pb age have been studied to meet a requirement of geological “point-like” event and dated with Rb-Sr, K-Ca and Ar-Ar methods. Biotite of the Bolgohtock intrusion, Kotuy, Russia was dated with Ar-Ar age at 225.0 ± 4.8 Ma; lepidolite (Rubikon pegmatite, Namibia) with Rb-Sr at 504.7 ± 4.2 Ma and Ar-Ar at 494.5 ± 8.9 Ma. The Archean Siilinjärvi carbonatite (Finland) Rb-Sr age records a post-emplacement metamorphic event at 1869 ± 10 Ma and Ar-Ar at 1879 ± 23 Ma. The 2058.9 Ma Rb-Sr age of the Phalaborwa coincide with previous U-Pb published ages. K-Ca and Ar-Ar dating for this complex resulted in *ca.* 1% younger ages. Phalaborwa complex may represent a “point-like” magmatic event and was suitable for the ^{40}K decay constant intercalibration. We propose that the ^{40}K decay constant of Min et al. (2000) is the most suitable decay constant for ^{40}K geochronometers, it brings the K-Ca age into an agreement with U-Pb.

1. Introduction

One of the most popular dating systems Ar-Ar (Begemann et al., 2001) was used for determination of the ages for the majority of Geologic Time Scale units (Gradstein et al., 2012; Smith et al., 1998) and its accuracy plays an important role in constraining the age of the planets, durations of processes and their sequence of occurrence. Ar-Ar ages rely on the decay constants of the parent radioactive isotope ^{40}K , which undergoes β^- decay to ^{40}Ca (branch B_{β^-}) as well as decay to ^{40}Ar . The decay scheme to ^{40}Ar consists of three

paths: electron capture with emission of 1460 eV γ -rays (branch $B_{EC,1460}$), which can be recorded with scintillation counting method; β^+ decay (branch B_{β^+}), which contribution is very small; and hypothetical electron capture decay to the ground state of ^{40}Ar (branch $B_{EC,g.s.}$), without emission of the γ -ray. The $B_{EC,g.s.}$ branch was calculated by Bé et al. (2004), but its existence is questioned by some authors (Kwon et al., 2002). Decay branches $B_{Ca} = B_{\beta^-}$ and $B_{Ar} = B_{EC,1460} + B_{EC,g.s.} + B_{\beta^+}$ are equally relevant for Ar-Ar dating, as the total decay constant λ and decay branch of ^{40}Ar (B_{Ar}) are a part of the age equation.

1.1. ^{40}K decay constant determination

The decay constant can be determined by scintillation counting of activity, by accumulation experiments and by geological intercomparison. ^{40}K decay constant was determined with scintillation counting, when either β^+ decay or γ -rays or both together were measured. β^+ decay is experimentally rare, only three experiments were performed to measure it (Engelkemeir et al., 1962; Leutz et al., 1965; Tilley and Madansky, 1959). Electron capture to the ground state cannot be observed directly and must be calculated theoretically. The summary of such experiments have been made by (Audi et al., 1997; Audi et al., 2003; Bé et al., 2014; Beckinsale and Gale, 1969; Endt and van der Leun, 1973). A recent compilation of available physical measurements is present in an online data-base (Bé et al., 2014). This evaluation uses a statistical approach assuming Gaussian distribution of the data. Based on available data, Bé et al. (2014) proposed the total decay constant to be $\lambda_{\text{tot}} = 5.530 \pm 0.013 \cdot 10^{-11} \text{ a}^{-1}$. They calculated branching ratios from the B_{β^-} and $B_{EC, 1460}$ published in 1940-60s. The branch of electron capture to Ar ground state cannot be measured and was calculated theoretically. The suggested branching ratios were $B_{\beta^-} = 89.25 \pm 0.19 \%$, $B_{EC, 1460} = 10.55 \pm 0.11 \%$, $B_{ECgs} = 0.20 \pm 0.10 \%$, $B_{\beta^+} = 0.00100 \pm 0.00012\%$, which sums up to $B_{Ca} = 89.25 \pm 0.17 \%$ ($\pm 0.19 \%$), $B_{Ar} = 10.75 \pm 0.15 \%$ ($\pm 1.40 \%$), 1σ uncertainties. The uncertainties of previously published decay constants were not evaluated for systematic errors by Bé et al. (2014). The dataset uncertainties were treated as purely statistical repeatability of results (Type A evaluation (JCGM, 2012)).

Geological intercomparison is another approach to estimate decay constants. This method is close to accumulation experiments, which can be described as following: the sample of well-known composition and consisting mostly of a pure parent element is measured after a well-defined time span. The amount of accumulated daughter elements produced after decay is a function of the decay constant. The same approach can be used with natural samples containing a parent element in a mineral lattice. A determination of the ^{40}K decay constant by a pure accumulation experiment is complicated due to a low ^{40}K natural abundance. However this approach can be used with old natural minerals containing high amount of K and no Ca in the lattice, which can be measured. The reference age of a sample is determined with other geochronological methods, for example precise U-Pb or Rb-Sr. This approach for the ^{40}K decay system was first performed with comparison of K-Ar and U-Pb ages for a wide range of rocks from 4500 to 267 Ma by

Wetherill et al. (1956). Though some of their samples had discrepancies in ages up to 7%, constants determined with this method were in use by the geochronological community for a decade.

1.2. ^{40}K decay constant in geochronology

The recommended decay constant for geochronological community became the value of Steiger and Jäger (1977) $\lambda_{\beta^-} = 4.962 * 10^{-10} \text{ a}^{-1}$ and $\lambda_{^{40}\text{Ar}} = 0.581 * 10^{-10} \text{ a}^{-1}$, $\lambda_{\text{tot}} = 5.543 * 10^{-10} \text{ a}^{-1}$. This decay constants were based on the compilation of activity data of Beckinsale and Gale (1969) recalculated to the precise $^{40}\text{K}/\text{K}$ value of Garner et al. (1975). Later works criticized the value of Steiger and Jäger (1977) as being too high. Min et al. (2000) performed the comparison of U-Pb and Ar-Ar ages for a 1.1 Ga rhyolite and assumed that Ar-Ar ages were too low due to an inaccurate ^{40}K decay constant. They mentioned the best fit ^{40}K total decay constant of $5.37 * 10^{-10} \text{ a}^{-1}$, however Min et al. (2000) recommended the decay constants of Endt and van der Leun (1973) based on activity data compilations: $\lambda_{\beta^-} = 4.884 \pm 0.099 * 10^{-10} \text{ a}^{-1}$ and $\lambda_{^{40}\text{Ar}} = 0.580 \pm 0.014 * 10^{-10} \text{ a}^{-1}$, $\lambda_{\text{tot}} = 5.464 * 10^{-10} \text{ a}^{-1}$. Later Kwon et al. (2002) performed the comparison of Ar-Ar and U-Pb ages of five reference samples whose ages span from 1.9 ka to 4.5 Ga and estimated the total decay constant to be $\lambda_{\text{tot}} = 5.4755 \pm 0.0170 * 10^{-10} \text{ a}^{-1}$ (1 σ). The publication of Krumrei et al. (2006) also compares Ar-Ar and U-Pb ages of the Ilimaussaq complex assuming an age of 523.1 Ma for the irradiation monitor McClure Mountain hornblende (MMhb). They obtained a spread of ages 1-2% younger than the U-Pb age of baddeleyite and concluded that the decay constants published by Kwon et al. (2002) give coinciding Ar-Ar and U-Pb ages. Renne et al. (2010) using the approach of simultaneously determining the age of the irradiation monitor (Fish Canyon sanidine FCs) and the decay constants for 17 samples obtained $\lambda_{^{40}\text{Ar}} = 0.5755 \pm 0.0016 * 10^{-10} \text{ a}^{-1}$ and $\lambda_{\beta^-} = 4.9737 \pm 0.0093 * 10^{-10} \text{ a}^{-1}$, $\lambda_{\text{tot}} = 5.5492 * 10^{-10} \text{ a}^{-1}$. Later elimination of liquid scintillation data from the calculation resulted in $\lambda_{^{40}\text{Ar}} = 0.5757 \pm 0.0016 * 10^{-10} \text{ a}^{-1}$ and $\lambda_{\beta^-} = 4.9548 \pm 0.0134 * 10^{-10} \text{ a}^{-1}$, $\lambda_{\text{tot}} = 5.5305 * 10^{-10} \text{ a}^{-1}$ (Renne et al., 2011). One has to note that an important part of the Ar-Ar age calculation is the branching ratio of $B_{\text{Ca}}/B_{\text{Ar}}$. Compared to the uncertainty of the total decay constant of 0.2-0.5%, the branching ratio is still not known better than 1.5%. The only independent approach to estimate the branching ratio from molar amount of radiogenic Ar and Ca was performed by Nagler and Villa (2000) on a single sample and resulted in $B_{^{40}\text{Ar}} = 0.1067$ and $B_{\beta^-} = 0.8933$ (1% uncertainty).

1.3. Our approach

So far one branch (B_{Ca}) was measured with high precision using scintillation counting; another branch (B_{Ar}) was attempted to be estimated from geological intercomparison. The branching ratio relies on scattered activity data measured in the 20th century, and the theoretical calculation of the electron capture decay to the ground state. To improve the precision on the decay constant and the branching ratio we attempt to intercalibrate Ar-Ar, K-Ca, Rb-Sr ages with well-known U-Pb ages of the samples with

“point-like” geological history. This approach allows to calculate directly the total decay constant and the branching ratio if the age distribution of the samples is wide enough. This has not been performed before due to high complexity and high uncertainty of the K-Ca method. First discussed by Holmes (1932) the K-Ca method was used only in a few cases for minerals with high K content such as K-feldspars, muscovites, sylvite, langbeinite, to build mineral-whole rock isochrones of igneous, sedimentary rocks, some meteorites and lunar samples (e.g. Ahrens, 1951; Ovchinnikova et al., 1980; Marshall and DePaolo, 1982; Shih et al., 1993, 1994; Fletcher et al., 1997; Gopalan, 2008; Simon et al., 2011; Yokoyama et al., 2015). Since we improved the Ca measurement method (Naumenko-Dèzes et al., 2015) we aimed for K-Ca age determination with an uncertainty lower than 1%. This will allow us to assess the ^{40}K total decay constant and the branching ratio comparing an age offset of the K-Ca system with a reference sample age.

2. Samples

Sample selection plays a crucial role for this study. The main criteria for choosing samples are 1) to be old enough to accumulate measurable quantity of radiogenic Ca; 2) to be geologically “point-like” event (Begemann et al., 2001) with all isotopic systems closed at the same time; 3) dated mineral should not be affected by low-temperature alteration; 4) the chemical composition of dated minerals should be homogenous.

An initial selection of eight samples was evaluated based on the literature data about their geological history, thin-sections as well as microprobe study for some of them. Description of each sample and elimination details can be found in Appendix 2. Here we describe and discuss three samples, which were eventually chosen for the Rb-Sr and K-Ca study and one sample which was dated only with the Ar-Ar method.

The **Phalaborwa** phoscorite comes from a well-studied carbonatite complex, north-eastern Transvaal, South Africa. Phalaborwa carbonatite is an intracratonic alkali intrusive complex composed mainly of clinopyroxenites with minor carbonatites and phoscorites (in some studies called micaceous pyroxenite (Eriksson, 1984)). It intruded an Archean terrain of granites, gneisses, quartzites, granulites, amphibolites, talc and serpentine schists. (Eriksson, 1984). Phalaborwa has been dated by numerous workers (Table 1). Wu et al (2011) dated different layers and found coincident ages for all of them, which conforms to the requirement that a sample has to be a “point-like” event. The carbonatite sample was also used previously for the evaluation of the Rb-Sr decay constant by comparison with U-Pb age (Nebel et al., 2011).

Our sample (PhB-2) is a phoscorite that consists of large crystals (up to 10 cm) of phlogopite (*ca.* 45%), apatite (*ca.* 35%), diopside (*ca.* 14%), ilmenite (*ca.* 5%) and calcite (*ca.* 1%) (Fig. 1.). Apatite forms both large idiomorphic grains (up to 10 cm) and small mineral inclusions (1-200 μm) located inside phlogopite and diopside grains. Small (20-200 μm) ilmenite and calcite grains fill crystal boundaries interspace. Inclusions of apatite and calcite make it difficult to achieve high radiogenic values of ^{40}Ca . We observe signs of serpentinisation along diopside cleavage planes; phlogopite appears visually to be pristine.

The homogeneity of phlogopite was confirmed with microscope pictures, microprobe quantitative profile analysis and element maps. We found no signs of alteration or zonation of phlogopite at the resolution of an electron microprobe analysis (EMPA) (ca.1-2% relative uncertainty for major elements).

The Rubikon lepidolite comes from the Rubikon mine, which is located within the Karibib pegmatite belt, Namibia. Rubikon pegmatites have intruded into medium- to high-grade metamorphic rocks in between a quartz monzonite of Neoproterozoic age (700 – 500 Ma), and a pegmatitic granite of Ordovician-Cambrian age (600 – 460 Ma). Columbite from the Rubikon pegmatite has been dated with the U-Pb (TIMS) method at 505.5 ± 2.6 Ma (Melcher et al., 2015).

Our lepidolite sample (Lep) consists of pristine big pink sheets, which can be easily sliced along their cleavage planes with a blade into thin transparent pieces. The microprobe analysis shows that the sheets have no visible inclusions of other minerals, no zonation or signs of alteration. Element maps show uniform distribution of Al, F, K, Mn and Rb. Quantitative profile analysis also confirms homogeneity of the sample within the uncertainty of the microprobe method (1-3%). Very high K and Rb contents make this sample a good candidate for simultaneous dating with the Rb-Sr and K-Ca methods.

The third sample was a phlogopite from a **Siilinjärvi** carbonatite complex situated in the Karelian Craton in eastern Finland within the Ladoga-Bothnian deep fracture zone. Pb-Pb dates the intrusion of the complex at 2594 ± 13 Ma. (Rukhlov and Bell, 2010). Despite the pristine look of the sample in thin-sections (Fig. 2) literature data point to a post-emplacement metamorphic event at ca. 1900 Ma (summary of available ages in Rukhlov and Bell (2010)). Nevertheless simultaneous dating of Siilinjärvi mica with the Rb-Sr, K-Ca and Ar-Ar methods was attempted in this study.

A biotite of Bulgokhtokh granodiorite intrusion, **Kotuy**, Russia was dated with Ar-Ar method in this study. The Bolgoghtokh stock is situated at the far north-west end of the Norilsk flood basalt field and is younger than the Norilsk and Maymecha-Kotuy provinces. It has been interpreted to be formed out of lower crust melts (Wooden et al, 1993) during a later tectonic reactivation at 229.05 ± 0.36 Ma (U-Pb concordant ages of zircon (Kamo et al, 2003)). Ar-Ar ages of the stock are 227.1 ± 1.2 Ma for the biotite and 228.0 ± 1.9 Ma and 224.7 ± 1.0 Ma for hornblends (Dalrymple et al., 1995). Nebel et al (2011) argued that the discrepancy between originally published Ar-Ar and U-Pb ages might be due to offset of a flux monitor or the ^{40}K decay constant. Indeed recalculation of the Ar-Ar ages to the recently published McClure Mountain syenite (MMhb-1= 522.98 ± 1.00 Ma (Schoene and Bowring, 2006)) monitor ages bring the Ar-Ar biotite and hornblende ages closer to and U-Pb zircon age, though they still remain ca. 0.5 % younger. Wooden et al. (1993) describe certain weathering and alteration phenomena on the thin section scale, as well as Nebel et al (2011) point out minor sericitization of feldspars. The microprobe analysis revealed irregular zonation of mica (see Appendix 2) and thus this sample was not approved for ^{40}K decay constant intercalibration.

Table 1. Literature ages of the Phalaborwa complex.

* Rb-Sr age recalculated to $\lambda_{87} = 1.3972 \times 10^{-11} \text{ a}^{-1}$ (Villa et al., 2015), assuming that originally the ^{87}Rb decay constant of Steiger and Jäger (1977) was used

Age (Ma)	Method	Mineral	Rock type	Reference
2060	U-Pb	uranothorianite		Holmes and Cahen (1956)
2047 ± 19*	Rb-Sr	phlogopite	clinopyroxenite, carbonatite and phoscorite	Eriksson (1984)
2047 +11 / -8	U-Pb	thorianite and baddeleyite	carbonatite and phoscorite	Eriksson (1984)
2059.8 ± 0.8	U-Pb	baddeleyite	carbonatite	Heaman and LeCheminant (1993)
2060.6 ± 0.5	U-Pb	baddeleyite		Reischmann (1995)
2057 ± 8	U-Pb	baddeleyite	<i>not indicated</i>	Horn et al. (2000)
2057.1 ± 2.6	U-Pb	baddeleyite	<i>not indicated</i>	Wingate and Compston (2000)
2059.6 ± 0.4	U-Pb	baddeleyite	carbonatite	French et al. (2002)
2026 +46 / -47	U-Th Pb	total baddeleyite	carbonatite	French et al. (2002)
2062±74	Rb-Sr	hornblende, felsic fraction, clinopyroxene	dolerite	Yuhara et al. (2005)
2013±93	Rb-Sr	whole rock and mineral	phoscorite	Yuhara et al. (2005)
2060.1±4.1 2050±13	U-Pb (in situ)	baddeleyite zircon	outer pegmatitic pyroxenite of Loolekop pipe	Wu et al (2011)
2061.72±2.4 2047±27	U-Pb (in situ)	baddeleyite zircon	main phoscorite	Wu et al (2011)
2060.0±2.2	U-Pb (in situ)	baddeleyite	banded carbonatite	Wu et al (2011)
2056.7±2.7 2059.8±1.3 2053±14	U-Pb(in situ)	baddeleyite baddeleyite zircon	transgressive carbonatite	Wu et al (2011)
2068±17 2049±28	U-Pb (in situ)	baddeleyite zircon	satellite syenite (plug-like bodies outside the border of main complex)	Wu et al (2011)
2035±35	U-Pb (in situ)	baddeleyite	later mafic dyke	Wu et al (2011)
2060.3±0.4	Pb-Pb	baddeleyite	carbonatite	Kumar et al. (2014)

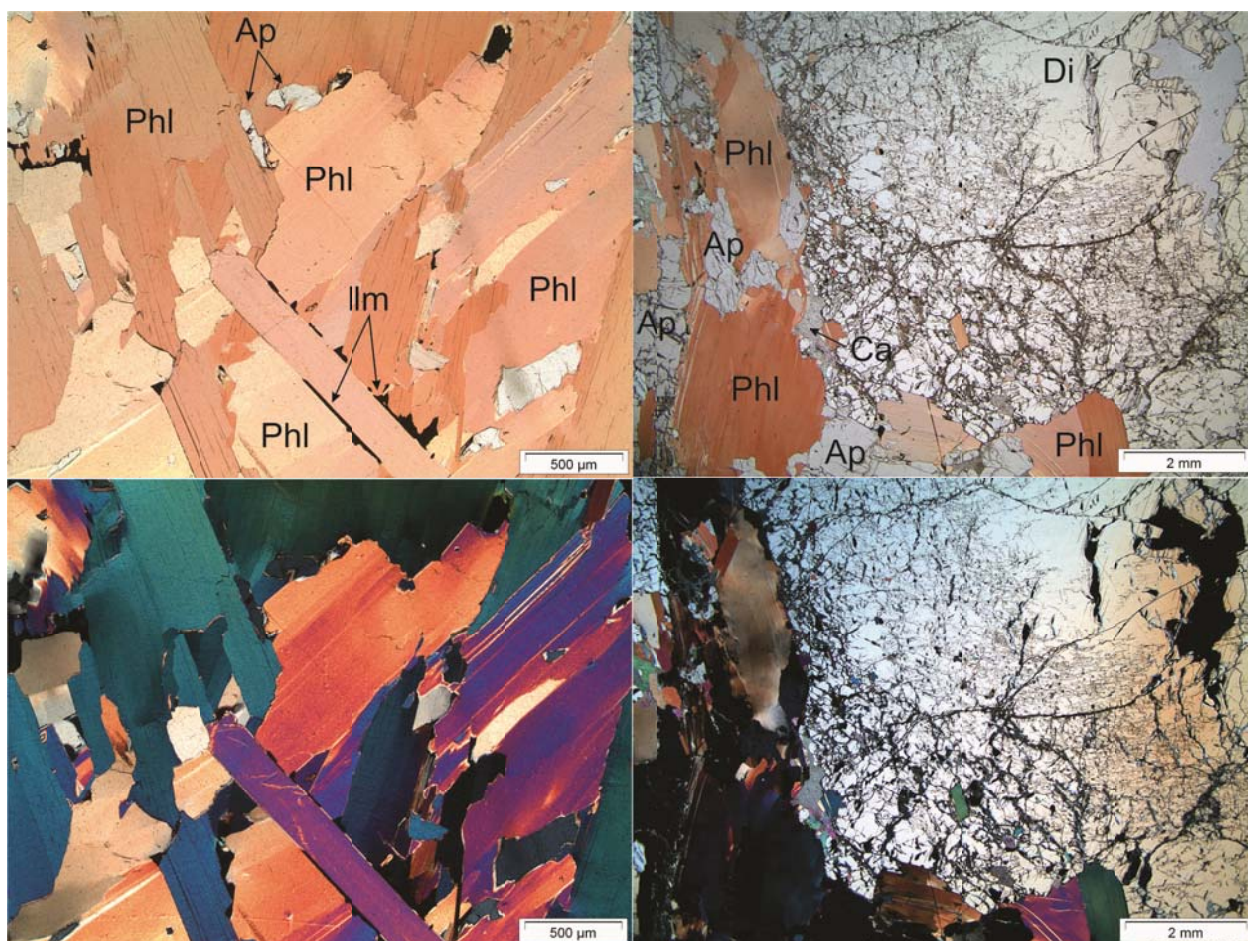


Fig 1. The Phalaborwa phoscorite thin section: upper row plane-polarized light, lower row cross-polarized light.

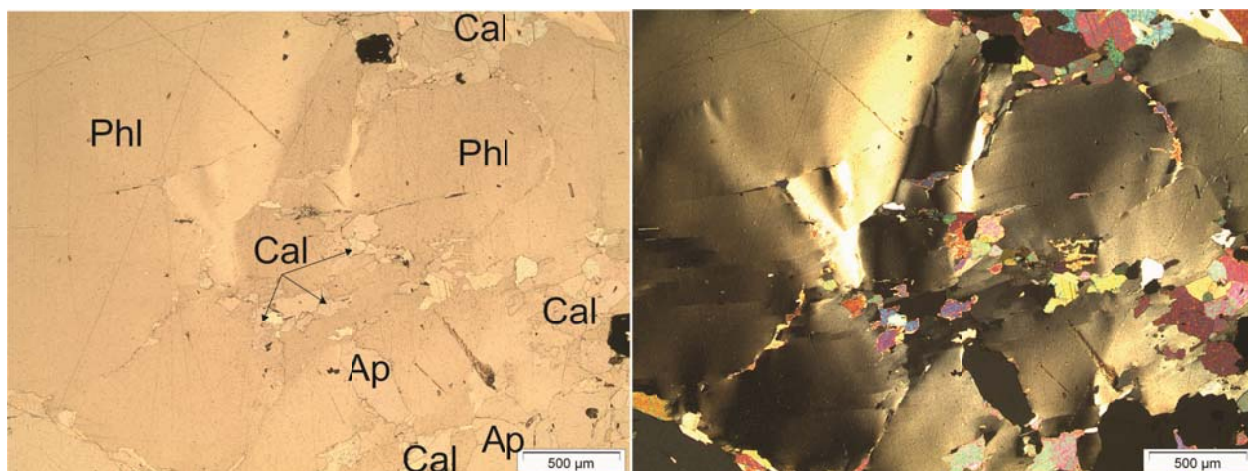


Fig. 2. The Siilinjärvi carbonatite thin section: to the right cross-polarized light, to the left plane-polarized light.

3. Method

3.1. Sample preparation

Phlogopite, apatite and calcite were detached from our samples with a steel Milli-Q pre-cleaned scalpel into a Petri dish. Sheets of phlogopite were disconnected from each other to obtain as thin and transparent sheets as possible. Grinding of samples (see PhB2c2d in the Table 2) resulted in Ca blank contamination and therefore was not performed for the rest of the samples. Transparent mica flakes were picked under the binocular microscope to ensure that no other minerals are present in the mica fraction, though apatite or calcite micro inclusions might have been present. After picking minerals, they were put in Petri dishes with Milli-Q and submitted to ultrasonic treatment. The samples were dried at 50°C overnight and then weighed. *Circa* 5 mg of phlogopite and 30 mg of lepidolite were used for dating. Samples were spiked with K-Ca and Rb-Sr mixed spikes separately, due to the presence of ⁸⁶Sr isotope in ⁴³Ca spike, which was used for preparation of our K-Ca mixed spike. The presence of Sr in the Ca spike was also reported by Baadsgaard (1987) and Gopalan (2008).

Three different procedures were applied to K-Ca samples: 1) dissolution in HF and HNO₃ on a hot plate at 100°C for two weeks 2) leaching in HCl and HNO₃ at 100°C for two weeks and 3) first leaching with HCL and HNO₃ for one week, then pipetting it out, dissolution of the residue with HF + HNO₂ on the hot plate at 100°C for a few days, evaporating, joining again the leach and dissolved residue. All samples at the end were converted into chlorides with 6.4M HCL, evaporated and diluted with 2.5 M HCl for column chemistry. The results of all three approaches plot on the same isochron (see below), however the last one is more likely to be contaminated with a random Ca blank. Therefore leaching with HCl and HNO₃ mixture is preferred for small amounts of mica. The K-Ca column chemistry was performed with handmade Teflon columns of 300 µl volume filled with Dowex AG 50WX8. K-Ca columns were substantially pre-cleaned to reach column blanks of <0.5 ng. Procedure blank was variable *ca.* 1.5 ng with casual spikes up to 35 ng and was monitored on the routine basis. The K-Ca separation followed Nögler and Villa (2000). The Rb-Sr columns of 6.5mm diameter were filled with 6ml of the Dowex AG 50WX8 resin. The Rb and Sr were separated with distilled 2.5 M HCl. Sr fraction was later purified with Sr resin SR-B50-a (100-150 µm (Triskem int.)). (Detailed clean laboratory protocols can be found in Appendix 1)

3.2. Measurements

K-Ca and Rb-Sr measurements

Calcium, K and Sr were measured in static mode on multicollector thermal ionization mass-spectrometer (TIMS) ThermoScientific Triton Plus™ specially designed for Ca measurements and installed at the Geological institute of the University of Bern (Switzerland). Detailed Ca measurement description can be found in Naumenko-Dèzes et

al. (2015). Ca was measured mostly on amplifiers having $10^{12}\Omega$ resistors except ^{40}Ca , which was measured on one amplifier with a $10^{11}\Omega$ resistor. ^{39}K and ^{41}K were measured in $10^{11}\Omega$ and ^{40}K in $10^{12}\Omega$ amplifiers. Strontium was measured with application of only $10^{11}\Omega$ amplifiers. Gain calibration of amplifiers was performed on each day measurements and made with a built-in stable tension source of 3V. The discussion on the gain calibration and on the strong signal tail of ^{39}K can be found in Naumenko et al. (2013). Rubidium was measured on multicollector ICP-MS Nu Instruments with a sample-bracketing technique with an in-house Rb standard and IUPAC Rb isotopic composition (de Laeter et al., 2003). All data were corrected for an instrumental fractionation offline. Double spike iteration correction protocol was used for Ca, and single-spike iteration protocol was used for Sr isotopes. K sample-spike mixtures were fractionation corrected following Chu et al. (2011) adapted for K. Error magnification was calculated for $^{40}\text{K}/^{44}\text{Ca}$ and $^{87}\text{Rb}/^{86}\text{Sr}$ based on spike/sample ratio (detailed description and formulas can be found in Appendix 3). Errors for Rb-Sr and K-Ca are presented as 2σ , Ar-Ar as 1σ according to the common procedure in the respective community, if not stated differently. Isochrons were calculated with Isoplot 3.75 (Ludwig, 2012).

Ar-Ar measurements

Few milligrams mica flakes were detached from a rock sample with a scalpel and picked under the binocular microscope, wrapped in aluminum foil and irradiated at the McMasters nuclear reactor (Ontario, Canada) with a Fish Canyon sanidine as a monitor (reference age used for J calculation 28.201 Ma (Kuiper et al., 2008)). Ar ratios were measured in Milano Bicocca University on a Nu Instruments Noblesse TM mass-spectrometer equipped with one Faraday cup and two ion counters. ^{40}Ar , ^{39}Ar were measured on Faraday cups ^{38}Ar , ^{36}Ar , ^{37}Ar and ^{35}Ar were measured on ion counters, if the intensity was below 15 mV. The gain intercalibration was calculated offline using the isotopic intensity of ^{39}Ar (faraday over ion counter 0) and ^{36}Ar (ion counter 0 over ion counter 1), gain variations over 5 measurement days was *ca.* 1.5%. Mass fractionation was determined with air pipettes relative to the ratio $^{40}\text{Ar}/^{36}\text{Ar} = 298.55$ (Lee et al., 2006), fractionation factor was calculated according to the linear law; variation of the fractionation factor per 2 amu over 5 days was within 0.7%. Raw data was reduced offline: measured intensities were regressed, corrected for baseline, gain and fractionation. The J-factor was calculated from two Fish Canyon sanidine monitors. Due to unstable behavior of the ion counters during the measurements its uncertainty was estimated to be 1%. Data is reported according to the data reporting norms given in Renne et al. (2009).

3.3. K-Ca mixed spike calibration

The K-Ca mixed spike was prepared from an enriched ^{40}K spike and a ^{43}Ca - ^{48}Ca double spike. The isotopic composition of K was measured with a total evaporation technique with a precision of $\pm 0.30\%$ (2σ) for $^{40}\text{K}/^{41}\text{K}$ and $\pm 0.12\%$ (2σ) for $^{39}\text{K}/^{41}\text{K}$. No additional fractionation correction was applied to the K fraction of the K-Ca mixed spike:

due to very low spike-sample ratios the measured K ratios were close to the natural concentration and uncertainties of spike ratios had negligible effect on the resulting calculations. The first approximation of Ca isotopic composition was also measured with a total evaporation technique and then fractionation corrected with an iterative protocol to three spike-standard mixtures, which gave an uncertainty of 0.2 % (2σ) on the Ca isotopic composition of the K-Ca mixed spike.

The K-Ca mixed spike was calibrated with two NIST mixtures (NIST SRM 3109a, NIST SRM 3141a) and mixed ICP mixtures traceable to NIST (Certipur 1.70342.0100, Certipur 1.70308.0100). Three mixtures for each NIST and Certipur reference samples were prepared in Savillex Teflon beakers. Each weighing step was performed five – six times to ensure that there were no weighing artefacts. The deviation during weighing was below 0.2‰. The deviation during weighing was included into calculation of concentration uncertainties. Due to high concentration of Ca original standard mixtures, they were diluted. The uncertainty on the weighing (2 ‰ for diluted Ca NIST SRM 3109a) is also included into total uncertainty calculation.

Potassium and Ca of standard-spike mixtures were separated in K-Ca columns and measured following the same procedure as for samples. The procedure was repeated several times for each mixture to monitor for blanks. Column blanks were below 1ng, but some Ca fraction suffered from a random contamination, which shifted the resulting Ca spike concentration downwards. Such erratic results were eliminated. Due to the high K concentration in the sample-spike mixtures the calculated K concentration were not affected by external contamination.

The summary of 36 measurements of six spike-standard mixtures for Ca yielded repeatability of results of 0.5 ‰. The uncertainty of NIST standards was the dominant source of uncertainty for K-Ca mixed spike concentrations. The propagation of weighing repeatability, measurement uncertainty and NIST standard concentration uncertainty resulted in 0.17 % uncertainty for Ca and 0.29 % for K concentrations at 95 % confidence level.

4. Results

The **Phalaborwa** sample was dated with K-Ca, Rb-Sr and Ar-Ar systems. K-Ca dating was performed on 19 phlogopite fragments and five apatites of different weight (Table 2, Fig. 3b). A spread of points along the isochron is due to the microscopic inclusions of the apatite in phlogopite. Seven points have been eliminated due to incomplete fractionation correction of the measured Ca data. The issue of incomplete fractionation correction is more pronounced for the samples with minor amount of Ca compared to the more concentrated standards discussed in Naumenko-Dèzes et al (2015). The calculated concentration of K corresponded to those measured with the microprobe. The K-Ca isochron has a slope of 1.8781 ± 0.012 (2σ) which corresponds to the age of

2040.0 ± 13 Ma (2σ) (decay constants of Steiger and Jäger (1977)). Rb-Sr dating of phlogopite was performed to confirm that our samples correspond to the age of the complex and has not suffered alteration and loss of Sr. Eleven phlogopite fragments and one apatite resulted in a Rb-Sr age of 2058.9 ± 5.2 Ma (Table 3, Fig. 3a), one phlogopite aliquot was rejected due to anomalously low Rb content. Step-heating Ar-Ar dating gave plateau age of 2000 ± 40 Ma (Table 8, Fig. 4). The high uncertainty of the Ar-Ar data is due to unstable behavior of the ion counters. During Ar-Ar measurements the first four and the last one steps contained elevated Ca/Cl ratio (Fig. 5.a), which implies that the phlogopite sample was mostly but not entirely a pure mica phase. Early four high Ca steps might correspond to a calcite micrograins or calcium dust present in the interlayers of mica and the last step may correspond to the micro inclusion of apatite. Overall the Rb-Sr age overlap with the U-Pb age of 2060 Ma, K-Ca and Ar-Ar ages are *ca.* 1 % younger within the uncertainties.

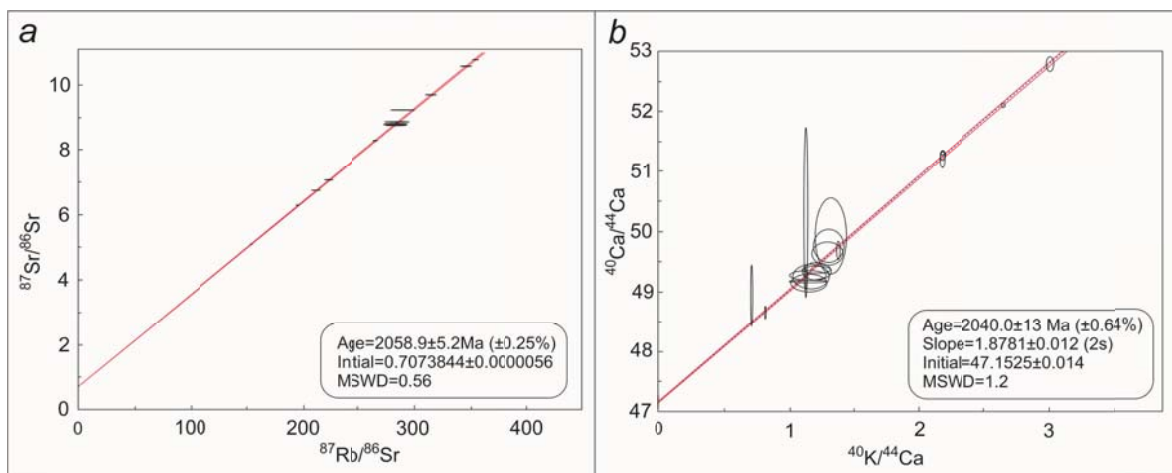


Fig. 3. Isochrons for Phalaborwa phoscorite (PhB-2). a) Rb-Sr isochron for 11 phlogopites and an apatite calculated with a decay constant $\lambda_{87} = (1.3972 \pm 0.0045) \times 10^{-11} \text{ a}^{-1}$ (Villa et al., 2015). b) K-Ca isochron for 19 phlogopites and five apatites defining a slope of 1.8781 ± 0.011 , which corresponds to an age of 2040 ± 13 Ma with constants of Steiger and Jäger (1977)

Table 2. Results for K-Ca dating of Phalaborwa phoscorite. Samples

Sample	$^{40}\text{K}/^{44}\text{Ca}$	$\pm 2\text{SD}\%$	$^{40}\text{Ca}/^{44}\text{Ca}$	$\pm 2\text{SD} \%$	$\text{K} \cdot 10^4 \text{ ppm}$	Ca ppm
PhB2b10A1	2.175	0.7	51.184	0.21	8.94	259
PhB2b10B1	2.178	0.7	51.271	0.13	8.93	259
PhB2b10C1	2.185	0.7	51.299	0.05	8.94	258
PhB2c2d1A1	1.143	10.3	49.275	0.13	8.46	449
PhB2c2d1B1	1.150	10.3	49.148	0.24	8.48	447
PhB2c2d2B2	1.308	7.3	49.755	0.45	5.92	277
PhB2c2d2C1	1.301	7.3	49.632	0.32	8.60	404
PhB2c2d2C2	1.323	7.5	49.932	1.03	8.71	405
PhB2c2d1A1	1.164	10.5	49.252	0.33	8.54	445
PhB2c2d2A2	1.205	7.5	49.367	0.10	8.78	443
PhB2c2d3B1	1.212	7.3	49.344	0.25	8.64	433
PhB2c2d4B2	1.135	10.4	49.171	0.04	8.75	467
PhB91	1.381	0.7	49.692	0.24	8.76	388
PhB92	3.003	0.7	52.792	0.19	8.39	181
PhB101aliqu	0.813	0.7	48.658	0.17	8.52	387
PhB102aliqu	0.708	0.8	48.944	0.85	8.48	444
PhB103aliqu	1.117	0.7	49.205	0.31	8.35	279
PhB104aliqu	1.120	1.1	50.322	2.32	9.56	326
PhB105	2.649	0.5	52.102	0.06	8.86	214
PhB25ap			47.153	0.13		$1.50 \cdot 10^5$
PhB27tr			47.163	0.18		$38.0 \cdot 10^5$
PhB27ap1			47.163	0.18		$3.98 \cdot 10^5$
PhB27ap2			47.133	0.07		$3.37 \cdot 10^5$
PhB28Ap3c not spiked			47.157	0.04		

Table 3. Results for Rb-Sr dating of Phalaborwa phlogopite.

Sample	$^{87}\text{Rb}/^{86}\text{Sr}$	$\pm 2 \text{ SD } \%$	$^{87}\text{Sr}/^{86}\text{Sr}$	$\pm 2\text{SD} \%$	Rb ppm	Sr ppm
PhB2c11	282.62	3.0	9.214	0.028	563	11
PhB2c12	277.68	3.0	8.836	0.023	563	11
PhB2c13	276.16	3.1	8.764	0.273	566	11
PhB262	189.99	0.6	6.259	0.001	651	15
PhB26b	149.79	0.7	5.070	0.000	611	17
PhB281s	259.06	0.6	8.263	0.002	624	12
PhB282s	345.06	0.6	10.760	0.002	650	11
PhB2101	205.64	1.5	6.718	0.008	676	15
PhB2102	216.47	1.2	7.037	0.025	670	15
PhB2103	306.74	1.2	9.676	0.009	691	12
PhB2104	337.09	1.1	10.556	0.011	539	9
PhB28 Ap not spiked			0.70739	0.00002		

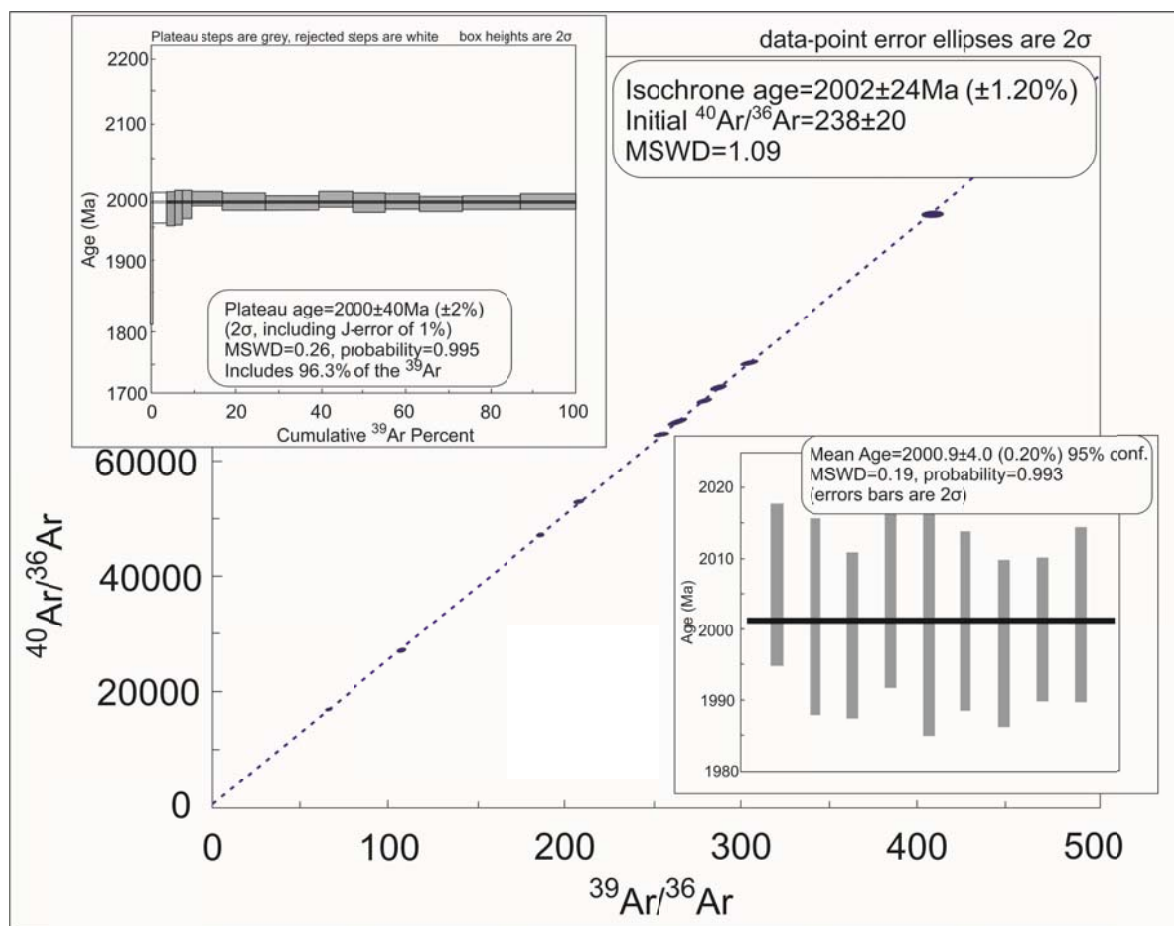


Fig. 4. Ar-Ar ages of the Phalaborwa phlogopite. High uncertainties of a plateau and an isochrone age are due to the high uncertainty of J calculated from the FC sanidine standard. A mean age is calculated for a low Ca/Cl fraction, the uncertainty of J is not propagated into the mean age. All calculations performed with Isoplot 3.75 (Ludwig, 2012) to the constants of Steiger and Jäger (1977).

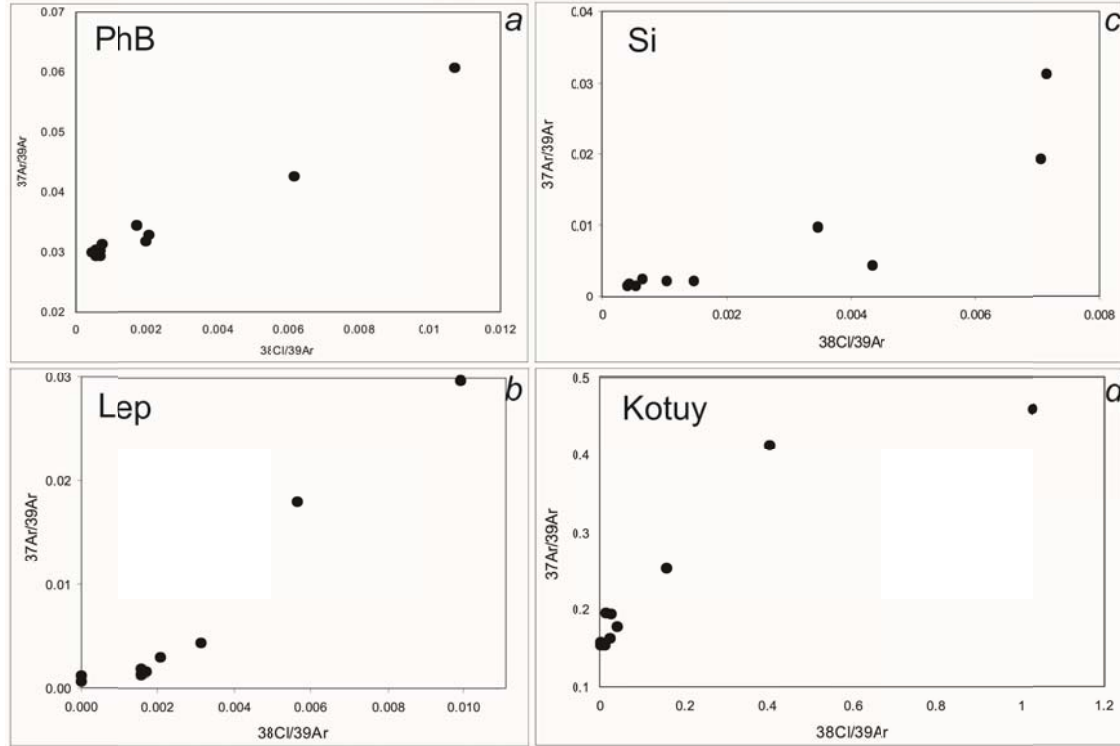


Fig. 5. $^{37}\text{Ar}/^{39}\text{Ar}$ vs $^{38}\text{Cl}/^{39}\text{Ar}$ representing Ca/K vs Cl/K ratios showing non-homogeneity of the samples
a) the Phalaborwa phlogopite. Five high Ca-Cl points corresponds to four first and one last step of the measurement.
b) the Rubikon lepidolite. Two high Cl points of the first and the last steps are not included. Another three highest points correspond to steps 2-4, their results were not included into the weighted mean age calculation.
c) the Siilinjärvi phlogopite. Two high Ca/Cl points of the first two steps are not included. Another four highest points correspond to steps 3, 10-12.
d) the Kotuy biotite. First two high Ca/Cl points are not included. Another three highest points correspond to the last steps.

The **Rubikon** lepidolite was dated with Rb-Sr, K-Ca and Ar-Ar methods. Due to a very high Rb-Sr ratio of the sample the Rb-Sr spike used in this study was not optimal, which limited our precision on $^{87}\text{Rb}/^{86}\text{Sr}$ ratio to the minimum of 0.7%. Only four chips were in an acceptable spike/sample range, they resulted in an age of 504.7 ± 4.2 Ma (Fig. 6.a, Table 5.). The initial $^{87}\text{Sr}/^{86}\text{Sr}$ ratio was fixed to 0.710. Due to a highly radiogenic $^{87}\text{Sr}/^{86}\text{Sr}$ ratio of more than 500 the variation of the initial Sr in the natural limits does not affect the resulting age. The K-Ca dating resulted with a low precision age of 481 ± 51 Ma (Fig. 6.b, Table 4.). A plateau Ar-Ar age gave 493.8 ± 9.9 Ma (Fig. 7, Table 9). Step heating of the Rubikon lepidolite showed signs of non-homogeneity despite a uniformity of the microprobe analysis results. The first four and the last two steps are showing high Cl content, which might be due to some accessory phase (Fig. 5.b). Pure mica steps were used to calculate a weighted mean age. The high precision Rb-Sr and low precision Ar-Ar and K-Ca ages overlap with the published U-Pb age of columbite (505 Ma) (Melcher et al., 2015). However the precision of K-Ca and Ar-Ar ages is too low to assess the ^{40}K decay constant intercalibration.

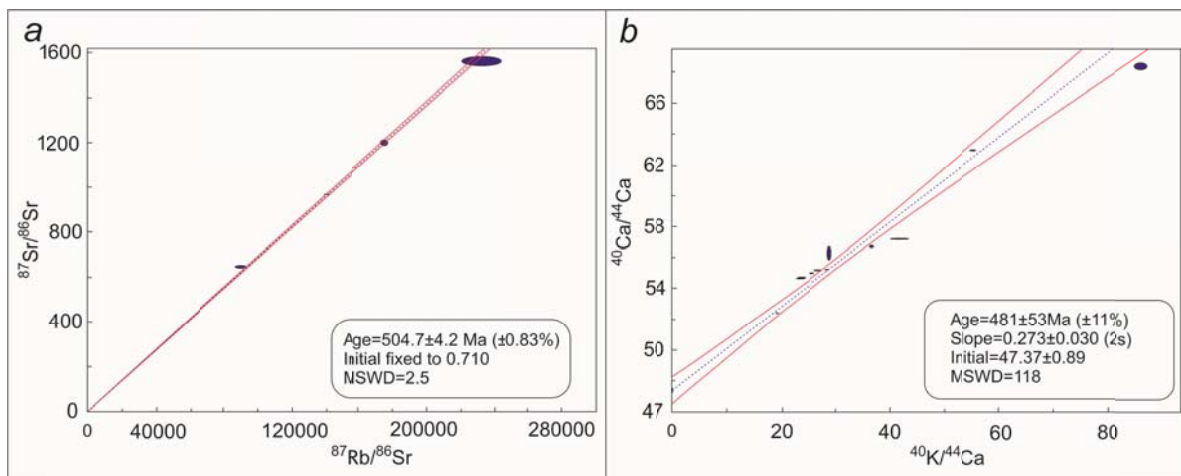


Fig. 6. Isochrons for the Rubikon lepidolite: *a*) Rb-Sr isochron for four lepidolite chips. The initial fixed to 0.710. The age is calculated with a decay constant $\lambda_{87} = (1.3972 \pm 0.0045) \cdot 10^{-11} \text{ a}^{-1}$ (Villa et al., 2015). *b*) K-Ca isochron with a slope 0.273 ± 0.030 corresponds to the age of $481 \pm 53 \text{ Ma}$ with constants of Steiger and Jäger (1977)

Table 4. Results for the K-Ca dating of the Rubikon lepidolite.

Sample	$^{40}\text{K}/^{44}\text{Ca}$	$\pm 2\sigma \%$	$^{40}\text{Ca}/^{44}\text{Ca}$	$\pm 2\sigma \%$	$\text{K} \cdot 10^4$	Ca ppm
Lep-9-4c	19.02	0.91	52.34	0.00	8.57	29.00
Lep-9-3c	36.50	0.79	56.66	0.10	9.14	17.41
Lep-8-2c	86.20	1.03	68.34	0.27	9.63	9.32
Lep2wA1	25.39	1.65	54.96	0.04	7.44	19.78
Lep2wA2	26.67	1.66	55.14	0.02	7.52	19.10
Lep3eB1	23.49	2.51	54.66	0.02	6.66	19.05
Lep2eB2	23.20	2.49	54.61	0.03	6.59	19.05
Lep92c	28.76	0.83	56.23	0.63	8.59	20.61
Lep5	55.36	0.70	62.92	0.03	8.46	11.77
Lep91c	28.32	0.61	55.16	0.03	8.60	20.56
Lep72	41.70	3.29	57.15	0.01	9.69	16.29

Table 5. Results for the Rb-Sr dating of the Rubikon lepidolite.

Sample	$^{87}\text{Rb}/^{86}\text{Sr}$	$2\sigma\%$	$^{87}\text{Sr}/^{86}\text{Sr}$	$2\sigma\%$	$\text{Rb} \cdot 10^4 \text{ ppm}$	Sr ppm
Lep6	86928	3	640.81	1.29	0.86	18
Lep83s	225605	4	1562.72	2.05	1.12	22
Lep81s	136720	1	966.68	0.23	1.13	23
Lep82s	170372	1	1200.19	1.71	1.12	23

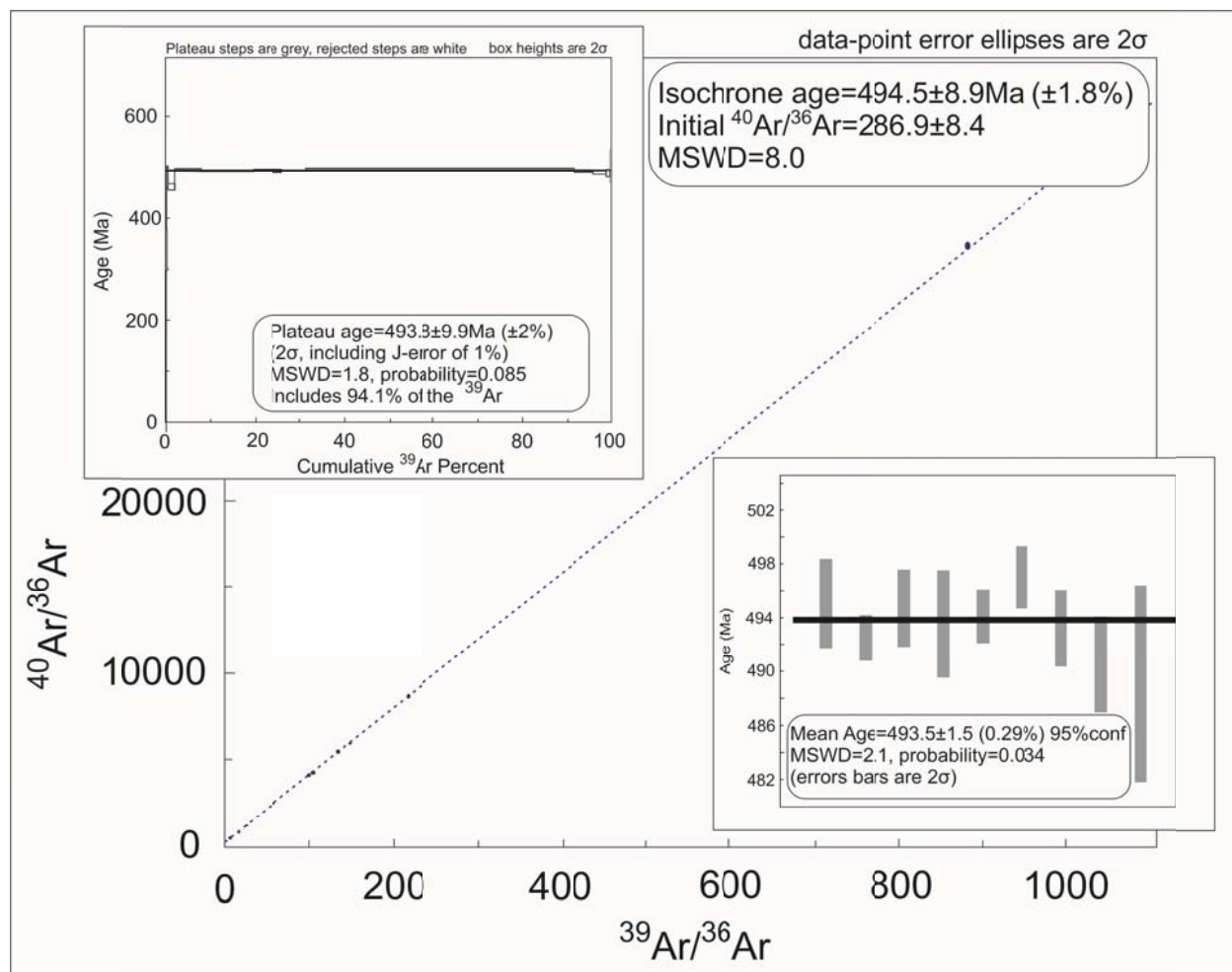


Fig. 7. Results of the Ar-Ar dating of the Rubikon lepidolite. Plateau and isochrone ages include J uncertainty of 1%. A mean age is calculated for a low Ca/K fraction, the uncertainty of J is not propagated. All calculations performed with Isoplot 3.75 (Ludwig, 2012) to the constants of Steiger and Jäger (1977).

The **Siilinjärvi** carbonatite (sample Si-102) with a Pb-Pb age of 2594 ± 13 Ma and 1.8% discordance was known to be altered by post-emplacement event approximately dated with the lower discordia intercept at 1894 ± 78 Ma (Rukhlov and Bell, 2010). Thus limited attempts to date this sample were made. A Rb-Sr age of 1826 ± 10 Ma (Fig.6.a, Table 7) is within the lower limit of the lower discordia intercept. The K-Ca dating gave a low precision age of 1786 ± 112 Ma and overlaps with the discordia age within uncertainty (Fig. 6.b, Table 6). An Ar-Ar age gave a bit older age of 1879 ± 23 Ma (Fig. 9, Table 10). The Siilinjärvi phlogopite despite a pristine view under the microscope is not homogenous. Step heating Ar-Ar measurements reveal high Ca and Cl contents for the first three and the last three steps (Fig.5.c). Transition from the high Ca/Cl ratio to the low and backwards is continuous. Higher Ca/Cl steps produced higher Ar-Ar ages. The phlogopite mean ages were calculated only for Ca/Cl low steps 3-9.

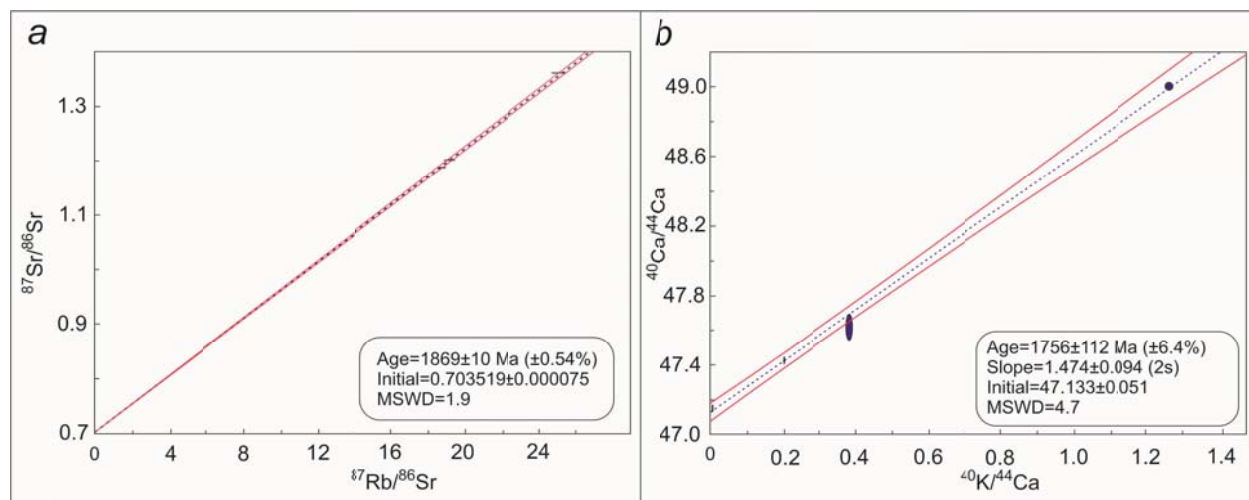


Fig.6. Isochrons for the Siilinjärvi carbonatite: *a*) Rb-Sr isochron for 3 phlogopites and a calcite. The age is calculated with a decay constant $\lambda_{87} = (1.3972 \pm 0.0045) \cdot 10^{-11} \text{ a}^{-1}$ (Villa et al., 2015). *b*) K-Ca isochron for three phlogopites and a calcite with a slope 1.474 ± 0.094 corresponds to the age 1756 ± 112 Ma with constants of Steiger and Jäger (1977)

Table 6. Results for the K-Ca dating of the Siilinjärvi carbonatite

Sample	$^{40}\text{K}/^{44}\text{Ca}$	$\pm 2\sigma \%$	$^{40}\text{Ca}/^{44}\text{Ca}$	$\pm 2\sigma \%$	Ca ppm	K ppm
Si5Bi	1.264	0.66	49.001	0.036	2212	$4.6 \cdot 10^5$
Si7Bi2	0.379	1.83	47.608	0.126	1590	$1.0 \cdot 10^5$
Si7Bi1	0.195	0.76	47.415	0.029	2526	$0.8 \cdot 10^5$
Si7cal1	0.000001	32.64	47.141	0.030	$3.6 \cdot 10^5$	65

Table 7. Results for the Rb-Sr dating of the Siilinjärvi carbonatite. A sample Si5Bi is not included to the isochron (Fig 6.a) due to high uncertainty, which masks other points, it does not affect the age or the uncertainty.

Sample	$^{87}\text{Rb}/^{86}\text{Sr}$	2 $\sigma\%$	$^{87}\text{Sr}/^{86}\text{Sr}$	2 $\sigma\%$	Rb ppm	Sr ppm
Si5Bi	223.14	6.25	6.55	6.197	305	6
Si61	18.74	0.99	1.20	0.016	368	60
Si62	18.35	0.85	1.19	0.009	350	58
Si8Bi1s	24.59	1.29	1.36	0.027	336	42
Si8cal3s not spiked			0.703521308	0.011		

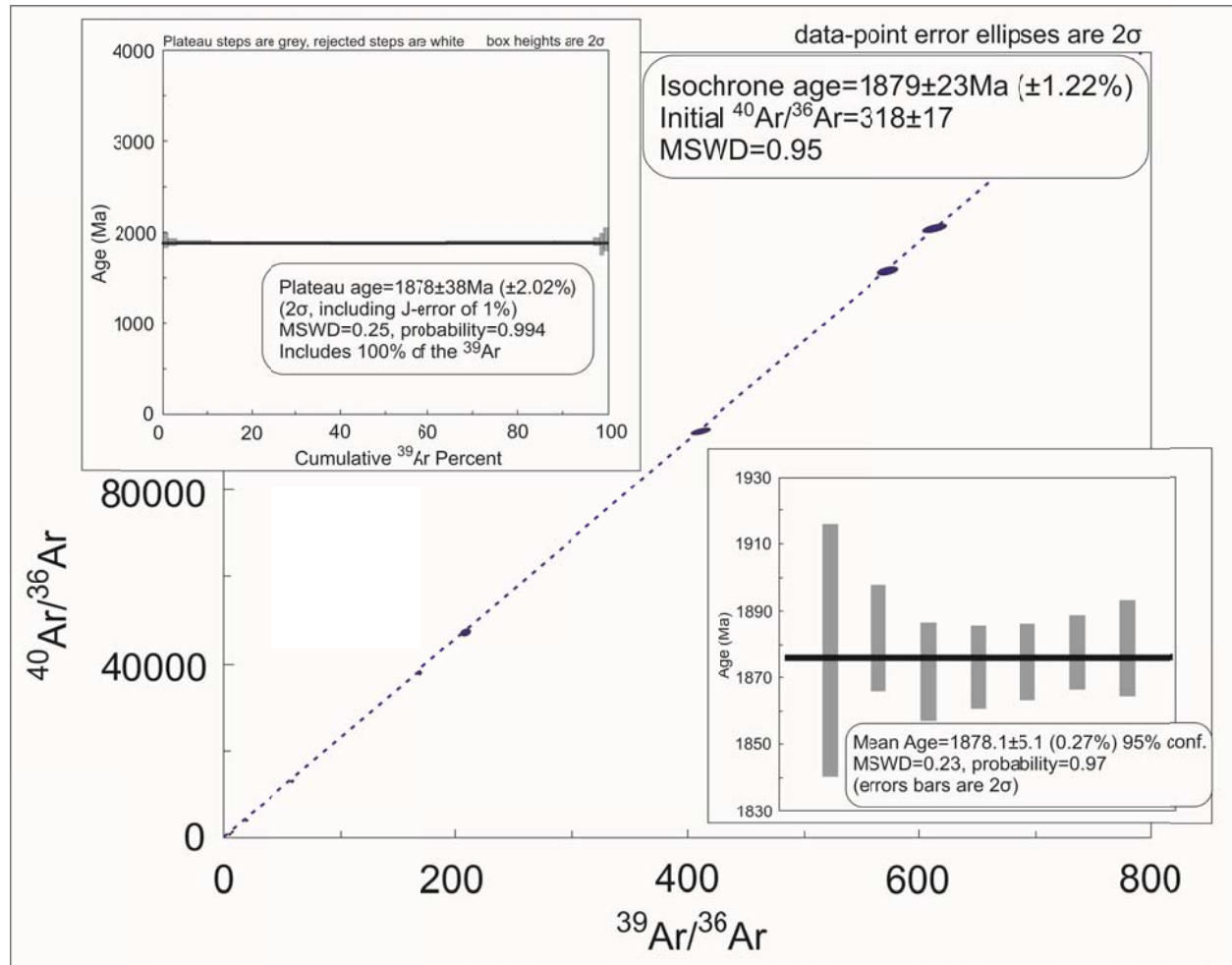


Fig.9. Results for the Ar-Ar dating of the Siilinjärvi phlogopite. Plateau and isochrone ages include J uncertainty of 1%. The mean age is calculated for low Ca/Cl steps 3-9, the uncertainty of J is not propagated. All calculations performed with Isoplot 3.75 (Ludwig, 2012) to the constants of Steiger and Jäger (1977).

The **Kotuy** sample was dated only with an Ar-Ar method (Fig. 10, Table 11). The isochron age of 225.0 ± 4.8 Ma coincides with previously published 223.2 ± 1.2 Ma for biotite and 224.1 ± 1.9 Ma for hornblende (Dalrymple et al., 1995). Ar-Ar ages are *ca.* 1% lower than the U-Pb zircon age of 229.05 ± 0.36 Ma (Kamo et al., 2003) despite that the new calibrated age of FCs was used for this study. We confirm the signs of alteration described previously by (Wooden et al., 1993). High Ca/Cl ratio at the beginning and the end of the step-heating shows non-homogeneity of the sample (Fig.5.d). Only steps 5-7 correspond to a low Ca fraction and presumably a clean mica part. Steps 5-9 with a low Ca and uniform Cl composition were chosen for the weighted mean age calculation and resulted in 223.32 ± 0.89 Ma without propagated 1% uncertainty on the J value.

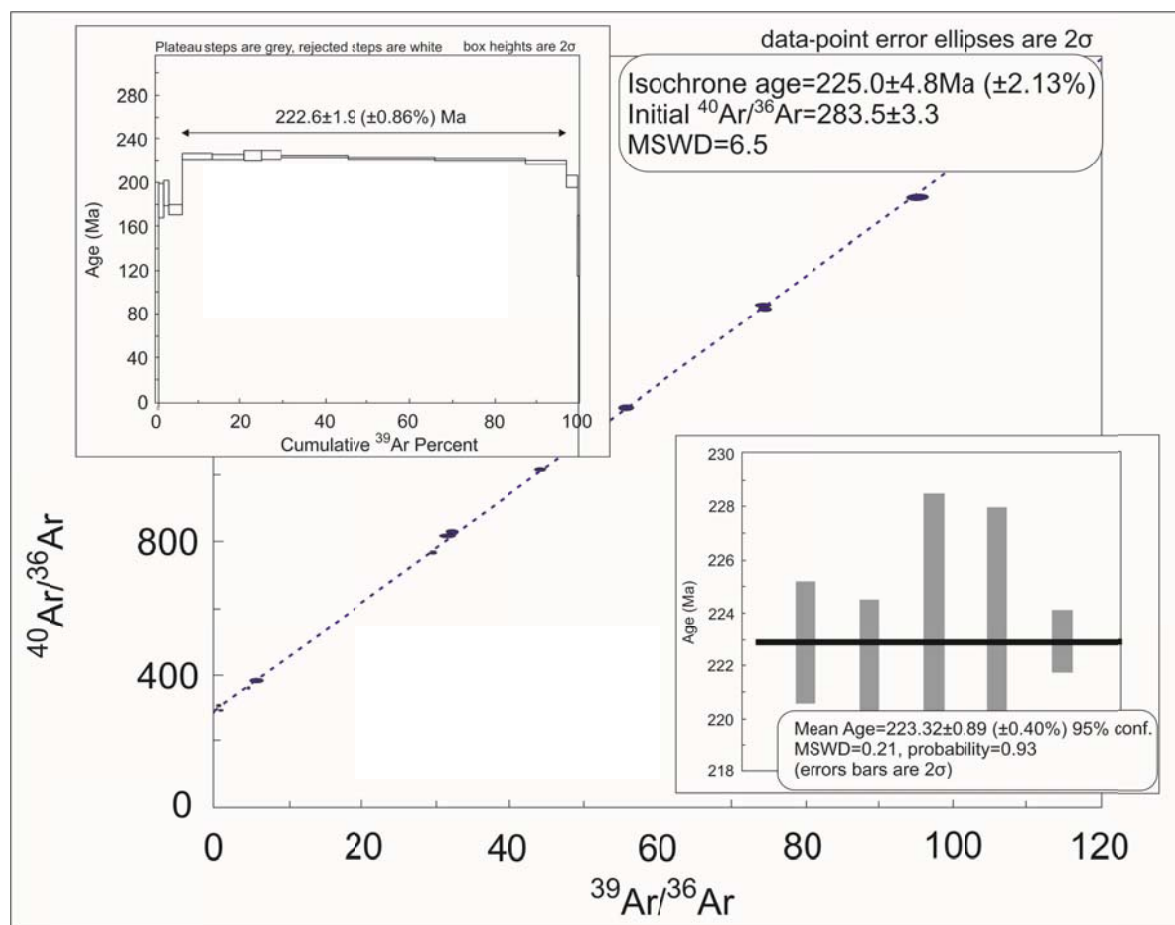


Fig.10. Results for the Ar-Ar dating of the Kotuy biotite. Isoplot 3.75 does not define a plateau; the isochron age includes J uncertainty of 1%. The mean age is calculated for low Ca/Cl steps 3-9, the uncertainty of J is not propagated. All calculations performed with Isoplot 3.75 (Ludwig, 2012) to the constants of Steiger and Jäger (1977).

Table 8. Results for the Ar-Ar step heating of the Phalaborwa phlogopite.

Step	40Ar(mV)	±	39Ar(mV)	±	38Ar (mV)	±	37Ar (mV)	±	36Ar (mV)	±	35Cl (mV)	±	40Ar/36Ar	±	
PhB step 1	251.70	0.16	0.830	0.022	0.9125	0.001	0.02458	0.00013	0.19432	0.0004	0.01803	0.0001	1295.27	1.91	
PhB step 2	1796.71	0.72	6.765	0.022	0.4452	0.000	0.04228	0.00018	0.40590	0.0008	0.01826	0.0001	4426.49	7.35	
PhB step 3	977.46	0.54	3.887	0.022	0.1773	0.000	0.00786	0.00009	0.03582	0.0002	0.01778	0.0001	27287.17	82.22	
PhB step 4	866.77	0.61	3.414	0.020	0.1628	0.000	0.00722	0.00010	0.05053	0.0002	0.01774	0.0001	17151.99	52.48	
PhB step 5	1156.46	0.50	4.538	0.021	0.2243	0.000	0.00804	0.00011	0.06813	0.0003	0.01791	0.0001	16973.99	48.72	
PhB step 6	3988.18	3.40	15.716	0.029	0.6958	0.001	0.01176	0.00013	0.07514	0.0002	0.01753	0.0001	53077.45	89.34	
PhB step 7	5055.70	6.90	20.025	0.042	0.8403	0.001	0.01356	0.00016	0.07189	0.0002	0.01740	0.0001	70323.12	152.36	
PhB step 8	6349.81	6.20	25.151	0.045	1.0637	0.001	0.01442	0.00014	0.13469	0.0005	0.01856	0.0001	47142.80	85.14	
PhB step 9	4270.29	4.20	16.873	0.037	0.7177	0.001	0.01086	0.00013	0.06612	0.0003	0.01778	0.0001	64585.82	107.93	
PhB step 10	4098.44	5.60	16.244	0.037	0.6973	0.001	0.01118	0.00013	0.06146	0.0002	0.01860	0.0001	66687.96	179.41	
PhB step 11	4138.44	4.60	16.401	0.031	0.7027	0.001	0.01054	0.00014	0.05702	0.0002	0.01822	0.0001	72576.74	148.92	
PhB step 12	5142.81	4.90	20.435	0.040	0.8803	0.001	0.01157	0.00013	0.07108	0.0003	0.01831	0.0001	72355.78	121.14	
PhB step 13	7173.89	5.00	28.495	0.045	1.2062	0.001	0.01266	0.00016	0.06988	0.0003	0.01804	0.0001	102665.46	155.04	
PhB step 14	6212.81	6.40	24.618	0.039	1.0305	0.001	0.01403	0.00019	0.08101	0.0003	0.01863	0.0001	76692.57	156.67	
PhB step 15	189.17	0.08	0.583	0.020	0.0673	0.000	0.00631	0.00011	0.13413	0.0003	0.01929	0.0001	1410.35	4.90	
Sum			203.976												
Step	40Ar/39Ar	±	40*Ar	±	40*Ar/39Ar	±	37Ar/39Ar	38Cl/39Ar	39Ar/36Ar	±	40Ar/36Ar	±	% Ar	Age (Ma)	± (Ma)
PhB step 1	303.11	8.07	193.7	0.4	233.24	6.23	0.0293	1.039	4.27	0.11	1295	2	0.4	1911.8	51.0
PhB step 2	265.57	0.87	1675.5	3.3	247.66	0.95	0.0062	0.043	16.67	0.06	4426	7	3.7	1983.2	7.6
PhB step 3	251.49	1.44	966.8	3.1	248.74	1.63	0.0020	0.032	108.50	0.93	27287	82	5.6	1988.4	13.0
PhB step 4	253.87	1.51	851.7	2.8	249.45	1.68	0.0021	0.033	67.56	0.49	17152	52	7.3	1991.9	13.4
PhB step 5	254.84	1.19	1136.1	3.5	250.36	1.40	0.0018	0.035	66.61	0.43	16974	49	9.5	1996.2	11.1
PhB step 6	253.76	0.52	3965.7	8.5	252.33	0.71	0.0007	0.031	209.16	0.82	53077	89	17.2	2005.7	5.7
PhB step 7	252.47	0.63	5034.2	13.8	251.40	0.87	0.0007	0.029	278.54	1.27	70323	152	27.1	2001.3	6.9
PhB step 8	252.47	0.52	6309.6	14.4	250.87	0.73	0.0006	0.029	186.73	0.79	47143	85	39.4	1998.7	5.8
PhB step 9	253.09	0.61	4250.6	9.3	251.92	0.78	0.0006	0.030	255.19	1.32	64586	108	47.7	2003.8	6.2
PhB step 10	252.30	0.67	4080.1	13.0	251.17	0.98	0.0007	0.030	264.32	1.38	66688	179	55.6	2000.1	7.8
PhB step 11	252.32	0.56	4121.4	10.5	251.28	0.80	0.0006	0.030	287.63	1.42	72577	149	63.7	2000.7	6.3
PhB step 12	251.67	0.55	5121.6	11.1	250.63	0.73	0.0006	0.030	287.51	1.49	72356	121	73.7	1997.5	5.9
PhB step 13	251.76	0.44	7153.0	13.9	251.03	0.63	0.0004	0.030	407.79	2.20	102665	155	87.6	1999.5	5.0
PhB step 14	252.37	0.48	6188.6	15.5	251.38	0.74	0.0006	0.029	303.89	1.26	76693	157	99.7	2001.2	5.9
PhB step 15	324.73	11.2	149.1	0.5	255.99	8.88	0.0107	0.061	4.34	0.15	1410	5	100.0	2023.2	70.2
Sum / age calculated out of sum			51197.8		251.00										2028.7
Fractionation correction per 2 amu			1.0099		Air ⁴⁰ Ar/ ³⁶ Ar=298.55 (Lee et al, 2006)										
J=0.0080842±1% (FCs)					λ=5.543*10 ⁻¹⁰ (Steiger and Jäger, 1977)										

Chapter 3. ^{87}Rb - ^{87}Sr , ^{40}K - ^{40}Ca and ^{40}Ar - ^{39}Ar intercalibration.

Table 9. Results for the Ar-Ar step heating of the Rubikon lepidolite.

Step	40Ar (mV)	±	39Ar (mV)	±	38Ar (mV)	±	37Ar (mV)	±	36Ar (mV)	±	35Cl (mV)	±	40Ar/36Ar	±	
Lep step 1	192.90	0.92	0.1848	0.0190	0.3150	0.0015	0.00506	0.00013	0.6468	0.0036	0.016821	0.00015	298.26	2.02	
Lep step 2	83.82	0.32	0.3238	0.0190	0.1357	0.0007	0.00534	0.00014	0.2531	0.0011	0.016928	0.00016	331.18	2.14	
Lep step 3	136.35	0.37	1.1777	0.0260	0.1060	0.0005	0.00591	0.00015	0.3074	0.0010	0.017806	0.00014	443.61	2.29	
Lep step 4	351.64	1.00	6.0221	0.0260	0.2634	0.0009	0.02840	0.00018	0.4509	0.0013	0.017903	0.00014	779.93	3.51	
Lep step 5	1060.18	1.70	23.8981	0.0008	0.3884	0.0009	-0.00691	0.04100	0.4265	0.0002	0.019106	0.00018	2485.76	6.84	
Lep step 6	1922.63	1.20	47.0573	0.0009	0.6742	0.0007	-0.00661	0.04200	0.3234	0.0001	0.018221	0.00017	5944.32	7.25	
Lep step 7	732.59	0.36	17.7601	0.0200	0.2680	0.0006	0.02237	0.00038	0.1336	0.0003	0.018124	0.00016	5482.30	13.08	
Lep step 8	350.72	0.19	8.3632	0.0200	0.1393	0.0004	0.01140	0.00022	0.0851	0.0003	0.018507	0.00014	4120.55	12.44	
Lep step 9	886.56	0.79	21.9767	0.0006	0.2949	0.0003	-0.00598	0.03400	0.1024	0.0001	0.016303	0.00012	8656.65	12.69	
Lep step 10	9645.08	14.00	243.8699	0.0039	3.1028	0.0008	-0.00605	0.40000	0.2771	0.0002	0.016526	0.00015	34801.70	51.36	
Lep step 11	701.16	0.41	17.0510	0.0220	0.2483	0.0005	0.02162	0.00036	0.1286	0.0005	0.017627	0.00014	5451.37	12.39	
Lep step 12	511.82	0.38	12.3185	0.0240	0.1871	0.0005	0.01558	0.00033	0.1206	0.0004	0.017569	0.00013	4245.61	11.66	
Lep step 13	161.78	0.08	3.1422	0.0190	0.0762	0.0003	0.00413	0.00012	0.1367	0.0004	0.017353	0.00011	1183.76	4.90	
Lep step 14	122.57	0.06	0.6774	0.0210	0.0831	0.0003	0.00177	0.00010	0.3203	0.0007	0.017616	0.00013	382.69	1.59	
sum			403.83												
Step	40Ar/39Ar	±	40*Ar	±	40*Ar/39Ar	±	37Ar/39Ar	38Cl/39Ar	39Ar/36Ar	±	40Ar/36Ar	±	% Ar	Age (Ma)	± (Ma)
Lep step 1	1043.65	107.91	-0.194	-0.002	-1.05	-0.11	0.0570	1.0393	0.29	0.03	298	2	0.05	-15.39	-1.59
Lep step 2	258.89	15.30	8.3	0.1	25.50	1.52	0.0335	0.2612	1.28	0.08	331	2	0.13	338.10	20.10
Lep step 3	115.77	2.59	44.6	0.3	37.86	0.87	0.0099	0.0298	3.83	0.09	444	2	0.42	481.66	11.06
Lep step 4	58.39	0.30	217.0	1.2	36.04	0.25	0.0056	0.0180	13.36	0.07	780	4	1.91	461.27	3.20
Lep step 5	44.36	0.07	932.8	3.1	39.03	0.13	0.0000	0.0011	56.03	0.02	2486	7	7.83	494.77	1.65
Lep step 6	40.86	0.03	1826.1	3.1	38.81	0.07	0.0000	0.0012	145.49	0.05	5944	7	19.48	492.23	0.84
Lep step 7	41.25	0.05	692.7	1.8	39.00	0.11	0.0016	0.0019	132.91	0.35	5482	13	23.88	494.42	1.42
Lep step 8	41.94	0.10	325.3	1.0	38.90	0.16	0.0021	0.0029	98.26	0.45	4121	12	25.95	493.25	1.98
Lep step 9	40.34	0.04	856.0	1.7	38.95	0.08	0.0000	0.0007	214.59	0.19	8657	13	31.39	493.83	0.98
Lep step 10	39.55	0.06	9562.3	22.0	39.21	0.09	0.0000	0.0007	879.94	0.57	34802	51	91.78	496.73	1.14
Lep step 11	41.12	0.06	662.8	1.7	38.87	0.11	0.0016	0.0013	132.57	0.50	5451	12	96.00	492.94	1.41
Lep step 12	41.55	0.09	475.8	1.4	38.63	0.14	0.0017	0.0015	102.18	0.40	4246	12	99.05	490.25	1.76
Lep step 13	51.49	0.31	121.0	0.5	38.50	0.29	0.0031	0.0043	22.99	0.15	1184	5	99.83	488.84	3.63
Lep step 14	180.94	5.64	26.9	0.1	39.78	1.25	0.0111	0.0232	2.12	0.07	383	2	100.00	502.97	15.82
Sum / age calculated out of sum			15751.4		39.01									494.45	
Fractionation correction per 2 amu	1.0096		Air ⁴⁰ Ar/ ³⁶ Ar=298.55 (Lee et al, 2006)												
J=0.0080842±1% (FCs)	λ=5.543*10 ⁻¹⁰ (Steiger and Jäger, 1977)														

Table 10. Results for the Ar-Ar step heating of the Siilinjärvi phlogopite.

Step	40Ar (mV)	±	39Ar (mV)	±	38Ar (mV)	±	37Ar (mV)	±	36Ar (mV)	±	35Cl (mV)	±	40Ar/36Ar	±
Si step1	63.93	0.03	0.062	0.02	0.0389	0.000	0.12265	0.00032	0.16047	0.0004	0.01843	0.0001	398.39	1.97
Si step2	327.09	0.25	0.977	0.02	0.0884	0.000	0.04202	0.00022	0.33611	0.0006	0.01842	0.0001	973.18	2.97
Si step3	545.26	0.36	2.345	0.01	0.0460	0.000	0.01021	0.00013	0.04240	0.0001	0.01782	0.0001	12859.85	82.00
Si step4	2066.76	1.00	9.016	0.02	0.1343	0.000	0.01327	0.00013	0.04404	0.0002	0.01769	0.0001	46932.64	156.27
Si step5	2312.75	1.30	10.160	0.02	0.1538	0.000	0.01045	0.00013	0.06104	0.0002	0.01777	0.0001	37891.63	108.64
Si step6	5031.73	5.30	22.183	0.04	0.3046	0.000	0.01190	0.00013	0.05404	0.0003	0.01754	0.0001	93111.32	195.44
Si step7	7150.79	7.60	31.517	0.04	0.4313	0.000	0.01294	0.00012	0.05509	0.0003	0.01767	0.0001	129800.5	291.89
Si step8	6630.51	5.10	29.154	0.04	0.4034	0.000	0.01275	0.00013	0.04757	0.0002	0.01802	0.0001	139391.9	317.46
Si step9	2417.63	1.90	10.574	0.02	0.1606	0.000	0.00686	0.00009	0.05121	0.0002	0.01839	0.0001	47213.29	126.77
Si step10	418.64	0.35	1.666	0.01	0.0591	0.000	0.00580	0.00009	0.12452	0.0003	0.01880	0.0001	3362.13	15.69
Si step11	187.54	0.09	0.775	0.02	0.0333	0.000	0.00551	0.00007	0.04948	0.0001	0.01861	0.0001	3790.49	20.66
Si step12	210.13	0.12	0.730	0.02	0.0556	0.000	0.00526	0.00008	0.13008	0.0004	0.01858	0.0001	1615.41	6.49
Sum			119.16											

Step	40Ar/39Ar	±	40*Ar	±	40*Ar/39Ar	±	37Ar/39Ar	38Cl/39Ar	39Ar/36Ar	±	40Ar/36Ar	±	% ³⁹ Ar	Age (Ma)	± (Ma)
Si step1	1034.55	352.5	16.0	0.1	259.23	88.36	1.9738	0.1340	0.39	0.13	398.39	1.97	0.1	2038.5	694.8
Si step2	334.86	6.88	226.7	0.7	232.13	4.83	0.0428	0.0147	2.91	0.06	973.18	2.97	0.9	1906.1	39.6
Si step3	232.47	1.80	532.6	3.5	227.07	2.29	0.0043	0.0044	55.32	0.47	12859.85	82.00	2.8	1880.3	18.9
Si step4	229.24	0.55	2053.6	7.2	227.78	0.96	0.0015	0.0022	204.73	1.13	46932.64	156.27	10.4	1883.9	7.9
Si step5	227.64	0.55	2294.5	7.1	225.84	0.88	0.0010	0.0022	166.46	0.83	37891.63	108.64	18.9	1874.0	7.3
Si step6	226.83	0.53	5015.6	12.8	226.10	0.74	0.0005	0.0015	410.49	2.65	93111.32	195.44	37.5	1875.3	6.2
Si step7	226.89	0.42	7134.3	19.1	226.36	0.69	0.0004	0.0016	572.10	3.23	129800.50	291.89	64.0	1876.6	5.8
Si step8	227.43	0.37	6616.3	17.2	226.94	0.67	0.0004	0.0017	612.90	3.83	139391.94	317.46	88.5	1879.6	5.6
Si step9	228.63	0.57	2402.3	7.1	227.18	0.86	0.0006	0.0025	206.51	1.08	47213.29	126.77	97.3	1880.9	7.1
Si step10	251.32	2.88	381.5	1.8	229.00	2.84	0.0035	0.0098	13.38	0.16	3362.13	15.69	98.7	1890.2	23.5
Si step11	242.01	7.52	172.8	1.0	222.94	7.03	0.0071	0.0193	15.66	0.49	3790.49	20.66	99.4	1858.9	58.7
Si step12	287.90	9.10	171.3	0.7	234.69	7.48	0.0072	0.0312	5.61	0.18	1615.41	6.49	100.0	1919.0	61.2
Sum / age calculated out of sum			27017.6											1878.6	

Fractionation correction per 2 amu	1.0056	Air ⁴⁰ Ar/ ³⁶ Ar=298.55 (Lee et al, 2006)
J=0.0080842±1% (FCs)		λ=5.543*10 ⁻¹¹ (Steiger and Jäger, 1977)

Chapter 3. ^{87}Rb - ^{87}Sr , ^{40}K - ^{40}Ca and ^{40}Ar - ^{39}Ar intercalibration.

Table 11. Results for the Ar-Ar step heating of the Kotuy biotite

Step	40Ar(mV)	±	39Ar(mV)	±	38Ar (mV)	±	37Ar(mV)	±	36Ar(mV)	±	35Cl (mV)	±	40Ar/36Ar	±
Ko step 1	57.28	0.02	0.243	0.02	0.6989	0.0008	0.00227	0.00008	0.19213	0.0003	0.01799	0.0001	298.1	0.3
Ko step 2	30.8	0.02	0.509	0.021	0.1428	0.0004	0.03103	0.00019	0.08065	0.0002	0.01816	0.0001	381.9	1
Ko step 3	41.91	0.02	0.694	0.02	0.1642	0.0003	0.01299	0.00015	0.1084	0.0003	0.01789	0.0001	386.6	0.8
Ko step 4	121.19	0.06	1.674	0.021	0.4112	0.0008	0.01959	0.00014	0.33543	0.0006	0.01823	0.0001	361.3	0.8
Ko step 5	92.15	0.04	3.998	0.019	0.696	0.001	0.00398	0.00012	0.09039	0.0003	0.01821	0.0001	1019.4	1.5
Ko step 6	86.39	0.04	3.995	0.018	0.6783	0.0009	0.00196	0.00009	0.07187	0.0002	0.0182	0.0001	1202	1.6
Ko step 7	57.38	0.03	2.224	0.022	0.3882	0.0007	0.00115	0.00009	0.0702	0.0002	0.01819	0.0001	817.4	1.5
Ko step 8	61.99	0.03	2.42	0.02	0.4212	0.0008	0.00532	0.00011	0.07478	0.0003	0.018	0.0001	829	1.6
Ko step 9	169.25	0.06	8.328	0.018	1.4168	0.0014	0.05344	0.00023	0.11216	0.0003	0.01759	0.0001	1509.1	1.6
Ko step10	214.44	0.12	11.118	0.017	1.8741	0.0021	0.12378	0.00033	0.11683	0.0003	0.01811	0.0001	1835.5	2.3
Ko step11	233.38	0.11	11.61	0.02	2.0706	0.0019	0.28766	0.0006	0.15592	0.0005	0.01834	0.0001	1496.8	1.6
Ko step12	133.03	0.05	5.139	0.019	1.0092	0.0011	0.2044	0.00046	0.17271	0.0005	0.01845	0.0001	770.2	0.9
Ko step13	89.18	0.03	1.351	0.019	0.4053	0.0008	0.21018	0.00048	0.23286	0.0005	0.01867	0.0001	383	0.7
Ko step14	66.65	0.03	0.233	0.022	0.1392	0.0004	0.09037	0.00032	0.21533	0.0004	0.0181	0.0001	309.5	0.9
Ko step15	124.83	0.06	0.146	0.017	0.1484	0.0004	0.14748	0.00041	0.43138	0.0007	0.01865	0.0001	289.4	0.8
Sum			53.68											

Step	40Ar/39Ar	±	40*Ar	±	40*Ar/39Ar	±	37Ar/39Ar	38Cl/39Ar	39Ar/36Ar	±	40Ar/36Ar	±	% 39Ar	Age (Ma)	± (Ma)
Ko step 1	235.24	19.5	-0.0829		-0.34	-0.03	0.033	2.686	1.267	0.104	298.1	0.3	0.45	-4.97	-0.41
Ko step 2	60.55	2.53	6.72	0.02	13.21	0.55	0.0713	0.2374	6.306	0.261	381.9	1	1.4	183.04	7.66
Ko step 3	60.36	1.76	9.55	0.02	13.75	0.4	0.0267	0.1939	6.406	0.186	386.6	0.8	2.69	190.14	5.55
Ko step 4	72.38	0.92	21.04	0.05	12.57	0.16	0.015	0.195	4.992	0.063	361.3	0.8	5.81	174.54	2.25
Ko step 5	23.05	0.11	65.16	0.12	16.3	0.08	0.0024	0.1564	44.229	0.268	1019.4	1.5	13.26	223.28	1.15
Ko step 6	21.63	0.1	64.93	0.11	16.26	0.08	0.002	0.153	55.579	0.312	1202	1.6	20.7	222.74	1.09
Ko step 7	25.8	0.26	36.42	0.08	16.38	0.17	0.0032	0.1553	31.68	0.338	817.4	1.5	24.85	224.31	2.3
Ko step 8	25.62	0.21	39.67	0.09	16.39	0.14	0.0046	0.1549	32.364	0.299	829	1.6	29.35	224.48	1.94
Ko step 9	20.32	0.05	135.77	0.21	16.3	0.04	0.007	0.1542	74.254	0.276	1509.1	1.6	44.87	223.34	0.59
Ko step10	19.29	0.03	179.56	0.31	16.15	0.04	0.0114	0.1531	95.164	0.342	1835.5	2.3	65.58	221.38	0.51
Ko step11	20.1	0.04	186.83	0.28	16.09	0.04	0.0248	0.1623	74.46	0.271	1496.8	1.6	87.21	220.63	0.51
Ko step12	25.89	0.1	81.46	0.13	15.85	0.06	0.0401	0.1765	29.752	0.14	770.2	0.9	96.78	217.53	0.88
Ko step13	66.01	0.94	19.66	0.04	14.55	0.21	0.1569	0.2539	5.802	0.083	383	0.7	99.29	200.62	2.89
Ko step14	286.53	27.3	2.36	0.01	10.13	0.97	0.4057	0.4126	1.08	0.102	309.5	0.9	99.73	142.05	13.59
Ko step15	855.59	100.	-3.96	-0.01	-27.16	-3.2	1.0314	0.4591	0.338	0.039	289.4	0.8	100	-447	-52.68
Sum / age calculated out of sum			849		15.82									217.08	
Fractionation correction per 2 amu			1.0056	Air ⁴⁰ Ar/ ³⁶ Ar=298.55 (Lee et al, 2006)											
J=0.0080842±1% (FCs)				λ=5.543*10 ⁻¹⁰ (Steiger and Jäger, 1977)											

5. Discussion

A precise and accurate decay constant intercalibration with geological methods requires an exceptional accuracy to achieve the uncertainty lower than 1%. Although the individual dating methods like U-Pb, Ar-Ar, Rb-Sr and now even K-Ca can reach low uncertainties on the individual ages, there are a number of other conditions that have to be met. The successful intercalibration requires samples with a wide age spread, with a “point-like” geological history (samples have been formed rapidly and have not been altered, exchanged or lost radiogenic daughter isotopes since); it involves precise measurements in well constrained conditions. Such calibration includes accurate and precise spike calibrations with spike ratios optimally suited to the isotopic ratios of each individual sample. And the last but not the least successful intercalibration requires well known reference constants like the age of the flux monitor for Ar-Ar and the decay constant for U-Pb or Rb-Sr systems. Here we tested the intercalibration of the four dating systems with the aim to obtain an accurate and precise ^{40}K decay constant and its branching ratio. Even if precise ages with three dating systems were obtained for the Phalaborwa sample, two main requirements still must be met: a well calibrated Ar-Ar flux monitor and a “point-like” geological history of the sample.

5.1. Ar-Ar flux monitor

Fish Canyon sanidine (FCs) is often used as a flux monitor and has been dated with a number of methods by various workers: Renne et al (1994) with age spread of 27.91–28.09 Ma; Renne et al (1998) with age of 28.02 ± 0.28 Ma; Jourdan and Renne (2007) with more precise age of 28.03 ± 0.08 Ma; Kuiper et al (2008) with astronomically calibrated age of 28.201 ± 0.046 Ma; Renne et al. (2010) with Ar-Ar and U-Pb intercalibrated age of 28.305 ± 0.036 Ma; Channell et al. (2010) with best-fit age of 27.93 Ma (without published uncertainty band) to astrochronologically calibrated lava flows on Maui; and Rivera et al (2011) with a precise astronomically calibrated age of 28.172 ± 0.028 Ma. Each of these methods can be the subject of inaccuracies and interlaboratory calibration issues, moreover each of this methods uses different ^{40}K total decay constant, for example Kuiper et al (2008) and Rivera et al (2011) used Min et al. (2000) value of $(5.463 \pm 0.214) \times 10^{-10} \text{ a}^{-1}$, Renne et al (2010) used estimated by U-Pb and Ar-Ar age intercomparison value of $(5.5492 \pm 0.0093) \times 10^{-10} \text{ a}^{-1}$; the difference in calculated Ar-Ar age between first and second decay constants would be 1.55%. The U-Pb zircon ages were also obtained for the FCs and represent a discrepancy in the data, some overlap with Ar-Ar ages 27.98 ± 0.15 Ma (Villeneuve et al., 2000), some indicate older ages 28.41 ± 0.05 Ma (Oberli et al., 1990), 28.498 ± 0.035 Ma (Schmitz and Bowring, 2001); or even variable zircon population 28.67–28.03 Ma (Bachmann et al., 2007).

During step-heating measurements of our FCs monitor we observed signs of non-homogeneity. ^{37}Ar and ^{38}Ar release during the first and the last steps indicate high Ca and

Cl concentrations at the released phases (Fig.11). We also observed the age variation depending on the steps: early steps correspond to the younger and later to the older ages. The core 8 steps gave the age discrepancy of 0.5%, and the first and the last excluded high Ca/Cl steps gave difference of 24%. This strongly indicates that the standard itself is not uniform. A similar dishomogeneity was observed for other natural mineral monitors (Heri et al., 2014), who also had predicted that Fish Canyon sanidine would as well be inhomogeneous on the basis of its polyphaser petrogenesis. Such heterogeneities can be crucial for the precise age determination and make the desirable precision of 0.1% on the current flux monitor questionable. Depending of the method one uses (a step heating, a total gas release) the resulting age for the J determination might be either a few middle steps, or, in the case of the total release, a sum of different phases. Moreover step heating may or may not include the first cleaning step, which releases Ar of the first low temperature phase, the total gas release with a laser integrates Ar of all phases of a mineral. Thus the problem of the flux monitor standard is not yet resolved. A choice of the technique and the reference standard age might produce a systematic shift in Ar-Ar ages. Therefore the preferred reference age of the FC sanidine standard and the chosen measurement technique might produce an additional artifact while used for the determination of the ^{40}K decay constant.

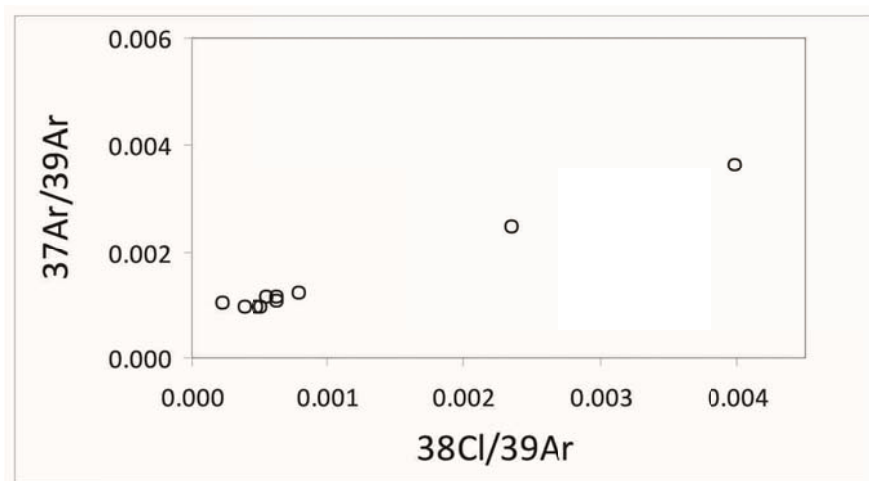


Fig. 11. $^{37}\text{Ar}/^{39}\text{Ar}$ vs $^{38}\text{Cl}/^{39}\text{Ar}$ representing Ca/K vs Cl/K ratios showing non-homogeneity of the Fish Canyon sanidine. First high Cl step eliminated.

5.2. “Point-like” event

Not all our samples reflect geologically “point-like” event. Siilinjärvi carbonatite sample Si102 was dated by Rukhlov and Bell (2010) with a $^{207}\text{Pb}/^{206}\text{Pb}$ in situ method on zircon at 2594 ± 13 Ma. Their high MSWD=21 indicates that the complex was not a true “geologically point-like” rock. The same authors pointed that the complex underwent a post-emplacement metamorphic event, which was dated with a lower discordia intercept at 1894 ± 78 Ma and at ca. 2000 - 2100 Ma with the $^{208}\text{Pb}/^{232}\text{Th}$ method. Our Ar-Ar isochron

age of 1879 ± 24 Ma confirms the post emplacement event and the Rb-Sr age place it more precisely at 1869 ± 10 Ma. The overlapping Ar-Ar and Rb-Sr ages suggests that the mica was reset during a post-emplacement metamorphism. A fresh appearance of the Siilinjärvi phlogopite under a binocular microscope (Fig.2) shows that mica crystallized during the post-emplacement event. Because the system was not monogenetic, it is imprudent to assume that the K-Ca and K-Ar ages should be equal.

Within the uncertainty (0.83% for Rb-Sr, 6.4% for K-Ca and 2% for Ar-Ar) the age of the Rubikon lepidolite coincide with the U-Pb age of columbite 505.5 ± 2.6 Ma (Melcher et al., 2015), indicating that the sample has a “point-like” geologic history. However the resolution unfortunately does not allow us to assess the intercalibration of the U-Pb, Rb-Sr, Ar-Ar and K-Ca systems with the Rubikon sample. Current scatter on the K-Ca isochron most likely can be explained not by an open system behavior, but by an incomplete fractionation correction of the data with a conventional exponential law. The application of an additional correction term (Caro et al., 2003; 2006) adapted to Ca (Naumenko-Dèzes et al., 2015) has to be tested for spiked samples and may reduce the scatter.

The Kotuy sample (Bolgoghtokh intrusion) was drilled out of a stock emplaced at the north-west end of the Norilsk area and represents a younger event than a main phase of the volcanism in the area. The main U-Pb age of the Siberian flood basalts is 251 Ma and point to a very large rapid eruption. Ar-Ar ages for the area are consistently younger 248-249Ma (Reichow et al., 2002; Renne and Basu, 1991), which is explained with the probable 1 % offset of the ^{40}K decay constant or the Ar-Ar flux monitor miscalibration. Thereby the Siberian flood basalts either were not affected by later alteration or it affected the Ar-Ar system less than by 1%. Our sample belongs to the later magmatic reactivation (*ca.*229Ma) of the region. The Rb-Sr age of this sample obtained by Nebel et al (2011) with the $\lambda = 1.3975 \times 10^{-11} \text{a}^{-1}$ (almost identical to those used by us) gave the age of 229.04 Ma indistinguishable from the U-Pb age of 229.05 ± 0.36 Ma (Kamo et al., 2003). Our Ar-Ar ages within the 2% analytical uncertainty coincide with U-Pb and Rb-Sr ages. The signs of alteration observed by us on the electron back-scattered image (see Appendix 2) and the non-homogeneity during step-heating Ar-Ar measurements, which might be attributed to an alteration, did not affect the Ar-Ar system higher than the limit of our uncertainty. Therefore this sample appears to represent a “point-like” event and have to be investigated further. Initially due to zonation of the mica this sample was not approved for the K-Ca and Rb-Sr intercalibration; in a view of our findings this sample is considered to be a decent candidate for the future intercalibration work.

Our best candidate for the geologically “point-like” event was the Phalaborwa complex. It was studied and dated by multiple workers (see Table 1). The homogenous U-Pb age distribution for the complex shows that it was intruded and cooled down to the temperature of baddeleyite and zircon crystallization rapidly. Attempts of the Rb-Sr dating

were less broad. Eriksson (1984) mentioned a Rb-Sr age without specifying of the decay constant used for calculations. We assumed it was the recommended ^{87}Rb decay constant (Steiger and Jäger, 1977) of that time. The recalculated to the modern constant (Villa et al, 2015) the Rb-Sr age is 2047 ± 19 Ma which overlaps with the U-Pb age and coincide with a low precision Rb-Sr age of 2013 ± 93 Ma published by Yuhara et al. (2005). Nebel et al. (2011) used a carbonatite of the Phalaborwa complex for the ^{87}Rb decay intercalibration with the U-Pb system. Their data, recalculated with a modern ^{87}Rb decay constant (Villa et al, 2015), gave the Rb-Sr age of 2050 ± 4.8 Ma (2σ). Our attempt to achieve a high precision Rb-Sr age resulted in 2058.9 ± 5.2 Ma (2σ), which overlaps with all previous Rb-Sr and U-Pb ages. K-Ca and Ar-Ar ages calculated with the decay constants of Steiger and Jäger (1977) are younger by approximately 1%.

It should be specified that the coincidence of the K-Ca and Ar-Ar ages is within 0.5-2% of uncertainty. Moreover the coinciding age does not yet rule out the possible alteration, whose impact on different systems was not yet profoundly studied. Phalaborwa phlogopite which looks pristine coexists with a diopside that has signs of weathering: serpentinisation along cleavage planes. Alterations of element concentrations of phlogopite below 1% cannot be resolved with the resolution of microprobe analysis, whose sensitivity is few percent. Indeed, stepwise heating shows a slightly discordant age spectrum and Ca/Cl/K systematics. This is proof of the presence of minor contamination by younger phases. Inability to prove the point-like geological history of the sample to the limit of <1% makes the intercalibrations attempts to reach 0.1 % uncertainty on the ages subject of a chance.

5.3. ^{40}K decay constant

The discrepancies between two mostly used and precise U-Pb and K-Ar, Ar-Ar dating systems have been a subject of critical reviewing (e.g. Renne et al., 1998, 2000, 2010; Min et al., 2000, 2001; Nomade et al., 2004; Schmitz and Bowring, 2001; Villeneuve et al., 2000; Schoene et al., 2006, Jourdan et al., 2009) and were attributed to the offset of the ^{40}K decay constant. Multiple attempts to recalibrate the ^{40}K decay constants and to reevaluate the available counting experiments data did not bring the consistency. The ^{40}K total decay constant and the branching ratio recommended by Bé et al. (2004) is higher than proposed by Min et al. (2000) and (Renne et al. (2010).

A Phalaborwa phlogopite age calculated with the K-Ca isochron strongly depends on the decay constants used for the calculations (Table 12). Currently recommended ^{40}K constants of Steiger and Jäger (1977) gives the age approximately 0.5-1% younger, the same effect have the constants of Bé et al (2014), Kossert and Günter (2004) and the constants modeled by Renne et al. (2010). Constants recommended by Min et al. (2000), used for calibration of irradiation monitor standards (Kuiper et al., 2008; Rivera et al., 2013; Rivera et al., 2011), give 0.5% higher age, but overlap within the analytical uncertainty of the K-Ca age. The decay constants recalculated by Renne et al. (2011) also

give the K-Ca age consistent with the Rb-Sr age of the complex but do not overlap with the U-Pb age of 2060.4 ± 0.4 Ma (Kumar et al., 2014).

Table 12. Various combinations of the ^{40}K total and beta decay constants, represented by branching ratio B ($\lambda_{\text{tot}}/\lambda_{\beta^-}$), and the Phalaborwa phoscorite K-Ca age calculated with the slope of 1.8781 ± 0.012 (2σ).

λ_{tot} (10^{-10})	λ_{β^-} (10^{-10})	B ($\lambda_{\text{tot}}/\lambda_{\beta^-}$)	Age (Ma)	$\pm 2\sigma$ (Ma) ($\pm 0.64\%$)	Reference
5.543	4.962	0.8952	2040.0	13.0	Steiger and Jäger, 1977
5.549	4.974	0.8963	2036.2	13.0	Renne et al., 2010
5.531	4.955	0.8959	2043.6	13.1	Renne et al., 2011 (recalc)
5.543	4.947	0.8925	2043.5	13.1	Bé et al, 2014
5.551	4.959	0.8933	2039.5	13.0	λ_{β^-} from Kossert and Günter, 2004; B Nögler and Villa, 2000
5.464	4.884	0.8939	2071.3	13.2	Min et al., 2000
5.491	4.911	0.8944	2060.4	13.2	"best fit" this work

The constants themselves have various uncertainties, for example ^{40}K decay constants of Min et al. (2000) have an uncertainty band of *ca.* 2%, Renne et al. (2011) *ca.* 1 %, Bé et al. (2014) *ca.* 0.5%, the branching ratio of Bé et al. (2014) has an uncertainty of *ca.* 1.5 %, and Nögler and Villa (2000) 1%. These uncertainties on the decay constants are neglected during Ar-Ar age calculation procedures, thus we also treated them as absolute values without uncertainties.

The attempt to assess the best fit for the ^{40}K total decay constant with a combination of a possible branching ratio is shown on the fig.13. So far the minimum branching ratio (B_{min}) was calculated by Bé et al. (2014) and the maximum branching ratio (B_{max}) was estimated by Renne et al. (2010). The only independent branching ratio measured by Nögler and Villa (2000) is lying in between and has an uncertainty of 1% which is marked on the figure. This range of B coincides with our band of the age-fit likelihood. Within 2σ uncertainty of our slope two decay constants are the most suitable: Min et al (2000) and recalculated values of Renne et al. (2010) (Renne et al., 2011). B_{max} and B_{min} mark the range of reported branching ratios without their uncertainties and states that two ^{40}K decay constants are most likely be accurate for the K-Ca system. The best fitting values we can derive from this sample are $\lambda_{\text{tot}} = (5.491 \pm 0.035) \times 10^{-10} \text{ a}^{-1}$, $\lambda_{\beta^-} = (4.911 \pm 0.031) \times 10^{-10} \text{ a}^{-1}$, which gives $\lambda_{\text{Ar}} = (0.580 \pm 0.005) \times 10^{-10} \text{ a}^{-1}$, the same λ_{Ar} as suggested by Min et al. (2000).

This work managed to narrow down the range of possibilities of ^{40}K decay constants combinations, however the high accuracy and precision Ar-Ar data is required to assess the independent evaluation of the branching ratio as well as additional samples of the wide time range to establish simultaneously also the ^{40}K total decay constant. The single most important factor is the choice of natural samples whose internal heterogeneity (chemical and isotopic) must be lower than 1%. At the present stage no such homogeneous minerals have been observed, especially not the "age standards" used by the Ar-Ar community.

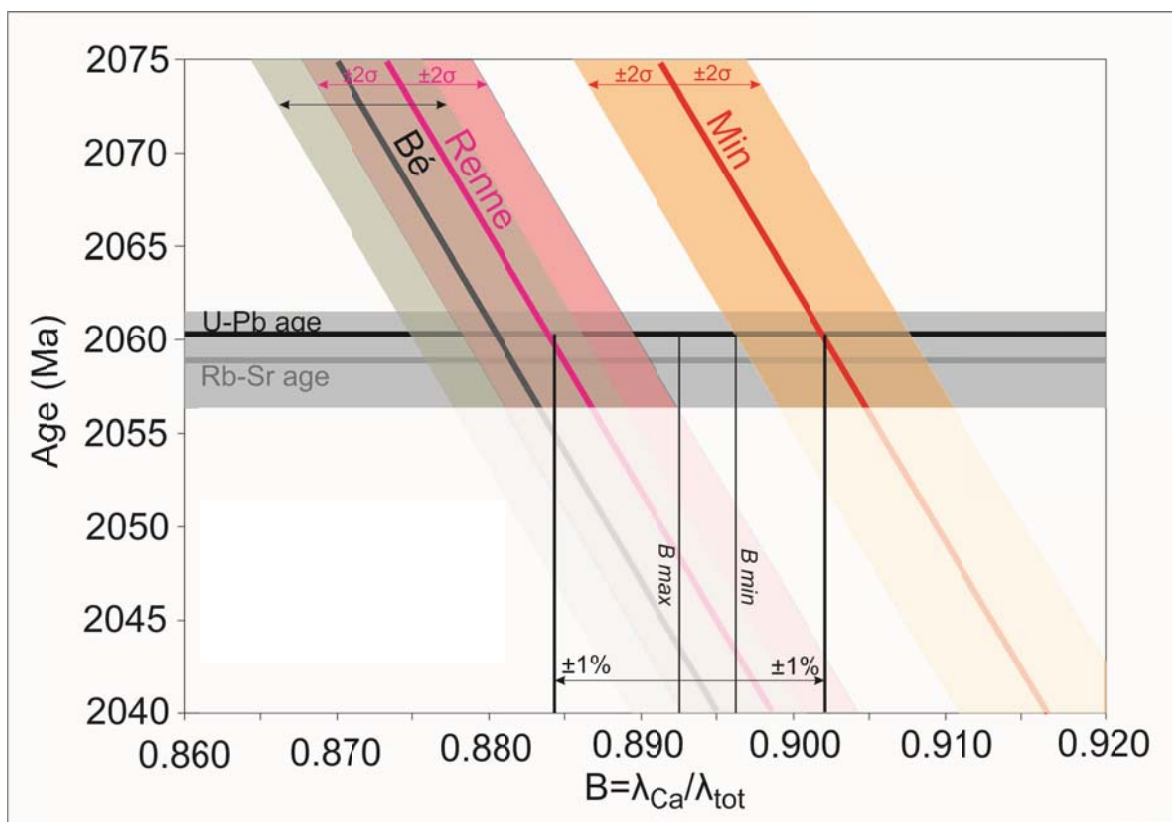


Fig. 13. The dependency of the K-Ca age on the decay constants. The black horizontal line and the grey horizontal band represent reference U-Pb and Rb-Sr ages of the complex. The dark gray inclined line represents the K-Ca age calculated with the ^{40}K total decay constant of Bé et al. (2014) and variable branching ratio B . The gray inclined band represents the uncertainty on the K-Ca slope. The uncertainty of the decay constant was not included. The magenda and the orange lines with uncertainty bands represent accordingly age calculated with the ^{40}K total decay constant of Renne et al. (2011) and Min et al. (2000). Decay constants of Renne et al. (2010) and Kossert and Günter (2006) were not plotted here, they lie within the uncertainty range from Bé et al. (2014). B_{max} represent maximum value of published branching ratio $B = \lambda_{\text{Ca}} / \lambda_{\text{tot}}$ (Renne et al., 2010) and B_{min} accordingly minimum value (Bé et al., 2014). Most of other published B lie in between. The uncertainties of B_{max} and B_{min} are not plotted; minimum uncertainty on B published by Nägler and Villa (2000) is represented as $\pm 1\%$ band, this range also indicates the range of ^{40}K total decay constant with the combination of the branching ratios which gives the proper K-Ca age.

6. Conclusions

Four samples have been chosen for the ^{40}K decay constant intercalibration with geological methods. Four samples were dated with an Ar-Ar method, and three samples were dated with Rb-Sr and K-Ca methods. The biotite of the youngest sample from a dolerite dike, Kotuy region, Norilsk resulted in the Ar-Ar isochron age of 225.0 ± 4.8 Ma coinciding within the uncertainty with U-Pb and Rb-Sr ages of 229 Ma (Kamo et al., 2003; Nebel et al., 2011). The Rb-Sr age of 504.7 ± 4.2 Ma for the Rubikon pegmatite and the low precision Ar-Ar and K-Ca ages confirmed the U-Pb columbite age of 505.5 Ma (Melcher et al., 2015). Rb-Sr, Ar-Ar and K-Ca dating of the Siilinjärvi carbonatite complex established a post-emplacement event ca. 1900 Ma, the high precision Rb-Sr age place it at 1869 ± 10 Ma. The 2058.9 Ma Rb-Sr age of the Phalaborwa phoscorite coincide with 2060 Ma previously dated with U-Pb method by multiple workers (see Table 1). K-Ca and Ar-Ar dating for this complex resulted in ca. 1% younger ages.

High precision K-Ca dating also allowed to calculate a possible combination of the ^{40}K total decay constant and the branching ratio. This study confirms stated earlier that the ^{40}K decay constants recommended for the geochronological use (Steiger and Jäger, 1977) give 1% younger Ar-Ar and K-Ca ages. The decay constants of Min et al. (2000) and Renne et al. (2011) with the range of branching ratios ($B (\lambda_{\text{tot}}/\lambda_{\beta^-})$) from 0.8925 to 0.8963 gives the best fit of K-Ca age with the reference age of the Phalaborwa complex.

Acknowledgements

This work was sponsored by Swiss National Foundation grants 200021-131916 and 200020-153126. We are grateful to Dr. Beda Hofman (Naturhistorisches Museum der Burgergemeinde Bern) for the contribution of the Rubikon lepidolite sample and to Prof. Keith Bell (Carleton University, Department of Earth Sciences) for carbonatite samples among which a Siilinjärvi sample (Si102). MND is thankful to Emelie Axelsson for her introduction to the Rb-Sr procedure.

References

- Ahrens, L.H., 1951. The feasibility of a calcium method for the determination of geological age. *Geochimica et Cosmochimica Acta* 1, 312-316.
- Audi, G., Bersillon, O., Blachot, J., Wapstra, A.H., 1997. The Nubase evaluation of nuclear and decay properties. *Nuclear Physics A* 624, 1-124.
- Audi, G., Bersillon, O., Blachot, J., Wapstra, A.H., 2003. The Nubase evaluation of nuclear and decay properties. *Nuclear Physics A* 729, 3-128.
- Bachmann, O., Oberli, F., Dungan, M.A., Meier, M., Mundil, R., Fischer, H., 2007. $^{40}\text{Ar}/^{39}\text{Ar}$ and U–Pb dating of the Fish Canyon magmatic system, San Juan Volcanic field, Colorado: Evidence for an extended crystallization history. *Chemical Geology* 236, 134-166.
- Bé, M.-M., Christè, V., Dulieu, C., Browne, E., Chechev, V., Kuzmenko, N., Helmer, R., Nichols, A., Schönfeld, E., Dersch, R., 2004. Table of Radionuclides, A=1 to 150 ed. Bureau International Des Poids et Mesures, Pavillon de Breteuil, F-92310 Sèvres, p. 285.
- Bé, M.-M., Dulieu, C., Mougeot, X., Kellett, M., 2014. HALF-LIVES. Table of recommended values, 2014 ed. Bureau International Des Poids et Mesures, Pavillon de Breteuil, F-92310 Sèvres, p. 13.
- Beckinsale, R.D., Gale, N.H., 1969. A reappraisal of the decay constants and branching ratio of ^{40}K . *Earth and Planetary Science Letters* 6, 289-294.
- Begemann, F., Ludwig, K.R., Lugmair, G.W., Min, K., Nyquist, L.E., Patchett, P.J., Renne, P.R., Shih, C.Y., Villa, I.M., Walker, R.J., 2001. Call for an improved set of decay constants for geochronological use. *Geochimica et Cosmochimica Acta* 65, 111-121.
- Caro, G., Bourdon, B., Birck, J.-L., Moorbath, S., 2003. ^{146}Sm - ^{142}Nd evidence from Isua metamorphosed sediments for early differentiation of the Earth's mantle. *Nature* 423, 428-432.
- Channell, J.E.T., Hodell, D.A., Singer, B.S., Xuan, C., 2010. Reconciling astrochronological and $^{40}\text{Ar}/^{39}\text{Ar}$ ages for the Matuyama-Brunhes boundary and late Matuyama Chron. *Geochemistry, Geophysics, Geosystems* 11, n/a-n/a.
- Chu, Z.-y., Yang, Y.-h., Jinghui, G., Qiao, G.-s., 2011. Calculation methods for direct internal mass fractionation correction of spiked isotopic ratios from multi-collector mass spectrometric measurements. *International Journal of Mass Spectrometry* 299, 87-93.
- Dalrymple, B.G., Czamanske, G.K., Fedorenko, V.A., Simonov, O.N., Lanphere, M.A., Likhachev, A.P., 1995. A reconnaissance $^{40}\text{Ar}/^{39}\text{Ar}$ geochronologic study of ore-bearing and related rocks, Siberian Russia. *Geochimica et Cosmochimica Acta* 59, 2071-2083.
- de Laeter, J.R., Böhlke, J.K., De Bièvre, P., Hidaka, H., Peiser, H.S., Rosman, K.J.R., Taylor, P.D.P., 2003. Atomic weights of the elements. Review 2000 (IUPAC Technical Report), *Pure and Applied Chemistry*, p. 683.
- Endt, P.M., van der Leun, C., 1973. Energy levels of A=21-44 nuclei (V). *Nuclear Physics* 214, 1-625.
- Engelkemeir, D.W., Flynn, K.F., Glendenin, L.E., 1962. Positron Emission in the Decay of K40. *Physical Review* 126, 1818-1822.
- Eriksson, S.C., 1984. Age of carbonatite and phoscorite magmatism of the Phalaborwa Complex (South Africa). *Chemical Geology* 46, 291-299.
- Fletcher, I.R., McNaughton, N.J., Pidgeon, R.T., Rosman, K.J.R., 1997. Sequential closure of K–Ca and Rb–Sr isotopic systems in Archaen micas. *Chemical Geology* 138, 289-301.
- French, J.E., Heaman, L.M., Chacko, T., 2002. Feasibility of chemical U–Th–total Pb baddeleyite dating by electron microprobe. *Chemical Geology* 188, 85-104.
- Garner, E., Murphy, T., Gramlich, J., Paulsen, P., Barnes, I., 1975. Absolute Isotopic Abundance Ratios and the Atomic Weight of a Reference Sample of K. *J. Res. Natl. Bur. Stand., A* 79, 713-725.
- Gopalan, K., 2008. Conjunctive K–Ca and Rb–Sr dating of glauconies. *Chemical Geology* 247, 119-123.
- Gradstein, F.M., Ogg, J.G., Schmitz, M., Ogg, G., 2012. The Geologic Time Scale. *Newsletters on stratigraphy* 45, 171-188.
- Heaman, L.M., LeCheminant, A.N., 1993. Geochemistry of Accessory Minerals Paragenesis and U–Pb systematics of baddeleyite (ZrO_2). *Chemical Geology* 110, 95-126.
- Heri, A.R., Robyr, M., Villa, I.M., 2014. Petrology and geochronology of ‘muscovite age standard’ B4M. Geological Society, London, Special Publications 378, 69-78.
- Heumann, K., Kubassek, E., Schwabenbauer, W., Stadler, I., 1979. Analytisches Verfahren zur K/Ca-Altersbestimmung geologischer Proben. *Z. Anal. Chem.* 297, 35-43.
- Holmes, A., 1932. The Origin of Igneous Rocks. *Geological Magazine* 69, 543-558.

Holmes, L., Cahen, L., 1956. Geochronologie Africaine. Mem. Cl. Sci. Nat. Med., Acad. R. Sci. Colon.(Brussels), Fasc 1, 169.

Horn, I., Rudnick, R.L., McDonough, W.F., 2000. Precise elemental and isotope ratio determination by simultaneous solution nebulization and laser ablation-ICP-MS: application to U–Pb geochronology. *Chemical Geology* 164, 281-301.

JCGM, 2012. Joint Committee for Guides in Metrology - The International Vocabulary of Metrology - Basic and General Concepts and Associated Terms, 3rd ed., JCGM 200:2012. JCGM.

Jourdan, F., Marzoli, A., Bertrand, H., Cirilli, S., Tanner, L.H., Kontak, D.J., McHone, G., Renne, P.R., Bellieni, G., 2009. $^{40}\text{Ar}/^{39}\text{Ar}$ ages of CAMP in North America: Implications for the Triassic–Jurassic boundary and the ^{40}K decay constant bias. *Lithos* 110, 167-180.

Jourdan, F., Renne, P.R., 2007. Age calibration of the Fish Canyon sanidine $^{40}\text{Ar}/^{39}\text{Ar}$ dating standard using primary K–Ar standards. *Geochimica et Cosmochimica Acta* 71, 387-402.

Kamo, S.L., Czamanske, G.K., Amelin, Y., Fedorenko, V.A., Davis, D.W., Trofimov, V.R., 2003. Rapid eruption of Siberian flood-volcanic rocks and evidence for coincidence with the Permian–Triassic boundary and mass extinction at 251 Ma. *Earth and Planetary Science Letters* 214, 75-91.

Kossert, K., Gunther, E., 2004. LSC measurements of the half-life of ^{40}K . *Applied radiation and isotopes : including data, instrumentation and methods for use in agriculture, industry and medicine* 60, 459-464.

Krumrei, T.V., Villa, I.M., Marks, M.A.W., Markl, G., 2006. A $^{40}\text{Ar}/^{39}\text{Ar}$ and U/Pb isotopic study of the Ilímaussaq complex, South Greenland: Implications for the ^{40}K decay constant and for the duration of magmatic activity in a peralkaline complex. *Chemical Geology* 227, 258-273.

Kuiper, K.F., Deino, A., Hilgen, F.J., Krijgsman, W., Renne, P.R., Wijbrans, J.R., 2008. Synchronizing Rock Clocks of Earth History. *Science* 320, 500-504.

Kumar, A., Nagaraju, E., Srinivasa Sarma, D., Davis, D.W., 2014. Precise Pb baddeleyite geochronology by the thermal extraction-thermal ionization mass spectrometry method. *Chemical Geology* 372, 72-79.

Kwon, J., Min, K., Bickel, P.J., Renne, P.R., 2002. Statistical Methods for Jointly Estimating the Decay Constant of ^{40}K and the Age of a Dating Standard. *Mathematical Geology* 34, 457-474.

Lee, J.-Y., Marti, K., Severinghaus, J.P., Kawamura, K., Yoo, H.-S., Lee, J.B., Kim, J.S., 2006. A redetermination of the isotopic abundances of atmospheric Ar. *Geochimica et Cosmochimica Acta* 70, 4507-4512.

Leutz, H., Schulz, G., Wenninger, H., 1965. The decay of potassium-40. *Z. Physik* 187, 151-164.

Ludwig, K.R., 2012. Isoplot3_75, A Geochronological Toolkit for Microsoft Excel, 3.75 ed, Berkley Geochronology Center

Marshall, B.D., DePaolo, D.J., 1982. Precise age determination and petrogenetic studies using the K–Ca method. *Geochimica et Cosmochimica Acta* 46, 2537-2545.

Melcher, F., Graupner, T., Gäbler, H.-E., Sitnikova, M., Henjes-Kunst, F., Oberthür, T., Gerdes, A., Dewaele, S., 2015. Tantalum-(niobium-tin) mineralisation in African pegmatites and rare metal granites: Constraints from Ta–Nb oxide mineralogy, geochemistry and U–Pb geochronology. *Ore Geology Reviews* 64, 667-719.

Min, K., Mundil, R., Renne, P.R., Ludwig, K.R., 2000. A test for systematic errors in Ar–Ar geochronology through comparison with U–Pb analysis of a 1.1-Ga rhyolite. *Geochimica et Cosmochimica Acta* 64, 73-98.

Nägler, T.F., Villa, I.M., 2000. In pursuit of the ^{40}K branching ratios: K–Ca and ^{39}Ar – ^{40}Ar dating of gem silicates. *Chemical Geology (Isotope Geoscience Section)* 169, 5-16.

Naumenko-Dèzes, M.O., Bouman, C., Nägler, T.F., Mezger, K., Villa, I.M., 2015. TIMS measurements of full range of natural Ca isotopes with internally consistent fractionation correction. *International Journal of Mass Spectrometry* 387, 60-68.

Nebel, O., Scherer, E.E., Mezger, K., 2011. Evaluation of the ^{87}Rb decay constant by age comparison against the U–Pb system. *Earth and Planetary Science Letters* 301, 1-8.

Nelson, D.R., McCulloch, M.T., 1989. Petrogenetic application of the ^{40}K – ^{40}Ca radiogenic decay scheme - A reconnaissance study. *Chemical Geology (Isotope Geoscience Section)* 79, 275-293.

Nomade, S., Renne, P.R., Merkle, R.K.W., 2004. $^{40}\text{Ar}/^{39}\text{Ar}$ age constraints on ore deposition and cooling of the Bushveld Complex, South Africa. *Journal of the Geological Society, London* 161, 441-420.

Oberli, F., Fischer, H., Meier, M., 1990. High resolution ^{238}U – ^{206}Pb zircon dating of Tertiary bentonites and Fish Canyon tuff: a test for age concordance by single-crystal analysis, Seventh international conference on geochronology, cosmochronology and isotope geology.

Reichow, M.K., Saunders, A.D., White, R.V., Pringle, M.S., Al'Mukhamedov, A.I., Medvedev, A.I., Kirda, N.P., 2002. $^{40}\text{Ar}/^{39}\text{Ar}$ Dates from the West Siberian Basin: Siberian Flood Basalt Province Doubled. *Science* 296, 1846-1849.

- Reischmann, T., 1995. Precise U/Pb age determination with baddeleyite (ZrO_2), a case study from the Phalaborwa igneous complex, South Africa. *South African Journal of Geology* 98, 1-4.
- Renne, P.R., 2000. $^{40}\text{Ar}/^{39}\text{Ar}$ age of plagioclase from Acapulco meteorite and the problem of systematic errors in cosmochronology. *Earth and Planetary Science Letters* 175, 13-26.
- Renne, P.R., Balco, G., Ludwig, K.R., Mundil, R., Min, K., 2011. Response to the comment by W.H. Schwarz et al. on "Joint determination of ^{40}K decay constants and $^{40}\text{Ar}^*/^{40}\text{K}$ for the Fish Canyon sanidine standard, and improved accuracy for $^{40}\text{Ar}/^{39}\text{Ar}$ geochronology" by P.R. Renne et al. (2010). *Geochimica et Cosmochimica Acta* 75, 5097-5100.
- Renne, P.R., Basu, A.R., 1991. Rapid Eruption of the Siberian Traps Flood Basalts at the Permo-Triassic Boundary. *Science* 253, 176-179.
- Renne, P.R., Deino, A.L., Hames, W.E., Heizler, M.T., Hemming, S.R., Hodges, K.V., Koppers, A.A.P., Mark, D.F., Morgan, L.E., Phillips, D., 2009. Data reporting norms for $^{40}\text{Ar}/^{39}\text{Ar}$ geochronology. *Quaternary Geochronology* 4, 346-352.
- Renne, P.R., Deino, A.L., Walter, R.C., Turrin, B.D., Swisher, C.C., Becker, T.A., Curtis, G.H., Sharp, W.D., Jaouni, A.-R., 1994. Intercalibration of astronomical and radioisotopic time. *Geology* 22, 783-786.
- Renne, P.R., Mundil, R., Balco, G., Min, K., Ludwig, K.R., 2010. Joint determination of ^{40}K decay constants and $^{40}\text{Ar}^*/^{40}\text{K}$ for the Fish Canyon sanidine standard, and improved accuracy for $^{40}\text{Ar}/^{39}\text{Ar}$ geochronology. *Geochimica et Cosmochimica Acta* 74, 5349-5367.
- Renne, P.R., Swisher, C.C., Deino, A.L., Karner, D.B., Owens, T.L., DePaolo, D.J., 1998. Intercalibration of standards, absolute ages and uncertainties in $^{40}\text{Ar}/^{39}\text{Ar}$ dating. *Chemical Geology* 145, 117-152.
- Rivera, T.A., Storey, M., Schmitz, M.D., Crowley, J.L., 2013. Age intercalibration of $^{40}\text{Ar}/^{39}\text{Ar}$ sanidine and chemically distinct U/Pb zircon populations from the Alder Creek Rhyolite Quaternary geochronology standard. *Chemical Geology* 345, 87-98.
- Rivera, T.A., Storey, M., Zeeden, C., Hilgen, F.J., Kuiper, K., 2011. A refined astronomically calibrated $^{40}\text{Ar}/^{39}\text{Ar}$ age for Fish Canyon sanidine. *Earth and Planetary Science Letters* 311, 420-426.
- Robinson Cecil, M., 2009. Development and application of geochronometric techniques to the study of Sierra Nevada uplift and the dating of authigenic sediments., Department of Geosciences. University of Arizona, p. 176.
- Rukhlov, A.S., Bell, K., 2010. Geochronology of carbonatites from the Canadian and Baltic Shields, and the Canadian Cordillera: clues to mantle evolution. *Mineralogy and Petrology* 98, 11-54.
- Schmitz, M.D., Bowring, S.A., 2001. U-Pb zircon and titanite systematics of the Fish Canyon Tuff: an assessment of high-precision U-Pb geochronology and its application to young volcanic rocks. *Geochimica et Cosmochimica Acta* 65, 2571-2587.
- Schoene, B., Bowring, S., 2006. U-Pb systematics of the McClure Mountain syenite: thermochronological constraints on the age of the $^{40}\text{Ar}/^{39}\text{Ar}$ standard MMhb. *Contributions to Mineralogy and Petrology* 151, 615-630.
- Schoene, B., Crowley, J.L., Condon, D.J., Schmitz, M.D., Bowring, S.A., 2006. Reassessing the uranium decay constants for geochronology using ID-TIMS U-Pb data. *Geochimica et Cosmochimica Acta* 70, 426-445.
- Shih, C.Y., Nyquist, L.E., Bogard, D.D., Wiesmann, H., 1994. K-Ca and Rb-Sr dating of two lunar granites: Relative chronometer resetting. *Geochimica et Cosmochimica Acta* 58, 3101-3116.
- Shih, C.Y., Nyquist, L.E., Wiesmann, H., 1993. K-Ca chronology of lunar granites. *Geochimica et Cosmochimica Acta* 57, 4827-4841.
- Simon, J.I., Shih, C.Y., Nyquist, L.E., 2011. K-Ca and Rb-Sr dating of lunar granite 14321 revisited, 42 Lunar and Planetary Science Conference, The Woodlands, Texas. , p. 2754.
- Smith, P.E., Evensen, N.M., York, D., Odin, G.S., 1998. Single-Grain ^{40}Ar - ^{39}Ar Ages of Glauconites: Implications for the Geologic Time Scale and Global Sea Level Variations. *Science* 279, 1517-1519.
- Steiger, R.H., Jäger, E., 1977. Subcommittee on geochronology: convention on the use of decay constants in geo- and cosmochronology. *Earth and Planetary Science Letters* 36, 359-362.
- Tilley, D.R., Madansky, L., 1959. Search for Positron Emission in K40. *Physical Review* 116, 413-415.
- Villa, I.M., De Bièvre, P., Holden, N.E., Renne, P.R., 2015. IUPAC-IUGS recommendation on the half life of ^{87}Rb . *Geochimica et Cosmochimica Acta* 164, 382-385.
- Villeneuve, M., Sandeman, H.A., Davis, W.J., 2000. A method for intercalibration of U-Th-Pb and ^{40}Ar - ^{39}Ar ages in the Phanerozoic. *Geochimica et Cosmochimica Acta* 64, 4017-4030.
- Wetherill, G.W., Wasserburg, G.J., Aldrich, L.T., Tilton, G.R., Hayden, R.J., 1956. Decay Constants of K40 as Determined by the Radiogenic Argon Content of Potassium Minerals. *Physical Review* 103, 987-989.

- Wingate, M.T.D., Compston, W., 2000. Crystal orientation effects during ion microprobe U–Pb analysis of baddeleyite. *Chemical Geology* 168, 75-97.
- Wooden, J.L., Czamanske, G.K., Fedorenko, V.A., Arndt, N.T., Chauvel, C., Bouse, R.M., King, B.-S.W., Knight, R.J., Siems, D.F., 1993. Isotopic and trace-element constraints on mantle and crustal contributions to Siberian continental flood basalts, Noril'sk area, Siberia. *Geochimica et Cosmochimica Acta* 57, 3677-3704.
- Wu, F.-Y., Yang, Y.-H., Li, Q.-L., Mitchell, R.H., Dawson, J.B., Brandl, G., Yuhara, M., 2011. In situ determination of U-Pb ages and S-Nd-Hf isotopic constraints on the petrogenesis of the Phalaborwa carbonatite Complex, South Africa. *Lithos* 127, 309-322.
- Yokoyama, T., Misawa, K., Okano, O., Shih, C.Y., Nyquist, L.E., Simon, J.I., Tappa, M.J., Yoneda, S., 2015. Early solar system alkali fractionation events recorded by K-Ca isotopes in the Yamato-74442 LL-chondritic breccia, 46th Lunar and Planetary Science Conference, p. 1695.
- Yuhara, M., Hirahara, Y., Nishi, N., Kagami, H., 2005. Rb-Sr, Sm-Nd ages of the Phalaborwa Carbonatite Complex, South Africa. *Polar geoscience* 18, 101-113.
- Овчинникова Г.В., Левчинков, О.А., Варшавская, Е.С., Кутявин, Е.П., Яковлева, С.З., 1980. Сравнительное изучение К-Са, Rb-Sr и К-Ar систем в лепидолитах. *Геохимия* 8, 1166-1173.



General conclusions and outlook

General conclusions and outlook

A range of questions has been addressed in this study. They can be divided into two main groups: the standardization of isotopic compositions of K and Ca, which is important for fractionation processes studies; and the assessment of the ^{40}K decay constant by geological age intercorrelation which is essential for the accuracy of K-Ar and Ar-Ar dating systems.

The isotopic compositions of K and Ca were measured on standard reference materials; they were compared among themselves and with terrestrial and extraterrestrial values published in the literature. I measured and compared isotopic composition of K reference materials NIST SRM 918b and SRM 985. SRM 985 was produced and certified over 20 years ago and never issued again since, thus the comparison of a new standard material to the old certified value is significant for studies of the potassium fractionation in geological processes. The isotopic abundance of ^{40}K is so low that its accurate and precise determination is challenging. The $^{40}\text{K}/^{39}\text{K}$ ratios of SRM918b and SRM 985 presented here are respectively $0.000\,125\,185 \pm 130$ and $0.000\,125\,116 \pm 57$, when normalized to $^{41}\text{K}/^{39}\text{K}$ of 0.721677. These results are consistent with the previous reference K isotopic composition and are *ca.* 5 times more precise.

High precision static Ca measurements that allow to resolve the variation on $^{40}\text{Ca}/^{44}\text{Ca}$ value down to 0.06‰ was developed in the frame of this study to determine the isotopic composition of Ca reference materials. This precision is owed to the ability to measure the full range of Ca masses statically. The method bears potential to bring new insights into the history of early Earth and modern processes.

The isotopic composition of the Ca reference material SRM 915a has been widely used for the studies of Ca fractionation in Earth processes and nucleosynthetic models. This standard is however not available anymore and has been substituted with SRM 915b. A comparison of the old and new standards is therefore essential. The results obtained here show that these two standards have identical $^{40}\text{Ca}/^{44}\text{Ca}$ ratios when mass-fractionation corrected: the $^{40}\text{Ca}/^{44}\text{Ca}$ ratios I measured for SRM 915b is 47.1613 ± 28 and 47.1649 ± 47 for SRM 915a, when mass-fractionation corrected to $^{42}\text{Ca}/^{44}\text{Ca} = 0.31221$. These values are indistinguishable from previously published data on SRM 915a as well as on average terrestrial and extraterrestrial samples.

The choice of reference Ca isotopic composition is also essential. Three Ca isotopic compositions published in literature were compared here. Using various normalization ratios ($^{42}\text{Ca}/^{44}\text{Ca}$, $^{43}\text{Ca}/^{44}\text{Ca}$ and $^{48}\text{Ca}/^{44}\text{Ca}$) we demonstrated that an internally consistent isotopic composition gives the same normalized $^{40}\text{Ca}/^{44}\text{Ca}$ ratio independently of the used normalization ratio. However two out of three Ca isotopic compositions compared in this study show dependencies of the normalized $^{40}\text{Ca}/^{44}\text{Ca}$ ratio on the chosen normalization ratio. Such Ca isotopic compositions are unreliable and should not be used further.

The drawbacks, which appear when such high precision data is accumulated, was observed and described in Chapter 2. The issue of incomplete fractionation correction becomes significant if smaller and smaller amounts of Ca are analyzed. It is relevant for

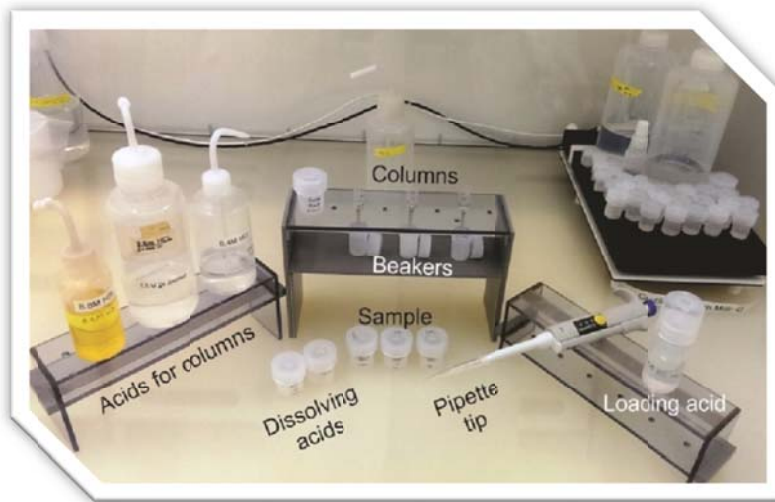
high precision Ca isotopic studies and K-Ca dating of small samples. The additional correction term adapted in this study for Ca reduces the effect of incomplete fractionation correction. The processes happening during thermal ionization in the high vacuum mass-spectrometers are not yet well understood and are described mainly on the basis of empirical observations. When a precision is aimed for better than a permille, empirical corrections are not sufficient anymore. A correct understanding of systematic effects, such as fractionation processes and accurate fractionation correction becomes essential.

Another direction of this research was dedicated to the improvement of two constants used for the Ar-Ar dating system: the ^{40}K isotopic abundance and the ^{40}K decay constant. The $^{40}\text{K}/\text{K} = (1.668 \pm 8) \cdot 10^{-4}$ value obtained in this study is coincident with previously published values for ^{40}K isotopic abundance, but with an uncertainty reduced from 0.35% to 0.07%.

The ^{40}K decay constant was assessed by an intercalibration of the four geochronometers U-Pb, Rb-Sr, Ar-Ar and K-Ca. The crucial point when performing such intercalibrations is to only use samples which meet the requirements of geologically “point-like” event; that is magmatic samples whose isotope record was not modified after intrusion or eruption. Within this work four samples were studied and dated because of their supposed “point-like” geological history. The Bolgokhtokh granodiorite intrusion, Kotuy, Russia, gave an Ar-Ar age of 225.0 ± 4.8 Ma coincident within uncertainty with previously published Ar-Ar, Rb-Sr and U-Pb ages. A Proterozoic post-emplacement metamorphic event was confirmed for the Archean Siilinjärvi complex; its Rb-Sr age is 1869 ± 10 Ma. The Rubikon lepidolite sample, from Karibib pegmatite, Namibia, gave a Rb-Sr age of 504.7 ± 4.2 Ma coincident with the baddeleyite U-Pb age from literature.

The fourth sample, a phoscorite from the Phalaborwa carbonatite complex, was demonstrated to meet the requirement of a “point-like” event. This sample was dated with Rb-Sr and K-Ca, as well as with Ar-Ar dating. Rb-Sr dating gave 2058.9 ± 5.2 Ma age, identical to previous U-Pb ages. This allowed us to compare the offset of K-Ca and Ar-Ar ages from reference Rb-Sr and U-Pb attributed to the inaccuracy of the ^{40}K decay constant. Based on the K-Ca age the range of possible ^{40}K decay constants was narrowed down. Our best estimate is the decay constants of Min et al. (2000) (see ref. in the chapter 3). This is consistent with a previously published “best-fit” decay constant for Ar-Ar with U-Pb dating. However one sample is not enough to assess independently both branches of the ^{40}K decay constant, moreover low precision Ar-Ar dating of our samples so far does not allow us to include the Ar branch of the ^{40}K decay constant into the intercalibration.

Another two samples appear to represent geologically “point-like” events: Kotuy and Rubikon. Three samples together and provisionally a K-feldspar of the Colomera meteorite will form four reliable geologically “point-like” samples with a wide age-span: 225 Ma, 505Ma, 2060Ma and 4610 Ma. High precision Ar-Ar and K-Ca dating of these four samples will allow us to perform full intercalibration with Rb-Sr and U-Pb dating systems and to assess independently the two branches of the ^{40}K decay constant.



Appendix 1.

Clean laboratory protocols

Appendix 1. Clean laboratory protocols.

Appendix 1. Clean laboratory protocols.

- K-Ca chemistry is extremely blank sensitive, therefore all procedures have to be performed with special care and concentration.
- avoid gloves when possible, better wash hands with distilled water approximately every 15 min or when you feel they become sweaty;
- always use triple or double distilled acids;
- always use specially cleaned beakers;
- avoid using HF when possible, CaF_2 is insoluble, HF has 5 ng/ml Ca blank;
- use separate Ca hood if possible;
- always use only Ca drop bottles, Ca beakers, Ca columns, everything reserved for this element;
- always keep everything closed, capped, when not used;
- always keep hood closed, when not working;
- always wipe the bottom of a hood with wet Kim-wipes before and after use.

Normal cleaning procedures:

All **new beakers** must be cleaned following normal beakers cleaning procedure:

- Soap step: rinse each individual beaker and its lid with Milli-Q and leave in “soap” for 12h,
 - wipe each beaker and lid with Kim-wipes, rinse each individual beaker and lid with Milli-Q. Put open beakers and lids in a 1 L beaker, fill it with Milli-Q and put it in an ultrasonic bath for 5 min. Dispose water, fill 1L beaker with Milli-Q twice. Dispose water.
- HCl step: put open beakers and lids in 1 time (1x) distilled HCl (6.4 M) + Milli-Q 1:1 for 24h on a hot plate, 100°C;
 - take beakers out of HCl, put in the 1 L beaker, fill with Milli-Q and put it in an ultrasonic bath for 5 min. Dispose water, fill the 1L beaker with Milli-Q twice. Dispose water.
- HNO_3 step: put open beakers and lids in 1x distilled HNO_3 (14 M) + Milli-Q 1:1 for 24h on a hot plate, 100°C;
 - take beakers out of HNO_3 , put in the 1 L beaker, fill with Milli-Q and put it in an ultrasonic bath for 5 min. Dispose water, fill the 1 L beaker with Milli-Q twice. Dispose water.
- Milli-Q step: put open beakers and lids in Milli-Q for 24h on a hot plate, 100°C;
 - take beakers out of Milli-Q. Dispose water, rinse each individual beaker and lid with Milli-Q.

Afterwards beakers should be dried and closed.

New bottles must be cleaned following the normal bottle cleaning procedure:

- 24h on a hot plate upside down on a glass beaker with 6.4 M HCl 1x distilled;
- 24h on a hot plate upside down on a glass beaker with 14 M HCl 1x distilled;

Appendix 1. Clean laboratory protocols.

- 24h on a hot plate upside down on a glass beaker with Milli-Q.

After normal beaker cleaning procedure, Ca cleaning should be applied before beakers or bottles can be used.

Ca specific cleaning procedures:

From here on **only three times (3x) distilled acids** should be used, if not specified differently.

Ca beakers cleaning

The cleaning procedure after using beakers for K-Ca chemistry or new beakers after normal cleaning is following:

- rinse lid and beaker 3x with Milli-Q ;
- fill with Milli-Q, close beakers, put in a 1 L beaker filled with Milli-Q;
- ultrasonic for 5 min;
- dispose water from each beaker, wipe with Kim-wipe and rinse 3x with Milli-Q;
- fill each beaker with Milli-Q , close and leave overnight;
- move beakers into the Ca hood;
- dispose Milli-Q;
- rinse each beaker and lid 3x with Milli-Q from a squeeze bottle;
- fill with 2.5 M HCl 3x distilled, close tightly and leave on a hot plate at 80-100°C for a minimum of 3 days;
- dispose acid;
- rinse 3x lid and a beaker carefully with Milli-Q from a squeeze bottle. Do not touch any inner surface with fingers!
- fill with Milli-Q, close tight and leave on a hot plate at 80-100°C for a minimum of 3 days;
- dispose Milli-Q;
- rinse 3x lid and a beaker carefully with Milli-Q from a squeeze bottle Do not touch any inner surface with fingers!
- fill with 1 M HCl 3x distilled, close tightly and store in a Ca drawer.

Ca bottles cleaning

- rinse 3x with Milli-Q in the Mo lab;
- fill 1/10 with 2.5 M HCl 3x distilled in the Ca hood;
- place the lid but do not close it;
- put on a hot plate in the Ca hood for at least one week. (I did Ca cleaning of bottles each step 1 month);
- dispose acid;
- rinse 3x with Milli-Q;
- fill 2/10 with Milli-Q;
- put on a hot plate in the Ca hood for at least one week;
- rinse with Milli-Q;
- dry bottle with open lid on HF hot plate in the Ca hood.

Appendix 1. Clean laboratory protocols.

Column chemistry

Ca column chemistry is an adaptation of the procedure from Nögler and Villa (2000). It was recalibrated in 2012 for handmade Teflon columns (300 μ l volume). The calibration plots can be seen in fig. A.1.1. Experiment was performed with a fake biotite solution. Two aliquots of a the sample was loaded into two columns A1 and A2. Fractions with steps of 120 μ l were collected into 7 beakers and the last fraction was 500 μ l, that is why the Ca peak is not visible on fig.A.1.1., most of the Ca fraction was collected in one step. Concentrations of Al, Mg, Ca and K were determined in each fraction.

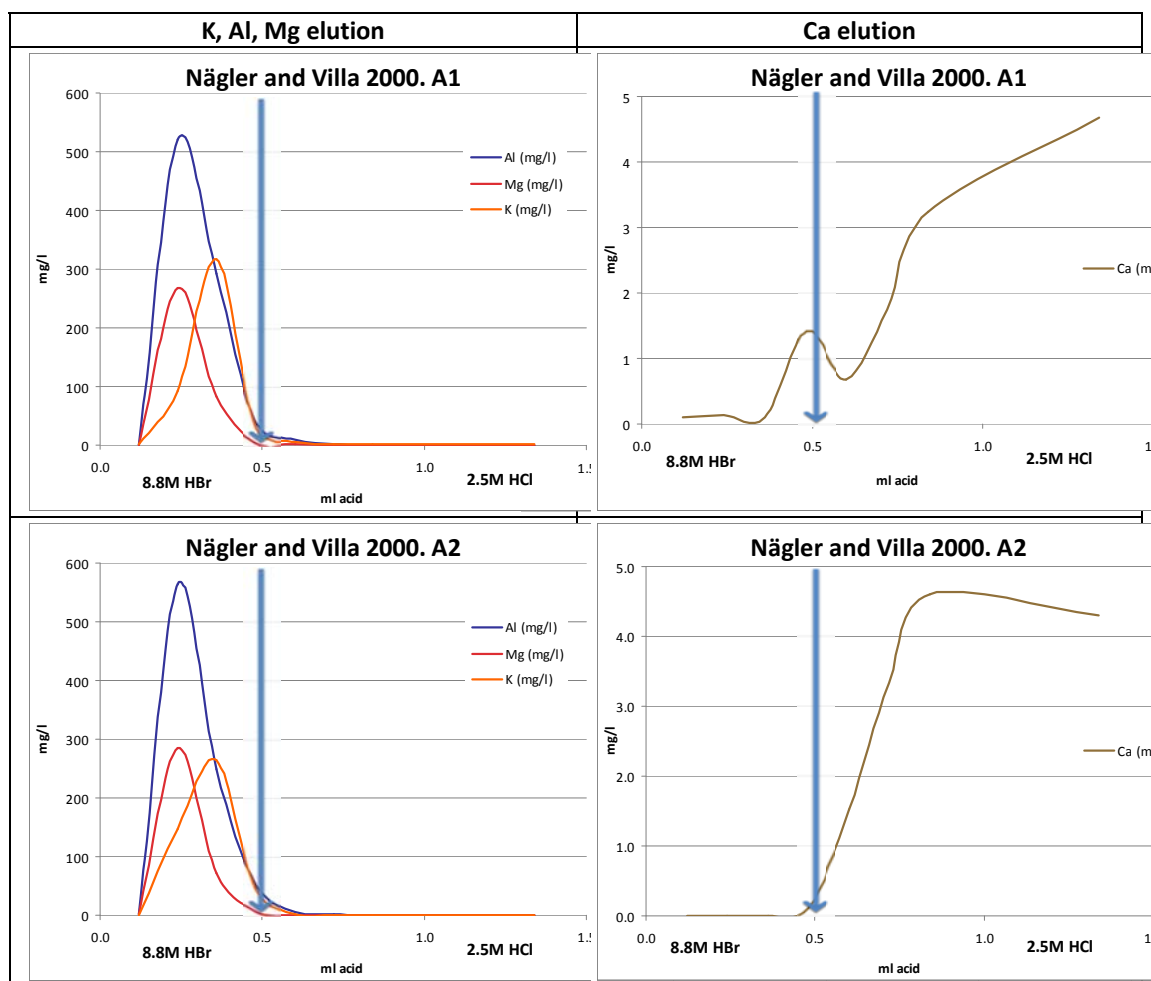


Fig. A1.1. Plots of an elution sequence in the hand-made Teflon columns filled with 300 μ l of Dowex AG 50WX8 resin. Blue line marks the transition from 8.8 HBr 2x distilled to 2.5 M HCl 3x distilled acids.

Appendix 1. Clean laboratory protocols.

Ca chemistry routine

Here are recommendations for low blank K-Ca column separations. The Ca Teflon columns are filled with 300 μ l of Dowex AG 50WX8 resin. The resin itself is dirty and needs substantial cleaning before it can be used for K-Ca. Initially all Dowex resin in the clean laboratory is pre-cleaned in a few consecutive repeating steps of 0.5 M, 2.5 M, 6.4 M HCl 1x distilled. After filling the Ca columns with a new resin, multiple pre-cleaning cycles are required until the column blank becomes 1ng. In between samples I did a minimum of 3 pre-cleaning cycles. The normal K-Ca pre-cleaning and column chemistry are described in tables A.1.1. and A.1.2. The longer one uses the resin the cleaner it becomes.

Pre-cleaning should always be done between column chemistry, at least one pre-cleaning cycle one day before columns. Acid cleaning steps can be repeated several times. If one has a few days in-between sample column chemistry, these days should be used for 2.5 M HCl-6.4 M HCl-2.5 M HCl cleaning as described in the table A.1.1 for days 1-3. One full pre-cleaning cycle should be done immediately before columns. One can use gloves for handling columns in-between column chemistry, but on the day sample chemistry is performed, gloves should not be used during pre-cleaning and separation; hands should be washed regularly with distilled water. Pre-cleaned columns are stored in Milli-Q or very weak HCl in clean beakers. I use open beakers and clean them with 2.5 M HCl 3x distilled on a hot plate each time I am working in the lab. Open beakers containing acid should not be left on a hot plate overnight otherwise the acid will evaporate and dirt will dry on the walls of the beakers. Open beakers with columns should be covered with “cupola” for overnight storage. If columns are not used for more than a week, they should be stored in closed Savillex beakers with clean very weak HCl. In case the procedure has to be speeded up, day 1 of Table A.1.1. can be skipped, days 2 and 3, as well as days 4 and 5 can be combined. It is better to not speed up the procedure if possible, as sample separation and handling around the columns need full concentration and attention to not contaminate them with a random blank from gloves and hands. Each cleaning step takes about 50-60 min. For cleaning purposes the columns should be filled with liquids till the top.

Pipette tips should be used as little as possible during samples chemistry, drop- and squeeze bottles are preferred. If pipette tips need to be used (for sample loading or if a bubble appears in the column), they should be filled immediately before use 3 times to maximum volume with 6.4 M HCl 3x distilled and three times with Milli-Q 3 distilled. Nothing should be touched with a pipette tip either before or after rinsing. The boxes with pipette tips should be filled with green tweezers from the Ca drawer. While refilling a box, the end of a pipette tip should not touch anything including the box itself.

Appendix 1. Clean laboratory protocols.

Table A.1.1. A protocol for column chemistry of samples for K-Ca dating:

Day 1	Day 2	Day 3	Day 4	Day 5
Pre-cleaning:	Pre-cleaning:	Pre-cleaning:	Pre-cleaning	Samples
-2.5M HCl -6.4M HCl -2.5M HCl <i>Optionally repeat</i>	-2.5M HCl -6.4M HCl -2.5M HCl <i>Optionally repeat</i>	-Milli-Q -Milli-Q -Ammonium acetate -2.5M HCl	-6.4M HCl -2.5M HCl -Milli-Q -Milli-Q -Ammonium acetate -2.5M HCl	-2.5M HCl -samples column chemistry from Table N
Open beakers for columns filled with 2.5M HCl 3x distilled and left on the hot plate for this day	Open beakers for columns filled with Milli-Q and left on the hot plate for this day	Open beakers for columns filled with 2.5M HCl 3x distilled and left on the hot plate for this day	Open beakers for columns filled with Milli-Q and left on the hot plate for this day	Open beakers for columns filled with 2.5M HCl 3x distilled and left on the hot plate for this day

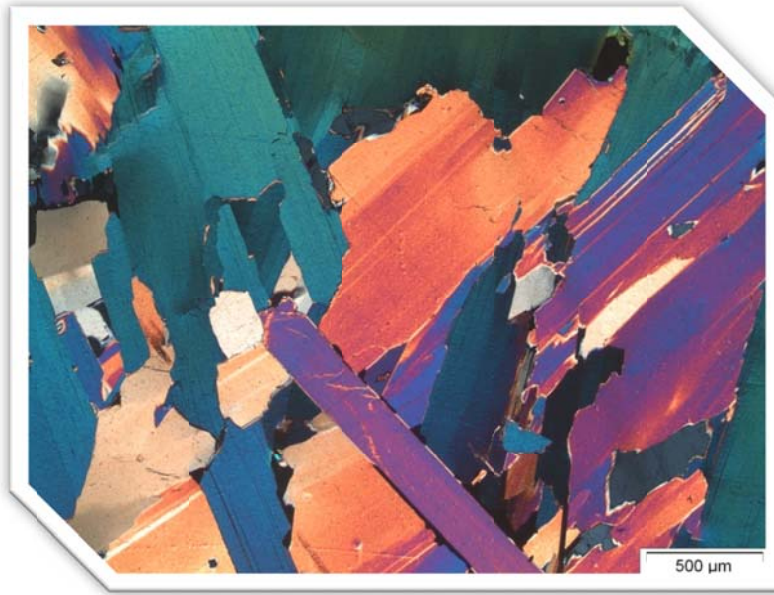
Appendix 1. Clean laboratory protocols.

Table A.1.2. K-Ca column separation protocol.

	acid	volume		A		B		C		D	Time
Column No				A1	A2	B1	B2	C1	C2	D1	
Pre-wash	2.5 M HCl	1 reservoir	<i>optional if afterwash was done before</i>								
	6 M HCl	1 reservoir									
	2.5M HCl	1 reservoir									
	Milli-Q	1 reservoir									
		1 reservoir									
	check neutrality (should be 5 or 7)										
	(am.acet.)	1/2 reservoir									
	2.5 M HCl	1 reservoir									
Here the break for the night can be done. In that case store pre-cleaned columns in Milli-Q in clean open beakers.											
conditioning	2.5 M HCl	1 reservoir	<i>optional if precleaning and columns are done the same day</i>								
sample in	2.5 M HCl	0.1 ml									
rinse 1	2.5 M HCl	0.1 ml									
add	8.8 M HBr	0.6 ml									
take:											
		0.3 ml	Elution Al, Mg (waste)								
beaker K		0.3 ml	Elution Al, K (1:1) collect								
add	2.5 M HCl										
		0.5ml	waste								
beaker Ca		1 reservoir	Elution Ca, collect								
After wash	2.5 HCl	1 reservoir									

References

Nägler, T.F., Villa, I.M., 2000. In pursuit of the ^{40}K branching ratios: K-Ca and ^{39}Ar - ^{40}Ar dating of gem silicates. Chemical Geology (Isotope Geoscience Section) 169, 5-16.



Appendix 2.

Sample description

Appendix 2. Sample description.

Appendix 2. Sample description.

Initially eight samples were available for this study from the following complexes:

- Klokken intrusion, South Greenland. Mineral separates;
- Bulgokhtokh intrusion, Kotuy, Russia. Mineral separates;
- Dolodau dyke, Canada. Piece of biotite sovite;
- Borden carbonatite complex, Canada. Mica separates;
- Prairie Lake, Canada. Piece of carbonatite;
- Siilinjärvi carbonatite complex, Finland. Piece of carbonatite;
- Phalaborwa carbonatite, Limpopo, South Africa. Piece of phoscorite.
- Lepidolite, Karibib, Namibia. Museum exemplar of lepidolite;

Samples acceptable for calibration study must fulfill the requirement as “point-like” geological event: minerals have to be in petrological equilibrium, without signs of any alteration, recrystallization, retrograde reaction or dissolution. Based on these criteria available samples were studied, evaluated and where necessary discarded.

A syenite piece from the **Klokken intrusion**, South Greenland, was originally collected for the study by Nebel et al. (2011) from the interior of syenodiorite sills. The Klokken syenite is a shallow layered intrusion in the south-western segment of the Gardar alkaline province. It is a 3x4 km onion-shaped body with sharp contacts against the basement and a thin outer gabbroic sidewall that encloses the syenitic magma chamber, which was intruded at a depth of less than 3 km and cooled below 300°C within 100ka. A more detailed description of the geology and age of this intrusion can be found in (e.g. Parsons, 1979, 1980, 1981; Parsons et al., 1991). Due to evidence of ⁴⁰Ar loss that resulted in low Ar-Ar ages (Burgess et al., 1992) this sample was considered as unfavorable for K-Ca and Ar-Ar ages intercomparison.

The Bulgokhtokh granodiorite intrusion, **Kotuy**, Russia, belongs to the Siberian flood volcanic province of the Norilsk-Maymecha-Kotuy area formed ca. 251 Ma ago. The Bolgoghtokh stock is situated at the far north-west end of the Norilsk flood basalt field and is younger than the Norilsk and Maymecha-Kotuy provinces. It has been interpreted to be formed during later tectonic reactivation (Kamo et al, 2003) out of lower crust melts (Wooden et al, 1993). The age of the Bolgokhtokh intrusion is well studied and is presented in the Table A.2.1. Nebel et al (2011) argued that the discrepancy between originally published Ar-Ar and U-Pb ages might be due to the offset of a flux monitor or the ⁴⁰K decay constant. Indeed recalculation of the Ar-Ar ages to the recently published McClure Mountain syenite (MMhb-1) monitor ages bring the Ar-Ar biotite and U-Pb zircon ages in the agreement; hornblende ages still remain younger, which might be a result of Ar loss during alteration. Indeed Wooden et al. (1993) describe certain weathering and alteration phenomena at thin section scale, moreover, Nebel et al (2011) point out

Appendix 2. Sample description.

minor sericitization of feldspars. Therefore biotite of the Bulgokhtokh was studied under a microprobe (fig. A.2.1), which revealed prominent zonation of mica, visible on the electron back-scattered image. We dated this sample with Ar-Ar method (see Chapter 3), but based on the microprobe data and results of the Ar-Ar dating it was not suitable for K-Ca dating.

Table. A.2.1. Literature ages for the Bulgokhtokh granodiorite intrusion (Kotuy). Ar-Ar ages are recalculated to MMhb-1 age of 522.98 ± 1.00 Ma (Schoene and Bowring, 2006) and are 1.736% older than originally published.

Age (Ma)	Details	Reference
229.05 ± 0.36	U-Pb concordia age for zircon (MSWD of concordance = 0.41)	(Kamo et al., 2003)
229.0 ± 0.4	²⁰⁶ Pb– ²³⁸ U for zircon (MSWD=0.11)	
229.3 ± 0.5	²⁰⁷ Pb– ²³⁵ U for zircon (MSWD=0.19)	
227.1 ± 1.2	⁴⁰ Ar– ³⁹ Ar for biotite	(Dalrymple et al., 1995)
228.0 ± 1.9	⁴⁰ Ar– ³⁹ Ar for hornblende	
224.7 ± 1.0		



Fig. A.2.1. Microprobe secondary electron scan of Kotuy biotite mounts (Bulgokhtokh granodiorite intrusion) revealing zonation.

Appendix 2. Sample description.

Dolodau dyke, Canada situated in the Abitibi greenstone belt together with Lac Shortt dyke. Complex has been extensively dated with various methods (Table A.2.1), and showed discrepancies between U-Pb and K-Ar ages. Furthermore study of a biotite + cordierite thin section under an optic microscope showed signs of partial dissolution and recrystallization of mica grains (Fig. A.2.2). This sample was therefore not used in this work.

Carbonatites were considered to be promising samples as carbonatite complexes have rapid cooling histories, and those located on platforms have the potential to be closed systems. Hence, three samples from carbonatite complexes were studied.

The Borden carbonatite complex from the Kapuskasing Structural Zone intruded upper amphibolite and granulite facies host rocks of the Canadian Shield. The minimum date of emplacement has been estimated to be 1882.0 ± 3.9 Ma (Pb-Pb, zircon), but other attempts to date this complex gave variable K-Ar, U-Pb, Rb-Sr ages (Rukhlov and Bell, 2010). Thus we consider this sample to be unsuitable for our study.

The Prairie Lake alkaline-carbonatite complex lies within the Archean-Proterozoic gneisses of the Quetico Subprovince of the Superior Province and is confined to the northern extension of the Big-Bay – Ashburton Bay Fault (Sage, 1987). It has an approximate age of 1.16 Ma (Table A.2.3) but variable K-Ar ages. Study of the sample under optical microscopy and microprobe analysis showed that micas have signs of recrystallization, dissolution and zonation (Fig. A.2.3 and A.2.4), making this sample also unsuitable for this study.

The Siilinjärvi carbonatite complex is situated in the Karelian Craton in eastern Finland within the Ladoga-Bothnian deep fracture zone. Sample Si-102 was available to us on courtesy of Keith Bell. The Pb-Pb dating places the emplacement of the complex at 2594 ± 13 Ma. Despite the pristine look of the sample in thin-sections (Fig. A. 2.5), literature data points to a post-emplacement metamorphic event ca. 1900 Ma (summary of available ages in Rukhlov and Bell, 2010, p.24). Nevertheless the attempt of simultaneous dating of Siilinjärvi mica with Rb-Sr, K-Ca and Ar-Ar methods was performed on this sample.

Appendix 2. Sample description.

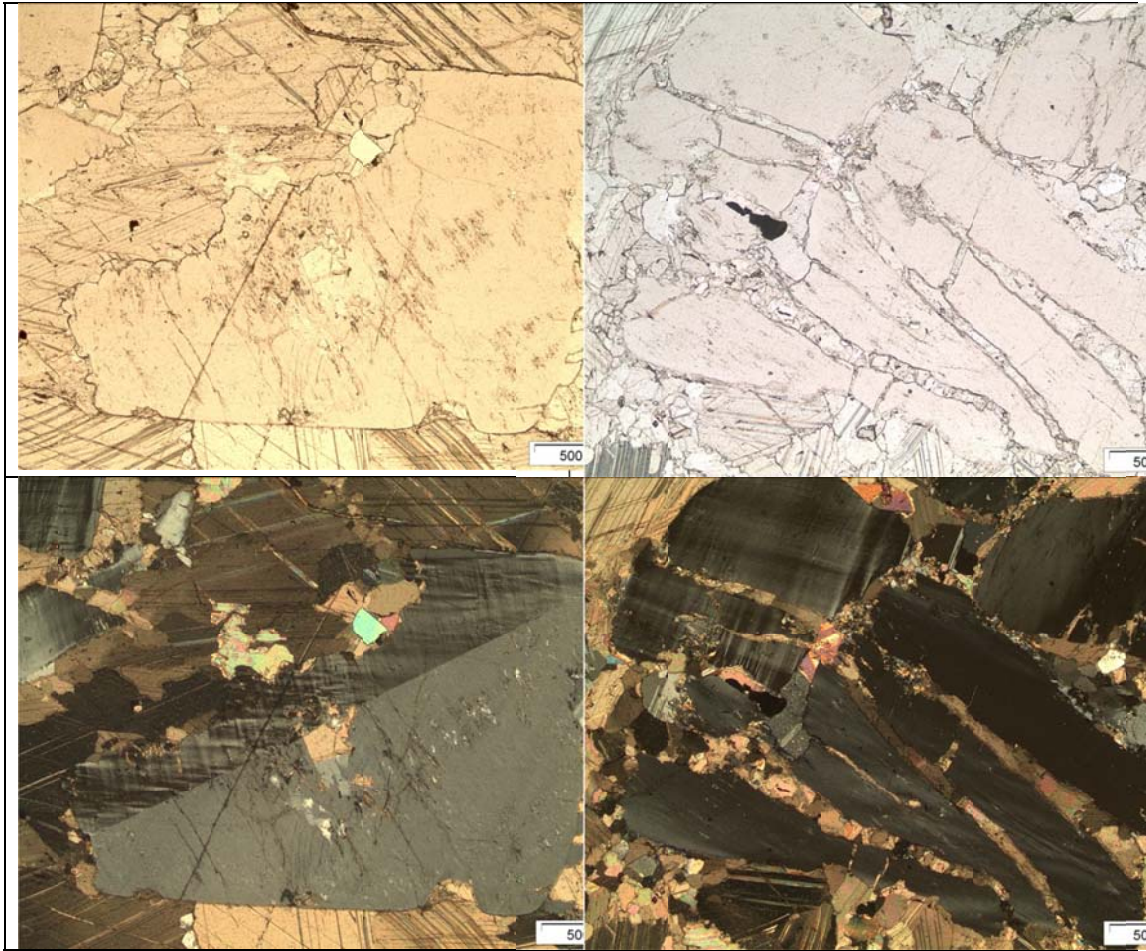


Fig. A.2.2. Two pictures of a the Dolodau muscovite under an optical microscope. Upper row plain polarized light, lower row cross polarized light.

Table A.2.2. Literature ages for the Dolodau dyke granodiorite intrusion

Age (Ma)	Method	Mineral / rock	Details	Reference
2684±170	U-Pb	zrn	LSC65, LSC7910, LSC7912(bi sovites), DOD77 (bi sovite), DOD91(bi-amf silicocarbonatite), Upper discordia intercept ($\pm 95\%$ -conf.), MSWD=8218, 6 fractions, 44–19% discordant	Rukhov and Bell (2010)
2680	U-Pb	ap	Upper discordia intercept, 2 samples	Tilton and Bell (1994)
2640 \pm 267	Rb-Sr isochron	whole rock	biotite sövites, biotite- 3 samples	Tilton and Bell (1994)
2677	Pb-Pb	ap	biotite sövite— $^{207}\text{Pb}^*/^{206}\text{Pb}^*$ date	Tilton and Bell (1994)
2479 \pm 79	K-Ar	bt	biotite sövite (dates from the bi concentrate)	Bédard and Chown (1992)

Appendix 2. Sample description.

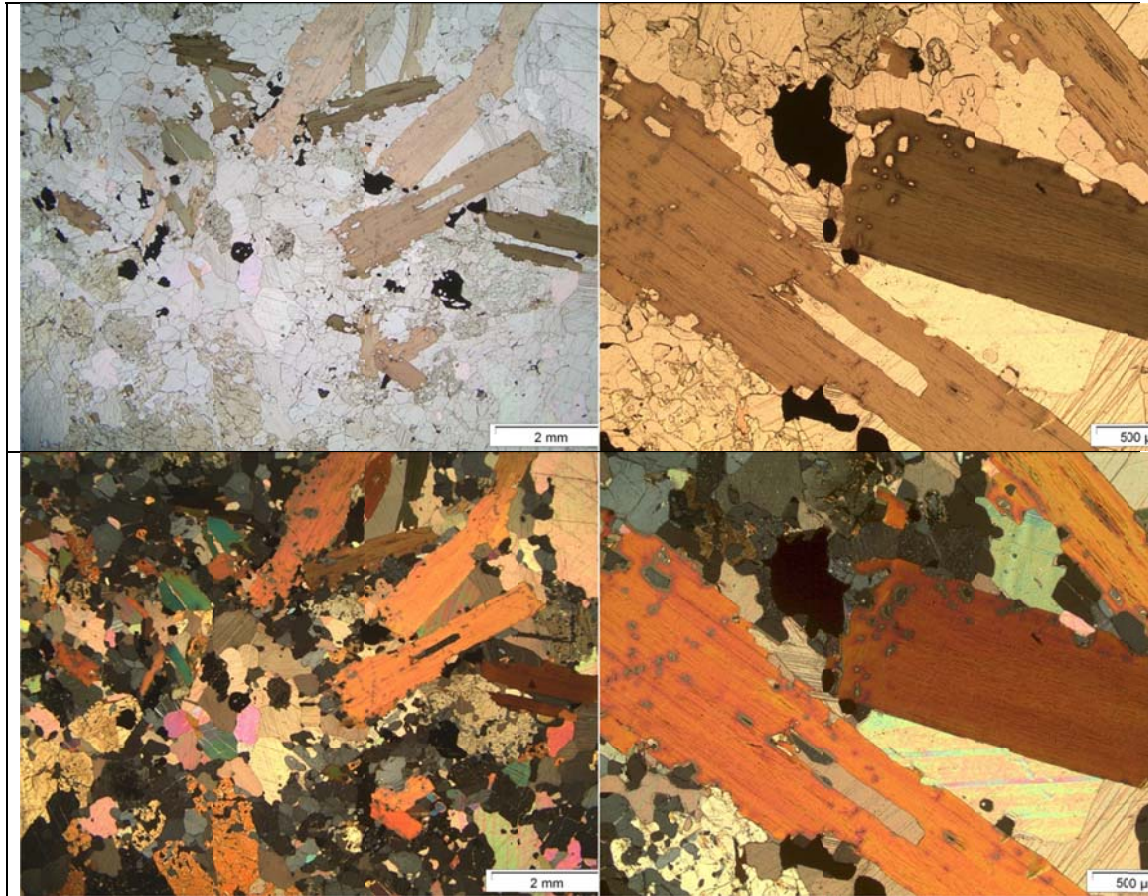


Fig. A.2.3. Microscope pictures of a Prairie Lake thin section, signs of dissolution and recrystallization. Upper row plain polarized light, lower row cross polarized light.

Table A.2.3. Literature ages for the Prairie Lake complex

Age (Ma)	Method	Mineral /rock	Details	Reference
1163.5 ± 3.5	U-Pb	zrn, bd	Sample: P21A/64.8, DP-26F. Upper discordia intercept ($\pm 95\%$ -conf.), 2 fractions	Rukhov and Bell (2010)
1157 ± 46	Pb-Pb isochron	ap	Sample: carbonatite. SHRIMP II. PRAP Model 1 date ($\pm 95\%$ -conf.), MSWD=0.61, 43 analyses, 1 sample	Sano et al. (1999)
1155 ± 36	Pb-Pb isochron	cal	Samples: carbonatites MSWD=6.2, 7 fractions, 5 samples	Kwon et al. (1989)
1023 ± 74	Rb-Sr isochron	WR	Sample: carbonatites $\pm 95\%$ -conf., MSWD=2.3, 7 samples	Bell and Blenkinsop (1980)
(1071–1174)*	K-Ar	bt	Sample: carbonatites 2 samples	Gittins et al. (1967)

Appendix 2. Sample description.

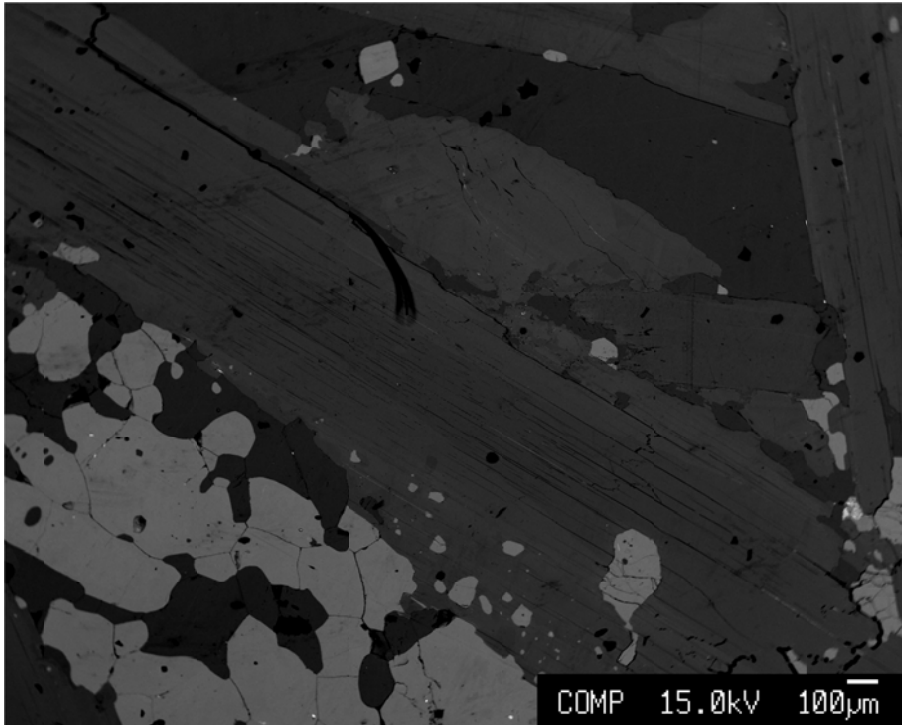


Fig. A.2.4. Microprobe secondary electron scan of Prairie Lake thin section, showing zonation of mica and signs of recrystallization.

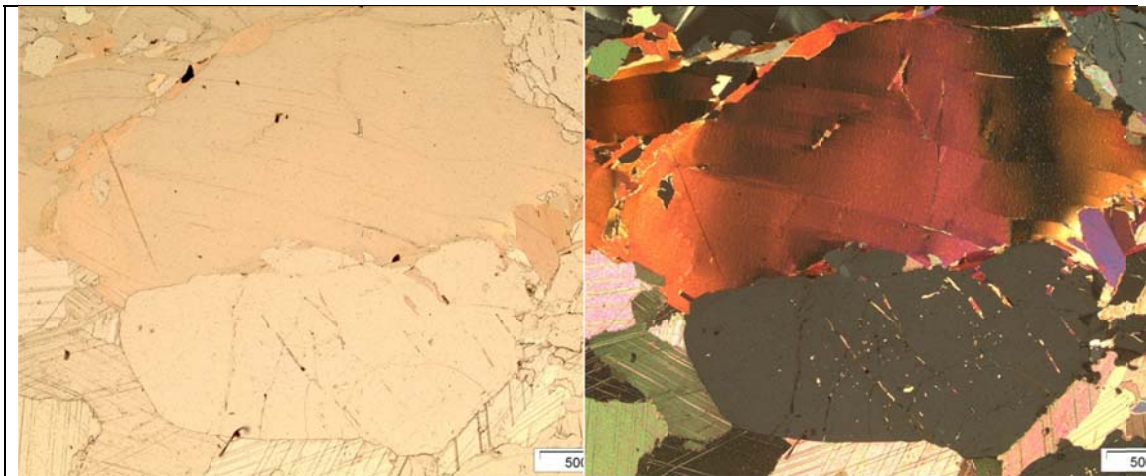


Fig. A.2.5. Microscope pictures of a Siilinjärvi carbonatite thin section. Biotite looks pristine, it shows signs of lamination which could be of magmatic origin. To the right cross polarized to the left plain polarized light.

Appendix 2. Sample description.

The most promising sample was a phoscorite from the **Phalaborwa** carbonatite complex, north-eastern Transvaal, South Africa. This is an intracratonic alkali intrusive complex of elongated form composed mainly of clinopyroxenites with minor carbonatites and phoscorites (in early works called micaceous pyroxenite). It intruded an Archean terrain composed of granites, gneisses, quartzites, granulites, amphibolites and talc and serpentine schists. (Eriksson, 1984). The complex has been dated by J.W.L de Villiers (Holmes and Cahen, 1956) with the U-Pb method on uranothorianite with a single analysis and gave an age of 2060 Ma. An age of 1000-2000 Ma was quoted by Heinrich, 1966, 1970. (Eriksson, 1984). Eriksson (1984) dated this complex with the U-Pb method on uranothorianites and baddeleyites and obtained an age of $2047 \pm 11 / -8$ Ma. He however cautions, that an additional 1% uncertainty may exist and states that the Rb-Sr age of phlogopites, phoscorite and clinopyroxenites give an isochron age of 2012 ± 19 Ma (2σ). I recalculated to the new $\lambda_{87} = 1.3972 \cdot 10^{-11} \text{ a}^{-1}$ (Villa et al., 2015) – assuming that Eriksson (1984) originally used the constant of (Steiger and Jäger, 1977) – and obtained a Rb-Sr age of 2047 ± 19 Ma. Later U-Pb dating confirmed an age of 2060 Ma (Heaman and LeCheminant, 1993; Reischmann, 1995; Horn et al., 2000; Wingate and Compston, 2000; French et al., 2002). Wu et al (2011) dated different layers of the Phalaborwa complex and found that they all are of the same age. (Table A.2.4). Rb-Sr dating on the other hand was less successful, it gives a high scatter of the isochrones (Eriksson, 1984, Yuhara et al, 2005), though successful attempts of precise dating with Rb-Sr method for this complex have been achieved (Nebel et al., 2011).

Our sample (PhB-2) is a phoscorite that consists of big crystals (up to 10 cm) of phlogopite (*ca.* 45%), apatite (*ca.* 35%), diopside (*ca.* 14%), ilmenite (*ca.* 5%) and calcite (*ca.* 1%). Apatite forms both big idiomorph grains (up to 10 cm) and small mineral inclusions (1-200µm) inside phlogopite and diopside grains. Small (20-200µm) ilmenite and calcite grains fill the spaces between crystal boundaries. Ilmenite also forms big massive crystals (in the current sample the crystal is 5x6 cm) surrounded by a reaction rim of diopside - serpentine. Diopside shows signs of serpentinisation along the cleavage (Fig. A.2.5, A.2.6.).

The detailed study of thin-sections under an optic microscope and using microprobe analysis showed that phlogopite is pristine and does not have any signs of alteration. Microprobe quantitative line analysis (Fig. A.2.7) and elemental mapping (Fig. A.2.8) demonstrated that micas are chemically homogenous without any zonation. This sample was thus considered as a suitable candidate for decay constant intercalibration.

Appendix 2. Sample description.

Table A.2.4. Literature ages for the Phalaborwa complex.

* Rb-Sr age recalculated to $\lambda_{87} = 1.3972 \cdot 10^{-11} \text{ a}^{-1}$ (Villa et al., 2015), assuming that Eriksson (1984) originally used the constant of (Steiger and Jäger, 1977)

Age (Ma)	Method	Mineral	Rock type	Reference
2060	U-Pb	uranothorianite		Holmes and Cahen (1956)
2047 ± 19*	Rb-Sr	phlogopite	clinopyroxenite, carbonatite and phoscorite	Eriksson (1984)
2047 +11 / -8	U-Pb	thorianite and baddeleyite	carbonatite and phoscorite	Eriksson (1984)
2059.8 ± 0.8	U-Pb	baddeleyite	carbonatite	Heaman and LeCheminant (1993)
2060.6 ± 0.5	U-Pb	baddeleyite		Reischmann (1995)
2057 ± 8	U-Pb	baddeleyite	<i>not indicated</i>	Horn et al. (2000)
2057.1 ± 2.6	U-Pb	baddeleyite	<i>not indicated</i>	Wingate and Compston (2000)
2059.6 ± 0.4	U-Pb	baddeleyite	carbonatite	French et al. (2002)
2026 +46 / -47	U-Th Pb	total baddeleyite	carbonatite	French et al. (2002)
2062 ± 74	Rb-Sr	hornblende, felsic fraction, clinopyroxene	dolerite	Yuhara et al. (2005)
2013 ± 93	Rb-Sr	whole rock and mineral	phoscorite	Yuhara et al. (2005)
2060.1 ± 4.1 2050 ± 13	U-Pb (in situ)	baddeleyite zircon	outer pegmatitic pyroxenite of Loolekop pipe	Wu et al (2011)
2061.72 ± 2.4 2047 ± 27	U-Pb (in situ)	baddeleyite zircon	main phoscorite	Wu et al (2011)
2060.0 ± 2.2	U-Pb (in situ)	baddeleyite	banded carbonatite	Wu et al (2011)
2056.7 ± 2.7 2059.8 ± 1.3 2053 ± 14	U-Pb (in situ)	baddeleyite baddeleyite zircon	transgressive carbonatite	Wu et al (2011)
2068 ± 17 2049 ± 28	U-Pb (in situ)	baddeleyite zircon	satellite syenite (plug-like bodies outside the border of main complex)	Wu et al (2011)
2035 ± 35	U-Pb (in situ)	baddeleyite	later mafic dyke	Wu et al (2011)
2060.3 ± 0.4	Pb-Pb	baddeleyite	carbonatite	Kumar et al. (2014)

Appendix 2. Sample description.



Fig. A.2.5. PhB-2 sample from Phalaborwa carbonantite complex.

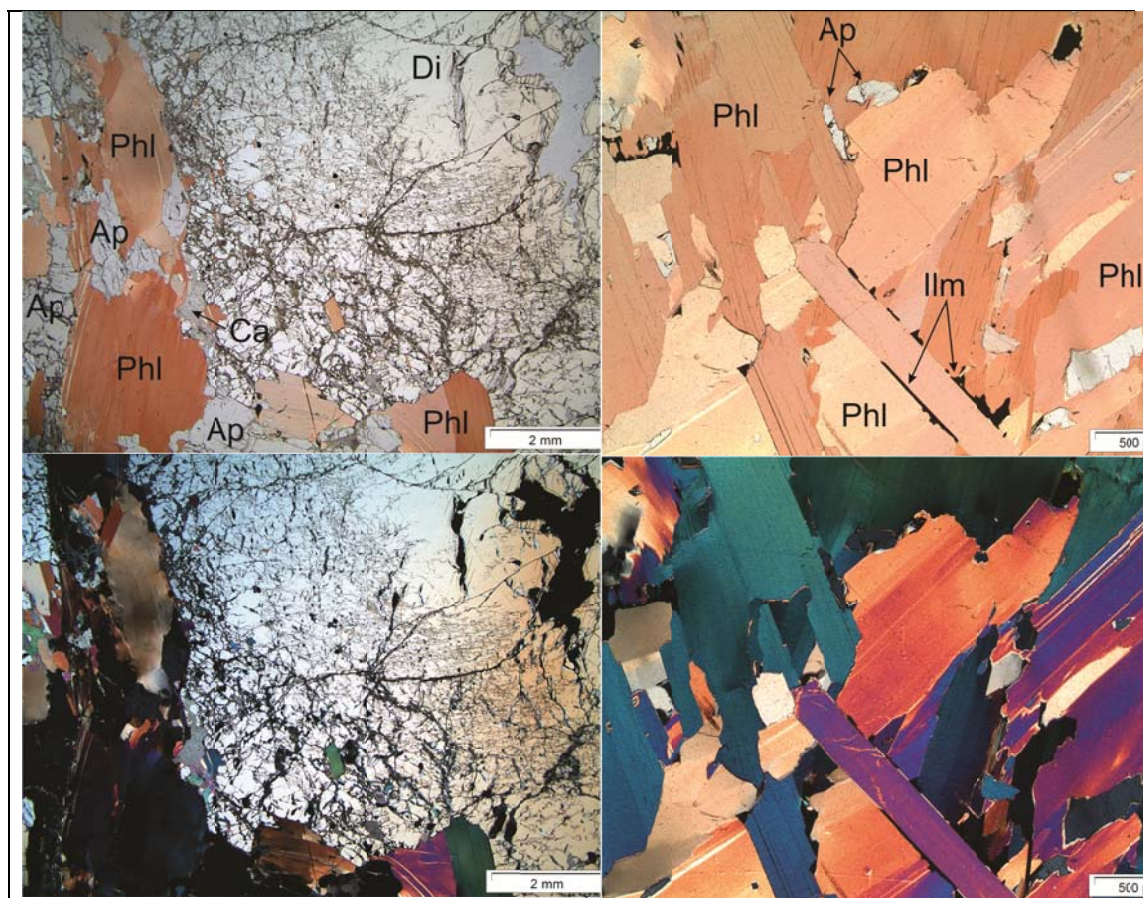


Fig A.2.6. Thin-section pictures of the PhB-2 sample: upper row plane polarized light, lower row cross polarized light.

Appendix 2. Sample description.

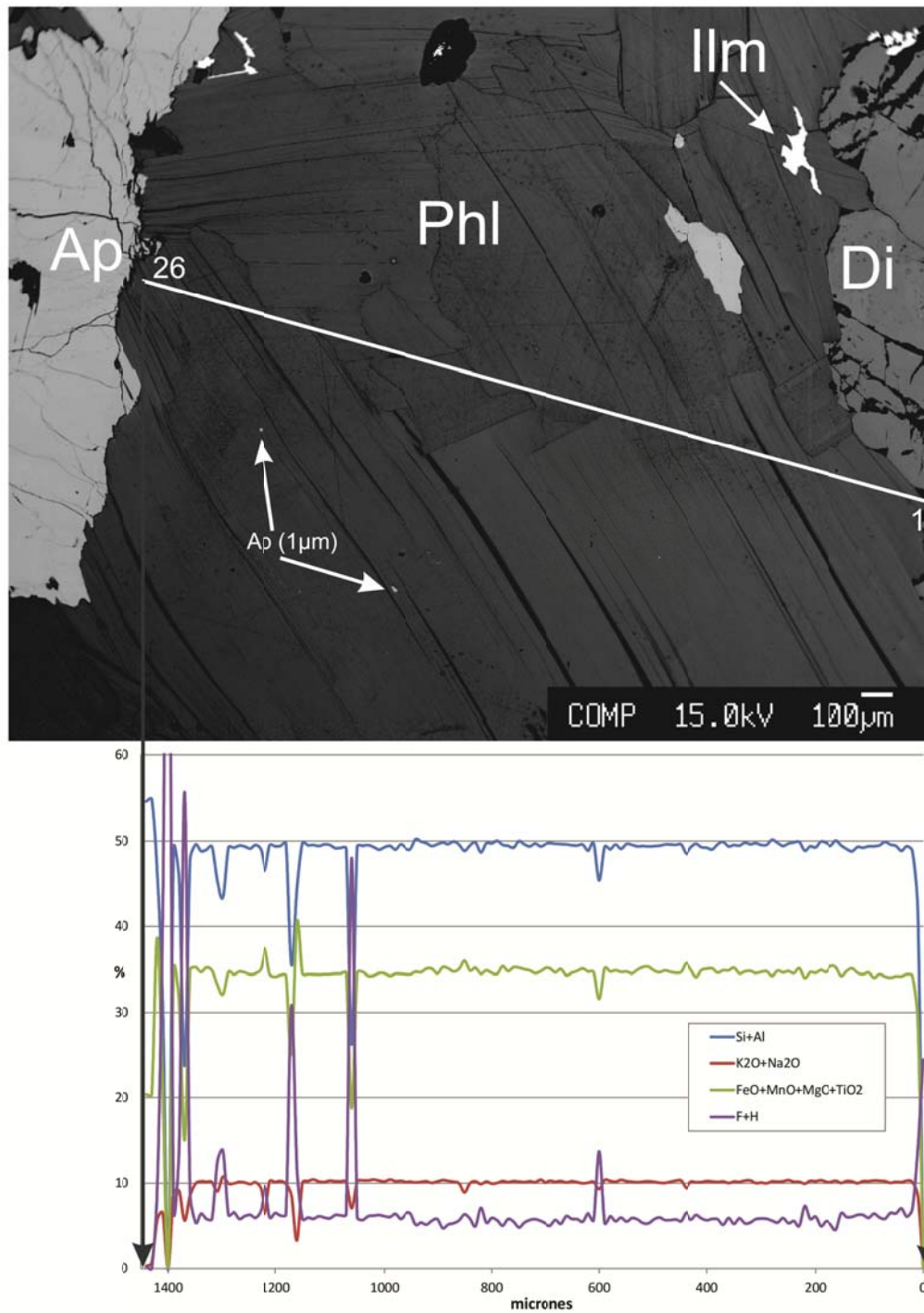


Fig. A.2.7. Microprobe quantitative analysis through a Phalaborwa phlogopite (PhB-2). Picks of F+H line shows mechanical cracks in the grain, probably due to thin-section preparation.

Appendix 2. Sample description.

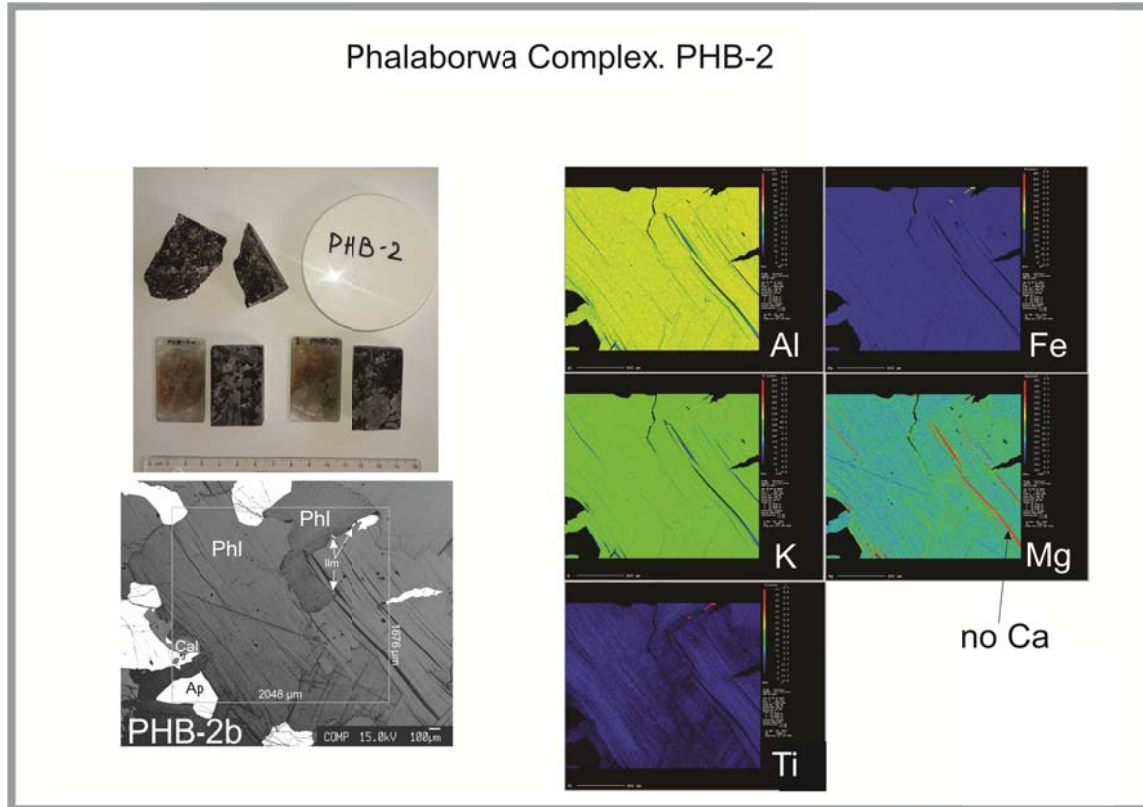


Fig. A.2.8. Microprobe maps of the Phalaborwa sample showing the uniform distribution within a single grain of phlogopite.

The lepidolite sample, Karib, Namibia was received courtesy of Dr. Beda Hofman (the Naturhistorisches Museum der Burgergemeinde Bern). It came from the Rubicon mine, which is located within the zoned Karibib pegmatite of the Dimara belt. Rubicon pegmatites have intruded into a medium- to high-grade metamorphic environment in between a quartz monzonite of Pan-African age (700-500 Ma), and a pegmatitic granite of late Pan-African age (600-460 Ma). U-Pb dating of the columbite gave an age of 505.5 ± 5.2 Ma (2σ) (Melcher et al., 2015).

The lepidolite sample (marked on the pictures as “Lep”) consists of pristine big pink sheets, that can be easily sliced along cleavage planes with a blade into thin transparent pieces. Microprobe analysis shows that the sheets have neither visible inclusions of other minerals, nor zonation or signs of alteration. Element maps show a uniform distribution of Al, F, K, Mn and Rb. Quantitative line analysis also confirms the homogeneity of the sample (Fig. A.2.9). Lepidolite has very high K and Rb contents and was considered as a good candidate for simultaneous dating with the Rb-Sr and K-Ca methods.

Lepidolite LEP-A8555

(obtained from Naturhistorisches Museum Bern.
Farm aria near mine Rubicon, Karibib, Namibia
1979. Dr.G.Jung)

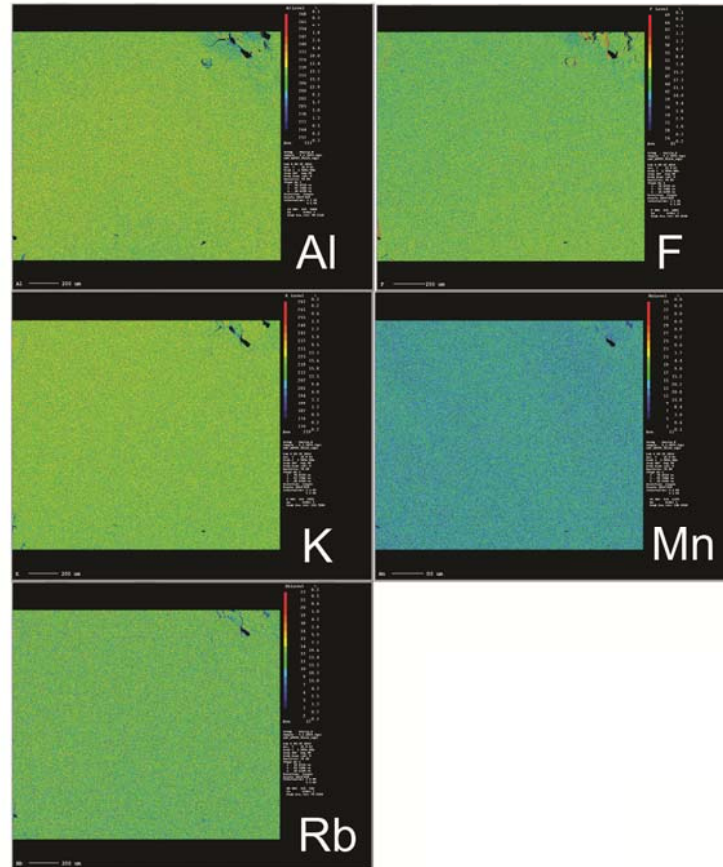
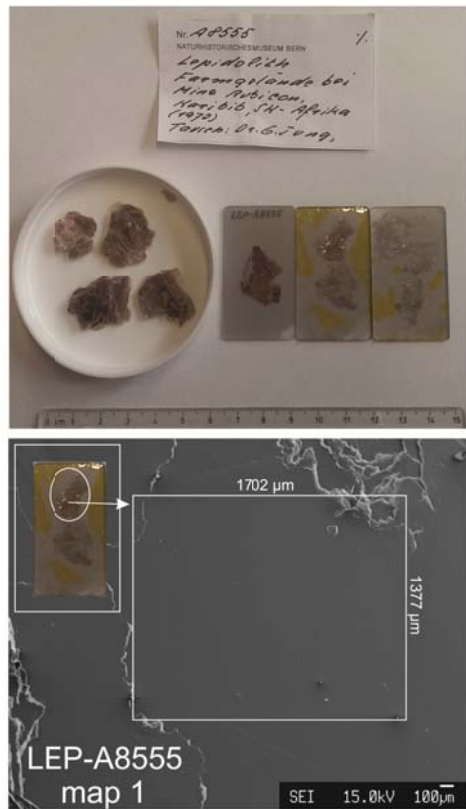


Fig.A.2.9. Lepidolite sample, backscattered electrons image of the mapped area and elemental maps.

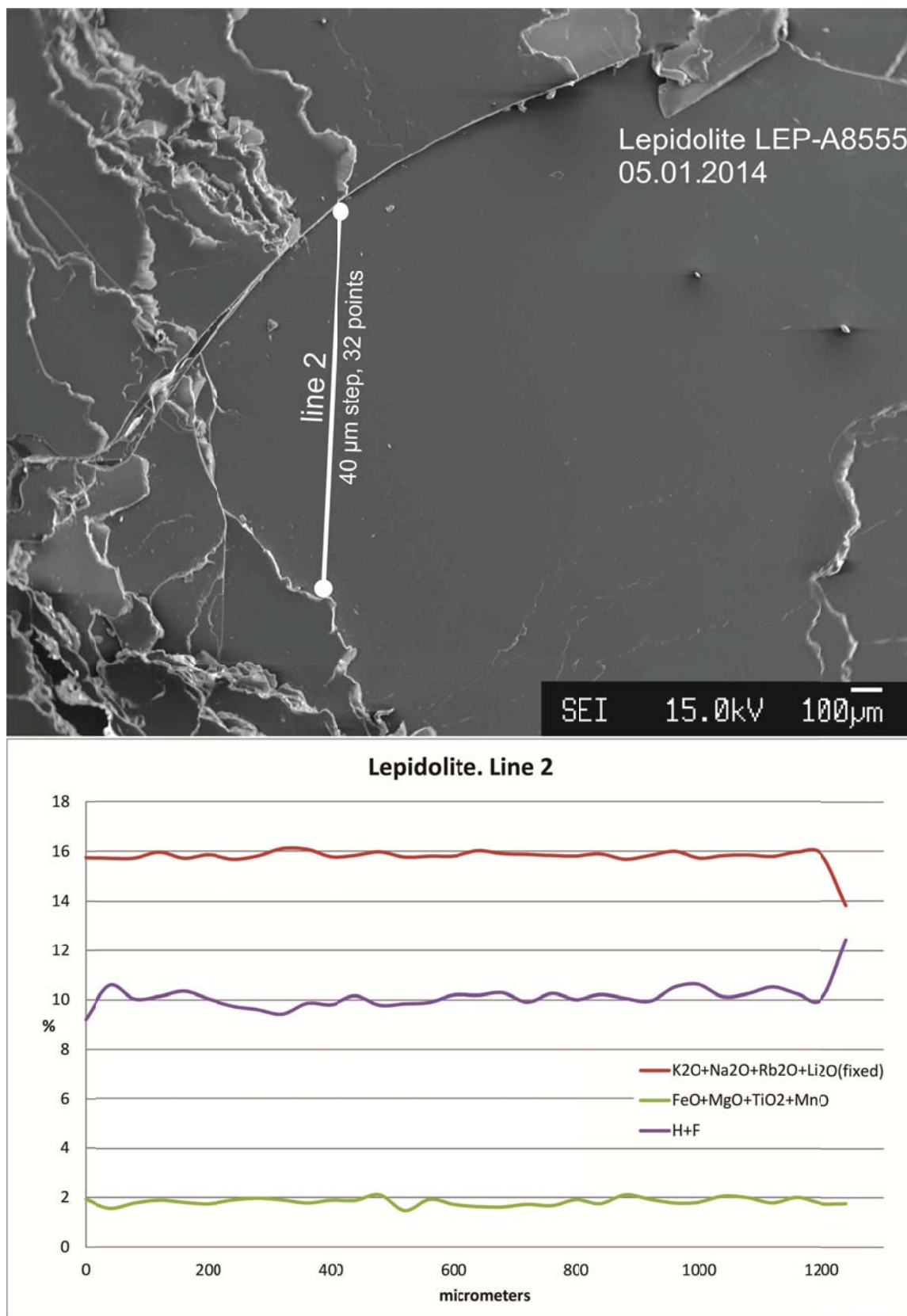


Fig. A.2.10. Quantitative microprobe line analysis of the Lepidolite sample.

Appendix 2. Sample description.

References:

- Bédard, L.P., Chown, E.H., 1992. The Dolodau dykes, Canada: An example of an archaean carbonatite. *Mineralogy and Petrology* 46, 109-121.
- Bell, K., Blenkinsop, J., 1980. Ages and initial $^{87}\text{Sr}/^{86}\text{Sr}$ ratios from alkalic complexes of Ontario. *Ont Geol Surv Misc Pap* 93, 16-23.
- Burgess, R., Kelley, S.P., Parsons, I., Walker, F.D.L., Worden, R.H., 1992. $^{40}\text{Ar}/^{39}\text{Ar}$ analysis of perthite microtextures and fluid inclusions in alkali feldspars from the Klokken syenite, South Greenland. *Earth and Planetary Science Letters* 109, 147-167.
- Dalrymple, B.G., Czamanske, G.K., Fedorenko, V.A., Simonov, O.N., Lanphere, M.A., Likhachev, A.P., 1995. A reconnaissance $^{40}\text{Ar}/^{39}\text{Ar}$ geochronologic study of ore-bearing and related rocks, Siberian Russia. *Geochimica et Cosmochimica Acta* 59, 2071-2083.
- Eriksson, S.C., 1984. Age of carbonatite and phosphorite magmatism of the Phalaborwa Complex (South Africa). *Chemical Geology* 46, 291-299.
- French, J.E., Heaman, L.M., Chacko, T., 2002. Feasibility of chemical U–Th–total Pb baddeleyite dating by electron microprobe. *Chemical Geology* 188, 85-104.
- Gittins, J., Macintyre, R.M., York, D., 1967. The ages of carbonatite complexes in eastern Canada. *Canadian Journal of Earth Sciences* 4, 651-655.
- Heaman, L.M., LeCheminant, A.N., 1993. Geochemistry of Accessory Minerals Paragenesis and U–Pb systematics of baddeleyite (ZrO_2). *Chemical Geology* 110, 95-126.
- Holmes, L., Cahen, L., 1956. *Geochronologie Africaine*. Mem. Cl. Sci. Nat. Med., Acad. R. Sci. Colon.(Brussels), Fasc 1, 169.
- Horn, I., Rudnick, R.L., McDonough, W.F., 2000. Precise elemental and isotope ratio determination by simultaneous solution nebulization and laser ablation-ICP-MS: application to U–Pb geochronology. *Chemical Geology* 164, 281-301.
- Kamo, S.L., Czamanske, G.K., Amelin, Y., Fedorenko, V.A., Davis, D.W., Trofimov, V.R., 2003. Rapid eruption of Siberian flood-volcanic rocks and evidence for coincidence with the Permian–Triassic boundary and mass extinction at 251 Ma. *Earth and Planetary Science Letters* 214, 75-91.
- Kumar, A., Nagaraju, E., Srinivasa Sarma, D., Davis, D.W., 2014. Precise Pb baddeleyite geochronology by the thermal extraction-thermal ionization mass spectrometry method. *Chemical Geology* 372, 72-79.
- Kwon, S., Tilton, G., Grünfelder, M., 1989. Lead isotope relationships in carbonatites and alkalic complexes: an overview. *Carbonatites: Genesis and Evolution*, 360-387.
- Melcher, F., Graupner, T., Gäbler, H.-E., Sitnikova, M., Henjes-Kunst, F., Oberthür, T., Gerdes, A., Dewaele, S., 2015. Tantalum-(niobium-tin) mineralisation in African pegmatites and rare metal granites: Constraints from Ta–Nb oxide mineralogy, geochemistry and U–Pb geochronology. *Ore Geology Reviews* 64, 667-719.
- Nebel, O., Scherer, E.E., Mezger, K., 2011. Evaluation of the ^{87}Rb decay constant by age comparison against the U–Pb system. *Earth and Planetary Science Letters* 301, 1-8.
- Parsons, I., 1979. The Klokken Gabbro-Syenite Complex, South Greenland: Cryptic Variation and Origin of Inversely Graded Layering. *Journal of Petrology* 20, 653-694.
- Parsons, I., 1980. Alkali-feldspar and Fe–Ti oxide exsolution textures as indicators of the distribution and subsolidus effects of magmatic-water in the Klokken layered syenite intrusion, South Greenland. *Earth and Environmental Science Transactions of the Royal Society of Edinburgh* 71, 1-12.
- Parsons, I., 1981. The Klokken Gabbro-Syenite Complex, South Greenland: Quantitative Interpretation of Mineral Chemistry. *Journal of Petrology* 22, 233-260.
- Parsons, I., Mason, R.A., Becker, S.M., Finch, A.A., 1991. Biotite Equilibria and Fluid Circulation in the Klokken Intrusion. *Journal of Petrology* 32, 1299-1333.
- Reischmann, T., 1995. Precise U/Pb age determination with baddeleyite (ZrO_2), a case study from the Phalaborwa igneous complex, South Africa. *South African Journal of Geology* 98, 1-4.

Appendix 2. Sample description.

- Rukhlov, A.S., Bell, K., 2010. Geochronology of carbonatites from the Canadian and Baltic Shields, and the Canadian Cordillera: clues to mantle evolution. *Mineralogy and Petrology* 98, 11-54.
- Sage, R.P., 1987. Geology of carbonatite-alkalic rock complexes in Ontario: Prairie Lake carbonatite complex, District of Thunder Bay. Ministry of Northern Development and Mines, Ontario Geological Survey, Study 46, p. 91.
- Sano, Y., Terada, K., Hidaka, H., Yokoyama, K., Nutman, A.P., 1999. Palaeoproterozoic thermal events recorded in the ~4.0 Ga Acasta gneiss, Canada: evidence from SHRIMP U-Pb dating of apatite and zircon. *Geochimica et Cosmochimica Acta* 63, 899-905.
- Schoene, B., Bowring, S., 2006. U-Pb systematics of the McClure Mountain syenite: thermochronological constraints on the age of the $^{40}\text{Ar}/^{39}\text{Ar}$ standard MMhb. *Contributions to Mineralogy and Petrology* 151, 615-630.
- Steiger, R.H., Jäger, E., 1977. Subcommittee on geochronology: convention on the use of decay constants in geo- and cosmochemistry. *Earth and Planetary Science Letters* 36, 359-362.
- Tilton, G.R., Bell, K., 1994. Sr-Nd-Pb isotope relationships in Late Archean carbonatites and alkaline complexes: Applications to the geochemical evolution of Archean mantle. *Geochimica et Cosmochimica Acta* 58, 3145-3154.
- Villa, I.M., De Bièvre, P., Holden, N.E., Renne, P.R., 2015. IUPAC-IUGS recommendation on the half life of ^{87}Rb . *Geochimica et Cosmochimica Acta* 164, 382-385.
- Wingate, M.T.D., Compston, W., 2000. Crystal orientation effects during ion microprobe U-Pb analysis of baddeleyite. *Chemical Geology* 168, 75-97.
- Wooden, J.L., Czamanske, G.K., Fedorenko, V.A., Arndt, N.T., Chauvel, C., Bouse, R.M., King, B.-S.W., Knight, R.J., Siems, D.F., 1993. Isotopic and trace-element constraints on mantle and crustal contributions to Siberian continental flood basalts, Noril'sk area, Siberia. *Geochimica et Cosmochimica Acta* 57, 3677-3704.
- Wu, F.-Y., Yang, Y.-H., Li, Q.-L., Mitchell, R.H., Dawson, J.B., Brandl, G., Yuhara, M., 2011. In situ determination of U-Pb ages and S-Nd-Hf isotopic constraints on the petrogenesis of the Phalaborwa carbonatite Complex, South Africa. *Lithos* 127, 309-322.
- Yuhara, M., Hirahara, Y., Nishi, N., Kagami, H., 2005. Rb-Sr, Sm-Nd ages of the Phalaborwa Carbonatite Complex, South Africa. *Polar geoscience* 18, 101-113.

Appendix 2. Sample description.



Appendix 3.

Measurement protocols

Appendix 3. Measurement protocols.

Loading procedures

Potassium was measured on TIMS. The routine for **K** measurements is described in Naumenko et al. (2013). Here is a short summary and tips and tricks.

Potassium was loaded on tantalum single filament, degassed at 2 A for 45 min, 3 A for 30 min and 5 A for 70 min. It was left to oxidize minimum two weeks, more often more than a month before being used. Potassium was loaded in a separate cupboard under a laminar flux with H_3PO_2 acting as a stabilizer. H_3PO_2 were pre-cleaned in a Savillex beaker with a cation exchange resin. It was kept in the resin for few weeks, being shaken every day, afterwards beaker was centrifuged and acid pipetted out into a drop-bottle.

The most suitable standard concentration for a routine K measurement is 100ng/ μl , though for a total evaporation one should consider much lower concentrations (10ng/ μl). Potassium ionizes up to 100% and total evaporation can take days if too much element is loaded.

Loading was done according to following procedure:

1. Ta filament heated at 0.1 A
2. H_3PO_2 drop from a drop-bottle places on a piece of parafilm
3. Pipette tip prewashed by soaking in 3 times 10 μl of 6.4 M HCl 3x distilled and 3 times 10 μl of Milli-Q. Usually all necessary pipette tips were pre-washed in a such way immediately before loading.
4. 1-2 μl of H_3PO_2 loaded onto a filament. Filament current can be increased to 0.5 A
5. When the acid is almost dry a sample is loaded. Better to limit a loaded amount to max. 3 μl . For standards I used 1-2 μl . If there was necessarily to load more than 3 μl then it was done stepwise.
6. A sample dried on a filament at 0.5 A, maximum at 1 A. Higher current can lead to drop being spread on a filament surface.
7. The light is switched off and the current is slowly increased until approximately 4 A, when filament starts to glow. Glowing is kept for 10 seconds and then the current is decreased with a moderate speed (approximately 4 A per 30s)

Afterwards filaments can be mounted on a TIMS turret, which should be done in gloves with two tweezers, to not touch a filament. Sometimes I can touch with gloves corners of a cover to mount it better.

The routine for **Ca** measurements is described in Naumenko-Dèzes et al. (2015). Rhenium single filaments were used for Ca measurements. It is described in literature that Ta double filaments are better for high-precision measurements of Ca, and it gives less fractionation. In the light of incomplete fractionation correction with

Appendix 3. Measurement protocols.

an exponential law, I would recommend to test the next measurements of Ca on double Ta filaments.

Here is the routine for Ca loading on a Re single filament. First, filaments have to be additionally pre-washed before degassing. Each filament holder with welded rhenium ribbon has to be immersed for 20s into 2.5 M HCl 1x distilled and 20s Milli-Q™, then dried under a glass cover in the 50°C hood overnight. Afterwards filaments can be degassed under vacuum at 1.5 A for 45min, 2 A for 30min and 4 A for 70min.

Calcium is loaded on a Re filament with Ta-activator (Birck, 1986; Nögler and Villa, 2000). The parafilm is not used in this case to avoid contamination. A drop of activator is placed into a clean beaker with a flat bottom. Pipette tips are washed the same way as described for K. Activator is loaded at 0.1 A. After it is almost dry the sample is loaded.

Initial sample loading included soaking 2 µl of 6.4 M HCl into pipette tip, wiping a bottom and walls of a beaker to collect a sample. After struggling with Ca blank the procedure that requires fewer operations above an open beaker outside of the clean lab have been developed. After a sample is dry I add three drops of 6.4 M HCl 3x distilled into a beaker in the clean lab. A beaker is closed, revolved and let all acid to flow down at the bottom, if necessary it can be centrifuged. Then the beaker is opened in the Ca hood with bare washed in deionized water hands and placed on HF hot plate at 90°C. It takes about 40 min to evaporate most of the acid. The beaker is kept on a hotplate until the size of a drop reach *ca.* 3-5 µl. Afterwards the beaker is closed. Remaining drop gets smaller while the beaker is cooling down, therefore the drop should not get too small while on a hot plate. Samples are loaded on filaments immediately after this procedure, maximum next morning, if the preparation was done in an evening.

Loading is performed under a laminar flux in a separate cupboard in the mass-spectrometry room. One µl of the activator is loaded onto a Re filament and brought to almost dry at 0.1 A, then 1-2 µl of a sample is loaded on the top of the activator. If the loading amount in the beaker is bigger than 2 µl, the sample should be loaded in steps. After a sample is loaded, and the filament is dry; the light switched off and the filament is slowly brought to glowing. It stats glowing at about 3-4 A. It is kept glowing for 15-20s to evaporate the acid and possible K. This loading procedure for 21 filaments can take up to 5-6h.

Strontium loading is almost identical to Ca except that filaments do not need to be pre-washed in acid or Milli-Q. Activator droplet can be placed on a parafilm piece.

Appendix 3. Measurement protocols.

During the writing of the K paper (Naumenko et al., 2013) we received a useful comment from our associates editor Dimitri Papanastassiou about filament preparation for different elements. It might be useful for future work. Here is his message enclosed:

“We use single Ta (zone refined, microcrystalline, super-annealed, obtained a while back from Rembar) for K, Sr, Ca, Ti, Ba. The Ta has to be microcrystalline and super annealed, otherwise work-hardened Ta shows large crystals that get oxidized in a patchy way (leading to hot spots), depending on orientation.

For these, the Ta filaments are first outgassed and then oxidized at 1.5 Torr (air, leaked back into the outgasser), in the outgasser, at 4.0 Amps (once for Sr, Ba; twice and at 4.2 Amp, for Ca, Ti). Our outgasser has a sensitive capacitance manometer, for setting the pressure. One has to instantly go to 4Amp, because otherwise the insulating posts for the filament provide enough cooling (the filament time constant is a few milliseconds) that the corners are not sufficiently oxidized. Then for Ca, Ti we add very fine Ta₂O₅ powder and cement it with 0.5 N H₃PO₄.

Then, I observed on the Lunatic that with a DC filament power supply, the + end got hotter than the – end. Hence we switched to a square wave filament power, where the square wave is produced at ground potential and then the voltage/wave go through an isolation transformer, with the transformer secondary raised to the acceleration voltage.

The Triton uses a DC power supply for the filaments, which may yield problems.

For high precision Ca, on the Triton, we have used double filaments, CaCl₂ (which decomposes to CaO), and phosphoric.

D. A. Papanastassiou”(Papanastassiou, 2013)

Measurements

Rubidium was measured on ICP-MS Nu Instruments with sample-bracketing technique. Usually Apex requires pre-cleaning before Rb can be measured without any background. Pre-cleaning of Apex can be done with filling it with 1 M HNO₃ for few days, then with Milli-Q for another few days. Additional step of cleaning with “soap” can be performed if necessarily. Usually 1 M HNO₃ and Milli-Q overnight is enough, but it depends which samples were measured before. Rubidium standard was prepared so that the concentration is few ppb, which gives up to 3 V signal. ICP-MS was equipped with multicollector array of Faraday cups which are able to measure up to 10 V. Samples were diluted substantially before measurement. Three standard runs were performed at the beginning of the measurement day to test the stability and reproducibility of results. Samples were measured with sample-standard bracketing

Appendix 3. Measurement protocols.

procedure. Then samples were interspaced with standard, usually one standard-one to three samples, with washing in between till background memory is at < 1 mV. The results were corrected for baseline in-run. The fractionation factor was calculated from standards with exponential law and applied to samples. Usually it stays stable over measurement day. Over a year of measurements the fractionation factor varied between -1.72 to -2.2.

Calcium, K and Sr were measured on TIMS Triton+ in the static mode. Our TIMS equipped with nine Faraday cups, two of which were specially designed for Ca measurements, and variable amplifiers 10^{10} (used only in 2013 for K), 10^{11} and 10^{12} Ω . Strontium was measured with application of only 10^{11} Ω amplifiers to avoid intercalibration problems. K for Chapter 1 (Naumenko et al., 2013) paper was measured on all three amplifiers 10^{10} Ω (^{39}K), 10^{11} Ω (^{40}K) and 10^{12} Ω (^{41}K), later 10^{10} Ω amplifier was disconnected and replaced with 10^{11} Ω amplifier which limited the further precision of K measurements. Ca was measured mostly on 10^{12} Ω except strong ^{40}Ca signal which was amplified with 10^{11} Ω analyzer. More detailed cup – amplifier description for Ca can be found in Naumenko-Dèzes et al. (2015). Gain intercalibration of amplifiers was performed with built-in stable source of 3 V current. Gain calibration issues are described in Naumenko et al. (2013). Samples were measured mostly manually to avoid loss of the signal. Standards and sometimes Ca in apatite were measured with automatic heating program.

Strontium was measured with cup configuration present on fig. A.3.1. The approximate heating program can be found on fig. A.3.2. Heating for samples was performed slower, with slope 180 mA / min till 1200 and then with 50 mA / min till the signal of ^{88}Sr appears. If some Rb present filament was left at 1800 mA for approximately 20 min to burn it out, and then heated till Sr gives desirable signal intensity. Usually Rb is burned out before Sr reaches full signal.

Appendix 3. Measurement protocols.

Actual Cup Positions

Cup Number	Species	Target [mm] CDD Defl.[V]	Actual Position[mm]	Single Cup Positioning	Status In position
L5-F					
L4-F		60.797	60.794	Set	Pos. OK
L3-F		41.489	41.377	Set	Undefined
L2-F	84Sr	32.200	32.203	Set	Pos. OK
L1-F	85Rb	15.063	15.072	Set	Pos. OK
Center-F	86Sr				
H1-F	87Sr	15.000	14.998	Set	Pos. OK
H2-F	88Sr	32.200	32.203	Set	Pos. OK
H3-F		41.416	41.137	Set	Undefined
H4-F		60.740	60.738	Set	Pos. OK

Buttons: Break, Set Collection, Read, Reset Low, Reset High, ☐ Advanced

Configuration

Triton_Sr_IC

Sub-Configurations

Main

Buttons: New..., Rename..., Delete

Zoom Optics

Focus [V]: 0.0
Dispersion [V]: 0.0

Buttons: Read, Set

Fig. A.3.1. Sr cup configuration.

Acquisition Control | **Evaluation**

Filament Heating

Settings: Pilot Mass: 88Sr, SUMI Cups, Max. Value: 3700 nA, ION, SUMI Cups, 0 nA

Interblock Actions

Heating: ☐ EVA int. Window [%]: 80 to 120, ☐ ION int. Window [%]: 80 to 120

Counter Calibration

☐ Plateau Voltage: At Start, 1, ☐ Dark Noise: At Start, 1, ☐ Yield: At Start, 1

Triton_Sr_HV_1V.fht - Filament Heater

Line	Estimated Start Time	Valve	Filam. Type	Function	Time [min:sec]	Value [mA,mV,°C,ps]	Slope [mA/min]	Steps	Action1	Action2	Action3	Action4	Action5
1	00:00:00	CLOSE	EVA	FILC	00:04:00	1800	450	1	NONE	NONE	NONE	NONE	NONE
2	00:04:00	CLOSE	EVA	WAIT	00:03:00				NONE	NONE	NONE	NONE	NONE
3	00:07:00	OPEN	EVA	IONC	00:01:00	20	100	1	PEAKCENTER	FOCUS	ZFOCUS	FILFOCUS	NONE
4	00:11:50	OPEN	EVA	IONC	00:01:00	250	50	1	FOCUS	ZFOCUS	NONE	NONE	NONE
5	00:15:02	OPEN	EVA	IONC	00:01:00	500	50	1	FOCUS	ZFOCUS	FILFOCUS	NONE	NONE
6	00:18:54	OPEN	EVA	WAIT	00:01:00				NONE	NONE	NONE	NONE	NONE
7	00:19:54	OPEN	EVA	IONC	00:01:00	1000	50	1	FOCUS	NONE	NONE	NONE	NONE
*	00:22:57			END									

Done with heating process at 18:02:56.

Line No.	Mass Set	L2	L1	IC0 C	H1	H2	Integration Time[s]	Number of Integrations	File Time [s]	Control Cup Peakcenter	Control Cup Focus
1	Main	84Sr	85Rb	86Sr	87Sr	88Sr	4.194	1	6.000	88Sr	88Sr
*											

Fig. A.3.2. Approximate Sr heating protocol.

Fractionation correction

Raw data after baseline and gain correction was used for further off-line fractionation correction. Fractionation correction for spiked samples was performed with an iterative process in Microsoft Excel adapted from the program for MC-ICP-MS written by Jan Krammers (Krammers, appr. 1990).

Strontium fractionation correction was performed according to following routine:

Shortening used for formulas:

88/86N=⁸⁸Sr/⁸⁶Sr natural, 88/86S=⁸⁸Sr/⁸⁶Sr spike, 88/86M=⁸⁸Sr/⁸⁶Sr measured ratios.
m88 stands for mass of ⁸⁸Sr, accordingly for all other isotopes.

The constant used for calculations:

88/86N=8.375209; 88/86S=3.92966;

84/86N=0.056795132; 84/86S=23.2399;

m86=85.909265; m84=83.913426; m88=87.905617.

1. Calculate the mixing line spike-sample: $y = S_{mix} \cdot x + I_{tmix}$
 $I_{tmix} = 84/86N - 88/86N$
 $S_{lmix} = (84/86S - 84/86N) / (88/86S - 88/86N)$
2. Make fractionation line first order as linear fractionation:
 $S_{lfrac} = ((84 - 86) / (88 - 86)) * ((84/86M) / (88/86M)) - 1 * ((84/86M) / (88/86M))$
 $I_{tfrac} = 84/86M - 88/86M * S_{lfrac}$

➔ Start iteration

3. Make intersection:
 $True_R = (I_{tfrac} - I_{tmix}) / (S_{lmix} - S_{lfrac})$
 $Obs_R = 88/86M$
4. Calculate fractionation factor:
 $Fract = \log(True_R / Obs_R) / \log(m86/m87)$
5. Calculate fractionation line again using exponential factor:
 $S_{lfrac\ 2} = (84/86M * (1 - (m86/m84)^{Fract})) / (88/86M * (1 - (m86/m88)^{Fract}))$
 $I_{tfrac\ 2} = 84/86M - 88/86M * S_{lfrac\ 2}$

Repeat iteration 5 times.

Correcting after iteration:

Use last $Fract_5$ as exponential correction factor in correction formula

$$\left(\frac{i_{Sr}}{86Sr}\right)_C = \left(\frac{i_{Sr}}{86Sr}\right)_M \times \left(\frac{im}{86m}\right)^{Fract_5}, \text{ where } i \text{ stands for any Sr isotopes } C \text{ marks}$$

fractionation corrected value, M measures ratio.

Appendix 3. Measurement protocols.

Spike correction was performed according to formula

$$\left(\frac{^{87}\text{Sr}}{^{86}\text{Sr}}\right)_{\text{spcorr}} = \left(\frac{^{87}\text{Sr}}{^{86}\text{Sr}}\right)_{\text{C}} - \frac{\left(\frac{^{87}\text{Sr}}{^{86}\text{Sr}}\right)_{\text{S}} - \left(\frac{^{87}\text{Sr}}{^{86}\text{Sr}}\right)_{\text{C}}}{\left(\frac{^{84}\text{Sr}}{^{86}\text{Sr}}\right)_{\text{S}} - \left(\frac{^{84}\text{Sr}}{^{86}\text{Sr}}\right)_{\text{C}}} \times \left(\left(\frac{^{84}\text{Sr}}{^{86}\text{Sr}}\right)_{\text{C}} - \left(\frac{^{84}\text{Sr}}{^{86}\text{Sr}}\right)_{\text{N}} \right), \text{ where N stands for}$$

natural, S for spike ratios

Fractionation correction protocol described for Sr above did not work properly for **K** correction due to an extreme spike isotopic composition and an extreme fractionation during measurement (fig. A.3.3). Thus adapted correction protocol from Chu et al. (2011) was applied.

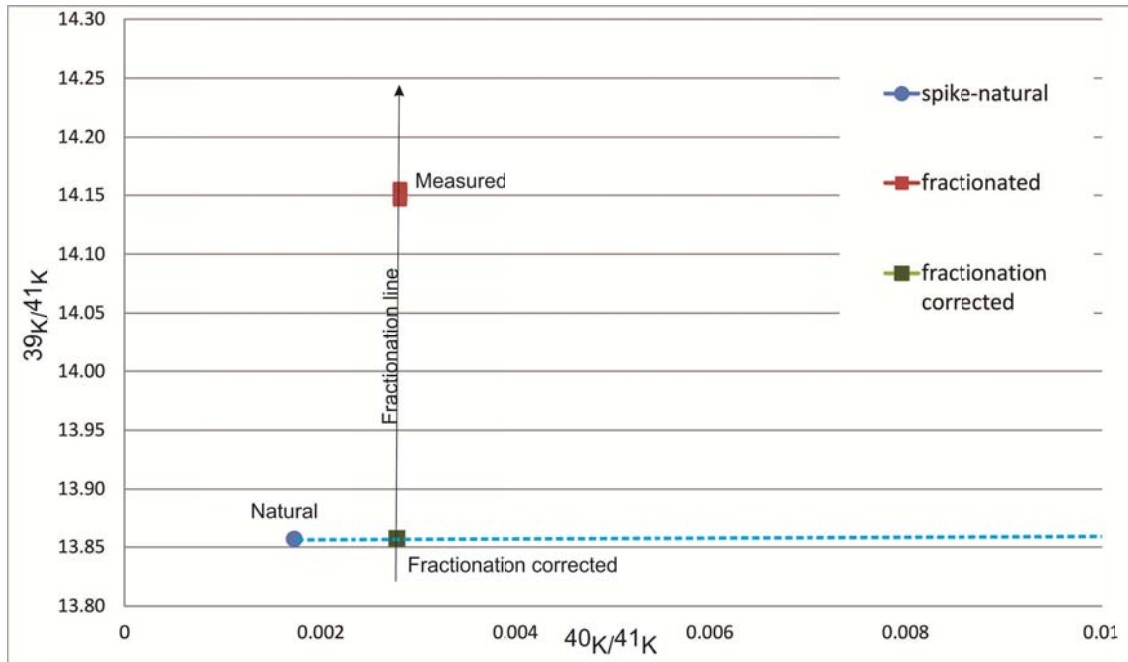


Fig. A.3.3. Fractionation correction of spike-sample mixture for K.

Designations are the same as for Sr.

1. Calculate fractionation factor accordingly to power law.

$$A = (39/44\text{N} - 39/44\text{S}) / (40/41\text{N} - 40/41\text{S})$$

$$B = \frac{\left(\frac{40}{41}\text{N} \times \frac{39}{41}\text{S}\right) - \left(\frac{39}{41}\text{N} \times \frac{40}{41}\text{S}\right)}{\left(\frac{40}{41}\text{N} - \frac{40}{41}\text{S}\right)}$$

$$\left(\frac{40}{41}\text{M}\right)_{\text{n1}} = \frac{-B + \sqrt{B^2 + 4 \times A \times \frac{40}{41}\text{M} \times \frac{39}{41}\text{M}}}{2 \times A}$$

$$\left(\frac{39}{41}\text{M}\right)_{\text{n1}} = \left(\frac{40}{41}\text{M}\right)_{\text{n1}} \times A + B$$

Appendix 3. Measurement protocols.

$$\text{Frac1} = \frac{\ln\left(\frac{\left(\frac{39}{41}M\right)_{n1}}{\left(\frac{39}{41}M\right)_{n1}}\right)}{\ln\left(\frac{m39}{m41}\right)}$$

2. Calculate fractionation factor (Frac.) accordingly to exponential law

$$\begin{aligned} &\left(\frac{40}{41}M\right)_{n2} \\ &= \frac{-B + \sqrt{B^2 + 4 \times A \times \frac{40}{41}M \times \frac{39}{41}M \times \left(\frac{m40}{m41}\right)^{-\text{Frac1}} \times \left(\frac{m39}{m41}\right)^{-\text{Frac1}}}}{2 \times A} \\ &\left(\frac{39}{41}M\right)_{n2} = \left(\frac{40}{41}M\right)_{n2} \times A + B \end{aligned}$$

$$\text{Frac2} = \frac{\ln\left(\frac{\left(\frac{39}{41}M\right)_{n2}}{\left(\frac{39}{41}M\right)_{n2}}\right)}{\ln\left(\frac{m39}{m41}\right)}$$

3. Calculated $\left(\frac{40}{41}M\right)_{n3}$ and $\left(\frac{39}{41}M\right)_{n3}$ like in step 2 but using Frac2, calculate Frac2 from $\left(\frac{40}{41}M\right)_{n3}$ and $\left(\frac{39}{41}M\right)_{n3}$. Repeat this step 8-10 times.

Calcium spiked samples were corrected with iterative process for double spiked samples. Following designations used in formulas:

43/44 and $\frac{43}{44}$ states for $\frac{^{43}\text{Ca}}{^{44}\text{Ca}}$ ratio, correspondingly other isotopic ratios are noted. M stands for measured, C for fractionation corrected, N for natural, S for spike ratios. Ratios from Russel et al. (1978) were used for fractionation correction. m43, m44, m48, m40m m42 stands for masses of corresponding isotopes.

The calculation protocol:

1. Calculate 43/44c and 48/44c with fractionation factor Frac.=0

$$43/44C = 43/44M \times (m43/m44)^{\text{Frac}}$$

$$48/44C = 48/44M \times (m48/m44)^{\text{Frac}}$$

2. Calculate natural 43/44N' out of 43/44M

$$\frac{43}{44}N' = \frac{43}{44}M + \left(\frac{\left(\frac{43}{44}M - \frac{43}{44}S\right) \times \left(\frac{48}{44}N - \frac{48}{44}C\right)}{\left(\frac{48}{44}C - \frac{48}{44}S\right)} \right)$$

3. Find ratio (Iter) between 43/44N' and 43/44N

$$\text{Iter} = (43/44N') / (43/44N)$$

Appendix 3. Measurement protocols.

4. Iterate fractionation factor (Frac) till Iter=1 with Excel tool “Goal Seek”.
5. Correct 42/44M and 40/44M for fractionation

$$42/44C = 42/44M * (m_{42}/m_{44})^{Frac}$$

$$40/44C = 40/44M * (m_{40}/m_{44})^{Frac}$$

6. Spike correction 40/44sp.corr.

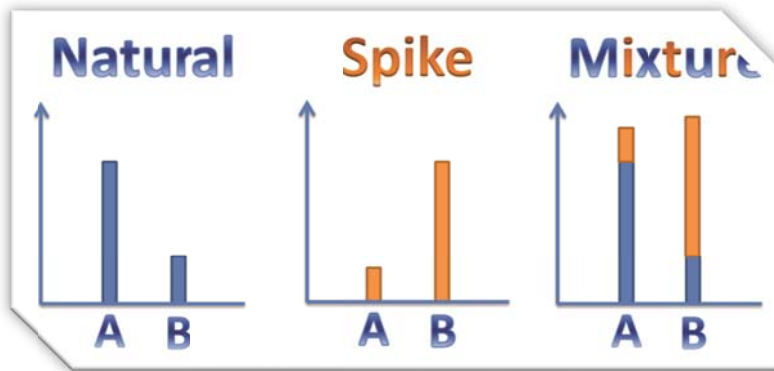
$$\frac{40}{44} \text{ sp. corr.} = \frac{40}{44} C + \frac{\left(\frac{40}{44} C - \frac{40}{44} S\right) \times \left(\frac{43}{44} N - \frac{43}{44} C\right)}{\left(\frac{43}{44} C - \frac{43}{44} S\right)}$$

Important! If calculations are made in Excel the precision preferences should be changed to 0.000 000 0001, otherwise shift downwards of fractionation and spike corrected $^{40}\text{Ca}/^{44}\text{Ca}$ is observed !

References:

- Birck, J.L., 1986. Precision K-Rb-Sr isotopic analysis: Application to Rb-Sr chronology. *Chemical Geology* 56, 73-83.
- Chu, Z.-y., Yang, Y.-h., Jinghui, G., Qiao, G.-s., 2011. Calculation methods for direct internal mass fractionation correction of spiked isotopic ratios from multi-collector mass spectrometric measurements. *International Journal of Mass Spectrometry* 299, 87-93.
- Kramers, J., appr. 1990. Fractionation correction program for Nd isotopes for spike-sample mixtures written for MC-ICP-MS. Institute of Geological Sciences, University of Bern.
- Nägler, T.F., Villa, I.M., 2000. In pursuit of the 40K branching ratios: K-Ca and 39Ar-40Ar dating of gem silicates. *Chemical Geology (Isotope Geoscience Section)* 169, 5-16.
- Naumenko-Dèzes, M.O., Bouman, C., Nägler, T.F., Mezger, K., Villa, I.M., 2015. TIMS measurements of full range of natural Ca isotopes with internally consistent fractionation correction. *International Journal of Mass Spectrometry* 387, 60-68.
- Naumenko, M.O., Mezger, K., Nägler, T.F., Villa, I.M., 2013. High precision determination of the terrestrial 40K abundance. *Geochimica et Cosmochimica Acta* 122, 353-362.
- Papanastassiou, D.A., 2013. Filament loading tips, in: personal communication to Villa, I.M. (Ed.).
- Russell, W.A., Papanastassiou, D.A., Tombrello, T.A., 1978. Ca isotope fractionation on the Earth and other solar system materials. *Geochimica et Cosmochimica Acta* 42, 1075-1090.

Appendix 3. Measurement protocols.



Appendix 4.

K-Ca mixed spike calibration

Appendix 4. K-Ca mixed spike calibration

Appendix 4. K-Ca mixed spike calibration

Isotopic composition

K-Ca mixed spike was prepared out of ^{40}K spike and ^{43}Ca - ^{48}Ca double spike. Ca double spike “Bern2” composition is present in Table A.4.1. The isotopic composition of K was measured with total evaporation technique with the precision showed in table A.4.2.

The first approximation of Ca isotopic composition was also measured with total evaporation technique. To calculate how much it is fractionated relatively to the true composition, three spike-standard mixtures were prepared and measured on TIMS. Twenty measurements for three spike-standard mixtures have suffered the instrumental mass-dependent fractionation. Each of these mixtures has been fractionation corrected with iteration method to natural Ca isotopic composition (Russel et al., 1978). Afterwards natural $^{40}\text{Ca}/^{44}\text{Ca}$ isotopic ratio was calculated out of the fractionation corrected mixtures. The δ deviation of this calculated ratio from published by Russel et al (1978) is due to incorrect, instrumentally fractionated isotopic spike composition. The exponential fractionation factor was calculated for spike isotopic composition with an iteration process by minimizing the δ deviation described above. With this method the Ca isotopic composition of Ca was calculated with uncertainty of 0.2%.

The uncertainty on the K ratios on the mixed spike did not affect the resulting uncertainty of the measured samples because K spike/sample ratio was very low. The further mixture is from the pure spike composition the less is an impact of the spike uncertainty on the resulting concentration calculation. For the K-Ca dating the measured K ratios of spiked micas are close to the natural composition and uncertainties of spike ratios have negligible effect on resulting calculation. The uncertainties on spike ratios were not included into the uncertainty propagation of spike concentration calculation.

Table A.4.1. Isotopic composition of the Bern2 Ca double spike used for preparation of the mixed spike.

“Bern 2” Ca double spike	
$^{40}\text{Ca}/^{44}\text{Ca}$	2.556
$^{42}\text{Ca}/^{44}\text{Ca}$	0.16858
$^{43}\text{Ca}/^{44}\text{Ca}$	16.422
$^{48}\text{Ca}/^{44}\text{Ca}$	18.905

Table A.4.2. Isotopic composition of the “Jäger” K spike used for preparation of the mixed spike.

“Jäger” K spike		
$^{40}\text{K}/^{41}\text{K}$	11.456	± 0.30
$^{39}\text{K}/^{41}\text{K}$	20.325	± 0.12

Isotopic concentration

Mixtures preparation

K-Ca mixed spike was calibrated to NIST mixtures and mixed ICP mixtures traceable to NIST. Ca NIST SRM 3109a with concentration 10.025 ± 0.017 mg/g [$\pm 0.17\%$ 2σ] mg/g and K NIST SRM 3141a 10.011 ± 0.029 mg/g [$\pm 0.29\%$ 2σ], K ICP standard (Certipur 1.70308.0100) 987 ± 3.9 $\mu\text{g/g}$ [0.4%] and Ca ICP standard diluted from Certipur 1.70342.0100 1.0198 ± 0.0042 $\mu\text{g/g}$ [0.4%] were used for preparation of calibration mixtures.

Three ICP-spike and NIST-spike mixtures were used for the spike calibration. Standard and spike were mixed in Savillex Teflon beaker, each weighing step was performed five – six times to ensure that there is no weighing artefacts. The deviation during weighing was below 0.2‰. The deviation during weighing was included into propagation of concentration uncertainties. Due to high concentration of Ca in the original standard mixtures, they had to be diluted before being used for preparation of K-Ca mixed standards. The uncertainty on the weighing (2‰ for Ca NIST diluted) is also included into the uncertainty propagation. All weighing and concentration together with each individual uncertainty can be found in the spread sheet “Original weighing spread sheet for mixtures”.

Mixtures measurement

Small amount of a mixture was loaded onto K-Ca columns for separation after mixtures have been equilibrated over few days. Potassium and Ca fractions were measured separately and fractionation corrected as described in Appendix 3. The procedure was repeated several times for each mixture. After measurements were completed they were compared between each other to eliminate those contaminated with blanks (Fig. A.4.1.). This test shows only those measurements which were contaminated with a blank during column separation or loading procedure. If blank was involved during mixture preparation, the calculated spike concentration will differ from concentrations of other mixtures. Due to high K concentration in mixtures no blank was observe to affect K measurements.

The summary on *ca.* 70 measurements of spike-standard mixtures for Ca yielded *ca.* 1% uncertainty on the resulting Ca concentration, which comes from blank contamination during mixture preparation or column chemistry. Therefore some of the outliers were additionally eliminated (orange and red data in the spreadsheet “K-Ca spike calibration summary”). This resulted in weighted average of 36 measurements: $^{43}\text{Ca} = 0.0020936 \mu\text{mol/g} \pm 0.053\%$ (fig.A.4.2), $^{48}\text{Ca} = 0.0024135 \mu\text{mol/g} \pm 0.055\%$ (fig.A.4.3). Despite such a small uncertainty on the weighted average for further calculation the certified uncertainty of the NIST SRM 3109a concentration ($\pm 0.17\%$, 2σ) was used for dating.

Appendix 4. K-Ca mixed spike calibration

Potassium calibration was not affected by a contamination problem. The spike concentration calculated from ICP mixture is 8% offset from those calculated from NIST. (Fig. A.4.3.). Since NIST mixtures are more trusted we have used only the results from NIST-spike mixtures for final calculation (fig. A.4.4.). The resulting concentration of $^{40}\text{K}=0.0053130\mu\text{mol/g}$ with uncertainty on NIST concentration (0.29%) were used for K-Ca dating.

The resulting spike data used for further concentration calculation is present in the Table A.4.3.

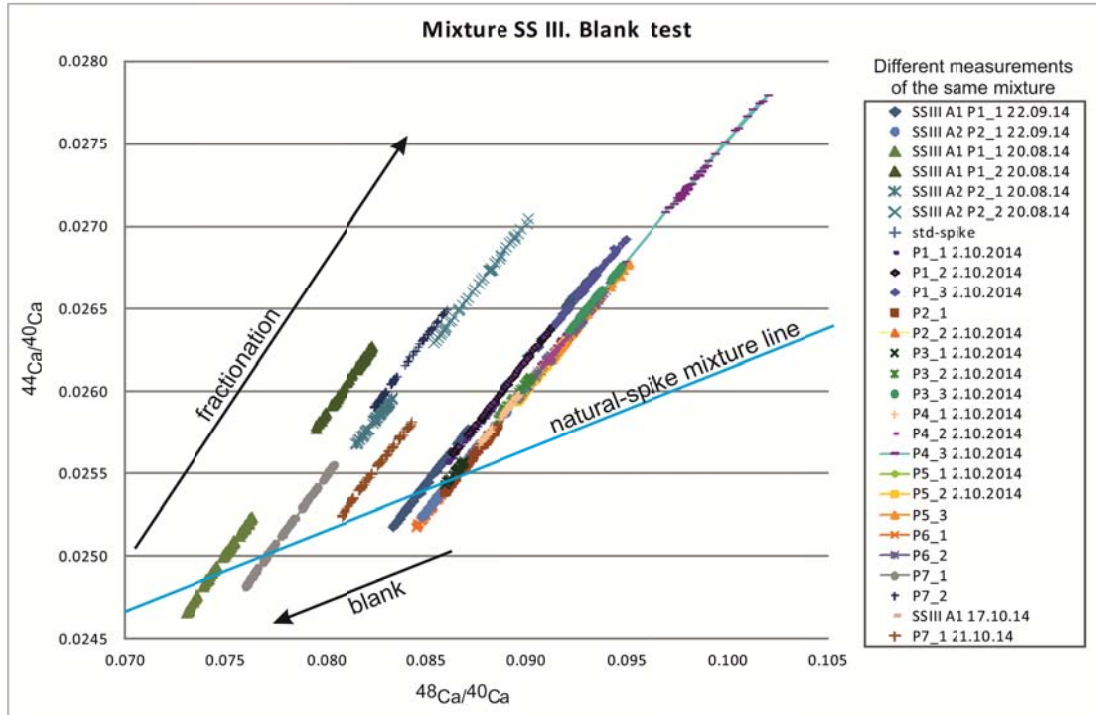


Fig. A.4.1. Example of the blank test for a mixture. All measurements which are towards the left from outside right are blank contaminated and shifted towards natural Ca isotopic composition.

Appendix 4. K-Ca mixed spike calibration

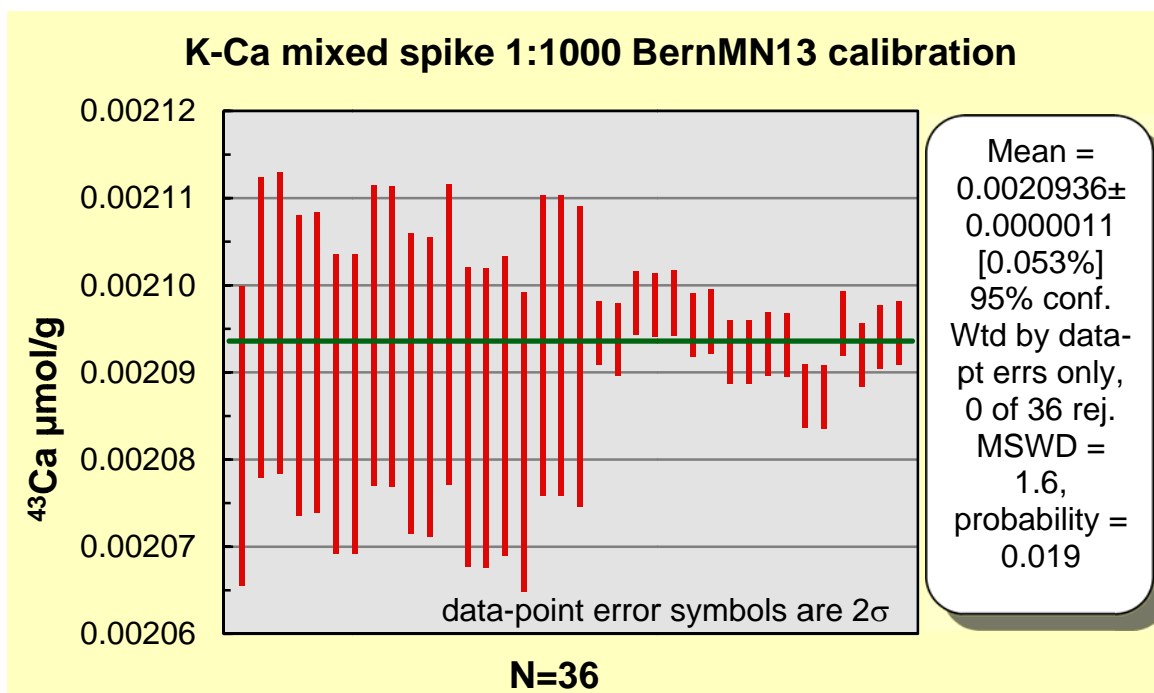


Fig. A.4.2. ^{43}Ca concentration. First 19 measurements of ICP mixture, last 17 of NIST mixture.

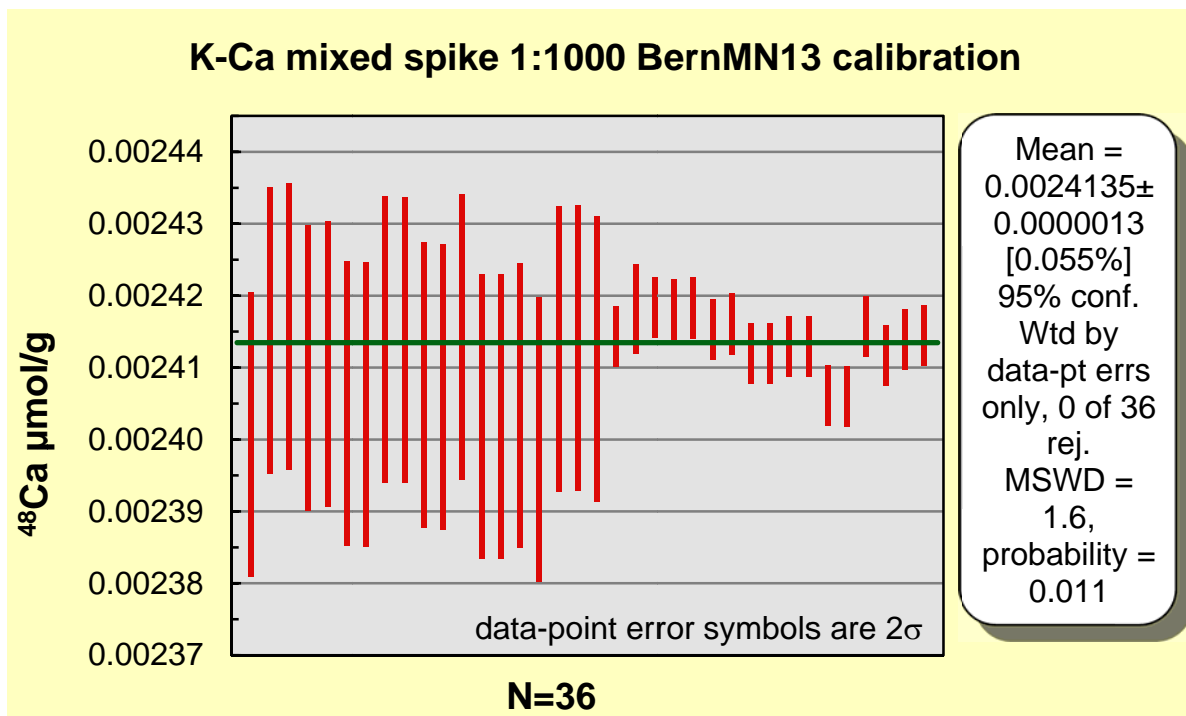


Fig. A.4.3. ^{48}Ca concentration. First 19 measurements of ICP mixture, last 17 of NIST mixture.

Appendix 4. K-Ca mixed spike calibration

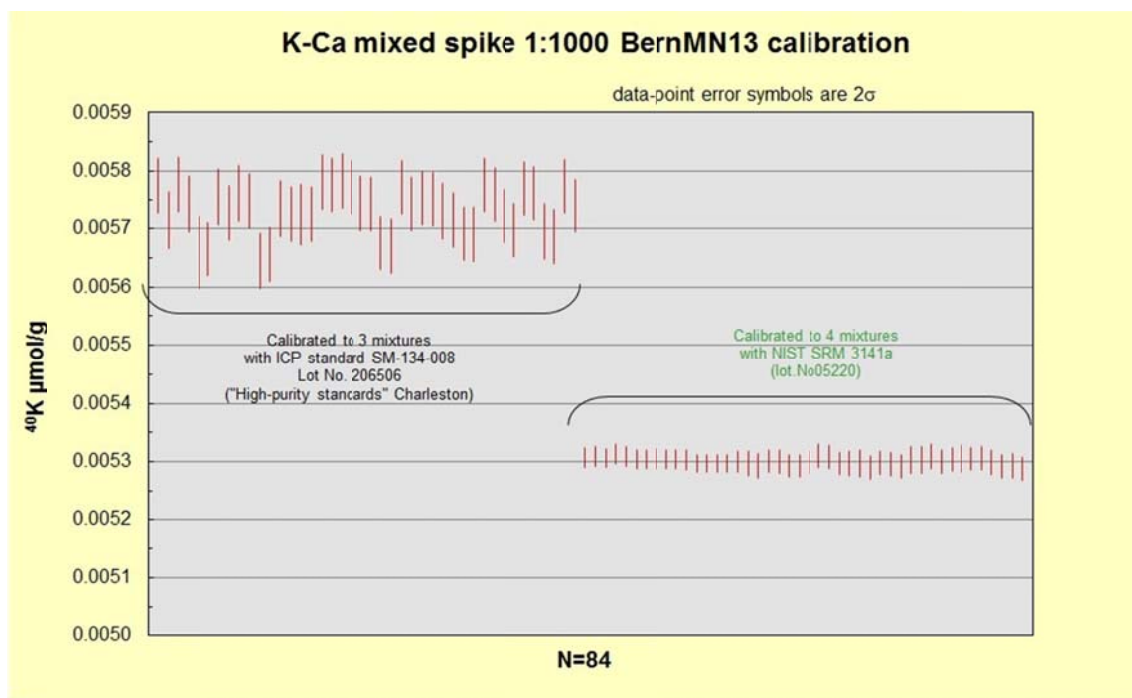


Fig. A.4.3. The results for ^{40}K concentration calculation showing the offset between ICP and NIST mixtures results.

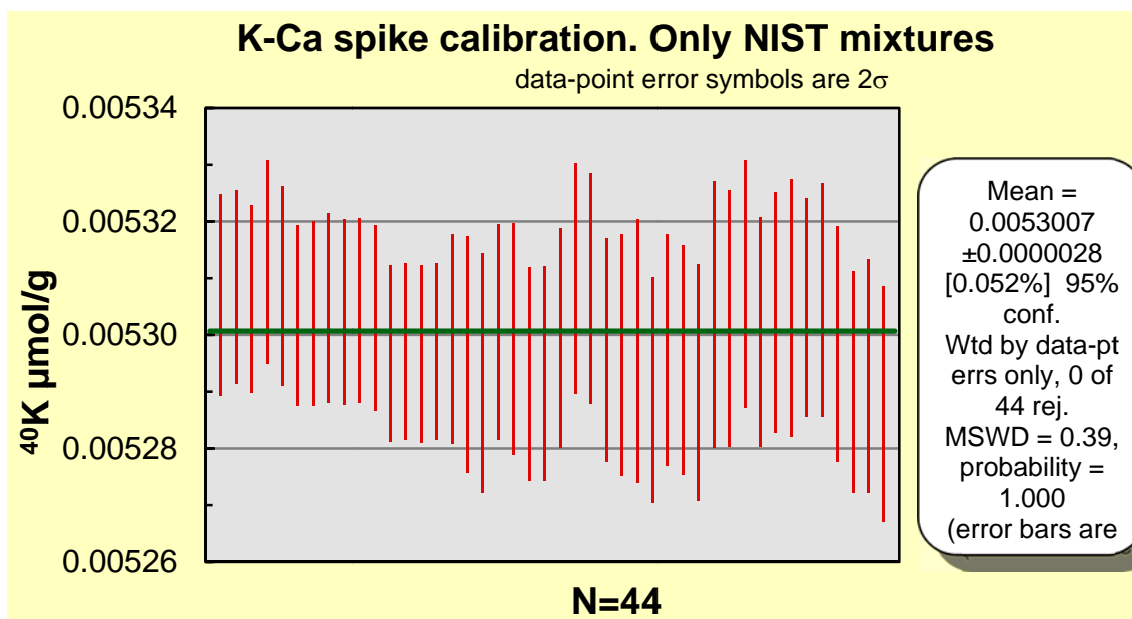


Fig. A.4.3. The results for ^{40}K concentration calculation, only for NIST mixture.

Appendix 4. K-Ca mixed spike calibration

Table A.4.3. The resulting K-Ca spike composition.

K-Ca mixed spike 1:1000 Bern13				
<i>calibrated 15.09.2015 to NIST SRM 3141a and NIST SRM 3109a</i>				
<i>Uncertainties 2 sigma</i>				
Ca tot	0.23217	±	0.00039	µg/g ±0.17%
K tot	0.59722	±	0.00173	µg/g ±0.29%
⁴³ Ca	0.0020936	±	0.0000036	µmol/g ±0.17%
⁴⁸ Ca	0.0024135	±	0.0000041	µmol/g ±0.17%
⁴⁰ K	0.0053007	±	0.0000154	µmol/g ±0.29%
⁴⁰ Ca/ ⁴⁴ Ca	3.7807	±	0.2%	
⁴² Ca/ ⁴⁴ Ca	0.1672			
⁴³ Ca/ ⁴⁴ Ca	15.9574			
⁴⁸ Ca/ ⁴⁴ Ca	18.3943			
⁴³ Ca/ ⁴⁸ Ca	0.86752			
⁴⁰ K/ ⁴¹ K	11.456	±	0.3%	
³⁹ K/ ⁴¹ K	20.325	±	0.12%	
⁴³ Ca/ ⁴⁰ K	0.39501	±	0.34%	
<i>mica : spike 1:100</i>				
<i>calcite : spike 1:200</i>				

References:

Russell, W.A., Papanastassiou, D.A., Tombrello, T.A., 1978. Ca isotope fractionation on the Earth and other solar system materials. *Geochimica et Cosmochimica Acta* 42, 1075-1090.

Declaration of consent

on the basis of Article 28 para. 2 of the RSL05 phil.-nat.

Name/First Name: Mariia Dèzes

Matriculation Number: 11-104-437

Study program: Doktorat PHIL NAT, Reglement 2008

Bachelor ☐

Master ☐

Dissertation ☒

Title of the thesis: Refined isotopic compositions of K, Ca and a complementary comparison of the ^{40}K - ^{40}Ca , ^{40}K - ^{40}Ar and ^{87}Rb - ^{87}Sr chronometers.

Supervisor: Prof. Dr. Igor M. Villa
Prof. Dr. Thomas F. Nägler

I declare herewith that this thesis is my own work and that I have not used any sources other than those stated. I have indicated the adoption of quotations as well as thoughts taken from other authors as such in the thesis. I am aware that the Senate pursuant to Article 36 para. 1 lit. r of the University Act of 5 September, 1996 is authorised to revoke the title awarded on the basis of this thesis. I allow herewith inspection in this thesis.

Bern, 04.02.2016

Place/Date

Signature

Mariia Dèzes née Naumenko

E-mail: marie@geosphere.ch
Phone: +41 78 605 37 87
Address: Depotstrasse 28, Bern 3012, Switzerland
Birth: 8.2.1986 - born in Kerch, Crimea, Ukraine
Nationality: Ukraine; Swiss working permit B
Marital status: Married
Languages: Ukrainian and Russian- native, bilingual;
English – fluent, German – beginner



Education

04.02. 2016	Examination for the PhD title. University of Bern, Geological Institute. Bern, Switzerland.
1.9.2007 – 30.6.2009	Master Degree with Honor at the Kyiv National Taras Shevchenko University. Kyiv, Ukraine.
1.9.2003 – 30.6.2007	Bachelor Degree with Honor at the Kyiv National Taras Shevchenko University. Kyiv, Ukraine.
1.9.1992 – 20.6.2003	Kotsubinsky Lycée. Silver Medal for Merits. Kotsubinsky, Kyiv region, Ukraine.

Working Experience

1.5.2011 – 04.02.2016	PhD candidate in University of Bern, Geological Institute, Isotope Geology Group. Bern, Switzerland. Topic: “Refined isotopic compositions of K, Ca and a complementary comparison of the ^{40}K - ^{40}Ca , ^{40}K - ^{40}Ar and ^{87}Rb - ^{87}Sr chronometers”. Academic supervisors Prof. Dr. Igor M. Villa, Prof. Dr. Thomas F. Nägler. Summary: Calibration of ^{40}K decay constants with geological methods in pursuit to improve the uncertainty of Ar-Ar dating systems.
3.5.2007 – 31.3.2011	Associate Analyst (50%) in the Department of Oil and Gas, Institute of Geology, National Academy of Science of Ukraine. Kyiv, Ukraine. Task: Creating and analyzing the data base of geochemical analysis for the petroleum bearing Donbass region, Ukraine.

Skills

Mass-spectrometry:

TIMS Triton plus: establishing, developing and testing a method for full range Ca isotopes measurements in static mode in cooperation with ThermoScientific; solving problems, measuring K, Ca, Sr on the routine basis. Five years daily work experience.

ICP-MS measurements (Rb, Sr). One year experience.

Ion exchange chemistry: developing and improving K-Ca method, routine Rb-Sr column chemistry.

Work in a **clean laboratory:** maintaining laboratory equipment, responsible for acid distillation, cleaning procedures. Four years of experience.

Isotope dating (Ar-Ar, K-Ca and Rb-Sr): preparing samples, measurements, writing calculation protocols, proceeding and interpreting data, spike calibration.

Familiarity with Microprobe, optic microscopy. Worked in CorelDraw, Excel, InDesign *etc.*

Featured courses: Academic writing; Presentation skills; Project management for research.

Publications

M. Naumenko-Dèzes, C. Bouman, K. Mezger, Nägler Th., I. Villa. TIMS measurements of full range of natural Ca isotopes with internally consistent fractionation correction. *International Journal of Mass Spectrometry*, – 2015. Vol. 387, pp. 60-68. [doi:10.1016/j.ijms.2015.07.012](https://doi.org/10.1016/j.ijms.2015.07.012)

M. Naumenko, K. Mezger, Nägler Th., I. Villa. High precision determination of the terrestrial ^{40}K abundance. *Geochimica et Cosmochimica Acta*, – 2013. Vol. 122, pp. 353–362.

A.D. Naumenko A.D., **M.O. Naumenko**, P.M. Korznev Some new features of the kerleutian sediments geological structure of the Azov-Kerch segment of the Black Sea shelf. *Geology and mineral resources of the oceans*. - 2010. Vol. 4. [Original paper in Russian](#).

M. Naumenko. To the methods of facies diagnostics of the terrigenous sediments using geochemical data, on an example of the terrigenous low carboniferous sediments of Dnieper-Donets basin. *Collection of scientific works of the Institute of Geological Science NAS of Ukraine*.– 2010. Vol.3. [Original paper in Russian](#).

M. Naumenko. Geochemical characteristics of deposits of the Sribnean syncline north-east side of the Dnepr-Donets depression. *Collection of scientific works of the Institute of Geological Science NAS of Ukraine*.– 2009. Vol.2. 280 p. [Original paper in Russian](#).

A.D. Naumenko, **M.O. Naumenko** The Major Regularities of the Location of Oil-Gas Perspective Objects in the NE Sector of the Black Sea. *Geology and Mineral Recourses of the World Ocean*. – 2008. Vol.4. [Original paper in Russian](#).

Conferences

M. Naumenko-Dèzes, C. Bouman, K. Mezger, Nägler Th., I. Villa. High accuracy analysis of the whole range of Ca natural isotopes by TIMS. 13th Swiss Geoscience Meeting, Basel 2015.

M. Naumenko, C. Bouman, K. Mezger, Nägler Th., I. Villa. Simultaneous measurements of the whole range of Ca isotopes (^{40}Ca - ^{48}Ca) by TIMS. 12th Swiss Geoscience Meeting, Fribourg 2014.

M. Naumenko, K. Mezger, Nägler Th., I. Villa. High precision determination of the terrestrial ^{40}K abundance. Goldschmidt2013, Florence, Mineralogical Magazine, Volume: 77(5).

M. Naumenko, K. Mezger, Nägler Th., I. Villa. High precision $^{40}\text{K}/^{39}\text{K}$ ratio determination. AGU Fall Meeting 2012, San Francisco. DOI: 10.13140/2.1.4369.6324.

M. Naumenko, K. Mezger, Nägler Th., I. Villa. Thermal ionization mass spectrometric determination of the $^{40}\text{K}/^{39}\text{K}$ ratio. 10th Swiss Geoscience Meeting, Bern 2012.

M. Naumenko. Features of the mineral kingdom of the Crimean mineralogical province.// Materials of Third Ukrainian scientific conference. “Mineral resources of Ukraine: the optimal use” (Volodarsk-Volyn, Ukraine. 9 December 2010.)

M. Naumenko. Changing of the grain size and geochemical properties of alluvial deposits on the tectonic structures.// Actual problems of geology, prediction, exploration and evaluation of mineral deposits. Abstracts of the international scientific-practical conference. (Sudak, Ukraine. Crimea Department UGGRI, September 27-October 3, 2010)

M. Naumenko, A. Naumenko: New features of the Kerleutian sediments geological structure, Kerch Peninsula.// AAPG European Region Annual Conference. Exploration in the Black Sea and Caspian Regions, 17–19 October 2010, Kiev, Ukraine.

Naumenko A.D., **Naumenko M.O.** Lithologic-facies regularity of tectono-geodynamic evolution of Kerch peninsula. // The study of geodynamic and fluid dynamic formation of oil and gas deposits at Azov and Black Sea polygon. The Collection of Papers of VIII International Conference. Simferopol. Ukraine. – 2009.

Recommendations:

<u>Name:</u>	Prof. Igor M. Villa	Prof. Thomas F. Nägler
<u>Title:</u>	Associate professor, Geochronology. University of Bern, Geological institute. Bern, Switzerland	Associate professor, Isotope geochemistry. University of Bern, Geological institute. Bern, Switzerland
<u>e-mail:</u>	igor.villa@geo.unibe.ch	naegler@geo.unibe.ch